DOSIMETRY OF THE TEFLON ENCASED STRONTIUM EYE APPLICATOR.

By

SEHLOHO NTLAMELE

Dissertation submitted in fulfillment of the requirement of the degree of

MASTER OF SCIENCE IN MEDICINE

in the

DEPARTMENT OF MEDICAL PHYSICS

in the

FACULTY OF MEDICINE

at the

UNIVERSITY OF LIMPOPO

SOUTH AFRICA.

Supervisor: D.P.A. Maboe

Co-supervisor: Dr. A.C. Chamberlain

May 26, 2010.

DECLARATION

"I, Sehloho Ntlamele declare that the mini-dissertation hereby submitted to University of Limpopo, for the degree of Master of Science in Medicine in Medical Physics has not previously been submitted by me for the degree at this or any other university; that it is my work in design and execution, and that all material contained herein has been duly acknowledged".

……..... …….

(Mr S Ntlamele) Date

Student Number: 200603418

DEDICATION

To my parents, especially for guidance and affectionate care showed to me by my mother Selloane Alina Ntlamele, and motivation and encouragements I acquired from my late father Lesole Teba Edward Ntlamele.

ACKNOWLEDGEMENTS

This dissertation was produced with the assistance and guidance of the following people to whom I would like to express my sincere gratitude.

- My co-supervisor, Dr A.C Chamberlain for his guidance, advice, support and surplus supervision through the study.

- Mr D.P.A Maboe, my supervisor for the basics in MCNP code.

- Dr M.E Sithole, my mentor for guidance, advices, discussions and help during typing of this manuscript.

- Ms N.V Uushona for been there when I needed help and sharing ideas behind MCNP code.

- Mrs P. Van der Westhuizen for encouragement and moral support.

- Ms C. Ueckermann for assistance in Corel Draw software used for Figures in this manuscript.

- Mr M.M Motshwane for statistical analyses in some of the results.

- Ms R.A Scheepers for the English editing of this manuscript.

- The financial assistance of Department of Health Free State Government (South Africa) is also acknowledged.

TABLE OF CONTENTS

Numbers *Pages*

APPENDICES

LIST OF FIGURES

LIST OF TABLES

ABSTRACT

Key words: Monte Carlo simulation, MCNP5 code, Beta irradiation, Teflon-encased eye applicator, Dosimetry, Strontium-90 (Sr-90)

Introduction: The treatment of various superficial lesions of the eye and skin has been conducted for many years, using Strontium-90 ophthalmic applicators. The dosimetry of the Sr-90 eye applicator is necessary, since it helps to determine a precise dose distribution within the eye globe. This also aids in optimizing the dose to be delivered to the target tissue of the eye without harming normal tissues, through surface dose rate determination. Thus, the surface dose rates are used to determine the lens and sclera dose, and also to specify the effectiveness of the applicator.

These eye applicators are no longer manufactured and are commercially unavailable, because they have gone out of fashion. Those available are more than 20 years old. Due to recurrence in pterygium, glaucoma surgery enhancement and treatment of conjunctivae, the resurgence of the Sr-90 eye applicator is clinically needed. Hence, the Department of Medical Physics (University of Limpopo, MEDUNSA) proposed a new model of the Sr-90 ophthalmic applicator called the Teflon-encased eye applicator.

Aim: To determine the radiation depth dose rate distributions of the Teflon-encased eye applicator, and to compare the calculated dose rates with that of the standard eye applicator (SIA. 8975) previously used and studied in MEDUNSA.

Material and method: MCNP5 version 1.20 based Monte Carlo code was used. The first step involves verification of strontium-90 (Sr-90) and Yttrium-90 (Y-90) spectra. Second step, a new applicator model was designed. The third step, applicator was setup with water phantom, to determine dose distribution in water. Surface dose rate and central axis depth dose rate distributions were calculated. These were obtained in three different phases by varying the thickness of Teflon, different sources and changing the surface source distance (SSD) in order to determine their effects on central axis depth dose rates

and surface dose rates. The relationship of results was verified by correlation and ANOVA F- tests.

Results and discussion: All spectra were demonstrated to be as reliable and accurate with relative errors ranging up to 7.9%, and correspond well to published available spectra. A Teflon thickness of 0.1 cm was sufficient to filter out and suppresses Sr-90 beta particles, and gave maximum beta penetration of 0.8 cm. No betas reached the back side of the applicator shaft. Only about 90% of the initial source dose escaped Teflon-encased eye applicator.

The surface dose rate increased exponentially with a decrease in Teflon thickness with regression coefficient of 97%. It also decreased linearly with increase in SSD and source thickness with a variation correlation of 99% and 99%, respectively. The source thicknesses of 0.03 cm, 0.04 cm, 0.045 cm and 0.05 cm gave closest results of 38.32 cGy/s ± 2.7%, 36.45 cGy/s ± 2.8%, 34.90 cGy/s ± 2.8% and 32.75 cGy/s ± 1.5% respectively, to the standard eye applicator having 36.55 cGy/s ± 2.5%. The depth dose results have a strong correlation and significance of 99%. An increased of Teflon thickness from 0.1 cm to 0.125 cm lead to a 27% decrease in central axis depth dose rate. All ten statistical checks from MCNP were passed with average relative error of ±3%, at one standard deviation. The accuracy of calculated central axis depth dose rates was within 5%.

Conclusion: The central axis depth dose rate of the Teflon-encased eye applicator can only be calculated at a distance less than 0.5 cm depth of water, due to the applicator's geometry. The geometry, materials, applicator shape, source size, and distance between source and phantom, input spectra and MCNP code used caused differences in results. However it was possible to minimise the differences. The surface dose rate can only be defined at a depth of 0.01 cm in a water phantom in order to accurately estimate the dose to lens and sclera. The dosimetry of the Teflon-encased eye applicator is similar to that of a standard eye applicator. Also, this newly modeled applicator is effective and it can be manufactured for clinical treatment purposes.

Chapter 1

INTRODUCTION

1.1 Aim of the study

According to the literature [Ali & Khan, 1990; ICRU 72, 2004; Maage, 2002; Reft *et al.*, 1990; Selman, 1976], Strontium-90 (Sr-90) eye applicators have been used for more than 50 years in the treatment of both benign diseases of the eye, and superficial disorders and malignant diseases of the eye. These conditions include pterygium, glaucoma, corneal vascularisation, vernal conjunctivitis, tumours of the cornea and eyelid, and occasionally skin keratoses and hemangiomas. Thus, radiotherapy has been employed in ophthalmology for many years.

Whenever radiation is used in the treatment of cancer, dosimetry is essential. The treatment must deliver the right dose to the target tissues, without harming those parts of the body that are unaffected. Modern diagnostic techniques allow all volumes of interest in the eye to be determined within 0.05 cm. The critical structures can in certain cases be as close as 0.2 cm to 0.3 cm to the tumor. It is thus very important to optimise the treatment by limiting the dose to these structures (critical organs or those at risk). This can be achieved through source shaping or collimation and also by controlling the position of the applicator. The goal in ophthalmic therapy is to reduce the incidence and severity of vision-limiting complications without compromising tumour control. In ophthalmic treatments, a precise dose distribution within the eye globe or within about 1 cm from the ophthalmic applicator is required [ICRU 72, 2004].

The knowledge of the exact dose distribution is crucial to clinical decision making and to the outcome of the treatment. The algorithms applied in the calculations must be precisely comparable to the anatomic determination of all structures in the treatment region. In addition, knowledge of dose distribution and the exact reporting of this are important in allowing comparison of the results of the treatment to different radionuclides or different treatment modalities [ICRU 72, 2004]. For this reason, surface dose rates are

used to determine the lens and sclera dose and also to specify the effectiveness of the applicator [Maage, 2002].

Eye applicators are no longer manufactured or commercially available. Those currently in use are more than 20 years old, especially the Sr-90 ophthalmic applicators. The manufacturers stopped producing these because they went out of fashion when patients in developed countries began to fear radiation. However, owing to a recurrence in pterygium prevention, glaucoma surgery enhancement and treatment of conjunctivae, all of which are increasing dramatically in HIV/AIDS affected patients, applicators have again become clinically relevant. The use of the Sr-90 eye applicator for reducing recurrence rates after pterygium excisions has long been an effective therapeutic procedure [Gleckler *et al.*, 1998].

Given this background, a new model of the Sr-90 eye applicator, the Teflon-encased eye applicator, has been proposed. This concave eye applicator has been designed in the Department of Medical Physics, University of Limpopo (MEDUNSA).

The purpose of this study is to simulate the dosimetry of the Teflon-encased eye applicator and the applicator geometries. This study is concerned with the source dimensions and source geometries of this newly designed model. This model can be manufactured, provided its dosimetry is clinically acceptable. The chief research question is, whether the dose distribution of the new eye applicator is clinically similar to that of the original, commercially available standard eye applicator.

The main aim of the study is to determine the radiation dose distribution of the Sr-90 Teflon-encased eye applicator, and to compare the calculated dose rate with that of the standard eye applicator. This will be achieved by determining the dimensions and geometries of the Teflon-encased eye applicator, since these differ from the standard eye applicator.

The most accurate, reliable and flexible calculation method is required to simulate the dosimetry of the Teflon-encased eye applicator because of the characteristics of the beta-ray source, Sr-90. Such characteristics include energetic dose, short range and fast fall off over a few millimeters of the beta ray (β-ray). Beta dosimetry refers to the technique which measures the β-dose component of the radiation. The Monte Carlo N-Particle (MCNP) code will be used in this study to simulate the setup and to determine the dose distribution as radiation passes from the source to the water phantom. This means that MCNP will be used to quantify the surface dose rate, and the dose rates at various depths in an object, such as the lens of the eye. The surface dose rate of the applicator will be used to determine radiation dose for an affected area. The MCNP results will be compared with those obtained in a previous study [Maage, 2002] on a standard eye applicator.

1.2 Summary of this dissertation

This work is divided into interconnected chapters. Chapters 2 to 4 contain the literature review, history and theoretical background to the study. The basic physics and dosimetry theory applied in beta radiation, particularly to the Sr-90 source and to an eye applicator, are also discussed in chapter 2. Chapter 3 covers aspects of the Monte Carlo transport code and focuses on the MCNP5 code which was used in this study. Chapter 4 presents the background and history of the Sr-90 eye applicator, the description of both Teflon-encased and standard eye applicators, Sr-90 eye applicator medical applications and ophthalmic treatment techniques. Chapter 5 outlines the material, method and procedure followed in this study. Chapter 6 provides the results and the discussion of the findings. Finally, the conclusions and recommendations are discussed in chapter 7.

Chapter 2

BASIC PHYSICS AND DOSIMETRY THEORY

2.1 Introduction

The physics of the interaction of radiation with matter is used in radiation therapy, diagnostic radiology and other areas of medical physics. In order to optimize treatment in therapy and ophthalmology, the way in which radiation energy is transferred to and absorbed by the patient's body must be investigated [Dendy & Heaton, 1999]. The main subject of interest in dosimetry is the mechanism of energy deposition in matter by radiation [Klevenhagen, 1993].

Photons require an intermediate interaction stage of transferring energy first to atomic electrons before any transfer of energy to the medium can take place, since charged particles lose energy in a totally different manner to photons. In contrast, electrons start to lose energy immediately to the medium [Klevenhagen, 1993]. The basic physics of beta (β) particles, photons, dosimetric quantities and radiation dose distributions are discussed in the next sections.

2.2 Main types of ionizing radiation

Ionizing radiation can be divided into two categories. The first is called directly ionizing radiation and is composed of charged particles. Such charged particles include beta (β) particles, protons and alpha (α) particles, which require sufficient kinetic energy to produce collisional and radiative ionization when penetrating the absorber. The ionizing particles which are most important biologically are the alpha and beta particles; they are also known as alpha rays and beta rays [Friedell *et al.*, 1950]. The second category is named indirectly ionizing radiation, which is composed of uncharged particles such as neutrons and photons. The latter type of ionizing radiation can be detected by determining the ionization effects the charged particles produce during their interactions

with matter [Donald, 1996; Johns & Cunningham, 1983; Khan, 2003; Podgoršak, 2006]. As there are so many ionizing particles, only the most important will be discussed here.

2.2.1 Beta (β)-particles

The β-particles are fast, energetic electrons (high speed electrons) arising not from orbital electrons but from nuclear decay or transformations. They are ejected from the nucleus of an unstable radioactive atom, with energies ranging from just above 0 MeV to the maximum energy ($E_{\beta\ max}$) available for a particular radionuclide. This range of energies forms a continuous spectrum [Dendy & Heaton, 1999; James, 2006]. The β-particles are single, negatively charged and have very small mass. They cause ionization just like the primary electrons produced by photons [Friedell *et al.*, 1950].

The only difference between β-particles and electrons is their energy. The β-particles are deflected through a rather tortuous path [James, 2006], due to light mass and high speed. They are more penetrating than α-particles, but can be stopped by a few millimeters of aluminum, so cannot penetrate deeply into tissues. Hence, these are used for superficial tumour treatment, such as those of the eye. Beta-particles lose energy in four ways: direct ionization, creation of delta rays by ionization, the production of bremsstrahlung and Cerenkov radiation. Although all such mechanisms may occur, the most common are direct ionization and bremsstrahlung production [James, 2006].

2.2.1.1 Transformation mode of beta particles

Radioactive nuclides, either naturally occurring or artificially produced by nuclear reactions, are unstable and strive to reach more stable nuclear configurations. These can be reached through various processes of spontaneous radioactive decay that involves transformation to a more stable nuclide, and emission of energetic particles. The radioactive transformation is chaotic process, and defined as spontaneous nuclear transformations that result in the formation of new elements. This process is also described as the change of radionuclide from one nuclear configuration to another [Donald, 1996]. Thus it is a process by which the nucleus attempts to achieve stability, it

is not always successful at the first attempt and further transformation process may be necessary [Dendy & Heaton, 1999]. The rate of transformation is not affected by natural processes, such burning, freezing, solidifying, dilution, etc, with exception of chemical change which can increase the electron density near the nucleus [James, 2006].

The process of radioactive transformation was first recognized by Rutherford. Commonly, the term radioactive decay is used, but transformation is more accurate description of what is actually happening. Decay suggests a process of disappearance, what in reality happens is an atom with excess energy transforms itself to another atom that is either stable or one with more favourable conditions to proceed on stability [James, 2006]. The radioactive transformation of an atom occurs because of the constituents in the nucleus are not arranged in the lowest potential energy states possible. Therefore, the rearrangement of the nucleus causes an excess energy to be emitted and nucleus is transformed to an atom of a new isotope. This process may involve the emission of alpha particles, beta particles, orbital electron capture, negatrons, positrons, electromagnetic radiation in the form of x-rays or gamma rays and to a lesser extend neutrons, protons, and fission fragments [James, 2006; Johns & Cunningham, 1983], depending on the characteristics of the radionuclide.

In actual fact the process is characterized by the transformation of an unstable nucleus into a more stable isotope that itself may be unstable, and will decay further through a series chain of decays until a stable nuclear configuration is reached [IAEA, 2003]. In a stable nucleus, no particle ever acquires enough energy to escape, however in radioactive nucleus it is possible for a particle by series of chance encounters to gain enough energy to escape from the nucleus. The ejection of a nuclear particle is pure chance, and there is no way to decide when any particular nucleus will disintegrate. However, if there are many nuclei a certain percentage will disintegrate in a given time. Nuclei are characterized by the number of protons, Z and the number of neutrons (N = A-Z) in the nucleus.

In such decay sequence the nuclide which decays is frequently called the parent and its decay product the daughter. If both the parent and daughter nuclides are radioactive and the parent has longer half-life than the daughter, the rate of decay of the daughter is determined not only by its own half-life but also by the rate at which it is produced. As a first approximation assume that if the activity of the parent remains constant, or is constantly replenished, so that the rate of production will at first exceed its rate of decay and equilibrium will be reached when rate of production is just equal to the rate of decay [Dendy & Heaton, 1999].

The rate of approach to equilibrium depends on half life of the daughter, for an example Strontium-90 + Yttrium-90 (Sr-90-Y-90), after 10 half lives the activity will be within 0.1% of equilibrium. The equilibrium activity is governed by the activity of the parent, Strontium-90 (Sr-90). Two practical situations should be distinguished [Cherry *et al.,* 2003; Dendy & Heaton, 1999; James, 2006]:

1. Secular equilibrium: Occurs when the half-life of parent is much longer than half-life of daughter. Thus daughter is much short lived than parent.
2. Transient equilibrium: Occurs when parent half-life is not that much longer than that of daughter, both are almost equal in terms of activity and parent activity is not constant.

The radioactive transformations are typically displayed in the decay schemes, which depict energy, E (vertical axis) versus atomic number, Z (horizontal axis), as shown in Figure 2.1 below for Strontium-90 + Yttrium-90. The decay scheme product is depicted below the radioactive nuclide (i.e. with less energy) and the direction of the arrow indicates the change in atomic number, Z [James, 2006].

Sr-90 is abundant long-lived fission product and Sr-90 decays with half-life of 28.90 years into short-lived daughter Y-90, which in turn decays with half-life of 64 hours into stable Zirconium-90. The maximum beta energy from the Sr-90 (E_{max}) is 0.546 MeV and with mean kinetic energy of 0.196 MeV, while Y-90 produces more energetic and penetrating beta particles with maximum energy (E_{max}) of 2.284 MeV and mean kinetic energy of 0.933MeV. Since the daughter, Y-90 has such a short half-life; its emission is

in secular equilibrium with its parent, Sr-90 [ICRU 72, 2004; James, 2006; Johns & Cunningham, 1983; Kearsley *et al.,* 1988].

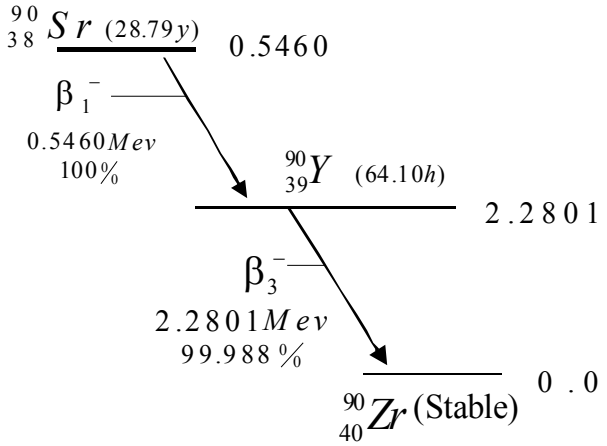

Figure 2.1: Decay scheme for Sr-90 + Y-90 isotopes [James, E.M., 2006; 775].

The decay scheme [Johns & Cunningham, 1983, Khan, 2003; Selman, 1976] of Sr-90 + Y-90 can also be presented by equations as follows:

$$^{90}_{38}Sr \rightarrow ^{90}_{39}Y + ^{0}_{-1}\beta(0.546MeV) + \bar{\nu} \tag{2.1}$$

$$^{90}_{39}Y \rightarrow ^{90}_{40}Zr + ^{0}_{-1}\beta(2.28MeV) + \bar{\nu} \tag{2.2}$$

where $\bar{\nu}$ and β are antineutrino and beta particle respectively. The antineutrino emitted in the beta emission process carries off a portion of the available energy; however this energy does not contribute to dose because of the negligibly small interaction of antineutrino's with matter [ICRP 38, 1983; Johns & Cunningham, 1983].

From Strontium-90 + Yttrium-90 decay scheme the emissions of the short lived daughter Y-90, are in secular equilibrium with long lived parent Sr-90, and only the beta energy of the daughter (Y-90) is of importance because of the relatively low energy beta-particles of the parent are usually absorbed by the source capsulation, thus the more effective source is Y-90 with the greater maximum energy of 2.28 MeV. Also the absence of

gamma ray makes Sr-90 + Y-90 special [IAEA, 2002; Friedell *et al.,* 1950; Maage, 2002]. Hence Sr-90 + Y-90 isotope is called a pure beta emitter.

From the medical physics point of view the mean energy ($\overline{E}$) deposited in tissue from β emitter is the quantity of interest, while for the nuclear physicists it is the maximum energy. The mean energy is expressed as a fraction of maximum energy (E_{max}). The ratio ($\overline{E}/E_{max}$) is different for each isotope and is determined from the shape of spectrum. The kinetic energy released can be found by noting the masses of each of the nuclei involved in the process of decay [Johns & Cunningham, 1983].

From Table A.1 (Appendix A), Sr-90 and Y-90 atomic masses are 89.9077376 and 89.9071514, respectively. The nuclear masses were obtained by reducing the atomic masses by the mass of the appropriate number of electrons, 38 for Strontium and 39 for Yttrium. Also the mass to energy conversion factors were used as in balanced equation below [Johns & Cunningham, 1983; Maage, 2002]:

1 electron mass = 0.511 MeV

1 amu = 931.6 MeV

Mass of Sr-90 nucleus		$89.9077376 - 38\ m_0$
Mass of Y-90 nucleus	$89.9071514 - 39\ m_0$	
Mass of β^-	$1\ m_0$	
Mass of antineutrino	0	
Total mass	$89.9071514 - 38m_0$	$89.9071514 - 38\ m_0$
Energy released		0.0005862 amu

Consequently, the energy released is 0.0005862 × 931.6 = 0.546 MeV which is in agreement with Table A.1 (Appendix A).

According to theory [Johns & Cunningham, 1983; IAEA, 2003], in dosimetry calculations involving decaying isotopes, there is need for one to know the total number of disintegrations (emission) that occur while the radioactive source is in or near the

patient. The number of atoms disintegrating per unit time is activity, which is a useful concept. When the number of atoms (N) present in the source and the activity of the source (A) are related by the transformation constant (λ), also called decay constant. Hence, activity is defined mathematically by:

$$(A) = \frac{\Delta N}{\Delta t} = -\lambda N \tag{2.3}$$

where ΔN and Δt are total number of radioactive atoms disintegrating and can be determined from the mass of isotope, and total time interval of measurement or transformation, respectively. The minus sign indicates that the number of radioactive atoms decreases with time. The use of this equation is further explained in Appendix A.

The beta decay energy is defined by the difference in mass-energy between the parent and the daughter nuclei beta particles; they exhibit continuous spectral kinetic energy distribution with only the maximum kinetic energy corresponding to the beta decay energy [Podgoršak, 2006]. The spectra for Sr-90, Y-90 and Sr-90 + Y-90 can be determined as number of beta rays per MeV against the energy (E). The knowledge of beta ray spectra is important for understanding of penetration and as input to calculations of dose distributions. The relative number of beta rays per MeV, N(W) can be calculated theoretically through the following:

$$N(W) = p \bullet W \bullet (W_0 - W)^2 \bullet F(Z,W) \bullet a_n(Z,W) \tag{2.4}$$

where W is the total energy of the electron (in units of $m_e c^2$), W_0 is the corresponding value at the maximum electron energy, $p = (W^2 - 1)^{1/2}$ is the electron momentum (in units of $m_e c^2$), m_e is the electron mass and c is the velocity of light, Z is atomic number of daughter nucleus, $F(Z,W)$ is the Fermi factor, $a_n(Z,W)$ is the shape factor for

transition of order of forbiddingness n, and when $a_n(Z,W)=1$ the spectrum is said to have allowed shape [ICRU 56, 1997].

The spectra shape is expected to deviate at certain degree by varying source thickness, back scatter and attenuation of air or any covering over the source, and because of the energy dependence of:

i) Attenuation in the source
ii) Backscatter from the source backing
iii) Interaction in the air between the source and detector.

These factors vary with maximum energy of beta rays, the cover thickness, the backing material and the distance between source and detector [Cross *et al.*, 1983; ICRU 56, 1997]. Differences in spectral shapes are primarily responsible for variations in shapes of dose distributions from different beta emitters. They also affect the interpretation of beta-ray measurements by their effect on the response of dosimeter and instruments [ICRU 56, 1997].

The variable attenuation of beta particle energy based on the initial energy serves both to continuously filter out lower energy betas and to continuously decrease the energy of higher betas. Thus, the average energy of beta radiation from radioisotopes decreases relatively slowly with increased thickness of absorbing material [ICRP 38, 1983]. This factors result in continuous change in beta spectrum as a function of penetration depth into a medium. Hence, beta dose delivered at any point is a strong function of the beta spectrum. It is important to note that all Sr-90 + Y-90 sources emit the same beta spectrum but different filter materials, filter thickness and applicator construction result in different beta spectra being emitted from applicators for each design [Gleckler *et al*., 1998]. For thickly encapsulated sources, the lower energy component from Sr-90 is nearly compressed [Reft *et al.*, 1990], that is there is always the possibility that the beta particles at the extreme low-energy end of the spectrum will be absorbed in the applicator window.

2.2.2 Gamma (γ)-rays

Gamma (γ)-rays are highly penetrating (more so than α- or β-particles) electromagnetic rays (photons) emitted from the nucleus of an atom. They are highly energetic photons emitted from a radioactive source with a variety of monoenergetic energies, ranging from a low value of 100 keV to as high as 3 MeV. This means that each gamma ray has a precise energy corresponding to the discrete energy transformation within the nucleus.

The energy of these rays is determined by the energy level structure of the particular radionuclide or the transition between the energy levels in the nucleus. Therefore, an emitted γ-ray is characteristic of that particular nucleus. Podgoršak (2006) found that in most α- and β- transformations the γ-rays are emitted by the daughter nucleus during de-excitation, and referred as if they were from the parent nucleus. Practically, it requires several centimetres of lead to reduce their intensity appreciably. γ-rays offer the most practical approach to external beam radiotherapy [IAEA, 2003].

2.2.3 X-rays

X-rays are electromagnetic radiation like γ-rays, but are produced during the interaction of incident beta-particles with atomic orbital electrons of a target nucleus or interaction with a target nucleus. This produces characteristic radiation and bremsstrahlung radiation, respectively. These types of radiation are discussed in more detail in sections 2.4.1 and 2.4.2, respectively.

As described in the literature [IAEA, 2003; Mosia, 2005], x-rays can be categorized in terms of their energy or clinical beams as follows:
Low-energy, “soft x-rays” or “Grenz rays”: 0.1 – 20 keV
Superficial x-rays: 10 keV – 100 keV
Diagnostic-range x-rays: 10 keV – 150 keV
Deep therapy or Orthovoltage x-rays: 100 keV – 500 keV
Intermediate x-rays: 300 keV – 1 MeV
Megavoltage x-rays: 1 MeV and above

X-rays are used mainly in diagnostic radiology for disease diagnosis, and in radiation therapy for disease treatment [IAEA, 2003].

2.3 Interaction of ionizing radiation with matter

When a photon beam travels through any material, it interacts with the atoms and atomic electrons of this material by transferring some or all of its energy to the material. These photon interactions with matter or the absorber can lead to biological, chemical or physical changes, depending on the material type and photon beam quality. The number of photons attenuated through matter depends on the number of incident photons, the type of material concerned and its density. The attenuation of photon beams follows an exponential relationship in a homogenous medium.

When considering a monoenergetic, narrow photon beam with N incident photons and the absorbing material of thickness Δx, with n photons that interact with the attenuator and are removed from the beam, then n is expressed by:

$$n = \mu N \Delta x \tag{2.5}$$

where proportionality constant μ, is called the linear attenuation coefficient with dimensions cm^{-1}, and defines the fraction of photons that interact per unit thickness of attenuator Δx. This coefficient depends on the photon and the nature of the material. Thus, this is the probability of whether or not particular photon will penetrate a given absorber.

By considering the change in the number of photons ΔN in the beam passing through material thickness Δx, the number of incident photons N is reduced by one for each interaction, $\Delta N = -n$.
Thus

$$\Delta N = -\mu N \Delta x \tag{2.6}$$

In order to determine the number of transmitted particles, equation 2.6 can be solved to

$$N = N_0 e^{-\mu x} \tag{2.7}$$

Equation 2.5 describes how incident photons N change as the beam passes through the attenuator, and equation 2.6 determines the number of interactions in the slab thickness bombarded by N incident photons.

Hence, the amount of attenuation depends on the number of atoms in any thickness of material, which is material density. The linear attenuation coefficient divided by the material density is referred to as the mass attenuation coefficient (μ/ρ) [Johns & Cunningham, 1983; Maboe, 2001].

Once a complicated series of processes has taken place, the average energy transferred ($\bar{E}_{tr}$) and the average energy absorbed ($\bar{E}_{ab}$) per interaction can be used to calculate the total energy transferred (ΔE_{tr}) and the total energy absorbed (ΔE_{ab}) in thickness Δx. These total energies are defined by Johns and Cunningham (1983) as follows:

$$\Delta E_{tr} = \overline{E}_{tr}\,\mu N \Delta x = \mu\left(\overline{E}_{tr} / h\upsilon\right) N h\upsilon \Delta x \tag{2.8}$$

$$\Delta E_{ab} = \overline{E}_{ab}\,\mu N \Delta x = \mu\left(\overline{E}_{ab} / h\upsilon\right) N h\upsilon \Delta x \tag{2.9}$$

where $Nh\nu$ is the energy carried by the beam, ratios ($\bar{E}_{tr}/h\nu$) and ($\bar{E}_{ab}/h\nu$) are energy transferred and energy absorbed, respectively and $\mu N\Delta x$ indicates the number of interactions occurring.

The dimensions of $\mu(\bar{E}_{tr}/h\nu)$ and $\mu(\bar{E}_{ab}/h\nu)$ are the same, and provide more fundamental coefficients called transfer (μ_{tr}) and absorption (μ_{ab}) coefficients which can also be used to find total energies transferred and absorbed respectively in equations 2.8 and 2.9. The coefficients (μ_{tr}) and (μ_{ab}) are used in radiation dosimetry, since μ explains only the local

removal of photons from a beam without directly providing a measure of the energy transferred to or absorbed around the removal site.

Other, more fundamental, attenuation coefficients are the electronic coefficient ($_e\mu$) and the atomic coefficient ($_a\mu$), defined by:

$$_e\mu = \frac{\mu A}{\rho N_A Z} \tag{2.10}$$

$$_a\mu = \frac{\mu A}{\rho N_A} \tag{2.11}$$

where (μ/ρ) is the mass coefficient which is more fundamental and independent of density. N_A is the Avogadro's number and ρ, Z and A are density, atomic number and atomic mass of attenuating material, respectively [Johns & Cunningham, 1983].

Since the mass, electronic and atomic coefficients are measured in terms of area per gram, area per electron and area per atom, the coefficients are often referred to as cross sections. The cross section can be defined as the ratio of probability of an interaction occurring from the photon beam incident on a slab of material containing a number of atoms per unit area.

2.3.1 Photon interactions

Photons are far more penetrating in matter than other known types of radiation. They have no specific depth range, and their interaction with matter is based only on cross sections. In matter, photons may undergo scattering (scatter) or may have no interaction with matter (transmission), or they may be completely absorbed (absorption) and disappear. Photons demonstrate five important types of interaction which will be dealt with in the following subsections. These interactions are the photoelectric effect, Compton Effect, Thompson scattering, coherent scattering and pair production.

2.3.1.1 Photoelectric Effect

The photoelectric effect process, also known as the photo effect, is an interaction that might take place between an incident photon beam and one of the tightly bound electrons of K, L, M or N atomic shells in matter. It occurs mostly in the K-shell, as illustrated in Figure 2.2.

During the process, the photon disappears and its energy is absorbed by the atomic electron. The requirement for the process to occur is that the incident photon energy ($h\nu$) must be greater but in the order of binding energy of the orbital electron. In addition, this $h\nu$ must be totally absorbed. The reason for this is that the electron must first absorb enough energy to overcome the binding energy (E_B) of its shell, and the remaining photon energy is then given to the electron in the form of kinetic energy (E_K). The electron is ejected and is now called a photo-electron, leaving the atom with kinetic energy of:

$$E_k = h\upsilon - E_B \tag{2.12}$$

An atom is left in an ionized state with vacancy created in the shell, thus the atom is left highly unstable. Very quickly, the vacancy will be filled by one of the outer shell L, M or N orbital electrons. During this transition, energy will be released as a photon (electromagnetic radiation), a process known as Characteristic radiation (Figure 2.2). This radiation is the binding energy difference between the two shells, with the exact specific characteristic value which is different for different elements. The energy of Characteristic radiation depends on the energy of photon and the atomic number Z of the material, and is found to be very low in biological absorbers.

The atom may also undergo a process known as the Auger effect, where the energy released during the filling of the vacancy, is absorbed by an orbital electron instead of being released from the atom. This excited and mono-energetic electron is then emitted from the atom. The emitted electron is called an Auger electron. Both Characteristic radiation and Auger electrons are emitted by all elements, but heavy elements are more

likely to emit radiation rays (Characteristic radiation), while light elements are more likely to emit electrons (Auger electrons).

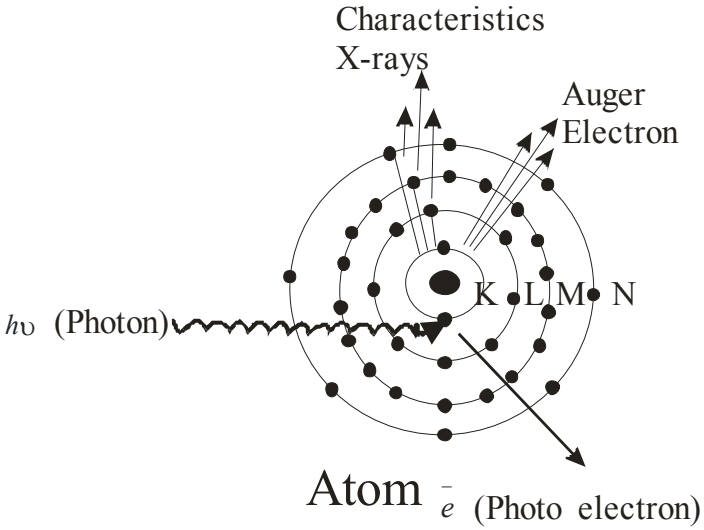

Figure 2.2: Illustration of Photoelectric Effect [Khan, 2003: 65].

The angular distribution of photo-electrons depends on incident photon energy: as the photon energy increases the photo-electrons are emitted in a more forward direction, although momentum and energy are conserved. The photo-electron is quickly brought to rest by surrounding atoms and delivers its energy to them in the process. A similar process occurs in Auger electrons.

The probability of the occurrence of the photoelectric interactions depends on photon energy (hv). Also the photoelectric attenuation depends strongly on the binding energy (E_B) of the atomic electrons (which is the atomic number Z of absorbing material). The photoelectric attenuation coefficient is zero when $hv << E_B$ and is inversely proportional to (hv). Hence, the following relationship between the mass photoelectric attenuation coefficient (τ/ρ), atomic number (Z) and incident photon energy (hv) holds true:

$$\tau/\rho \propto Z^3/h\upsilon^3 \tag{2.13}$$

Equation 2.13 applies to energies up to about 200 keV. At higher energies the term hv^3 approximates to hv^2 and eventually to hv [Donald, 1996; Khan, 2003; Johns & Cunningham, 1983].

2.3.1.2 Compton Effect

Compton scattering or effect is an incomplete absorption of a photon's energy or the scattering of photon radiation. It is also defined as incoherent scattering. This process involves the inelastic interaction of photons with free or loosely bound outer orbital shell electrons, as shown in Figure 2.3. This interaction is inelastic in that the photon energy is not conserved, although the total energy of the interaction is. By free electron it is meant that the electron has a much smaller binding energy fraction than the incident photon energy [ICRP 38, 1983]. Hence, the Compton Effect appears as a collision between a photon and a free electron [Cherry *et al.*, 2003; Johns & Cunningham, 1983].

In the process, some of the incident photon energy (hv_o) is absorbed while the scattered photon continues with a reduced energy. Then an emission of an electron (recoil or Compton electron) from the atom at recoil angle (Θ) occurs. This angle lies between the incident photon direction and the direction of the recoil electron. Thus, energy of the incident photon is shared between the scattered photon and the Compton electron. The sharing of energy depends on the scattering angle (ϕ) and the energy of the incident photon (hv_o) relative to the energy equivalent of the rest mass of the electron (m_0c^2) [Young, 1983].

The energy of the scattered photon (hv') is related to the angle of deflection (ϕ), and by applying the laws of conservation of momentum and energy, as expressed in Figure 2.3, the following relationships can be derived:

$$E = h\upsilon_0 \frac{\alpha(1-\cos\phi)}{1+\alpha(1-\cos\phi)} \tag{2.14}$$

and

$$h\upsilon' = h\upsilon_0 \frac{1}{1+\alpha(1-\cos\phi)} \tag{2.15}$$

where ϕ is the scattering angle at which the photon scatters, which lies between the incident photon direction and the scattered photon direction. *E* is the energy of a recoil or Compton electron, which may also be expressed by:

$$E = h\upsilon_0 - h\upsilon' \tag{2.16}$$

and $\alpha = \frac{h\upsilon_0}{m_0 c^2}$, and $m_0 c^2$ is the rest mass of the electron.

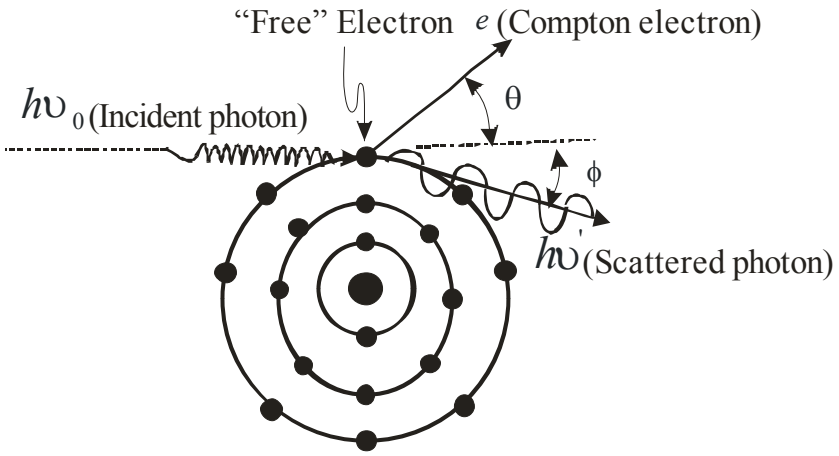

Figure 2.3: Diagram illustrating the Compton Effect [Khan, 2003: 67].

The scattering angle (ϕ) depends greatly on the amount of energy received by the scattered photon. For each collision the amount of the energy transferred to both recoil electron and scattered photon, depends on the energy of the incident photon and scattering angle. For a high energy incident photon the Compton electron acquires most of the energy, and the scattered photon will carry away only small fraction of energy. So, most of the energy is deposited in forward direction. For low energy incident photon very little energy is transferred to the recoil electron, and most is entirely scattered. So, the probability of photon being scattered forward and being scattered backward are almost equal, depending on the amount of incident photon energy. Thus, as energy of incident

photon increases the greater the energy of scattered photons at all scattering angles [Johns & Cunningham, 1983; Khan, 2003; Selman, 1976].

The scattering angle determines the decrease in energy of the scattered photon, thus the amount of energy ejected by the scattering photon depends only on the scattering angle. The greater the scattering angle the lower the energy of the photon will be scattered. Therefore, the lowest energy scattered photons occurs at 180 degrees, which occurs as a back-scatter radiation photons [Johns & Cunningham, 1983; Khan, 2003; Selman, 1976].

If the photon makes a direct hit:
The electron will travel straight forward and the photon will be scattered straight back. During this process the electron receives maximum energy compared to the scattered photon.

If the photon makes a grazing hit:
The electron will emerge nearly at right angles and the scattered photon will move almost straight forward. During this process the electron receives almost no energy and the scattered photon has essentially the full energy of the incident photon.

The Compton Effect depends strongly on incident photon energy and is independent of density, atomic number or any other property of the absorbing material. Hence, it follows that the Compton mass attenuation coefficient (σ/ρ) is independent of atomic number and depends only on the total number of electrons in absorbing material. In turn the Compton mass attenuation coefficient depends on material density and on the number of electrons per gram [Khan, 2003; Selman, 1976]. The mass attenuation coefficient (σ/ρ) is thus a measure of the total energy removed from the primary beam.

2.3.1.3 Thompson Scattering (Classical scattering)

This process is easily explained by classical electromagnetic theory, which states that when an electromagnetic wave passes near a free electron, the electron is sent into

vibration and accelerated by the electrical field of the wave. The electron will then radiate an electromagnetic wave of the same wavelength λ, and this wave will form the scattered radiation. According to Young (1983), the intensity of the radiation which is scattered at an angle θ to the direction of the incident radiation at a distance (*r*) from an electron of charge *e* and mass *m* is expressed as:

$$\frac{I}{2r^2}k^2(1+\cos^2\theta) \tag{2.17}$$

where *I* denotes the incident intensity and *k* is a constant.

If the fraction of the incident energy scattered by an electron into a solid angle $d\Omega = 1/r^2$ at an angle θ is denoted by $d\sigma_e$, then it follows that:

$$\frac{d\sigma_e}{d\Omega} = \frac{k^2}{2}(1+\cos^2\theta) \tag{2.18}$$

where $(d\sigma_e/d\Omega)$, is called the differential electronic cross section for classical scattering. This can be defined as a classical scattering coefficient per electron and per unit solid angle. The later is the function that allows the correct amount to be scattered for zero energy photons. During this process, no energy is transferred to the electron, since the frequency as well as the wavelength of the scattered radiation is the same as that of the incident radiation.

Since $d\Omega = 2\pi \sin\theta d\theta$ between cone of θ and θ + dθ, equation 2.18 becomes:

$$\frac{d\sigma_e}{d\theta} = \frac{k^2}{2}(1+\cos^2\theta)2\pi\sin\theta \tag{2.19}$$

By integrating equation 2.19 over all values of θ, that is, from zero to 180 degrees, the total cross section σ_e, defined as the Thomson classical scattering coefficient for free electrons, can be obtained [ICRP 38, 1983; Johns & Cunningham, 1983] as:

$$d\sigma_e = \frac{8}{3}\pi k = 66.525 \times 10^{-30} m^2 \tag{2.20}$$

This process occurs when the binding energy of the electrons is high which means that the atomic number of the scattering material is high, while the quantum energy of the incident photon is relatively low.

2.3.1.4 Coherent Scattering (Rayleigh scattering)

Coherent scattering, also known as classical scattering, Rayleigh scattering or elastic scattering, is a process that occurs between a photon and an atom as a whole. This process is an extension of the Thomson scattering theory. In this case, an electromagnetic wave of wavelength λ passes over the atom, with energy less than that of atomic electron binding energy. The electromagnetic wave has an oscillating electrical field associated with it, and this sends the atomic electrons into momentary vibration or oscillation. But this is not enough to put them into an excited or ionized state. These oscillating electrons emit radiation of the same wavelength λ as the incident photon beam (Figure 2.4).

The electrons return to their previous energy level by the emission of a photon that is equal in energy to the incoming photon but which is moving in a different direction. The scattered waves from the electrons within the atom combine to form a scattered wave, moving predominantly in a forward direction. The atom is left in the same energy state after the scattered photon departs in a direction different from that of the incident photon. That is, no energy is converted into kinetic energy or absorbed in the medium: all energy is scattered over a small angle. The scattering is a cooperative phenomenon and is thus referred to as coherent scattering [Johns & Cunningham, 1983].

The probability of coherent scattering occurring depends on the incident photon energy ($h\nu$) and the atomic number (Z) of the material. The cross section of coherent scattering decreases rapidly with the increase in photon energy, and is negligibly small for energies greater than about 100 keV in low atomic number materials. Hence the following relationship applies:

$$\frac{\sigma_{coh}}{\rho} \propto \frac{Z^2}{h\upsilon} \tag{2.21}$$

where (σ_{coh}/ρ) is the mass attenuation coefficient or cross section resulting from elastic scattering. Elastic scattering may occur as a result of a photon interacting with the nucleus of an atom of the attenuator. But the effect is even less, and so may safely be ignored in medical radiography or imaging. This process has an effect in slightly broadening the angular width of the beam [Donald, 1996; Johns & Cunningham, 1983]. From equation 2.21 it is clear that coherent scattering occurs mainly at low energies (about 50 keV) for larger atomic number values.

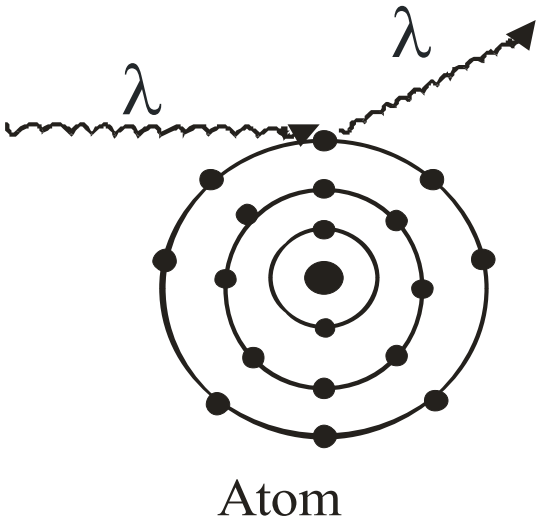

Figure 2.4: Diagram illustrating the process of coherent scattering. The scattered photon has the same wavelength as the incident photon. No energy is transferred [Khan, 2003: 65].

2.4 Electron (β-particles) interactions

All radiation particles or ionizing radiations (α-particles, β-particles, γ-rays and x-rays) interact differently with matter or tissue, since they have different characters. As a high energetic particle such as a β-particle transverses matter, it interacts with matter through coulomb interactions with atomic orbital electrons and atomic nuclei. Through these collisions, these β-particles may lose their kinetic energy (collision and radiative losses) or change their direction of travel (scattering) [IAEA, 2003], slowing down as they pass through matter as a result of these collisions with atoms and molecules. High energy electrons, which are also charged particles, are a by-product of these collisions. The energy losses occurring in a charged particle in ionization and excitation events are called collision losses, whereas those occurring in nuclear encounters resulting in bremsstrahlung production are called radiation losses.

The parameters used to describe the gradual loss of energy of a charged particle as it penetrates an absorbing medium are called stopping powers. Such parameters may be collisional (ionization) or radiative stopping powers. These parameters play an important role in radiation dosimetry, and are dependent on properties of the charged particle such as mass, charge, velocity and energy as well as on the absorbing medium's properties, such as density and atomic number [Podgoršak, 2006].

Energy losses are described in terms of stopping powers while scattering is described in terms of scattering powers [IAEA, 2003]. When attenuation is focused on the absorbing medium, we are interested in the linear rate of energy absorption (LET) by the absorbing medium as the ionizing particle transverses the medium a distance dl .

It is important to show the specific point at which the energy is absorbed. The energy transfer from the charged particle to matter in each individual atomic interaction is generally small, and the particle undergoes a large number of interactions before its kinetic energy is spent. Figure 2.6 indicates the initial point of interaction occurring at (A), where the photon of energy $h\upsilon$ is scattered with reduced energy as $h\upsilon'$. The kinetic

energy gained by the electron may be lost through the following processes, some of which are illustrated in (B):

i) Bremsstrahlung (inelastic collision as the electron nears the nucleus)
ii) Ionization and excitation (inelastic collision with atomic electrons)
iii) Elastic collision in which the electron may lose a maximum of half its original energy
iv) Violent electron-electron interaction causing delta ray.

As a result of the abovementioned processes, electron tracks are tortuous and their exact shape and length are unpredictable.

A given kinetic energy electron travels at a much higher speed than a heavy particle with similar energy. Such an electron thus spends a briefer time in the vicinity of an atom than a heavier particle and is therefore less likely to interact with the atom. Such an electron also carries only one unit of electrical charge, and thus exerts weaker forces on orbital electrons. These electrons experience less frequent interactions than heavy particles and lose their energy more slowly than heavy particles. Electrons are much less densely ionizing and travel further before they are stopped, unlike heavy particles of similar energy [Cherry *et al.*, 2003].

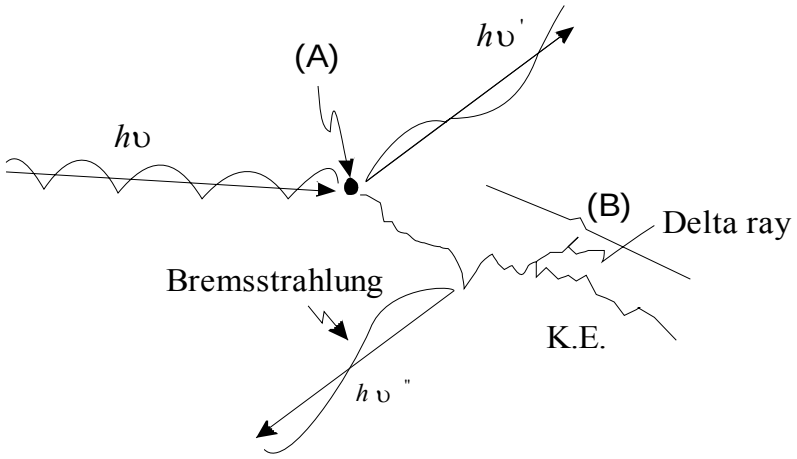

Figure 2.5: Schematic representation of the transfer of energy from a photon (hν) to the medium [Johns & Cunningham, 1983: 218].

Figure 2.5 above indicates that the transfer of energy from a photon beam to the medium takes place in two stages. The first stage (A) involves the interaction of the photon with the atom, causing an electron or electrons to be set in motion. The second stage (B) involves transfer of energy from the high energy electron to the medium through excitation and ionization [Johns & Cunningham, 1983].

2.4.1 Collisional interaction

The collision that occurs between a charged β-particle and atoms involves electric forces of attraction or repulsion, rather than actual mechanical contact [Cherry *et al.*, 2003]. In close encounters, the strength of coulomb forces may be sufficient to cause orbital electrons to separate from the atom during the interaction of β-particle with atom, thus causing ionization. The ionization interaction appears as a collision between the β-particle and an orbital electron, and the β-particle loses energy in the process. Part of this energy is used to overcome the binding energy of the electron from the atom, and what remains is given to the ejected secondary electron as kinetic energy. Thus ionization involves the ejection of an individual electron to a higher energy orbital after gaining energy from a β-particle.

The ejected electron may be sufficiently energetic to cause secondary ionizations on its own. Such an ejected secondary electron is called a delta (δ) ray, and occasionally causes longer side tracks when it is energetic enough [Cherry *et al.*, 2003; Klevenhagen, 1993]. The effects of the δ-ray are accounted for by using the energy limit Δ, below which the energy transfer is considered dissipative. Ionization involving an inner shell electron eventually leads to the emission of characteristic x-ray or Auger electrons, as described in the photoelectric effect process. However, these effects are generally small, since most ionization interactions involve outer shell electrons.

If the energy lost by the incident β-particle is not enough to eject an electron from the atom, it is used to raise the electron to a higher level by the process known as excitation, thus causing atomic or molecular excitation. These interactions result in smaller energy

losses than in ionization events. The energy transferred to an atom in an excitation interaction is dissipated in molecular vibrations, atomic emissions of infrared, visible, ultraviolet light, and so forth.

The inelastic collisions responsible for energy deposition locally in the irradiated medium result in excitation or ionization of an atom. The probability of their occurrence depends on the energy of the passing electron, the distance of closest approach and the atomic number Z of the medium [Klevenhagen, 1993].

2.4.2 Radiative interaction

Radiative interaction occurs when the high speed β-particle penetrates the orbital electron cloud of an atom, and interacts with its nucleus. The particle is rapidly decelerated and may be deflected from its original path, and through the process it loses energy. The energy appears as a photon of electromagnetic radiation, called bremsstrahlung (braking radiation). The energy of the bremsstrahlung photon can range anywhere from nearly zero (events in which the particle is only slightly deflected) to a maximum equal to the full energy of the incident particle. Bremsstrahlung depends on the atomic number of an absorber and the energy of the beta-particle. These photons are governed by the Larmor relationship [IAEA, 2003], which is expressed by:

$$P = \frac{q^2 a^2}{6\pi\varepsilon_0 c^3} \tag{2.23}$$

where P is the power in the emitted photon, q is the electronic charge, a the acceleration of the β-particle, ε_0 the permittivity of free space and c the speed of light in free space.

Radiation losses through bremsstrahlung increase with increasing β-particle energy, and with increasing atomic number Z of the absorbing medium. Hence, low atom number materials like plastic and aluminium are more efficient as protective shields for beta-particle emitters like Sr-90 + Y-90 sources. This is because they are poor bremsstrahlung radiation emitters and at the same time, they are good absorbers of beta particles [Selman,

1976]. This type of energy loss is characterized by radiative stopping power [Cherry *et al.*, 2003; IAEA, 2003]. An approximation of percentage radiation losses for beta-particles having maximum energy $E_\beta^{\max}$ (MeV) is:

$$\text{Percentage radiation losses} \approx \left({ZE_\beta^{\max}}/{3000} \right) \times 100\% \tag{2.24}$$

where Z is the atomic number of the absorbing material. This approximation is accurate to within about 30% [Cherry *et al.*, 2003].

The total kinetic energy KE loss by the beta-particle per unit length x can be described as the total mass stopping power given by combination of collisional and radiative interactions as follows:

$$\left({S}/{\rho} \right)_{tot} = \frac{1}{\rho}\frac{d(KE)}{dx} = \left({S}/{\rho} \right)_{col} + \left({S}/{\rho} \right)_{rad} \tag{2.25}$$

where $(S/\rho)_{col}$ is the mass collision stopping power resulting from β-particle and orbital electron interactions (atomic excitation and ionizations) and $(S/\rho)_{rad}$ is the mass radiative stopping power resulting from β-particle and nucleus interactions (bremsstrahlung).

2.4.3 Continuous Slowing Down Range (CSD range)

As a beam of beta particles passes through matter, the interactions cause the particles to slow down and change direction. Eventually, particles will lose all their kinetic energy and come to rest. There will be a finite distance beyond which there will be no particles, and this distance is called the particle range. This gradual and continuous loss of kinetic energy is often referred to, as the continuous slowing down approximation (CSDA).

The CSDA is used to obtain the actual range covered by the particle, taking into consideration the variation of the total mass stopping power with respect to the energy.

The distance covered by the electron during its energy drops in the intervals, is calculated by adding up all the increments of the length to get the actual range [Johns & Cunningham, 1983; Klevenhagen, 1993]. Thus, the CSDA range is a measure of total path length traveled in the course of slowing down, representing the mean path length and not the depth of penetration in a defined direction. The path of a β-particle is tortuous or zigzag with a much more devious track, because the charge and small mass may easily be deflected (scattering effects) from a straight line path. This deviation will lead to variations in actual penetration of β-particles into the absorbing medium, depending on the initial energy of the β-particles. Thus, β-particles do not have a well-defined range [Young, 1983].

In CSDA, energy loss fluctuations are neglected, and the beta-particle is assumed to lose energy along its track according to the mean energy loss per unit path length given by the stopping power. That is, inelastic energy losses by beta-particles moving through a medium with density ρ are described by the total mass energy stopping power $(S/\rho)_{tot}$ (in $MeV.cm^2/g$). Stopping power defines the effect of material in beta dosimetry [Klevenhagen, 1993].

Hence, the CSDA range or mean path-length for a β-particle of initial kinetic energy E_0 can also be found by integrating the reciprocal of the total stopping power:

$$R_{csda} = \int_0^{E_0} \left(\frac{S(E)}{\rho} \right)_{tot}^{-1} dE \qquad (2.26)$$

where R_{csda} is the range of the β-particle with initial energy of E_0 and $(S(E)/\rho)_{tot}^{-1}$ is the total mass stopping power with respect to energy, specifically total unrestricted mass stopping power. In the restricted collision stopping power it is generally accepted that β-particles lose their energy in a large number of interactions with small energy losses. Thus, during CSDA the energy transferred to the medium may be assumed to be absorbed locally, in a small volume, close to the point of interaction [Klevenhagen, 1993].

2.4.4 Mass Scattering Power

Collisions that occur between β-particles themselves, between β-particles and electrons or between β-particles and a nucleus not only contribute to the energy absorbed but also increase the scatter of a beam of β-particles. The energy loss and change of direction by the β-particle as it passes through a medium are described respectively by the stopping and scattering power ratios.

The scattering angle depends on the atomic number Z of the medium, as well as on the cross section of radiation loss of the β-particles. The mean square angle of scattering related to the mass of scattering material is recommended for characterizing the "angular scattering power" of a given medium. Multiple scattering of β-particles as they traverse, a path length (l) of an absorbing medium is commonly described by the mean square angle of scattering ($\overline{\theta^2}$) which is proportional to the mass thickness (ρl) of the absorber.

The mass scattering power (T/ρ) expresses the increase in the mean square angle of scattering ($d\overline{\theta^2}$) per unit mass thickness (ρl), and can be defined as follows [IAEA, 2003; Klevenhagen, 1993]:

$$\frac{T}{\rho} = \frac{1}{\rho}\frac{d\overline{\theta^2}}{dl} = \frac{\overline{\theta^2}}{\rho l} \tag{2.27}$$

This equation emphasizes that the scattering power is analogous to stopping power in a given medium [Klevenhagen, 1993]. Khan (2003) observed that scattering power varies approximately as the square of the atomic number (Z) of the absorbing medium and inversely as the square of the kinetic energy (KE) of the incident electron (β-particle).

$$\frac{T}{\rho} \propto \frac{Z^2}{KE^2{}_{e^-}} \tag{2.28}$$

2.4.5 Dosimetric quantities

There are two chief considerations in dosimetry: to describe a radiation beam itself and to describe the amount of energy it may deposit in the medium. In this subsection the description of the amount of energy deposited in the medium and the relationship between quantities will be considered. In general, dosimetric quantities are used to describe photon beams and charged particle beams.

Figure 2.6 in section 2.4 is useful in defining important dosimetric quantities, such as KERMA (K) and absorbed dose (D). The quantity KERMA (K) was introduced by the International Commission on Radiation Units and Measurements (ICRU) in 1980, to describe the initial interaction at (A) in Figure 2.6 [Johns & Cunningham, 1983: 218]. It is an acronym for Kinetic Energy Released in the Medium per unit mass. The "A" has been added for phonetic reasons and K is defined as the quotient of $d\overline{E_{tr}}$ by dm, where $d\overline{E_{tr}}$ is the sum of the initial kinetic energies of all the charged ionizing particles (electrons and positrons) liberated by uncharged particles in a material of mass dm :

$$K = \frac{d\overline{E_{tr}}}{dm}\left[\frac{energy}{mass}\right]\left(J/Kg\right) \tag{2.29}$$

KERMA (K) quantifies the average amount of energy transferred from indirectly ionizing radiation to directly ionizing radiation. When the absorbing medium is air the term used is air KERMA.

A major portion of the initial kinetic energy of electrons in low atomic number materials (e.g. air, water, soft tissue) is expended by inelastic collision (ionization and excitation) with atomic electrons. Only a small part of this energy is expended in radiative collisions with atomic nuclei (bremsstrahlung). Hence, KERMA can be divided into two parts [Khan, 2003:107]:

$$\mathrm{K} = \mathrm{K}^{\mathrm{col}} + \mathrm{K}^{\mathrm{rad}} \tag{2.30}$$

where K^{col} and K^{rad} are the collision and radiation parts of KERMA, respectively.

In all forms of ionizing radiation the biological impact is evaluated by introducing the absorbed dose. The absorbed dose (D) is the measure of energy absorbed or deposited in the medium by a radiation beam per unit mass of absorbing material. Absorbed dose is defined [Johns & Cunningham, 1983; Young, 1983] as the quotient $d\bar{E}_{abs}$ by *dm*, where $d\bar{E}_{abs}$ is the average energy of all ions released or lost at the point in the medium of mass *dm*:

$$D = \frac{d\overline{E}_{abs}}{dm}\left[\frac{energy}{mass}\right]\left(J/Kg\right) \tag{2.31}$$

Johns and Cunningham (1983) found that KERMA and absorbed dose do not take place in the same location, but can be related when there is charged particle equilibrium (CPE) between the two. The charged equilibrium exists only at the point where the fluence of the charged particles in the area of that point is constant. In special cases where such equilibrium occurs, absorbed dose is given by:

$$D = \Phi\left(\frac{\mu}{\rho}\right)\overline{E}_{abs} = K\left(1-g\right) \tag{2.32}$$

where Φ is the photon fluence and (μ/ρ) is the mass attenuation for the medium and *g* is the average fraction of an electron energy lost through radiative processes. Both absorbed dose and KERMA have the SI unit known as Gray (Gy).

2.5 Surface dose rate

One of the objectives of this study is to use the MCNP5 code to determine the dose distribution, that is, to quantify the dose rate at the surface of the applicator and also at some depth in an object such as the lens of the eye during the treatment. Therefore, to

evaluate the dose to the lens, the limiting tissue is lens. It does not receive a blood supply and has no biological mechanism, and so is defenseless against radiation. In practice it is difficult to estimate lens dose accurately as there are many factors affecting dose rate. These include variability in applicator placement, exposure variability, inconsistent eye applicator characterization and calibration, insufficient observation follow-up times after treatment and uncertainties in spatial distribution of the dose through the eye [Gleckler *et al.*, 1998].

The surface dose rate of the applicator is used to determine radiation dose to the affected area. The absorbed dose rates to water at the surface of the source are determined as the average of the dose rate across the central area of the source surface [Soares, 1992]. The surface dose rates for ophthalmic applicators are used mainly to determine the lens and sclera dose but also to specify the comparative means of the effectiveness of the applicator and applicator characteristics [Gleckler *et al.*, 1998].

The term "surface dose" implies a quantity determined extremely close to the skin surface. This term has, however, been found to be misleading as determination of such a quantity is virtually impossible. Therefore, the definition of the surface dose or the entrance dose should be related to the depth at which the radiation sensitive layer begins, which is 0.1 mm to 0.15 mm beneath the epidermis. Recently, it has become common to define the surface dose at 0.5 mm depth [Klevenhagen, 1993]. According to Gleckler *et al*. (1998), the surface dose rate is defined by the National Institute of Standards (NIST) as the dose rate to an infinitesimal layer of water at the exact surface of the applicator. Surface dose rates are therefore defined for the active area of an applicator, where the active area is defined as the area on the surface of the applicator in which the dose rate is at least 50% of the maximum dose rate. Thus, in order to determine the active area, the dose rate distribution across the surface of the applicator must be established.

The surface dose rate depends on the following factors: applicator design and construction such as source-binding method, source thickness, and encapsulation material thickness. The critical dimensions of the eye affect the distance and the location of the

lens relative to applicator which normally ranges from 2 mm to 3 mm. The placement of the applicator at a certain angle relative to the eye and the pressure being applied can also affect the dose rate [Gleckler *et al.*, 1998; ICRU 72, 2004]. In other words, to quantify the beta dose rate near the surface of the applicator is difficult and it becomes significantly more complex to quantify the resulting beta dose at some depth in an object such as the lens of the eye.

Although surface dose rate has no true physical meaning since it is defined on a per mass basis, there is a mathematical method which uses the extrapolation of measured values to find the theoretical values. In this way, the surface dose rate has the advantage of estimating the dose delivered to the sclera during treatment, although there is variability in calculated surface dose rate because of the rapid attenuation of beta-particles [Gleckler *et al.*, 1998]. Owing to the complexity of beta-ray absorption and scattering, it is not possible to calculate the dose rate reliably [ICRP 38, 1983]. The dose to the lens is estimated by extrapolating the surface dose rate to the lens. To estimate the lens dose due to beta irradiation, the curve of dose against the depth has been developed [Gleckler *et al.*, 1998].

The dose to be delivered at any point to an individual patient is calculated with the knowledge of the absorbed dose, which would be delivered by the same beam at some convenient reference point under specified conditions [Young, 1983]. According to the literature [Gleckler *et al.*, 1998; Young, 1983], with the knowledge of the surface dose rate, and how the dose rate varies with distance from the source and duration of irradiation, the dose to the sclera can be estimated. The sclera irradiation after pterygium removal relies heavily on the knowledge of the surface dose rate in order to prevent complications and to make easy the comparison of patients in follow-up studies. In practice, what is of concern is the surface dose rate at the centre of the applicator [Selman, 1976].

The accurate determination of absorbed dose rate of both planar and concave sources at the recommended reference distance of 1 mm from the centre of the source requires careful measurement [IAEA, 2002], usually several measurements at a few distances from the zero distance at which the detector is in contact with source surface or as close

as possible. Measurement should include a point at which the effective point of measurement is at reference distance or close to it. The absorbed dose rate at the reference distance should be determined from the measurement results, either directly or by accurate interpolation of values close to the reference point [ICRU 72, 2004].

Dose rates may be expressed as Gy/s, mGy/m, etc., but are more often expressed as μGy/h or cGy/s [James, 2006]. According to Johns and Cunningham (1983), Strontium eye applicators give an absorbed dose rate of about 1 Gy/min at the surface. The dose rate at the centre of an applicator surface may be as high as 100 cGy/s. The dose rate towards the surface of applicator decreases to about 50% at a depth of 1 mm in tissue and becomes 5% of surface dose rate at a depth of 4 mm. With a new source, a dose of 1000cGy (rad) may be administered over approximately 20 seconds [Kirwan *et al*., 2003].

A dose prescription at a greater distance on the source surface, preferably measured with detector integrating over the extent of the tumour, would seem more representative for radio-therapeutic treatment [Davelaar *et al.*, 1992].

2.6 Extrapolation Ionization Chamber (Ext IC)

The Extrapolation Ionization Chamber (Ext IC) is a device capable of providing a reading which is a measure of the average absorbed dose deposited in its sensitive volume by ionizing radiation. The extrapolation chamber is designed according to BGC theory.

This device is used mainly as a primary standard for determination of absorbed dose rate of the beta-ray sources and to measure patient doses in radiotherapy. NIST also uses it for calibration of sealed beta sources [IAEA, 2002; James, 2006; Pearce *et al.*, 2006; Soares *et al.*, 2001]. The extrapolation chamber can be used for all types of beta-ray sources, with the exception of concave sources due to the source geometry. When used with applicator, the air gap between the surface of the applicator and the extrapolation chamber's front face should be kept to about 0.2 mm or less. As a result, the

extrapolation chamber can only be used for calibration of those applicators with flat or slightly convex surfaces [IAEA, 2002; ICRU 72, 2004; Maage, 2002].

The requirements of the chamber are that it must have small air volumes such that does not disturb the particle flux, that satisfy the BGC theory and also satisfy the requirements described in the code of practice [Oliveira & Caldas, 2005; Soares *et al.*, 2001]. That is, the applicator must be placed in contact with the thin entrance foil of the extrapolation chamber in order to take absorbed dose-rate measurements. The extrapolation chamber requires no radiation calibration as it is absolute.

The determination of the geometrical properties of a chamber, in particular the effective area (sensitive volume) of the collecting electrode, is a major limitation in the absolute accuracy of the measurements [Soares *et al.*, 2001]. Chamber construction should be as homogenous and water equivalent as possible, so that both mass stopping powers and linear scattering powers are similar to those of water. The walls should be made of a material with water-like properties, and the air cavity must be vented to allow rapid equilibrium with the ambient pressure [Pearce *et al.*, 2006].

The beta dose rate is correctly measured by a thin window chamber, because it responds to actual energy deposited. The electrical signal produced is directly proportional to the energy deposited in the chamber gas [James, 2006]. The measured current as a function of distance between the electrodes, is then fitted to the slope of the graph to a limit of zero air gap [IAEA, 2002; Muench *et al.*, 1991; Oliveira & Caldas, 2005]. Through this extrapolation method, the absorbed dose rate at the applicator surface can be determined [Oliveira & Caldas, 2005].

The absorbed dose measurement is based on ionization and then followed by correction factors, such as temperature and pressure, which must always take place in the charged particle equilibrium (CPE) region, according to BGC theory [Maage, 2002]. The calculation of absorbed dose rate in water (as a reference material) from extrapolation chamber is obtained by following the BGC theory as follows:

$$\dot{D}_w = \frac{\left(\overline{W}/e\right)}{\rho_o a}.\overline{S}_{Air}^{Water}.B.U.\left(\Delta I/\Delta\lambda\right)_{\lambda\to 0} k_{back} \qquad (2.38)$$

where:

1. $\overline{S}_{Air}^{Water}$ is the ratio of the mean mass collision stopping power of water to that of air (taken as 1.12, can change up to 1.13) [IAEA, 2002; ICRU 56, 1997; Soares, 1995],
2. ρ_o is the density of air at the reference temperature (1.197 kg/m^3) [IAEA, 2002],
3. a is the effective ionization collecting area of electrode (m^2); this parameter is taken as the area corresponding to the radius of the collecting electrode plus one-half of the thickness of the insulating gap between the electrode and guard ring for electrodes which are smaller than the active area of the radiation or ionization source [IAEA, 2002; NCS 14, 2004],
4. $\left(\Delta I/\Delta\lambda\right)_{\lambda\to 0}$ is the rate of change of corrected current (normalized to reference temperature 22^{0}C and pressure 101.3 kPa of air) with extrapolation chamber air gap thickness as thickness approaches zero [IAEA, 2002; Oliveira & Caldas, 2005],
5. k_{back} is the correction factor that accounts for the difference in backscatter from the collecting electrode compared to that of water [IAEA, 2002; Oliveira & Caldas, 2005],
6. B is a correction for reduced backscatter from the graphite-collecting electrode relative to that of water (taken to be 1.005) [Soares *et al.*, 2001],
7. U is the correction for attenuation by the high voltage electrode (measured as 1.003) [Maage, 2002].

Since the ophthalmic applicator is used in contact with the patient's eye, the soft tissue dose rate at the external applicator surface can be determined when the applicator is placed in contact with the extrapolation chamber window. The extrapolation chamber is

discussed further in literature [IAEA, 2003; ICRU 56, 1997; ICRU 72, 2004; Pruitt *et al.*, 1988].

2.7 Theoretical calculation of dose distribution around a point source

Problems in determining the absorbed dose around localized beta-particle sources in tissue can be separated into two steps: firstly, determination of the absorbed dose distribution around a point source; and secondly, the dose distribution in and around a localized beta-particle source is calculated by a suitable summation of the elementary point source distribution [ICRP 38, 1983]. Direct measurement of the dose distribution in tissue around sources of β-emitting radionuclides raises difficulties as a result of the sharp dose gradient and the limited range of the β-particles. These difficulties can be approached in two ways in practice:

i. First, the function representing the dose distribution in tissue (water) around a "point source" of a β-emitting radionuclide – sometimes called "point kernel", must be determined.
ii. Secondly, the dose distribution around a β-particle source of a given shape and given dimensions can be computed, by integrating the point kernel over the whole volume of the source. This approach requires the point kernel to be accurate and presented in a mathematical form suitable for integration [Cross *et al.*, 2001; Vynckier & Wambersie, 1982].

Measurement of the dose distribution around a β-emitter point source, in tissue, is rather complicated for the following practical reasons:

i. Measurements can only be performed on extended plane sources using the extrapolation chambers [Vynckier & Wambersie, 1982].
ii. Measurements must be performed in a homogenous medium, with large source dimensions compared to the chamber diameter, or *vice versa*.

iii. Direct measurement of the dose around a point source of a β-emitting radionuclide can be performed in air where the isodose surfaces are sufficiently extended to allow for detectors of reasonable size.
iv. Measurements must be made in free air and scattering by other objects should be negligible.

The determination of dose distribution from the beta-ray ophthalmic applicator is particularly difficult because of the high dose gradients over the distances compared with the dimensions of the detectors [Cross *et al.*, 2001]. Another approach to estimate the β dose is to find the dose distribution for a point source, and then numerically integrate the point source over the actual radiating body. The calculation of the eye applicator doses made by integrating a point-source dose function or point kernel over the source make case-specific dose planning quick and efficient, and are much faster, provided that a software program is available and that it is easy for the user to learn. But in many circumstances the calculations may be considerably less accurate [Cross *et al.*, 2001; Hokkanen *et al.,* 1997].

Such a computer program for approximating dose distributions of differently sized, curved beta-ray eye applicators by theoretical calculations have been developed. Previously, only dose distributions around point or plane sources had been calculated. The present program runs on a microcomputer and was written using commercial software [Hokkanen *et al.*, 1997].

When comparing water and air, absorption and scattering of electrons is to a large extent dependent on atomic number (*Z*). Thus, when dose distributions in tissue are derived from dose distributions in air, corrections must be applied to take account of the differences in medium compositions and density. Besides experimental determinations, point kernels can be obtained from theoretical calculations [Cross *et al.*, 2001; Vynckier & Wambersie, 1982]. The analytical and numerical methods based on beta-ray point-source dose functions (point kernels) can be used to determine dose distributions. These methods are fast and easy to apply. However, they are valid strictly in a homogenous

medium of uniform density. The issues of air gaps, exit windows, backscatter from the applicator, or source encapsulation, all of which can introduce errors especially at clinical level applications, are not taken into account [ICRU 72, 2004].

The point source dose distribution can be estimated experimentally using a source of finite but small dimensions. From a distance such a source behaves like a point. Combining the experimental results with theory, a mathematical point source function, simple enough for numerical integration, can be found [Hokkanen *et al.,* 1997]. Beta-particle dose functions of a point source must be satisfactory and be simple enough for calculation purposes, while at the same time representing the dose distribution with reasonable accuracy over a wide range of energies and distances [ICRP 38, 1983].

2.8 Dose distribution

According to international recommendations [IAEA, 2002; ICRU 72, 2004], the quantity for the specification of the Sr-90 + Y-90 applicator (beta-ray source) is the reference absorbed dose rate in water at the reference distance from the source. The reference distance for planar and concave sources is 1 mm from the centre of the source. Measurements are difficult at this small distance, hence the distance is chosen from the point of the lowest penetration of the beta rays and the relevance to clinical application.

The principal difficulties in determining beta-ray doses and their significance are caused by:

a) Larger variation of dose over short distances.
b) The need to measure doses in a very thin layer, such as that of basal cells in the skin or TLDs in practical aspects. In order to simulate such volumes, a detector must be extremely thin with consequent reduction in sensitivity.
c) The strong scatter of beta radiation in air, which changes the energy and angular characteristics of the beta-ray beam with varying distance from the source [ICRU 56, 1997].

The conditions required for dose distribution calculation [ICRU 38, 1983] are:

i) The source activity must be uniformly distributed in material of known dimensions and density near unity,
ii) The applicator must be placed in or on tissue without appreciable air gaps and covered with enough material to produce complete scatter.

Beta dose distributions in tissue, where the beta-particles come from a small radioactive source, are difficult to determine experimentally because of the steep dose gradient and the short range of the electrons [Hokkanen *et al.,* 1997]. The actual dose distributions, especially in eye treatment, are influenced mainly by treatment geometry, individual source and how much Sr-90 is in the particular emitter, possible air gaps, different density of lens and other tissues, etc. [ICRU 72, 2004; Kirwan *et al.*, 2003]. The absorbed dose rate in tissue may be set as equal to the absorbed dose rate in water, so any soft tissue may be considered comparable to water [Friedell *et al.*, 1950; Pruitt *et al.*, 1988]. The ICRU report 72 (2004) shows the depth dose distribution results (Table 6.1) in water as well as the water spheres that simulate the eye. These were calculated by using MCNP for a planar source of Sr-90 + Y-90. The two results were significantly similar.

A tool that could be used to solve the problems of analytical and numerical methods in section 2.7 is the Monte Carlo method. This method can handle complex geometrical arrangements, multiple materials and the coupling of the electron and photon histories. The accuracy of the results from this method is often as good as physical measurements or even better [ICRU 72, 2004]. Dose distributions are calculated in water as this is closest to the clinical situation and because measurements are often made in water. The method can be used comprehensively to study the tissue, to which the dose is to be delivered before the actual treatment is carried out on the patient. The dose determination at the various depths in the patient's body is made using phantom materials.

2.8.1 Phantoms

During treatment of the patient with a beta irradiation beam of known quality and quantity, the beam will be absorbed and scattered and both its quality and quantity will be changed. In order to study these changes, experiments must be conducted using phantoms

to replace the patient or organ to be treated. In the context of dosimetry, a phantom is a medium with the same characteristics of absorption and scatter of the beam as the tissue to be irradiated or treated. The phantom material should have the same density as the tissue and should contain the same number of electrons per gram. Hence, in therapy the term phantom describes material and structures that model the radiation absorption and scattering proportionally to the human tissue of interest. Water and tissue absorb photons in almost the same way and for this reason water has been used in many investigations, and it will be used in this study [Johns & Cunningham, 1983; Klevenhagen, 1993; Young, 1983].

Water is the standard phantom material for the dosimetry measurements of photon and electron beams or beta-particles [IAEA, 2003] and it is the recommended phantom material for determination of absolute and relative absorbed dose and dose rate distributions [ICRU 72, 2004; Young, 1983]. The reasons for this are that it is universally available i.e. readily available, with reproducible radiation properties, it is liquid, cheap, and transparent and also has a simple chemical formula.

However, it is not always possible or practical to perform dosimetry in a water phantom, because it is difficult to take measurements near the surface of water because of its surface tension and because of the uncertainty in positioning the detector near the surface. It may also not be feasible because of leakages in radiation detectors. For this reason dosimetric measurements are often carried out using more practical solid materials, such as polystyrene, Lucite, A-50 tissue-equivalent plastic solid water WT1, RMI- 457 and others that mimic water in terms of mass density, number of electrons per gram and effective atomic number. The effective atomic number depends on the atomic composition of the mixture as well as on the type and quality of the radiation beam [IAEA, 2003; Klevenhagen, 1993].

For the phantom to be water-equivalent for electron or beta-particle dosimetry, it must have the same linear stopping power and the same linear angular scattering power. This can be achieved if the phantom has the same electron density and the same effective

atomic number as water. Hence, Khan's (2003) equation 2.42 is used during the built-up of phantom materials to bring them into line with water:

$$\rho_e = \rho_m \cdot N_A \cdot \left(\frac{Z}{A}\right) \tag{2.42}$$

where $\frac{Z}{A} = \sum_i a_i \cdot \left(\frac{Z_i}{A_i}\right)$, and (ρ_e) is the electron density, (ρ_m) is the mass density, N_A is Avogadro's number and a_i is the weight fraction of i^{th} element of atomic number Z_i and atomic weight A_i.

Water is tissue equivalent, which is essential because the data collected is to be used in tissue. Also the phantom must be of sufficient size and depth to allow an adequate amount of scattering material around the largest fields which are to be used and in order to obtain full backscattering beyond measurement point [Young, 1983]. In this study, a small cylindrical water phantom will be used to represent the eye in a clinical situation.

2.8.2 Depth dose distribution

Depth dose distribution is defined as the measure of energy variation with depth and deposited in a water phantom. Lower readings can be observed with increasing depth owing to the attenuation of radiation by the water. The degree of absorption or transmission of beta particles is determined by observing the change in source strength due to differences in thickness of the absorber in the beam. Even the smallest thickness of absorber can absorb beta-particles.

When the activity (count rate) or transmission curve plotted on a semi-logarithmic graph (Figure 2.9) decreases as a straight line, or nearly so, over a larger fraction of the absorber thickness, it eventually tails off into another straight line region represented by the background. This is always present and is a relatively flat tail. The point where the absorption curve meets the background is the range, $R_{\beta max}$, traversed by the most

energetic particle emitted. This type of curve can also be used to determine the maximum energy, $E_{\beta max,}$ for the beta source. It should be noted that the tail of the curve does not reflect β-particle transmissions, but rather represents the detection of relatively penetrating bremsstrahlung photons, generated by β-particles in the absorber and possibly in the source and the source holder. The extraneous instrument and radiation background may also contribute to the tail of the curve [Cherry *et al.*, 2003; James, 2006].

The thickness of the absorber corresponding to the intersection between extrapolation of the linear descending portion, and the tail of the curve is called the extrapolated range, R_e of the electrons. This is slightly less by a few percentage points than the maximum range, R_m. Although, R_m is the actual maximum thickness of the absorber penetrated by the maximum energy of β-particles, because the difference of R_e and R_m is so small. It is very difficult to measure R_m accurately. For this reasons, R_e is usually specified as the maximum β-particles range. The curve for β-particles (Figure 2.9) declines more rapidly for very thin absorbers, because of the rapid elimination of low energy electrons in the β-particles' energy spectrum [Cherry *et al*., 2003].

There is more than one way to specify the range of the beta-particles. Therefore, the relationship of range to beta-particle energy has been developed. The range in $mg.cm^{-2}$ for various energies in MeV has been empirically derived, independent of material density for energy range of $0.01 \leq E \leq 2.5$ MeV [James, 2006], as:

$$R = 412\ E^{1.265\ -\ 0.0954\ InE} \tag{2.43}$$

The range of beta-particles increases with increasing beta-particle energy. Ranges are also important for radiation dosimetry [Cherry *et al.*, 2003]. The β-particles of the radionuclide Sr-90 + Y-90 may reach a maximum depth of 0.8 cm to 1.2 cm in human tissue, and 10.62 cm maximum range in air. Whereas in water it has been found to be about 1.18 cm from the extrapolation method used in the curve of range against energy for maximum energy of 2.281 MeV [IAEA, 2003; Friedell *et al.*, 1950; Selman, 1976]. In general, penetration depends on the energy of particles released in the decay process of

the particular source and the material characteristics of the absorber [Kirwan *et al.*, 2003]. Hence, the β-particles cannot be used in treatment of deep-seated tumours by surface application, because of their mean range of a few millimeters in soft tissue [Selman, 1976].

Another empirical relation called Feather's rule (for beta-particles of $E \geq 0.6$ MeV) is given as:

$$R = 542E - 133 \tag{2.44}$$

The Feather analysis is described as the extrapolation of a straight line portion from activity against absorber thickness to the background, and the use of the extrapolated value as the maximum range [James, 2006]. The extrapolated ranges are found to be inversely proportional to the density ρ (g/cm^3) of the absorbing material. Hence, the following relation holds true and can be used for any material:

$$R_e(cm) = {R_e(g/cm^2)} \Big/ {\rho(g/cm^3)} \tag{2.45}$$

where $R_e(g/cm^2)$, is an electron range in absorber material (can be obtained from the curve). Electron ranges are usually expressed in g/cm^2 of absorber to normalize for density effects [Cherry *et al*., 2003].

The percent surface dose for β-particles increases with their energy, and this can be explained by the nature of β-particles' scatter. At lower energies, the β-particles are scattered more easily and over larger angles. This causes the dose to build up more rapidly and over a shorter distance, thus the ratio of surface dose to maximum dose is lower for lower energy electrons than for higher energy electrons [IAEA, 2003]. The surface dose increases with increase in energy as result of the decrease in mass scattering power with increase in energy.

The comparisons of actual dose distributions are not always straightforward. The dose distributions calculated using different methods are usually compared at the few relevant points and consistency is expressed in percentages [ICRU 72, 2004]. The central-axis depth dose distribution depends on [ICRP 38, 1983]:

(i) Filtration over source

(ii) Size of active area

(iii) Degree of uniformity with which the source is made

(iv) Method of measurement

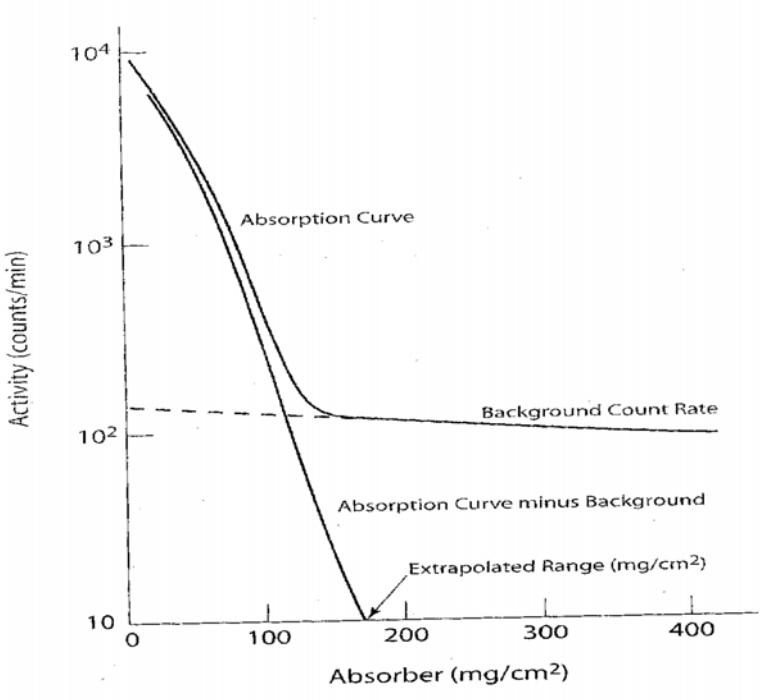

Figure 2.6: Decrease in measured activity of beta particle source versus absorber thickness (mg/cm^2) that trails off into the background of the detector system [James, 2006: 321].

Because the depth dose falls off more rapidly, a slightly concave applicator provides even more uniform contact. Better contact is achieved with a smaller applicator [Selman, 1976]. In this study depth measurement of the absorbed dose will be confined to the central axis of the source beam.

Chapter 3

MONTE CARLO N-PARTICLE TRANSPORT CODE

3.1 Introduction

The Monte Carlo N-Particle (MCNP) code, version 1.20, is the principal simulation program used in this study. MCNP is a general Monte Carlo N-Particle code [Briesmeister, 1997; X-5 Monte Carlo Team, 2003] that applies the Monte Carlo method to particle transport for single particles such as neutrons, photons, electrons and coupled neutron/ photon/ electron transport problems. The code is continuous energy, generalised-geometry, time-dependent and treats arbitrary three-dimensional geometries of material in geometric cells bounded by first and second degree surfaces, and fourth degree elliptic tori. The MCNP code uses point-wise cross-sectional data with the energy range of electrons, photons and neutrons extended from 1 keV to 1 GeV, 1 keV to 100 GeV and 10^{-11} eV to 20 MeV (up to 20 MeV neutrons for all isotopes and up to 150 MeV for some sources), respectively.

The MCNP code is a radiation transport code originally developed by the Monte Carlo Group to model neutron and photon radiation, with electron transport added later. The latter transport model was patterned after the Integrated Tiger Series (ITS) continuous slowing down approximation [Gleckler *et al.*, 1998]. MCNP is thus based on the early version of ITS. MCNP code uses an improved electron transport algorithm of ITS3.0, to correct the underestimated mean electron loss in the earlier version of ITS1.0 [Park *et al.*, 2008]. MCNP code appears to be a strong candidate compared to Electron Gamma Shower (EGS) and ITS, more especially when the powerful geometry capabilities of MCNP are taken into account [Ljungberg *et al.*, 1998].

The ITS, is based on Electron Transport (ETRAN) codes such as:
ZEBRA: presents an extension to multi-material slab geometry, treats electrons in continuous slowing down approximation, and has been extended to three dimensional geometries for application in beta dosimetry; TIGER: for multiple slab targets, allows

simulation in plane parallel slabs that are one-dimensional calculations; CYLTRAN: for general cylindrical geometries; and ACCEPT: uses general three-dimensional combination geometry or any complex geometry.

Currently, MCNP is upgraded by the diagnostic Applications Groups (Group X-5) in the Applied Physics Division (X-Division) at Los Alamos National Laboratory (LANL). MCNP has been made platform independent to enhance its portability, and written to comply with ANSI Fortran 90 standard. MCNP is distributed by the Radiation Safety Information Computational Center (RSICC) at the Oak Ridge National Laboratory. The Radiation Transport Group in Applied Theoretical Physics Division at LANL maintains and improves MCNP on a regular basis [Briesmeister, 1997; X-5 Monte Carlo Team, 2003; Mosia, 2005].

MCNP was among the first production physics codes to become commercially available as state of the art in computer architecture [Maage, 2002]. The first Monte Carlo code was written in 1963. Initially, its name stood for Monte Carlo Neutron Photon but now it stands for Monte Carlo N-Particle. In its long history since its inception at LANL, it had a variety of names, such as MCS, MCN, MCG, MCNG, MCP, and MCNP [Ljungberg *et al.*, 1998; X-5 Monte Carlo Team, 2003]. Initially, MCN and MCG merged to form MCNG; at a later stage, MCNG combined with MCP to form MCNP. Since 1983, MCNP also had various names and versions: MCNP3 (versions 3A and 3B), MCNP4 (versions 4B and 4C) and recently, since 2003, MCNP5.

During the years of World War II and the Manhattan project, Stan Ulam, John von Neumann and Nicholas Metropolis chose the name “Monte Carlo” for numerical simulation methods. These simulation methods describe statistical methods, using random numbers as a base to perform simulation of any specified situation. This name was chosen because of the close connection of the process to a game based on chance, and played in the casinos of Monte Carlo. Specifically, Metropolis told how Ulam’s uncle would borrow money from relatives to gamble in Monte Carlo, hence the name. The Monte Carlo method is generally accredited to scientists who were working on the

development of nuclear weapons in the 1940's at LANL [Ljungberg *et al.*, 1998; X-5 Monte Carlo Team, 2003].

3.2 Monte Carlo Method

The Monte Carlo method is nominally exact and is able to describe accurately the geometry of a system. It is a stochastic technique, which is based on random numbers and probability statistics. Answers are obtained by simulating individual particles and recording some aspects of their average behaviour, such as tallies. The average behaviour of particles in a physics system is then inferred by using the central limiting theorem from the average behaviour of the simulated particles [Mosia, 2005; X-5 Monte Carlo Team, 2003]. As the number of individual histories is increased, the quality of the reported average behaviour of the system increases, meaning that the statistical uncertainty decreases. Simulation is thus one of the most important tools in the study of particle transport and interaction with matter, including radiation protection and dosimetry.

The Monte Carlo method propagates individual particles from the source and through the patient or detector, tracking each particle history to detect where energy is deposited along the particle track. Each history represents the interactions undergone by single emitted photons or electrons [IAEA, 2002]. Individual particle histories are simulated based on the particle interaction cross section, particle transport and energy deposited characteristics.

A slightly faster program may save a few hours per simulation, depending on the geometry of the problem. Electron transport cut-off energy is an important factor affecting computation efficiency. This is because electron transport is halted below the user-defined energy, thus speeding up the simulation. Linux is found to be much faster than the MS DOS operating system. The code runs more quickly if the energy cut-off for photons and electrons is used. Consequently, the transport cut-off and energy threshold for the secondary electron and photon production, are extremely important. It is time

consuming to create particles which will not be simulated or used. Therefore, particles whose energy is out of the energy range of interest are terminated.

Simulation requires that system and physical processes be modeled from the known probability density function (PDFs). If the PDFs are accurately defined, then the simulation can be achieved by random sampling from PDFs [Ljungberg *et al.*, 1998; X-5 Monte Carlo Team, 2003].

Simulation studies have several advantages over experimental studies. In any given model, it is very easy to change parameters and investigate the effects of any alterations on the system under study. So the comparisons of eye applicators and their optimisation in performance can be studied through simulations. It is also important to note that some effects cannot be studied experimentally, but only through simulation. The simulation program allows a better understanding of underlying processes, since all the details of the simulation are accessible [Ljunberg *et al.*, 1998].

The Monte Carlo method is a calculation algorithm that most closely models the actual physics of the energy deposited. Monte Carlo algorithms are believed to be more accurate than any other kind of calculation algorithm. In actual fact, there are two algorithm approaches to numerical modelling: the deterministic method and the stochastic method [Maage, 2002; X-5 Monte Carlo Team, 2003]. The latter is very different from the former in solving a problem and constitution of solution. The commonly used deterministic method is a discrete ordinates method, which solves the transport equation for the behaviour of the average particle. The stochastic method, on the other hand obtains answers by simulating individual particles, and recording important aspects of their behaviour.

In principle, Monte Carlo techniques are capable of providing dosimetry data with high spatial resolution at a distance of millimetres. However, exact modelling of the source geometry and the radiation interaction are essential for the Monte Carlo calculation to be accurate. Monte Carlo calculations have also proved to be very useful in investigating

radiation transport phenomena and dosimetry, particularly in complex geometries where measurements can be difficult.

A better understanding of the physics of radiation transport in matter has been achieved, with the use of Monte Carlo techniques. These techniques duplicate statistical processes theoretically and the code can be used for complex problems. The individual events that comprise a process are sequential. The probability distributions governing these events are statistically sampled to describe the total phenomenon [Briesmeister, 1997; X-5 Monte Carlo Team, 2003].

The Monte Carlo codes have different applications in radiation dosimetry radiotherapy physics, radiation protection and in fields of nuclear physics, material science, high energy physics and medical physics. Important low energy phenomena such as production and transport of characteristic x-ray and Auger electrons, are accurately modeled no matter how difficult the geometry in question. Only geometry in the vicinity of particles for which a random walk is being constructed should be considered in any simulation [Maage, 2002; Park *et al*., 2008].

The code has been used for corrections and conversion factors currently used in dosimetry, treatment planning, etc. Thus, the Monte Carlo technique is vital in comparing international procedures and standards [Ljunberg *et al.*, 1998]. The technique provides a powerful tool for calculation of the dose and dose distributions. Such distributions help to predict and determine more accurately the dose and dose rate from various types of eye applicators of different shapes [Šolc, 2008].

It is important to take note of two modes of electron energy indexing algorithms that can be used in MCNP, the ITS-style energy indexing algorithm and the MCNP-style energy indexing algorithm. The default version uses the so-called MCNP-style energy indexing algorithm (bin-centred treatment). The ITS-style energy algorithm (nearest group boundary treatment) is used when a special switch on the DBCN card is used (for example, DBCN 17j 1). MCNP-style indexing uses the cross-sectional data from the

energy group in which the electron initiates the step (calculates for appearance boundary of the group). In MCNP, the electron cross-section data is tabulated on the predefined energy grid. The ITS-style indexing algorithm uses the data from the group with a boundary closest to the energy of the electron at the beginning of the step [Briesmeister, 1997; Maage, 2002].

These statistical processes are based on and dependent on the selection of random numbers. In actual fact, the Monte Carlo technique involves following many particles from the source throughout their lifetime until death [X-5 Monte Carlo Team, 2003].

Random numbers are the most fundamental part of the Monte Carlo simulation. Random sampling to solve mathematical problems dates back to 1772. Numbers are randomly distributed, hence they are unpredictable. MCNP uses a built-in pseudo random number generator instead of one supplied with a computer operating system where the code is running. A pseudo random number generator is used to generate numbers for each random variable with probability according to a probability density function. Thus, computer algorithms can be used to generate random numbers in practical considerations. The commonly used random technique is known as the multiplicative linear congruent method [Ljungberg *et al.*, 1998].

3.3 MCNP5

MCNP5 was released in 2003 [X-5 Monte Carlo Team, 2003] and includes new features such as the addition of photonuclear collision physics, superimposed mesh tallies, time splitting, plotter upgrades and parallel computer enhancement with the addition of support for OpenMP and MPI. These new features reflect advances in the Monte Carlo computer architecture, improvements in Monte Carlo methodology and better physics models.

MCNP codes have been extensively used in the field of medical physics in the investigation of Sr-90 + Y-90 eye applicators, Y-90 and P-32 [Park *et al.*, 2008; Vynckier

& Wambersie, 1982]. The use of the code in these fields has increased significantly in recent years for a combination of reasons. Some of these are the rapid increase in computer speed, the decrease in costs of data processing, and also the availability of larger general-purpose software packages. The range of MCNP applications is very broad.

MCNP5 was used in this study because of its ability to handle complicated geometries and multiple materials, as well as its user-friendliness (it is easy to understand). The code is ideal for dosimetric calculations of sources because it facilitates modelling of complicated geometry better than other transport codes [Park *et al*., 2008]. Many of the uncertainties and assumptions made in the theory of surface dose rate calculations corresponding to the lens dose can be avoided by using MCNP5 [Cross *et al.*, 2001; Gleckler *et al.*, 1998; Maage, 2002]. Monte Carlo calculations are more accurate and flexible, therefore more reliable solutions to the problem of dosimetry using the Teflon-encased eye applicator can be obtained using this simulation technique.

3.4 MCNP photon and electron interactions

There is variation between physical cross-section tables in Monte Carlo codes. These tables are important when comparing different codes, since the use of different cross-sectional data and approximation yield different results and the accuracy of results is not always obvious [Ljungberg *et al.*, 1998]. The photon interaction cross sections are required for all photon problems, and photon interactions account for both photoatomic and photonuclear events (new to MCNP5). The photonuclear interaction data describe nuclear events with specific isotopes.

3.4.1 Photon interactions

The MCNP has two photon interaction models, the simple and the detailed model. The simple physics treatment ignores coherent (Thompson) scattering and fluorescent photons caused by photoelectric absorption, and is usually intended for high-energy photon problems. The detailed physics treatment includes coherent (Thompson) scattering, and

also accounts for fluorescent photons after photoelectric absorption. The form factors and Compton profiles are used to account for the electron binning effects. The latter interaction model is regarded as the best one for most applications [X-5 Monte Carlo Team, 2003]. It is clear from the MCNP5 output file (Appendix C.2) that the detailed photon interaction model was applied in this study.

Scattering and absorption data from photons are fundamental to all Monte Carlo calculations: therefore, the accuracy of the simulation depends on the accuracy of the probability functions, that is, the cross-sectional tables. The total cross sections, attenuation coefficients, partial cross sections for incoherent and coherent scattering, photoelectric absorption and pair production in the field of the atomic nucleus and in the field of atomic electrons (Triplet production) are calculated. The sum of interaction coefficients for individual processes is equal to the total attenuation coefficient [Ljungberg *et al.*, 1998].

The simple physics model simulation processes include the photoelectric effect, pair production and Compton (scattering) effect. Therefore, the total cross section σ_t is regarded as the sum of cross sections of Compton (σ_s), photoelectric (σ_{pe}) and pair production (σ_{pp}) [X-5 Monte Carlo Team, 2003; Maage, 2002]:

$$\sigma_t = \sigma_{pe} + \sigma_{pp} + \sigma_s \tag{3.1}$$

3.4.1.1 Photoelectric Effect

The photoelectric effect is regarded as absorption without fluorescence, and treated as pure absorption by implicit capture with corresponding reduction in photon weight. The non-captured photon (1- $\sigma_{pe/}\ \sigma_t$) is forced to undergo either pair production or Compton scattering. The captured photon is assumed to have been deposited locally or to have become a photoelectron for electron transport [Briesmeister, 1997; X-5 Monte Carlo Team, 2003].

3.4.1.2 Pair Production

The collision of high energy photons and the strong electromagnetic fields of the nucleus results in pair production with probability [$\sigma_{pp/}$ (σ_t –σ_{pe})]. The electron-positron pair is created either for further transport and the photon disappears, or it can be assumed that the kinetic energy (E - 1.022) MeV of the produced electron-positron pair is deposited as thermal energy at the time and point of collision. This process leads to the isotropic production of two photons of energy 0.511 MeV, which are ejected in opposite directions [Briesmeister, 1997; X-5 Monte Carlo Team, 2003].

3.4.1.3 Compton Scattering

Compton scattering is an alternative to pair production on free electrons with probability ($\sigma_{s/}$ (σ_t –σ_{pe})). The process yields energy (E-E') to be deposited at the collision point and a new direction in the scattered photon. Such deposited energy (E-E') can be used to eject the Compton recoil electron for further transport [Briesmeister, 1997; X-5 Monte Carlo Team, 2003].

3.4.1.4 Coherent Scattering

The coherent scattering from the detailed physics is the only process that does not produces electrons for further transport, nor use the thick target bremsstrahlung (TTB) approximation. The TTB approximation is a default for MODE P problems, it also plays a role in MODE P E where is used in terminal process of electrons to account for the low energy bremsstrahlung photons produced at the end of electrons range. This process has a differential cross section:

$$\sigma_2(Z,\alpha,\mu)d\mu = C^2(Z,\nu)T(\mu)d\mu \tag{3.2}$$

$$\mu = \cos\theta \tag{3.3}$$

$$\nu = \sin(\theta/2)/\lambda = \kappa\alpha\sqrt{1-\mu} \tag{3.4}$$

where Z, α ,v, θ and κ are atomic number, photon energy, inverse length, angle of deflection from the line of photon flight and constant parameter with value 29.144 cm^{-1}, respectively. T (μ) and C (Z,v) are the Thompson cross section and the form factor. The function of the form factor is to modify Thompson cross sections. The Thompson cross section is defined by [Briesmeister, 1997; X-5 Monte Carlo Team, 2003]:

$$T(\mu) = \pi r_0^2 (1 + \mu^2) d\mu \tag{3.5}$$

where πr_0^2 has a value of 2494351, and r is the classical electron radius.

The fraction of form factor and the atomic number $C^2(Z,v)/Z^2$ have the general effect of decreasing the Thompson cross section for backward scattering, more especially in the case of high energy and low atomic number materials.

3.4.2 Electron interactions

In electron interactions, the data tables are required for problems in which electrons are transported, as well as for photon problems in which the thick target bremsstrahlung (TTB) model is used. The electron data tables are specially identified by ZAID in the form ZZZ000.nnE for two available interaction data libraries, el and e103. The data library contains energies for tabulation, electron stopping power parameters and ranges, bremsstrahlung cross section and energy distributions, the k-edge energies, and X-ray production probabilities [X-5 Monte Carlo Team, 2003].

The transport of charged particles and electrons is fundamentally different from that of neutrons and photons. Electron transport is dominated by long range Coulomb forces, which results in large numbers of small interactions. Theoretical work has been considered in developing various analytic, and semi-analytic multi-scattering theories for charged particles. These theories have attempted to use the fundamental cross sections and statistical nature of transport processes to predict distributions. The most important of these theories are the Goudsmit-Saunderson theory for angular deflections, the Landau

theory of energy-loss fluctuation and Blunk-Leisegang's enhancement of the Landau theory [X-5 Monte Carlo Team, 2003].

In order to follow an electron history through a significant energy loss, it is necessary to break the history into several steps. The energy loss and deflection of the electron during each of these steps can be sampled as probability distributions based on distribution theories. The condensed random walk for an electron can be considered for a sequence of set values [Briesmeister, 1997; X-5 Monte Carlo Team, 2003]:

$$(O,E_0,t_0,\mathbf{u}_0,\mathbf{r}_0),\ (s_1,E_1,t_1,\mathbf{u}_1,\mathbf{r}_1),\ (s_2,E_2,t_2,\mathbf{u}_2,\mathbf{r}_2),.....(\ s_n,E_n,t_n,\mathbf{u}_n,\mathbf{r}_n) \tag{3.6}$$

where s_n, E_n, t_n, u_n and r_n are total path length, energy, time, direction and position of the electron at the end of n steps, respectively.

The average energy and path length are expressed by:

$$E_{n-1} - E_n = -\int_{S_{n-1}}^{S_n} \frac{dE}{ds}\, ds \tag{3.7}$$

where dE/ds is the total stopping power in energy per unit length depending on the electron and material electron is moving through.

All the ETRAN-based codes choose the sequence of path length such that

$$E_n/E_{n-1} = k \text{ , where } k = 2^{-1/8} \tag{3.8}$$

All pre-calculated and tabulated data for electrons are stored on an energy grid whose consecutive energy values obey equation 3.8. This equation may result in 8.3% average energy loss per step. All the relevant data are pre-calculated and include electron energy grid, stopping powers, electron ranges, energy steps ranges, sub-step lengths and probability distribution [X-5 Monte Carlo Team, 2003].

The length of the sub-step can be derived from the total stopping power used in equation 3.7. The projected energy is based on non-radiative stopping power. Thus, the bremsstrahlung photon generated during the sub-step, is obtained by subtracting the photon energy from the electron energy at the end of the sub-step. The radiative energy loss is therefore taken into account, in contrast to the collisional (non-radiative) energy loss.

The restricted electron collision stopping power results in fractional energy transfer ε less than an arbitrary maximum value ε_m in the following form [Briesmeister, 1997; X-5 Monte Carlo Team, 2003]:

$$-\left(\frac{dE}{ds}\right)_{\varepsilon_m} = NZC\left\{\ln\frac{E^2(\tau+2)}{2I^2} + f^-(\tau,\varepsilon_m) - \delta\right\} \tag{3.9}$$

where

$$f^-(\tau,\varepsilon_m) = -\beta^2 + (1-\ln 2) + \left(\frac{1}{8}+\ln 2\right)\left(\frac{\tau}{\tau+1}\right)^2 \tag{3.10}$$

$$C = \frac{2\pi e^4}{m v^2} \tag{3.11}$$

In above equations *N, Z, E,* τ and δ represent the atomic density of the medium in cm^{-3}, average atomic number of the medium, electron kinetic energy, the electron kinetic energy in units of the electron rest mass and density effect correction, respectively. Whereas *m, e* and β represent electron rest mass, electron charge and ratio of electron speed (*v)* and light speed (*c)*, respectively.

In equation 3.9, *E* and *I* are expressed in terms of electron rest mass units, so *E* can be replaced by τ. By introducing the supplementary constants to equation 3.9, dividing by *N* and multiplying by a conversion factor 10^{24} barns/cm^2, and also using the fine structure constant α, the collisional stopping powers at the energy boundaries of the major energy steps can be represented [Briesmeister, 1997; X-5 Monte Carlo Team, 2003] by

$$-\left(\frac{dE}{ds}\right)=\frac{10^{24}\alpha^2h^2c^2}{2\pi mc^2}Z\left\{\ln\left[\tau^2(\tau+2)\right]-C2+C3-\beta^2+C4\left(\frac{\tau}{\tau+1}\right)^2-\delta\right\}\frac{1}{\beta^2} \quad (3.12)$$

where *C2, C3* and *C4* are supplementary constants defined by

$$\begin{aligned} C2&=\ln(2I^2)\\ C3&=1-\ln 2\\ C4&=\frac{1}{8}+\ln 2 \end{aligned} \quad (3.13)$$

and the fine structure constant defined by

$$\alpha=\frac{2\pi e^2}{hc} \quad (3.14)$$

where Planck's constant, *h,* is used to eliminate electronic charge. The radiative stopping power, on the other hand, is defined by [X-5 Monte Carlo Team, 2003]

$$-\left.\frac{dE}{ds}\right|_{rad}=10^{24}Z(Z+\bar{\eta})(\alpha r_e^{\,2})(T+mc^2)\Phi_{rad}^{(n)} \quad (3.15)$$

where $\Phi_{rad}^{(n)}$, $\bar{\eta}$, and r_e, and represent the scaled electron-nucleus radiative energy loss cross section, the parameter to account for electron-electron bremsstrahlung and the classical electron radius, respectively. The dimensions of both radiative stopping power and collisional stopping power are the same.

3.5 MCNP5 features and geometric setup

MCNP uses continuous-energy nuclear and atomic libraries. The nuclear data for photons and electrons are atomic rather than nuclear in nature, and photonuclear data are included. Each data table available is listed in a cross-section directory file XSDIR. Specific data can be selected by a unique identifier for each table, called a specific isotope identifier, ZAID. The general form of ZAID is ZZZAAA.nnX, where ZZZ is

atomic number, AAA is the atomic mass number, nn is the unique evaluation identifier, and X indicates the class of data [Briesmeister, 1997; X-5 Monte Carlo Team, 2003].

3.5.1 Input and Output files

The input file contains information about the problem in areas such as the geometry specification [Briesmeister, 1997], the description of materials, selection of cross-section evaluations, the location and characteristics of neutron, photon, or electron sources, the type of answers or tallies desired and any variance reduction techniques used to improve efficiency. MCNP uses units of cm, MeV and g/cm^3.

The electron trajectory and production of secondary particles are controlled at the sub-step level. The default value for the number of sub-steps per major step is assigned, based on material using empirically derived values within the MCNP code. The user can alter the default values for the number of sub-steps per major step, using the ESTEP option on the material card. ESTEP is the maximum fractional energy loss per electron step, which determines how far an electron can go in one step, the time required for the simulation and the accuracy of the simulation.

The input geometry is defined by three-dimensional configurations of the material in cells, bounded by cells and surfaces specified by the user. When the geometry is defined correctly, MCNP will track the particle path until the end. Information on the geometry input and output can be found in Appendix C. The cells are basic geometric units defined by geometric operators: intersections, unions and complements of regions bounded by surfaces [Briesmeister, 1997]. The geometric cells are defined by the user.

In the input file given in Appendix C.1 the first line, numbered 1 (As shown in output file Appendix C.2), is the title card. This describes what the study is about and is followed by line 2 which is the comment line, specifying details of the study. Line 4 starts with a comment line and represents the geometry of the phantom cells, and is also called the cell card. This is followed by line 5 in which the first number defines the cell number, 7,

which is followed by the material number, 4. If the material number is given as zero it means there is no particle cell and no material, and the cell is assumed to be a vacuum. The value following the material number is the density specification and, since this is negative density, is in the unit g/cm^3; it can also be defined by a positive entry to specify density in terms atoms per barn cm. Numbers following density are surface numbers or geometry identification numbers. Their negative sign indicates only that the area is defined inside such a surface, while the positive value means that the area is outside the surface.

Lines 155, 158 and 159 represent void cells between the source and the stainless steel, and between the water phantom and the applicator inside the sphere. The union operator (:) function to add surfaces, intersection operator (space) for the overlap of surfaces and complement operator (#), indicate that cells specified after the operator are not included in the cell. Line 160 defines the outside world of the geometry. Lines 162 and 240 represent comment lines for phantom and applicator surfaces, followed by the surface numbers and then the alphabetic mnemonic specifying the surface type. For example, cz 0.02 is a cylinder with radius 0.02 cm on the z-axis, pz -1.73 is the plane normal to the z-axis and sz -4.0, 2.482 is the sphere positioned at -4.0 on the z-axis with radius 2.482 cm.

The Data card MODE PE, specify that the photons and electrons should be transported through a total of 155 cells having the importance of 1 with the exception of the outside world cell which has an importance of zero. In order to fill a cell, homogenous source SDEF was used to define the volume source using volume distributions (Appendix C.1); the keyword SDEF means source definition. The example below of a source used in this study is cylindrical source based at location 0 0 -1.419, its axis in the negative direction of the z-axis, with a radius of 0.25 cm and a height 0.001 cm. The particles to be emitted from the source are electrons:

```
sdef pos 0 0 -1.419 axs 0 0 -1 rad d1 ext d3 par 3 erg d2 dir d4 Vec 0 0 -1
Si1 0 0.25 $ particles are to be born between zero and 0.25 cm in the radial direction
Sp1 -21 1 $ the probability of particle birth increases linearly with radial distance
```

Si2 H 0 0.1 ….. $ Energy values for source

Sp2 0 1.32…… $ probabilities for the source

Si3 H 0 0.001 $ the axial birth range if from zero to 0.001 cm in the axis direction from the position (pos)

Sp3 -21 0 $ the birth probability constant in axial direction

Si4 H 0 1 $ source particles produced in the forward direction at an angle of 180 degrees.

Sp4 d 0 1 $ the probability of the source particles

Si and Sp represent source information and source probability, respectively. The prefixes H and d represents the bin boundaries and distribution number, respectively. The former prefix is used for a histogram distribution of monotonically increasing scalar variables only. In this study, *Si_4 H 0 1*: are the source boundaries giving 180 degree direction. Whilest the latter gives the direction, for example *dir d4*: gives a monodirection of the source particles in the direction of *Vec: 0 0 -1*, thus gives a cosine angle between initial particle direction and vector direction. Vec is the reference direction for Dir. MCNP normalises the distributions to 1, and during the simulation process MCNP calculates fluence and also normalises tallies per source particle. The Scn card is the source comment card and *n* is the distribution number.

In material and tally cards, materials used for the phantom were described in the MCNP5 input data file by defining their composition and density. The material used for the phantom was water, and that for the radioactive source, $SrCl_2$ (Strontium Chloride) encased in Teflon, sponge (which was assumed to be a vacuum or void) and stainless steel.

The dose was calculated by tallying the energy deposited in each central axis cell of the phantom. The energies were represented by *F8: pe, giving the deposited energy in the tally cell in MeV. Thus, for each photon and electron entering the tally cell, the total energy deposited in that cell is calculated from the difference between the energy carried into (entered) and energy carried out of the cell by the particles. This is also known as the absorbed dose tally, and is considered as a surface estimator and scores energy deposited

only if there is a photon interaction or electron interaction within the cell, or when an electron crosses into the tally cell. In the case of both particles, if there is no interaction the net energy absorbed is zero. The absorbed dose is obtained by dividing the *F8 (MeV) by the mass (g) of the cell. For example, in our simulation cell 7 received an energy of $1.385 \times 10^{-5} \pm 2.5\%$ MeV per source particle, where the quoted uncertainty is 1σ.

The particles passing through each of the surfaces were tallied by tally type 1, i.e. an F1 tally with energy bins E1. Tally type F1 gives the electron current summed in both directions integrated over the surface. For example, in surface 3 between 1.012 MeV and 1.034 MeV, the current is $1.5897 \pm 1.01\%$ MeV per source particle within one standard deviation. The surface union is represented in tally type F1 by the symbol T, and is a short-hand for a region that is union of all other entries on the card. Thus symbol T is the average of the flux across all the surfaces included in the tally.

The DBCN card is useful in the identification of errors, and the entries are primarily used for debugging problems. The code itself is defined as DBCN X1 X2 X3 …X20, where X1 is the starting pseudorandom number , X2 the debug print interval number and X3 and X4 the history number limits for event log print. For this study DBCN 17j 1 was used. The FQn print hierarchy card changes the printing order of particles: for example, Fq8 f e indicates that for tally 8, cells will be printed as a function of energy [Briesmeister, 1997].

The ampersand (&) symbol at the end of lines indicates that the line continues on to the next line. The comment lines are distinguished from the execution lines by the use of lower case c as the first character. Also, the comments lines are found at the end of an execution line after the dollar sign "$". The outside world is defined as everything that is outside the union of all cells, and it is a special cell with a particular format. Any particles that enter the outside world are considered to have escaped, and their history is terminated. Such a special cell has the importance of zero.

The output file contains tables of standard summary information to offer a better idea of the problem run, insight into the physics of the problem concerned and the adequacy of the Monte Carlo simulation. The problem summary is a balance sheet with left hand side viewing how particle tracks, weight and energy were created and right hand side showing how they got lost. This sheet is a summary of both photons and electron in separate sheets. The last page of the output file gives the number of dump files, computer time in minutes and the reason for the termination of the run.

If errors occur during the simulations a detailed print for debugging is provided. A statistical relative error corresponding to one standard deviation is given with each tally [Briesmeister, 1997; X-5 Monte Carlo Team, 2003].

3.6 Accuracy and Precision of MCNP

The important distinction between accuracy and precision in the Monte Carlo results can be explained [X-5 Monte Carlo Team, 2003]. Accuracy is a measure of how close the expected value of the average $\overline{X}$ (mean) is, to the quantity being estimated. Factors affecting accuracy include the code, data libraries as defined by XS Lib acc, problem modelling by the user. The physical features in calculations and mathematical models must be accurately specified. Adequate energy and angular distributions of the source require accurate geometric description, and correct characteristics of materials involved in the problem. In addition, although some errors in the input file problem may be accepted by the system, the user should not abuse variance reduction techniques, and input and output files must be checked carefully.

Precision is the uncertainty in the mean value, caused by the statistical fluctuations of the values of physical phase space sampled by the calculations in the code. In the case of the results of the Monte Carlo calculations, uncertainty refers only to the precision of the results and not to their accuracy. Some user-controlled factors that affect the precision of the simulation include the number of histories, tally type and variance reduction techniques. The reduction technique is divided into four types [Maage, 2002]: the

truncation methods, population control methods, modified sampling methods and partially deterministic methods.

The estimate of efficiency on time required for desired precision can be achieved by using the figure of merit (FOM). The FOM is a tally reliability indicator for optimising the efficiency of Monte Carlo calculations, and estimating computer time required to reach the desired value of the relative error. FOM is calculated for each tally as a function of number of histories, and is one way of determining how well the simulation has performed by providing information about any unusual behaviour in the confidence interval. Big changes in FOM illustrate serious problems that need attention.

Results of FOM are printed in the TFC (tally fluctuation chart), and a well behaved tally is indicated by a fairly constant value of FOM. The TFC includes 10 statistical checks or tests. These tests are based on:

- Tally Mean, $\overline{X}$,
- Relative Error, R,
- Variance of the Variance, VOV,
- Figure of Merit, FOM, and
- Tally PDF (Probability Distribution Function), f(x) to test tally reliability.

If any of these tests fails, a warning is printed in the output and a plot of f(x) is produced. Valid formation confidence intervals for the results can be concluded from all the statistical information provided in TFC. The chart represents desired, observed and actual results along with pass/no pass message for each test.

3.7 Errors

MCNP uses a variety of external data sources, each with their own intrinsic errors. Cross-sectional data has errors which are well known to the data library. MCNP takes this into account when determining result errors (error bars) and tally FOM.

Every code has some limitations and no code is perfect [Ljungberg *et al.*, 1998]. It is thus very important to be aware of the limitations of the MCNP method in order to avoid systematic errors in simulation. Systematic and statistical errors may be small when results are obtained using similar codes, although differing physical modes and algorithms used in these codes might lead to significantly more erroneous results.

3.8 Monte Carlo calculations done in the water phantom

The source was constructed to emit the particles in a forward direction, and source emissions in directions away from the central axis of the applicator source were ignored for the purpose of this study. The back scatter from the eye applicator was negligibly small as explained in chapter 6 sections 6.1.2.2 and 6.2.1.2, hence was also ignored. MCNP5 tally type 8 (*F8) scores energy deposited in a cell by bookkeeping the difference between energy carried into and out of the cell by particles, and gives energy in MeV per source particle. By dividing the net energy deposited in the cell by the mass of a cell, an average dose in cell is obtained. Since dose SI units are Gray or J/kg, energy is converted from MeV to Joules by multiplying it by 1.602×10^{-13} J/MeV and the mass of the cell is converted from grams (g) to kilograms (kg).

For example, a dose in cell 7 which is enclosed by planes 26 and 27 at the centre of the water phantom (Appendix C.2 lines 5, 165 and 166) is calculated as follows:

$$\text{Dose (cell 7)} = dE/dm$$
$$1 \text{ eV} = 1.602 \times 10^{-19} \text{ J}$$
$$1 \text{ MeV} = 1.602 \times 10^{-13} \text{J}$$

In cell 7, 1.38495×10^{-5} MeV per source particle was deposited; the energy in Joules is thus 1.602×10^{-13}J/MeV $\times$ 1.385×10^{-5} MeV = 2.219×10^{-18} J per source particle. A mass is defined by volume and density of the material; the volume of the cell is 1.257×10^{-5} cm^3 and the density of water, 1g/ cm^3, hence the mass of cell 7 is 1g/ cm^3 $\times$ 1.257×10^{-5} cm^3 = 1.257×10^{-5} g = 1.257×10^{-8} kg.

$$\begin{aligned} \text{Therefore, Dose (cell 7)} &= 2.219 \times 10^{-18} \text{ J} / 1.257 \times 10^{-8} \text{ kg} \\ &= 1.765 \times 10^{-10} \text{ J/kg} \\ &= 1.765 \times 10^{-8} \text{ cGy per source particle} \end{aligned}$$

In order to calculate the dose rate, the relationship between the number of particles to be transported, the time and the activity is required, as shown in Appendix A. The activity of the source is given by the initial activity in disintegration per second (dps) [Maage, 2002]. Since the simulations were run with Sr-90 + Y-90 which give out two particles per disintegration, equation 3.16 taken from equation A10 in Appendix A holds true for dose rate:

$$\dot{D} = \frac{D}{t} = \frac{(E/n) \bullet 2A_0}{m} \tag{3.16}$$

So, Dose rate (cell 7) = $(2.219 \times 10^{-18}$ J) $\cdot 2$ $(1.338 \times 10^{9}$ $s^{-1})$/ 1.257×10^{-8} kg

= 0.4724 Gy/s

= 47.24 cGy/s

The relative error of the dose rate for cell 7 calculated above is 2.5 % at one standard deviation. Hence, dose rate for cell 7 can be given as 47.24 cGy/s ± 2.5%.

Two statistical tests were conducted on the Teflon-encased eye applicator results with Teflon thickness of 0.1 cm and sources of thickness 0.03 cm, 0.04 cm, 0.045 cm and 0.05 cm against the standard eye applicator. The first was the correlation test, which indicates

the strength and direction of the linear relationship between two random variables, and is defined by:

$$r_{xy} = \frac{\Sigma(x_i - \bar{x})(y_i - \bar{y})}{(n-1)S_x S_y} \tag{3.17}$$

where $S_x S_y$ are the standard deviations on x and y data values with averages $\bar{x}$ and $\bar{y}$.

The second test was the analysis of variance (ANOVA) test by the F-test method, also known as the ANOVA F-test. ANOVA provides a statistical test of whether the means of several groups are all equal.

Chapter 4

THE STRONTIUM EYE APPLICATOR

4.1 Introduction

The Strontium eye applicator (Ophthalmic Applicator), also called eye plaque, can be defined as a rigid device with the following characteristics: hollow, with a thin casing that encloses a radioactive Strontium-90 (Sr-90) powdered salt. Because of the properties and characteristic behaviour of the beta-particles produced from the radioactive decay of Sr-90, these applicators are used for very superficial lesions of the eye and skin, of less or equal to 1 mm in thickness. The Sr-90 applicators can also be used for technical purposes, such as routine dating and calibrations.

Cleaning of the applicators is necessary but must be done gently, because they are very small and the casing is usually thin and easily damaged. The applicators are sterilized with pure ethyl alcohol, any excess being wiped off with cottonwool before use. Heat of any form will damage the delicate covering [Fraser & Naunton, 1961]. Applicators are normally protected against corrosion by storing them in alloy case [Young, 1983]. Hence, safety in storage and consistency in management are required.

Since their acceptance, there have been further developments in design (construction and dimensions) based on studies of these applicators. The following sections, 4.2, 4.3, 4.4, 4.5 and 4.6 will focus respectively on the historical background, the description of the standard eye applicator used in this study, medical applications, a more specific ophthalmic treatment technique of the Sr-90 applicator device and the proposed Teflon-encased eye applicator.

4.2 Historical Background

The element strontium was discovered by Thomas Charles Hope in 1798. As a mineral, strontianite had been discovered in 1787 by William Cruikshank in a mine in the Scottish

village of Strontian. Many years after this discovery, in the early 1940's, gamma rays from Radium and "grenz rays" were being used in radiation therapy for various ophthalmologic conditions. In 1940, Burnam and Neil reported on the use of beta rays originating from the gas Radon, the daughter isotope of Radium, contained in a glass bulb enclosed within a brass cylinder as the source in an applicator. This type of applicator was in general use until artificially produced radioactive isotopes became available [Thomas *et al.*, 1962].

Following the report by Burnam and Neil, Iliff suggested in 1947 that beta radiation might be particularly useful in ophthalmology; however, its usefulness was limited by the need to use naturally occurring Radon seeds [Kirwan *et al.*, 2003].

The original applicators were lightly-filtered Radium sources, which are strong gamma ray sources [ICRP 38, 1983]. Later, Radium was found to be less than ideal for the purposes of beta radiation in radiotherapy used for certain diseases of the eye, and a number of the artificially produced radioactive isotopes were preferred. Two of these were Ruthenium 106 (Ru-106) and Cerium 144 (Ce-144), suggested by Freundlich (1949) and later developed by Haybittle (1953) [Sinclair & Trott, 1956].

These beta ray sources were found to be more effective than Radium-266 (Ra-266). This led Friedell, Thomas and Krohmer (1951) to model and described the use of plaques. Their model was using the fission product material Strontium-90 (Sr-90), with its daughter radionuclide Yttrium-90 (Y-90). A number of radioisotopes are now available which allow for a more desirable beta ray dose distribution than Radium. Among all the beta emitters available, Sr-90 was found to be most effective and compared well with the beta radiation administered by the Radon beta-ray applicator. Such ophthalmic applicators have been used for treatment of superficial eye disorders for many years now, because they have the required characteristics and they satisfy the criteria for element selection in beta therapy. These criterias are sufficient long half life, unaccompanied gamma rays, sufficient energy, and suitable chemical characteristics. Radium is no longer

used for clinical applications. [Friedell *et al.*, 1950; ICRP 38, 1983; Sinclair & Trott, 1956]

Some of the reasons that led to the selection of Sr-90 are the following [Friedell *et al.*, 1950; Kearsley *et al.*, 1988; Maage, 2002; Reft *et al.*, 1990; Selman, 1976; Sinclair & Trott, 1956; Thomas *et al.*, 1962]:

i) It has long half-life.
ii) It decays to Y-90, which emits energetic beta-particles which are suitable for biological purposes.
iii) Beta rays from the Sr-90 + Y-90 decay scheme have short range of 0.8 cm to 1.2 cm in human tissue.
iv) There is no accompanying gamma-radiation (pure beta emitter), thereby simplifying protection.
v) It has suitable physical and chemical properties, such as ease of manipulation, purity and high specific activity.
vi) It does not require frequent refilling.
vii) It is free of gaseous decay products.
viii) It delivers 100% dose in most of the superficial layers, while underlying tissues and lens receive a small dose, because of relative fall-off in dose over a few millimetres.
ix) The treatment procedure is simple and quick. However, patient co-operation is essential in maintaining the eye position constant. Thus, the application is rapid and simple. [Kirwan *et al.*, 2006].

The great advantage of the Strontium-90 eye applicator is that Sr-90 is a pure beta emitter, and the handling and storage are relatively simple and nonhazardous [Fraser & Naunton, 1961]. One of the reasons for developing Sr-90 applicators was that, they were a superior beta source compared to others, their focal nature of application reduces the risk of overdose and both dosimetry and area treated can be controlled accurately [Kirwan *et al*., 2003; Thomas *et al.*, 1962].

The first plane plaques or applicators were described by Friedell *et al*. (1951, 1954). The dosimetry of plane plaques has been extensively studied and reported [Supe *et al.*, 1975]. After unsatisfactory results using the small moulds (mixture of 50% P-32 and 50% Bakelite) which replaced the Radium beta ray applicator, a shell in the shape of a spherical cap was developed. This has proved very satisfactory, and was suitable for large and small eyes [Sinclair & Trott, 1956]. These spherical applicators were developed by Lederman (1953, 1956) and Ainslie *et al*. (1962).

The dosimetry of spherical applicators has not been widely studied owing to geometric problems. The construction and dosimetry of the plastic shell and spherical cap shape were described by Sinclair and Trott (1956). In recent years the spherical sources have been improved and metal containing silver has been used to serve both as backing and covering [Supe *et al.*, 1975].

In Friedell *et al.* study (1950) the applicator used consisted of a Lucite capsule which in turn was enclosed in an aluminium capsule. The ends of the Lucite capsule and the aluminum capsule were very thin (0.25 mm) to allow maximum beta rays to escape from the bulb. Strontium was introduced into the Lucite capsule in the form of a chloride solution. The aluminum covering of the Lucite provided additional strength and support. The calcium chloride was added to remove any moisture in the applicator; this also keeps the Strontium Chloride chemically inert and prevents corrosion.

Originally Perspex (Polymethyl Methacrylate) and later Polythene (Polyester) were used as materials for the shell, and strontium foil was embedded in them such that the front face was at a depth of about 0.5 mm. Different shapes and sizes of the plastic shell and strontium foil layer were made up [Sinclair & Trott, 1956].

Plastics are no longer used as backing material [Supe *et al.*, 1975]. Although, during the first stages of designing the spherical plastic cap applicators the advantages of Perspex had to be weighed against its known liability to break down under irradiation. In practice, following the increase in discolouration, the surfaces of some of the applicators

developed cracks after about 12 months of use. Although, Sisman and Bopp (1951) reported a serious breakdown of Polymethyl Methacrylate after a significant exposure, Linder (from Radio Corporation of America) suggested that Polystyrene, Polyester and Polyethylene were superior to Polymethyl Methacrylate. During 1956 these materials suggested by Linder were still being used clinically for applicators [Sinclair & Trott, 1956].

In the years before 1960, these applicators had a plastic covering but as this tended to crack it was replaced by a silver covering, and since then no problems have been experienced [Fraser & Naunton, 1961].

The first commercially available Sr-90 + Y-90 applicator was marketed by Tracerlab (model RA-1) in 1950. Subsequently, all manufacturers adopted a similar geometry for these applicators, with an activity of 2GBq, source diameters 10 mm to 14 mm mounted on the end of an approximately 15 cm-long shaft, with an approximately 10 cm diameter plastic shield mounted on the shaft [Soares, 1995]. In 1969 the source manufacturing and marketing of Tracerlab was sold to International Chemical and Nuclear (ICN), which continued to sell sources until the late 1970's under the name ICN/Tracerlab [Soares, 1995].

The first US competitor Tracerlab encountered was the Atlantic Research Corporation (ARC), which began marketing sources during the 1950s. Their source (Type B1), varied somewhat from the Tracerlab model in that the source diameter was smaller (10 mm as opposed to 13 mm), and it was encapsulated in silver rather than in stainless steel. It was also pivoted and the shield was free to slide along the shaft. ARC marketed these sources directly until 1969, when they sold the rights to Atomchem which marketed the B1 type sources until the late 1970s [Soares, 1995].

In Great Britain, the Radiochemical Centre at Amersham developed a fission product Sr-90 + Y-90 bonded in thin silver foils in 1952. Amersham introduced the planar applicator (model SIA 20) in 1975, and originally were producing only concave devices

[Sinclair & Trott, 1956; Soares, 1995]. The original Sr-90, foil-bonded in silver was covered with Polythene plastic to a thickness of about 0.5 mm, which is sufficient to stop the low energy beta-particles from the source Sr-90. The back of the foil was usually covered with a layer of silver to absorb all radiation [Johns & Cunningham, 1983].

During 1957, Mead and Robertson designed a tubular applicator. This applicator was pivot-mounted on the end of a long handle, and was placed on the anaesthetized eye surface such that the operational field could be seen within the circle made by the applicator. A flat Sr-90 plate was then seated on a narrow rim at the top of the applicator, in order to maintain the treatment distance of 5 mm between the plate and the eye surface, measured along the axis of the applicator [Kearsley *et al.*, 1988]. The tubular applicator had the unique advantage of providing the means of viewing the area to be treated so that the eye movement did not result in a geographical miss of part of the operation field.

During the 1960s and 1970s, manufacturers of applicators increased rapidly in the U.S. Between 1967 and 1976, 3M Corporation manufactured sources (model 6D1A) which were distinguished by the presence of screw threads on the source head for attaching Castroviejo field-shaping masks [Soares, 1995].

Between 1976 and 1983, New England Nuclear (NEN) manufactured sources (model NB-1) very similar to the model B-1 sources marketed earlier by ARC. Isotope Products Laboratory (IPL) manufactured sources during the period 1967 to 1976, selling some directly but marketing most of them through Nuclear Associates, which ceased selling sources in 1978. Other marketers or manufacturers of this period included Technical Operations and Manning Research, neither of which sold sources after the 1960's [Soares, 1995].

Strontium sources occurred in various chemical forms such as Strontium Carbonate ($SrCO_3$) bonded in silver foil. This source is regarded as an older source (1958), encapsulated in 50 mg/cm^2 silver plus 0.1 mm steel and made by Buchler-Amersham to

meet the ISO criteria [Pruitt *et al.*, 1988; Haybittle & Barber, 1973]. As already shown Strontium was introduced into the Lucite capsule in the form of a chloride solution, thus a Strontium Chloride source was used in this applicator.

The tubular applicators manufactured by Mead and Robertson (1957) were made with the sources Strontium titanium ($SrTi_2$), and Radio Chemical Centres Amersham were offering beta-ray sources made of Strontium titanate ($SrTiO_3$) bonded in plates of aluminium by 1972. The front face of the source comprised 27 $mg.cm^{-2}$ aluminium covered by 40 $mg.cm^{-2}$ of stainless steel [Haybittle & Barber, 1973]. There was also a $SrTiO_3$ source of 5 mm in with a glazed surface, backed by 3.5 mm ceramic (Al_2O_3) and covered with 100 $mg.cm^{-2}$ of titanium, made by Amersham to meet ANSI criteria [Pruitt *et al.*, 1988]. AB Atomenergi, Studsvik (Sweden) manufactured a Strontium sulphate ($SrSO_4$) source, with inner and outer diameters of 0.62 mm and 1 mm respectively with length 4.4 mm, and having a shutter that could move to cover the Sr-90 + Y-90 source [Ruden & Bengtsson, 1974].

The plane circular source used in the study of Chhabra (1962) was fabricated by the U.S. Radium Corporation in early 1955. It incorporated Sr-90 in the form of Strontium sulphate ($SrSO_4$) bound within a gold foil, which on the treatment side is set behind a Monel protective window. Of the ophthalmic applicators available, planar Sr-90 + Y-90 sources are used mainly in the U.S. for clinical purposes. A small number of concave applicators do exist and they are used mainly for technical purposes. Curved applicators, such as ^{106}Ru + ^{106}Rh (Rhuthenium-106 and Rhodium-106), are commonly used clinically in Europe for more deep-seated lesions [Soares, 1992]. This illustrate that applicators come in different shapes such as square, circular, and special shapes like planar and concave are for ophthalmic treatments [Young, 1983].

In the past there were several manufacturers of these sources, but during the 1990s only one commercial vendor existed, namely Amersham International. This was the only remaining company (vendor) to manufacture Sr-90 + Y-90 ophthalmic applicators [Ali & Khan, 1990; Gleckler *et al*., 1998; Reft *et al*., 1990; Soares, 1995]. According to the NCS

report 14 (2004), Amersham International has since stopped manufacturing the beta-ray sources. This means there are no more manufacturers of sources, including the Sr-90 + Y-90. Applicators in use today are often more than 20 years old but new ones are no longer commercially available.

4.3 Description of the standard eye applicator

The standard eye applicator is a planar, flat disk, cylindrical metallic rod mounted with a flat distributed 0.01 cm thick Strontium Carbonate ($SrCO_3$) source incorporated in 50 mg/cm^2 silver foil, as shown in Figure 4.1 below. The exit window is composed of 0.01 cm thick 316L stainless steel. Behind the stainless steel foil is a gap of 0.07 cm deep and 0.92 cm in diameter. There is a silver foil disc, which is 1 cm in diameter. It consists of silver face with 0.005 cm thickness, and then a 0.035 cm thick layer of silver backs the $SrCO_3$ source [Maage, 2002; Soares *et al*., 2001].

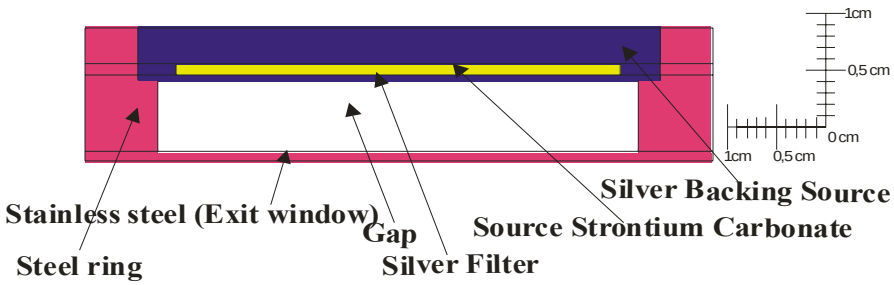

Figure 4.1: Standard eye applicator (SIA.8975).

4.4 Medical Applications

Many international protocols [ICRU 72, 2004; NCS 14, 2004], believe that the best beta-ray source for therapeutic applications dating back to the 1950s is the Sr-90 + Y-90 eye applicator which was firstly used for treatment of lesions of the eye. The Sr-90 source was first described and used clinically by C.I. Thomas and H.L. Friedell. In 1950, it was suggested for a variety of uses, especially in the treatment of ophthalmic diseases. Various morbid conditions of the eye, including superficial tumours, vernal

conjunctivitis, tuberculosis, corneal vascularisation, postoperative treatment of pterygia, and tumours of the cornea and eyelid, have been treated with Sr-90 eye applicators over the past five decades. Although, initially these applicators were only used for epibular malignant melanomas and corneal vascularization, they have also been used in preliminary studies for the treatment of macula degeneration [Hokkanen *et al.,* 1997; Kirwan *et al.*, 2003; Supe *et al.,* 1975; Thomas *et al.*, 1962].

Ruthenium (Ru-106) beta-ray applicators may also be used in the treatment of malignant melanoma of the uvea [Hokkanen *et al.,* 1997]. Sr-90 eye applicators can be used in the treatment of squamous cell carcinoma (SCC) of the conjunctiva. The SCC is a very rare tumour and appears as a slightly raised, gelatinous or white plaque at the cornea-scleral limbus, and is well defined in cattle and horses. This tumour might cause visual loss, local pain and the development of loco-regional metastasis. Since 1960 at the Queensland Radium Institute (Australia), SCC has been treated by delivering a dose in a single fraction to the post-operative bed, using the stand-off applicator for small lesions or the larger cup-shaped applicator for larger lesions. The enucleation is recommended for locally advanced or recurrent lesions [Kearsley *et al.*, 1988].

Concave sources can also be used for the treatment of pterygia; they are generally of lower activity than the planar sources. They are preferred by some physicians because of the large treatment area available. The available sizes range from 9 mm to 23 mm in diameter with a 10 mm or 15 mm radius of curvature [ICRU 72, 2004].

It is possible to design an eye applicator to treat the whole of the cornea or a part of it. The choice of an eye applicator depends mainly on the height of the tumour apex: only small tumours (height < 6 mm) are treated with Sr-90 beta-ray applicators [Hokkanen *et al.,* 1997].

In 1953, the first clinic was opened to study treatment with beta rays [Fraser & Naunton, 1961]. Beta-ray applicators are useful in medicine and biology as convenient sources with which to irradiate tissue to a depth of a few millimetres, while sparing deeper tissues [ICRP 38, 1983]. The beta-particles emitted by radionuclides can not be used in the

treatment of deep-seated tumours by surface application, because they have a short mean range of penetration.

The fibrovascular proliferative tissues can cover the cornea and cause visual disturbance, and possibly resulting in blindness [Oliveira & Caldas, 2005]. From the Barbados, Baltimore and Salisburg clinical studies it was established that black participants have twice much blindness than white participants, due to glaucoma. Glaucoma is described as the second most common blinding condition. Also the greater rates of pterygia in black participants were associated with African ancestry, age, fewer years of education, outdoor job location. Approximately one-fourth (25%) of black participants in those studies had pterygia and 10% of whites [Kirwan *et al.,* 2006; Viani *et al.,* 2008]. Although, blindness caused by cataracts is reversible, blindness caused by glaucoma is not [Kirwan *et al.*, 2006].

Pterygium is defined [Gleckler *et al.,* 1998; ICRU 72, 2004; NCS 14, 2004; Viani *et al.,* 2008] as the presence of raised fleshy growth that crosses the limbus, and encroaches on the clear cornea or having a history of pterygium surgery. It can also be defined as progressive, triangular, wing shaped, wedge growth of fibrovascular tissue and encroachment of the bulbar conjunctiva tissue onto the sclera of the human eye. It typically occurs medially on the ocular surface, extending horizontally from the nasal conjunctiva on to the cornea. It is classified as conjuctival degeneration, benign peribulbar lesion that mainly occurs at the nasal or temporal limbus, and can progress onto the cornea where it obstructs vision.

Pterygium causes irritation, photophobia, cosmetic problems, and visual loss from corneal astigmatism and growth over pupil. The incidence rates are high in hot, dry, dusty regions of the world but more commonly occur in the tropical regions of places such as USA, Brazil, Southern Africa and coastal regions of Japan and Australia. This lesion is related to ultra-violet exposure, and especially sun exposure [Kirwan *et al.,* 2003; Viani *et al.,* 2008].

In general, beta irradiation sources are also employed in brachytherapy, including ophthalmic, dermatological, intracranial and intravascular procedures because of limited range, and to achieve high rates of tumour control in patients with conjunctival carcinomas and conjunctival lymphomas or any benign diseases and malignant diseases. Moreover, Sr-90 + Y-90 sources are used in routine dating and radiation dosimetry, when luminescence readers and TLDs are calibrated [Oliveira & Caldas, 2005; Young, 1983; Viani *et al*., 2008].

The general aim of beta-ray dosimetry in radiation protection is to provide dosimetric information, which will help to keep any harmful effects of beta rays within acceptable limits. In the event of serious overexposure it may assist in medical treatment and prognosis [ICRU 56, 1997].

Beta-ray emitters may present hazards in a wide variety of circumstances, such as around nuclear reactors, particle accelerators, nuclear fuel processing facilities, as well as in biomedical applications of radioactive isotopes and research. Beta-ray emitters used for therapy also present external hazards [ICRU 56, 1997]. In the last half of 20^{th} century Sr-90 sources have gained wide acceptance, because of their long life and relative freedom from contamination hazards [Chhabra, 1962].

4.5 Ophthalmic treatment technique

A well known example of such ophthalmic treatments is the use of planar Sr-90 + Y-90 sources for the treatment of pterygia. The treatment consists of manual application of the source to the surface of the area where the pterygium had been removed. Typical treatment times might be shorter than one minute; such treatment greatly limits the chances of recurrence of the original growth [ICRU 72, 2004].

Usually the total dose to be delivered to the surface is fractioned in several radiation therapy sessions, and the applicator is positioned manually in contact with the area where the pterygium has been removed [ICRU 72, 2004]. Initially in the treatment of pterygium, the high dose of beta radiation was applied without surgical excision, the main aim being

to induce regression of the lesion. The administration after surgery was widely adopted with subsequent reports indicating the low recurrence rate.

The treatment combination of surgery and beta radiation was showed to give better results than the standard option. Many developing countries use surgery as a standard means of managing glaucoma [Kirwan *et al.,* 2003, 2006]. A high dose delivered at a high rate is radio-biologically effective in a cell kill; hence it takes a very short period to shrink a tumour. Also, the treatments should be completed more quickly.

The applicator is placed on the conjunctiva immediately following surgery rather than on the bare sclera. This reduces the dose received by the sclera, as a significant proportion of the radiation is attenuated passing through the conjunctiva (approximately 30% assuming a thickness of 1 mm) [Kirwan *et al.*, 2003].

The principle of holding a moulds radioactive source in contact with the lesion has been abandoned, where the radioactive mould (50% phosphorous and 50% bakelite) was held in contact with eye lesion in an angled metal applicator; instead, the idea of radioactive contact lens was adopted [Sinclair & Trott, 1956,] and had proved to be satisfactory and suitable for large and small eyes. All treatments have been administered by the direct-contact technique to the lens, since this was developed and this is still the only manner in which the actual dose to the eye tissue can be carefully regulated [Friedell *et al.*, 1950]. Dosage can be delivered to the surface area by placing the applicator manually in contact or near the area of the eye to be treated.

In practice, the eye is irradiated in several (weekly) fractions of dose, usually about 8 Gy to 10 Gy per fraction, and strontium sources with a concave or flat surface can be used for the treatment. The treatment times may vary from 20 seconds to 25 seconds, depending on the dose rate. The treatment period varies from 2 weeks to 14 weeks, depending on the activity of the source [NCS 14, 2004].

As the use of beta radiation may be especially suitable for use in the developing world, particularly in Africa, during 1999 up until 2002, Kirwan *et al*. (2006) started randomized trials of beta radiation in South Africa. During the trial study the β radiation was found to have a beneficial effect on intraocular pressure, and was also a useful adjunct to glaucoma drainage surgery. Reduction of intraocular pressure in the glaucoma patient is accepted as beneficial. Some evidence also suggests that the lower the intraocular pressure, the greater the protection that is afforded [Kirwan *et al.*, 2006].

Although β radiation could cause cataracts, it has extremely rapid attenuation, and the calculated amount of radiation reaching the germinal epithelium of the lens could be less than the minimum dose reported to cause cataracts. Thus, cataractogenesis is not a problem during the irradiation with the Sr-90 eye applicator. Cataracts are believed to originate in the radiosensitive germinative epithelium [Viani *et al.,* 2008; Gleckler *et al.*, 1998].

Post-operative radiation treatment of the sclera after pterygium excision is a common therapeutic procedure [Gleckler *et al.*, 1998]. Beta radiation has been used in management of pterygium, with the local application of a Sr-90 source to prevent recurrence [Kirwan *et al.*, 2003]. The use of encapsulated beta-ray sources for postoperative irradiation in the treatment of pterygium and other conditions has been described in many studies.

There are many types of surgical modes, such as excision, transplantation, bare sclera technique, keratectomy, the use of conjunctival flaps and autografts. However, the “bare sclera” is the most common. After surgery, therapy includes postoperative beta irradiation to the bare sclera and this is sufficient to reduce the potential regrowth. For simple surgery alone, recurrence rates to bare sclera are generally about 30% to 70% after completion. These recurrence rates drop to 0.5% to 33% with the use of the Sr-90 + Y-90 ophthalmic applicator technique. In this method the conjunctival edge near the limbus is sutured directly to the sclera tissue, leaving a bare sclera area after a simple excision of

pterygium. Surgery is not recommended for small pterygia [Gleckler *et al.,* 1998; Kirwan *et al.*, 2006; Viani *et al.,* 2008].

During a typical pterygium brachytherapy procedure, a dose is delivered to the area of the sclera from which the pterygium was excised, using beta-particles, by locating the edge of the applicator near the limbus. The limbus is located where the lens has the least amount of natural shielding; normally about 2 mm deep. Beta radiation deposits most of its energy within the first few millimetres of the tissue. While the whole lens dose remains well below the cataract threshold, the region of the lens nearest to the applicator receives a significantly higher dose than the rest of the lens [Gleckler *et al.*, 1998].

The long half-life of Sr-90 sources is clinically beneficial in the sense that the stability of source output may endure for some time, as long as care is taken in their use. The emitter may have a long working life (more than 20 years) with only occasional recalibration. The sources are stable and easily stored, with no refrigeration required [Kirwan *et al.*, 2003].

According to the literature [NCS 14, 2004], the use of the Sr-90 + Y-90 eye applicator is particularly attractive because the eye lens, with the edge 2 mm to 3 mm beneath the surface, is very sensitive to radiation and may suffer cataractous changes. Despite a larger dose of radiation to the lens, cataracts are not common [Friedell *et al.*, 1950; Kirwan *et al.*, 2006].

The beta-ray sources' speciality has been based on their physical characteristics, such as the short range of beta-particles resulting in rapid dose fall-off with distance, and lower doses to the neighbouring healthy tissues and to staff. The useful distance for treatment range is up to a few millimetres for beta rays. Such short distances are typical of treatment to the eye and skin [ICRU 72, 2004]. Hence, the procedure is very safe.

Such a low penetration of beta-particles from radioactive nuclides gives physicists the advantage of shielding the beta emitters with material of low atomic numbers, such as

Perspex, Lucite or Teflon materials. It must be kept in mind that the shielding of betas with high atomic number materials such as lead is to be avoided, since the interactions between the two can cause secondary electrons which might lead to bremsstrahlung radiation. Being photons, bremsstrahlung radiation is more penetrating and more difficult to shield than the original beta radiation. Operators can prevent exposure to beta rays by facing the applicators away from their bodies.

4.6 The proposed Teflon-encased eye applicator

The Teflon-encased eye applicator model consists of a concave Teflon cylinder of 1.5 cm height, 2 cm wide. The applicator is screwed onto a stainless steel 316L shaft, which is 15 cm long with radius 0.3 cm. This shaft compresses a spongy plug, backing a cylindrical volume Strontium Chloride ($SrCl_2$) source of 0.05 cm thick and 0.25 cm radius. The Teflon is 0.1 cm thick between the Teflon surface and the source. Thus, $SrCl_2$ is sealed into a shallow Teflon box as shown in Figure 4.2. The back and sides of the Teflon-encased eye applicator are thick enough to absorb the lower beta rays. The front surface is made thin enough to allow the beta particles to escape. Containers often allowed some of the beta particles to escape in great quantities to give an excessive dose in the immediate neighbourhood of the source [Johns & Cunningham, 1983].

The use of the concave shaped surface is to fit the contour or shape of the eye [Reft *et al.*, 1990], thus to have good contact with the cornea. Therefore the concave shape also gives a more uniform contact and focusing effect, which increases the depth dose along the central axis of the source. It is also important to use the smallest applicator consistent with the treatment of the disease not only to reduce the radiation to unaffected parts of the eye, but also to irradiate the diseased area adequately as the fall off of radiation is more rapid [Davelaar *et al*., 1992; Selman, 1976; Sinclair & Trott, 1956].

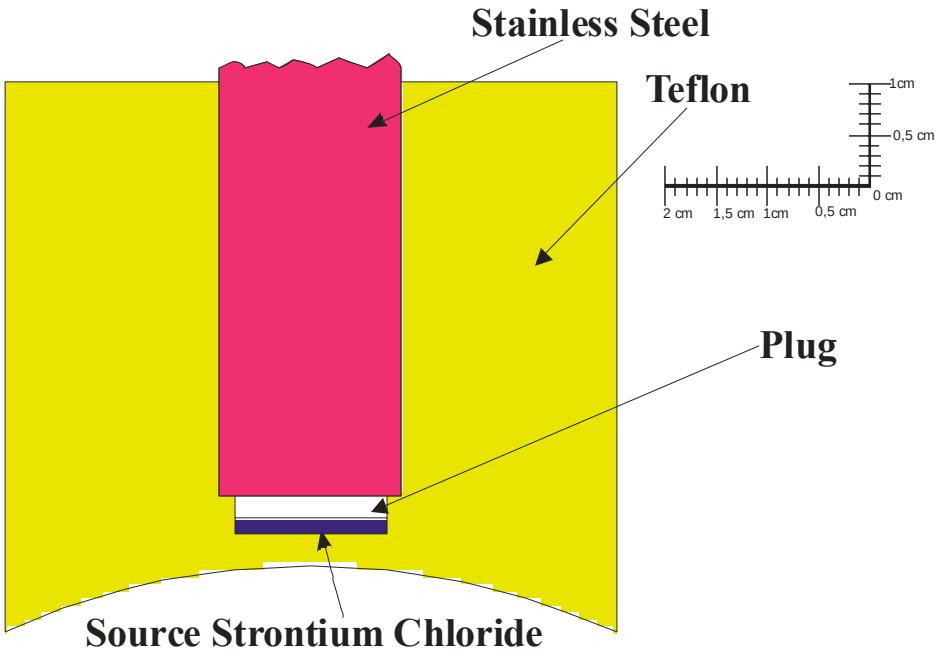

Figure 4.2: Teflon-encased eye applicator.

The Teflon-encased eye applicator differs from the standard eye applicator in terms of the material used. The standard eye applicator is made of cylindrical metal (316L Stainless steel) of 0.175 cm long, with 0.6cm radius, source $SrCO_3$ of radius 0.46 cm and thickness 0.01 cm, active area of 66 cm^2 and 0.01 cm thick, special plastic shield backing in the shaft to protect the operator. The Teflon-encased eye applicator is made from a cylindrical Teflon material of 1 cm radius and 1.73 cm long, source $SrCl_2$ of radius 0.25 cm and 0.05 cm thick, no backing material.

Chapter 5

METHODOLOGY

5.1 Introduction

This chapter outlines the method, the materials and the steps followed in this study. It includes a detailed description of the Monte Carlo simulations performed.

5.2 Materials

The Monte Carlo code employed in this study is MCNP5 disributed by RISCC, version 1.20 running on Linux-based Operating system, and 2.8 GHz Pentium IV processor, 512 MB memory with 120 GB hard drive. This code was used to simulate a Teflon-encased eye applicator, and an elliptical water phantom. Only the simulation was considered in this study.

The Teflon-encased eye applicator model was made out of a cylindrical flat anhydrous Strontium Chloride ($SrCl_2$) source which is the radioactive part of the applicator. This has a 0.25 cm radius and a thickness of 0.05 cm, unless otherwise specified. This concave eye applicator also has a Teflon cylinder with a radius of 1 cm and a length of 1.73 cm, attached by screwing to a stainless steel 316L shaft, with radius of 0.3 cm and a length of 15 cm. For the sake of simulations this was modeled as 3.41cm in length, since from the theory betas can not penetrate the stainless steel. The shaft compresses a spongy plug 0.009 cm thick with a radius of 0.25 cm, backing onto a Strontium Chloride ($SrCl_2$) source in order to keep the source flat.

The densities of the anhydrous source $SrCl_2$, stainless steel 3l6L and Teflon were taken as 3.052, 8.02 and 2.200 g/cm^3, respectively. The phantom material used for this study was water with a density of 1 g/cm^3. The elliptical water phantom was modeled to portray the actual clinical situation, and Figure 5.1 in section 5.4 can be used for reference.

The standard eye applicator [Maage, 2002] employed in this study as a reference, consists of a flat source, which was first calibrated and supplied on 4 December 1986 by Amersham International plc. During the calibration the source had a nominal activity of 1.85×10^9 Bq (50 mci). The measured surface dose rate supplied with the source on 4 December 1986 was 45.57 cGy/s ± 10%. On 25 April 2000, after applying the decay constant to account for the decayed activity of the source, this was found to be 32.95 cGy/s ± 10% and 10% was regarded as the acceptable error [Maage, 2002].

On 25 April 2000 the standard source was recalibrated with the source geometry from Amersham International plc. as initial calibration. This recalibration was done at the National Metrology Laboratory in Pretoria (CSIR) between two sources, SIA.20 (CSIR standard source) and SIA.8975 (MEDUNSA source). The comparison calibration technique was used. The surface dose rate was measured with a photomultiplier tube (PMT) detector with anthracene crystal of 0.3 cm diameter and 0.05 cm thick. The PMT detector was inserted inside the PMMA phantom with density of $1.19 g/cm^3$. The PMT detector was connected to a PC. The sources were position such that there is no air gap between detector and the source. From the measured doses a factor was determined and used to correct for accurate surface dose. The percentage difference between measured and the manufacturer activity was 1.14%.

The decay factor was found to be 0.723139 during the recalibration, and the remaining activity was calculated using a similar equation to equation A8 (Appendix A) below:

$$A(t) = A(0)e^{-\lambda t} \tag{5.1}$$

$$A(t) = 1.85 \text{ GBq} \times 0.723139$$

$$A(t) = 1.338 \text{ GBq}$$

where 1.85 GBq is the value which was quoted by Amersham International plc. [Maage, 2002].

For the purpose of this study, the old type model source SIA.8975 was regarded as the standard source, due to the fact that it was manufactured as an eye applicator and its

dosimetry had been completed. For the Teflon-encased source it was assumed that there was an activity of 1.338 GBq, although the simulations were conducted independent of source activity.

5.3 Simulation of the Sr-90 +Y-90 spectrum

The first step in the process was to determine and verify the spectra of $SrCl_2$ by simulating each of the Sr-90, Y-90 and Sr-90 + Y-90 spectra. These spectra were run in a spherical water phantom with a radius of 20 cm by a combination mode of photons and electrons using 2×10^6 histories, and this was found to be sufficient to cause beta interactions. The input values were taken from the international protocols [ICRU 56, 1997; ICRU 72, 2004]. The source was simulated as an isotropic point source centred in a water phantom, and isolated by a smaller sphere with a 0.05 cm radius. The fluence-rate energy spectrum data were scored using bin energies (0.00 MeV to 2.281 MeV), for tally type F8 in water medium and plotted from the system using MCPLOT [Briesmeister, 1997; X-5 Monte Carlo Team].

The second step was to develop an appropriate model of an ophthalmic applicator encased in Teflon. It was necessary to model the entire ophthalmic applicator, its physical dimensions, and all the materials to be used, with the exception of detailed information about the radiation source [Gleckler *et al.*, 1998]. The source used in this step is a point source, placed in the center of an empty and non material cylinder of 0.5 cm diameter and 0.001 cm thickness. This cylinder was made by surfaces 4, 5 and 6. The verified Sr-90 + Y-90 spectrum obtained from the first step was used as an input for the source. This spectrum was used since the energy spectrum and spatial distribution of the electrons leaving the applicator were unknown. Five cylindrical surfaces (14, 15, 16, 17 and 18) of radius 0.9 cm, positioned from 0.1714 cm to 0.406 cm away from the applicator's concave surface, were modeled. These surfaces were modeled in air, in front of the applicator. The entire setup was isolated from the outside world by enclosing it inside a sphere.

In order to increase accuracy of the calculation, 25×10^6 histories were run with no energy cut-off. The "electron energy spectra" were determined from surface 2 at the back of the applicator up to surface 18 on the cylindrical surface in front of the applicator, by using tally type F1 with 0.00 MeV to 2.281 MeV energy bins. This type of tally calculates the number of particles per MeV crossing each surface. The obtained emitted beta spectra through surfaces were compared by plotting them on the same graph as well as the input spectrum.

5.4 Simulation of the Sr-90 eye applicator with the water phantom

The geometry setup was defined by placing the Teflon-encased eye applicator on the surface of the water phantom (Figure 5.1). The geometry and the material used in the simulation reflect a realistic setup of a Teflon-encased eye applicator with a water phantom. The numbers in Figure 5.1 represent different planes of the applicator and the phantom. The distance between the applicator's concave surface and the phantom was kept at 0.21 cm due to the geometry of the eye applicator (curvature). This was regarded as a vacuum with an importance of 1 to allow the particles to pass through to the phantom [Maage, 2002]. This distance was kept constant for all simulations. The source was also kept 0.1 cm away from the surface of the Teflon for the study, unless otherwise specified. It was assumed that the radioactive material was distributed uniformly in the source core.

The assumption was made that backscatter is negligible from the applicator; hence backing material was not necessary. An area inside the sphere but outside the geometry of the applicator and water phantom was regarded as the vacuum with an importance of zero, to approximate the real clinical treatment situation.

The cylindrical water phantom was made large enough: 0.74 cm in length with a diameter of 2.5 cm, to obtain back scatter and to determine the central axis depth dose rate accurately beyond the range of the particles. Cylindrical cells of dimension 0.02 cm radius and 0.01 cm thickness, directly in the central axis of the source, were modeled in the water phantom. These cells were used to score the energies from the electrons passing

through each central axis cell by tally type 8 (*F8), which reflects energy deposited in each cell in MeV per source particle for all simulations in this section. Thus the surface dose rate was calculated by scoring the energy in the cell directly in the central axis of the source.

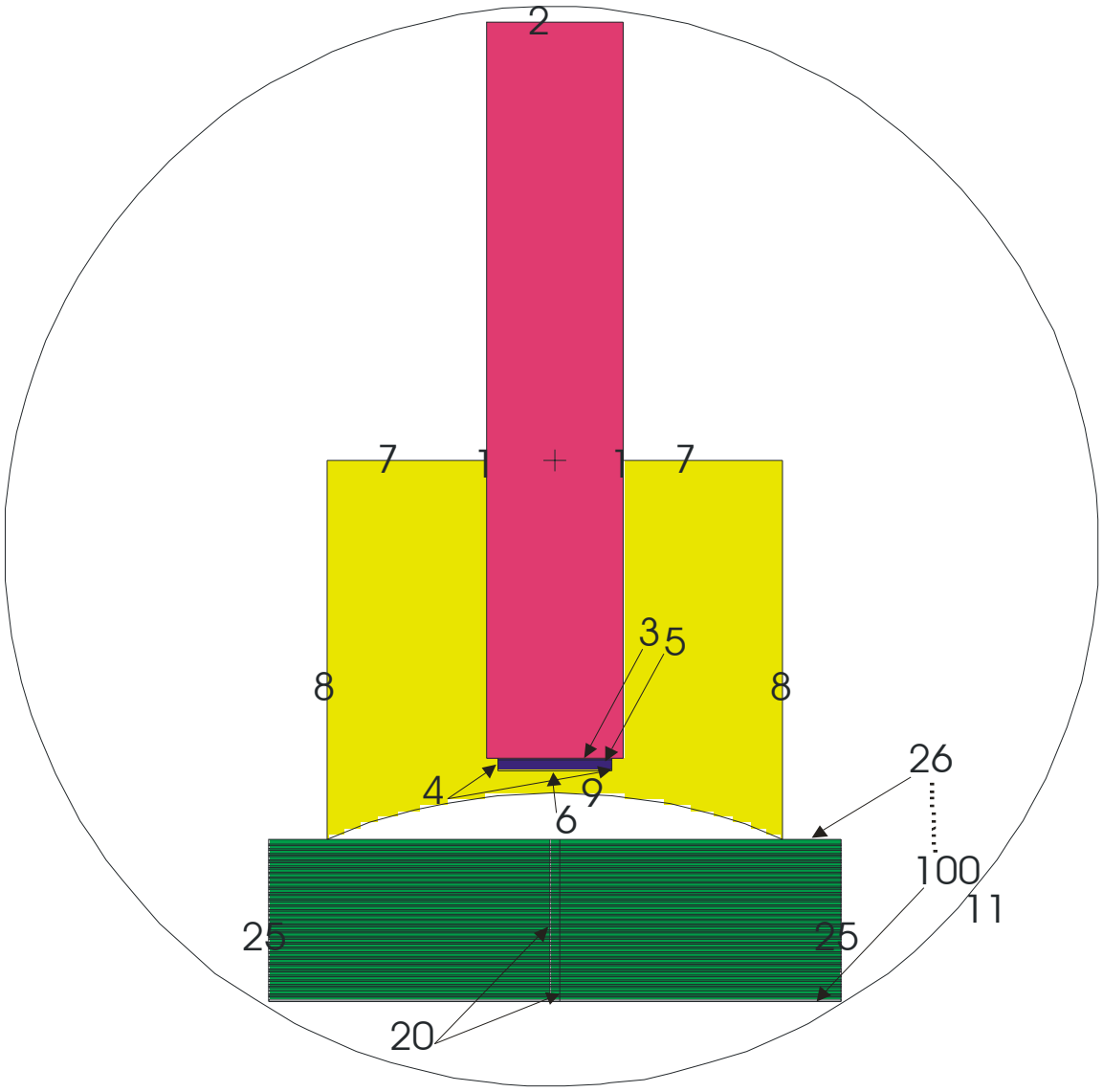

Figure 5.1: MCNP geometry specification setup for the simulation with water phantom.

The simulations for this part were run with 6×10^6 histories using the coupled photon-electron mode. Photons and electrons were tracked until they reached the energy cut-off of 0.02 MeV, so that the low energies could be assumed to be locally deposited, and any secondary particles (knock-on electrons and bremsstrahlung photons) of energy greater

than the cut-off energy were explicitly simulated [Park *et al.*, 2008]. This part of the study was divided into three phases.

In the first phase, the effect of Teflon material on the dose rate was determined by varying the case's thickness and using an anhydrous $SrCl_2$ source of 0.05 cm thickness and with a radius of 0.25 cm. The first run was made without Teflon material between the source and phantom at the surface source distance (SSD) of 0.02 cm. The SSD in this study was taken as the distance between the source and the concave surface of the eye applicator at the central axis of the source. Thus, SSD is the distance the electrons have to pass to reach the surface of the applicator. They also had to pass through the gap between the eye applicator and water phantom in order to contribute in dose rate.

Using a similar setup, Teflon was included and runs were conducted with the following Teflon thicknesses: 0.02 cm, 0.05 cm, 0.1 cm, 0.15 cm, 0.2 cm, 0.25 cm, 0.3 cm, 0.35 cm, 0.4 cm, 0.45 cm and 0.5 cm, in order to determine the central axis depth dose rate. This means that SSD increases with the same values of Teflon thicknesses, as shown also in Table 5.1. The data were obtained for all simulations and plotted graphically with the standard eye applicator data. From these results, the curve of the surface dose rate versus the Teflon thickness was constructed.

In the second phase, the effect of the source thickness on the depth dose rate was checked by determining the central axis depth dose rate, whiles the source thickness varied from 0.001 cm to 0.01 cm and increased by 0.01 cm thickness up to 0.10 cm with a Teflon thickness of 0.1 cm. The data were plotted on the same graph as the data from the standard eye applicator. The surface dose rate curve against the source thicknesses was constructed from the data obtained.

A further step was taken to check the Teflon and source effects by increasing the Teflon material to a thickness of 0.125 cm. The simulations were run with constant thickness, whereas the source thickness varied as follows; 0.04 cm, 0.045 cm and 0.05 cm. The results were compared to the standard eye applicator by plotting them on the same graph.

In the third phase, the effect of the surface source distance (SSD) was studied in the absence of Teflon material. The SSD was varied as follows: 0.02 cm, 0.05 cm and 0.10 cm with source thickness of 0.05 cm. The obtained central axis depth dose rate data were plotted on the same curve as the standard eye applicator results. The surface dose rate curve against the SSD was constructed from these data. The central axis depth dose curves on a semi-logarithmic scale were obtained for all the simulations in each of these phases.

Table 5.1: Input parameters into Monte Carlo Geometry for simulations with water phantom

PHASE	**1**	**2**		**3**
TEFLON (cm)	0, 0.02, 0.02, 0.05, 0.10, 0.15, 0.2, 0.25, 0.3, 0.35, 0.4, 0.45, 0.5	0.1	0.125	0
$SrCl_2$ (cm)	0.05	0.001, 0.01, 0.02, 0.03, 0.04, 0.05, 0.06, 0.07, 0.08, 0.09, 0.10	0.04, 0.045, 0.05	0.05
SSD (cm)	0.02, 0.02, 0.05, 0.10, 0.15, 0.2, 0.25, 0.3, 0.35, 0.4, 0.45, 0.5	0.1	0.125	0.02, 0.05, 0.10

To verify that the applicator was modeled correctly and represents the real applicator, the surface dose rate was calculated on MCNP results and compared to the previous published values [Maage, 2002]. The surface dose rate was calculated at surface cell of water phantom, which is the calculation of the dose to an infinitesimal thickness of water. Also the surface dose rate was assumed to be the dose rate at the surface of the Teflon-encased eye applicator.

Chapter 6

RESULTS AND DISCUSSION

6.1 Results

6.1.1 Introduction

The results presented here are divided into sections that cover the following: verifying the source model; strontium spectra through the central axis of the Teflon-encased eye applicator; the effect of Teflon thickness on the central axis depth dose rate and the surface dose rate; the effect of source thickness on central axis depth dose rate and surface dose rate; and also the surface source distance (SSD) effect on central axis depth dose rate, and the surface dose rate in the absence of Teflon.

6.1.2 Strontium spectra

6.1.2.1 Verifying the source model

Figures 6.1(a) and (b) illustrate the beta energy spectrum of Strontium-90 and Yttrium-90 respectively. Figure 6.2 shows the combination of the beta energy spectrum for Strontium-90 and Yttrium-90, as shown in Figure 6.1(a) and Figure 6.1(b). The dots and dashes on the spectra are error bars on Figures 6.1 and 6.2. The measured relative error ranges from 0.0023 to 0.079, for all spectra. All spectra are expressed in tally per energy (MeV) per particle against the energy (MeV). From Figure 6.2, it is clear that Yttrium-90 becomes dominant at energy of 0.5 MeV.

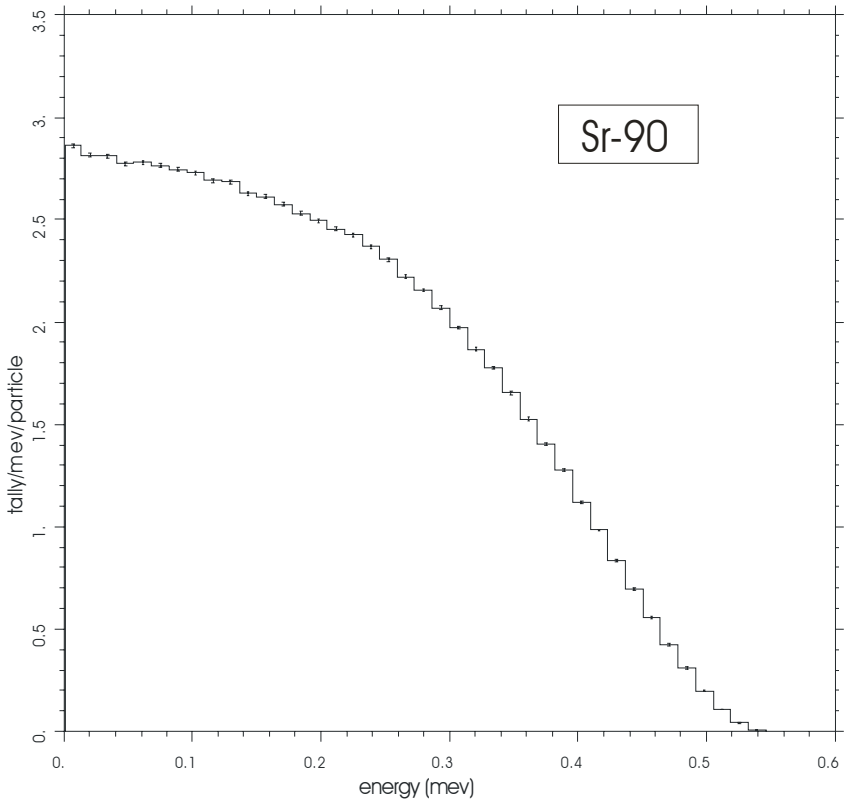

Figure 6.1(a): The beta energy spectrum from Strontium-90.

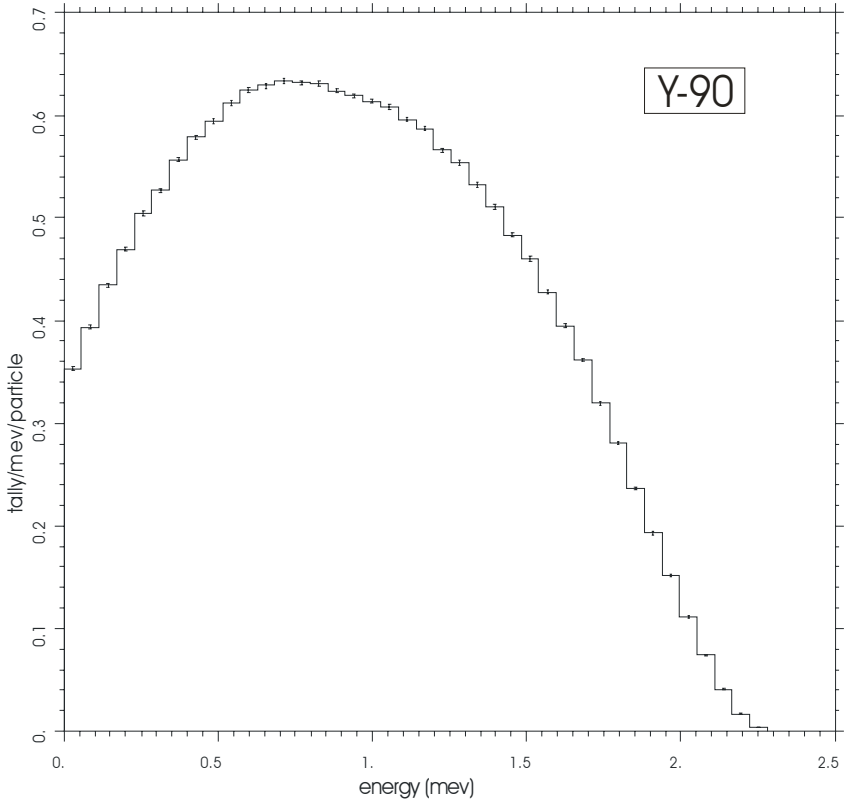

Figure 6.1(b): The beta energy spectrum from Yttrium-90.

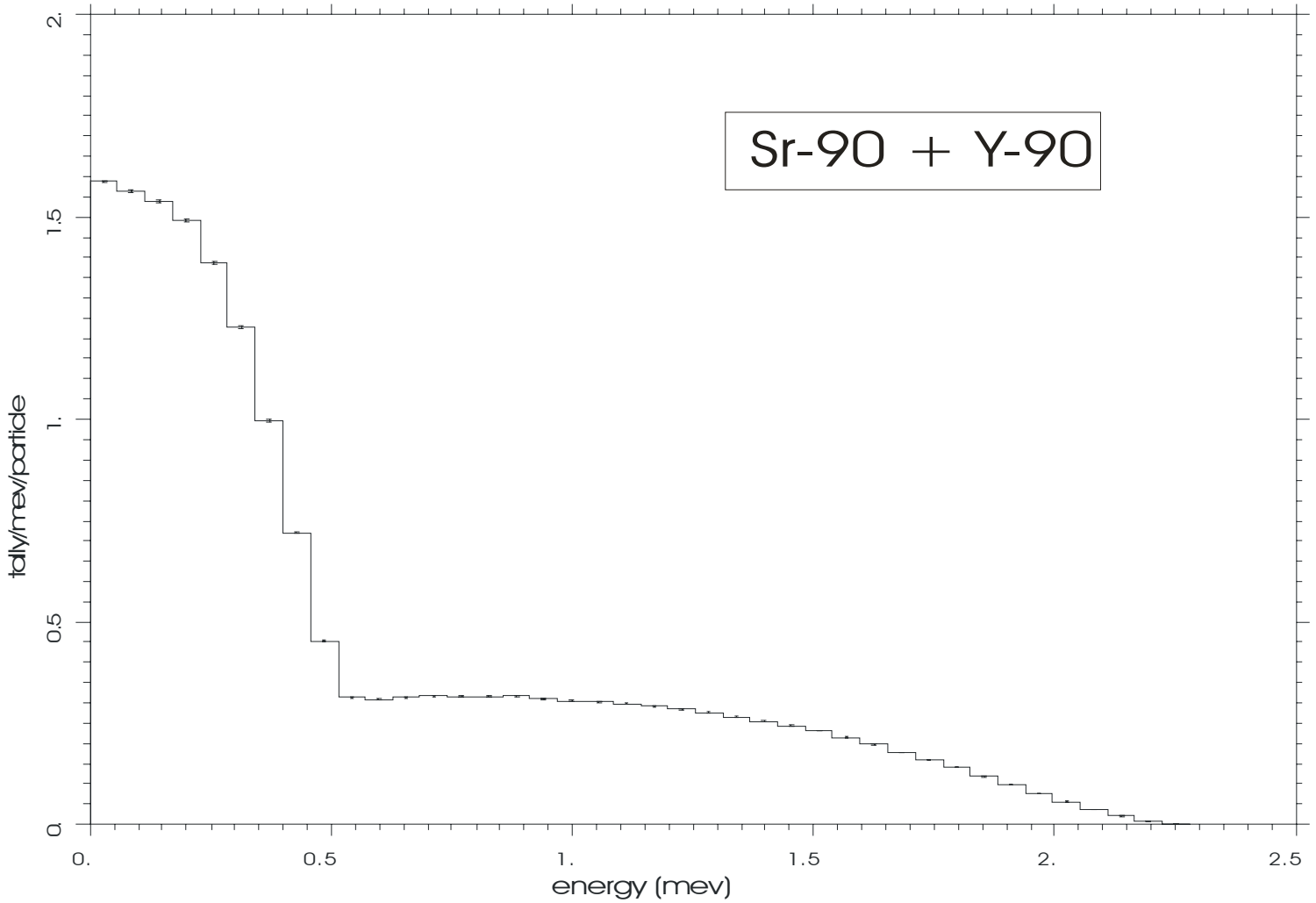

Figure 6.2: The combined beta energy spectrum of Strontium-90 and Yttrium-90.

6.1.2.2 Strontium spectra through the central axis of the Teflon-encased eye applicator

Figure 6.3 reflects the input spectrum of Sr-90 + Y-90 plotted together with the emitted number of electrons through various surfaces, 2 up to 9 on the central axis of the Teflon-encased eye applicator, and surfaces 14 up to 18 on the front side of the applicator. The surfaces are indicated in different colours, as reflected in the key.

Figure 6.4 illustrates the behaviour of electron energy spectra on the surfaces calculated on the back side, and on the front of the Teflon-encased eye applicator. The surfaces are represented by different colours and symbols, as indicated in the key. Figure 6.4 is an expansion of Figure 6.3.

Table B.1 reflects the percentage difference between the electron energy spectra as they pass through the surfaces inside, at the back and at the front of the Teflon-encased eye applicator on the central axis. These surfaces are numbered.

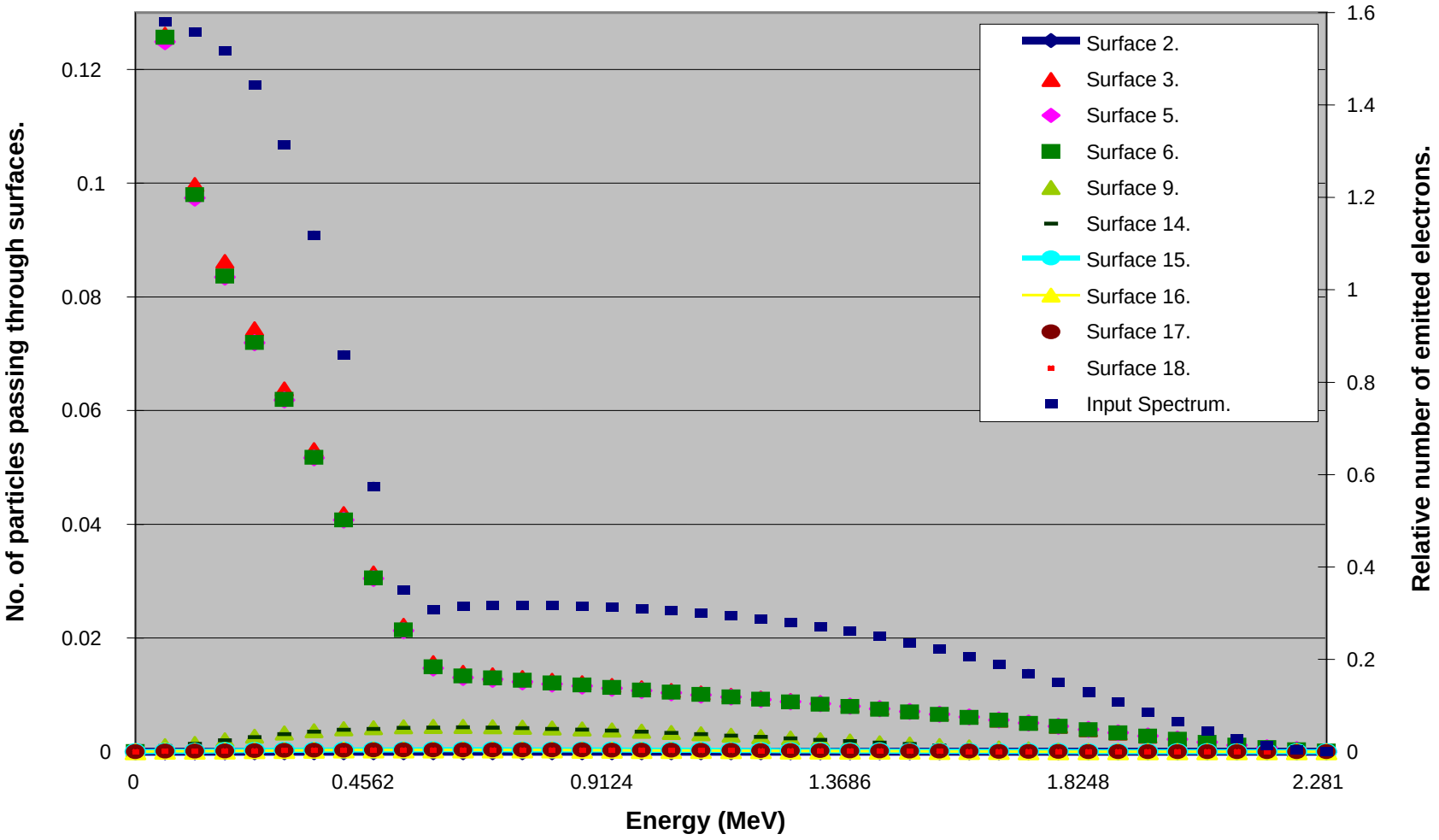

Figure 6.3: Electron energy spectra as a function of input spectrum of Sr-90 + Y-90.

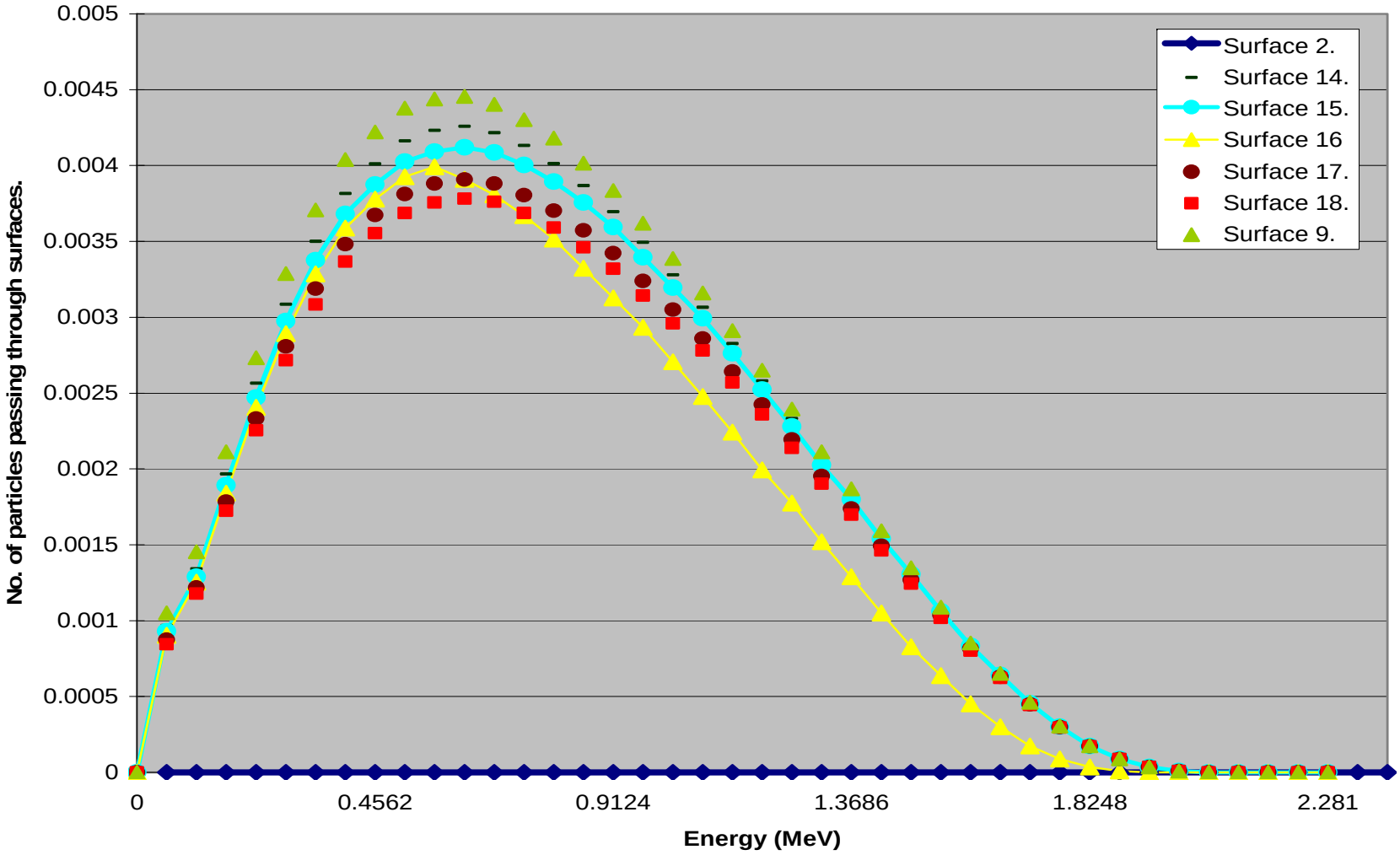

Figure 6.4: Electron energy spectra through applicator and the front surfaces.

6.1.3 Central axis depth dose rate and surface dose rate in water

6.1.3.1 Effect of Teflon thickness on central axis depth dose rate

Figure 6.5 illustrates the central axis depth dose rate curves for a source of thickness 0.05 cm, with various thicknesses of Teflon material ranging from 0 cm to 0.4 cm. The thicknesses are indicated by different colours and different symbols, as listed in the key. The Figure also includes the central axis depth dose rate curve of the standard eye applicator.

Figures E.1 (a) to E.1 (l), illustrate the central axis depth dose distribution curves at the various Teflon thicknesses as given by tally per particle versus cell binned, in semi-logarithmic scale. The lines in these curves are error bars.

In subsection 6.1.3.2, Figure 6.6 illustrates the decreasing tendency of the surface dose rate at the water surface as the Teflon thickness was increased at a constant source thickness of 0.05 cm. A solid, exponential, fitted line was defined by the equation given in the data label graph.

Table B.2 shows the percentage differences between surfaces in the water phantom when the Teflon material of the applicator is increased, and compared to standard eye applicator. The numbers shown in Table B.2 are Teflon thicknesses in centimetres.

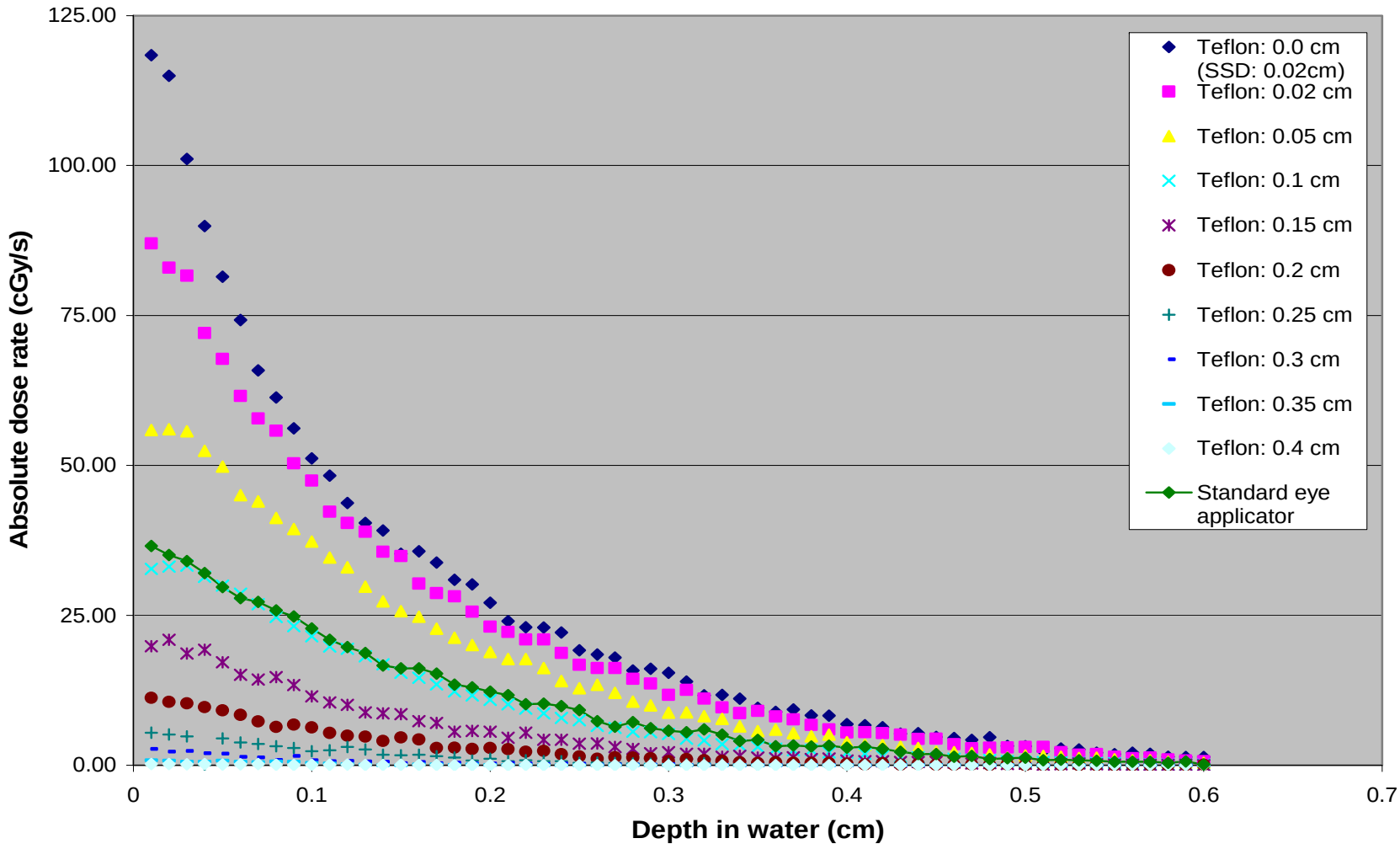

Figure 6.5: The central axis depth dose rate curves of varied Teflon thickness with 0.05 cm $SrCl_2$ and standard eye applicator.

6.1.3.2 Effect of Teflon thickness on surface dose rate

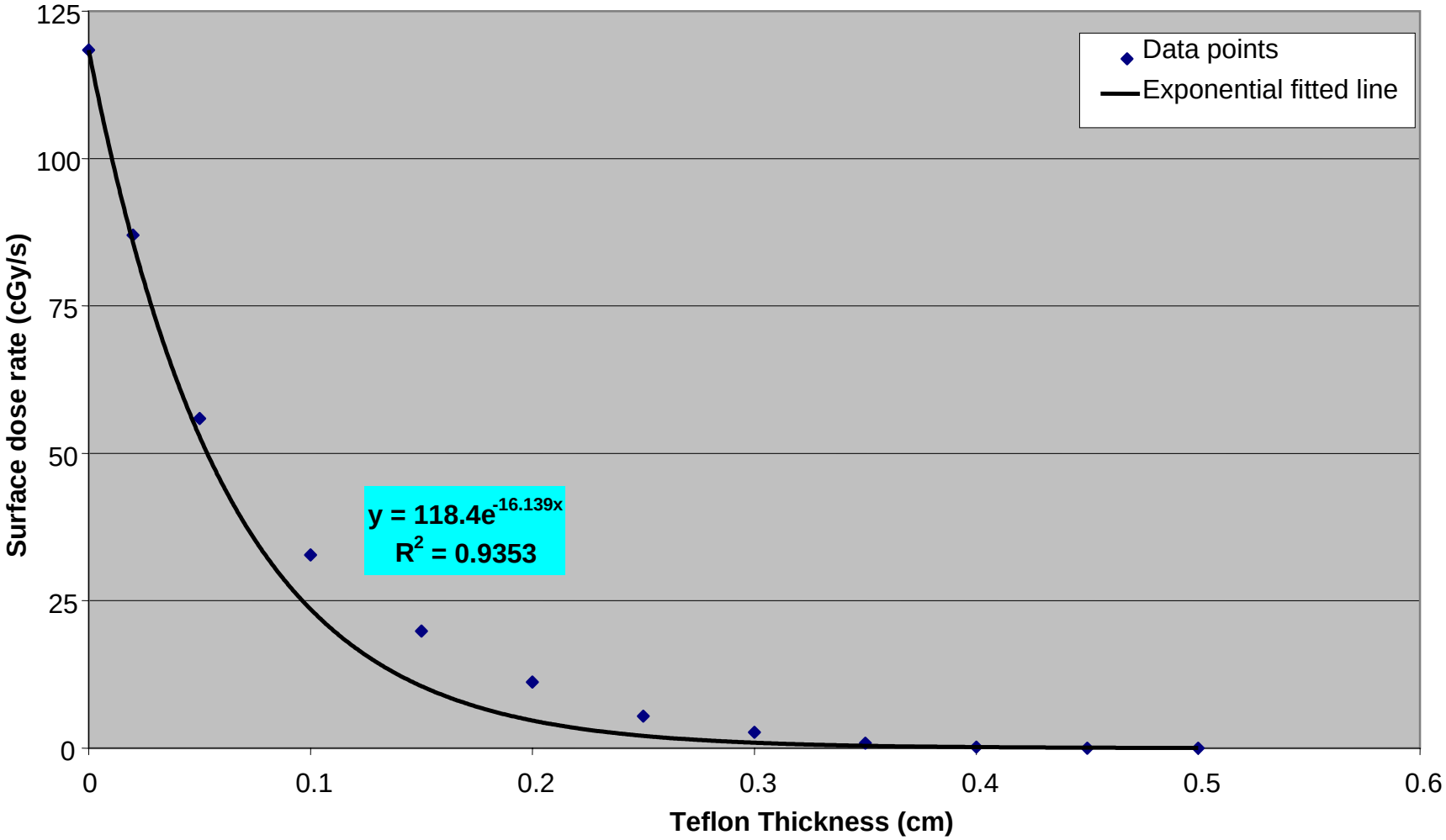

Figure 6.6: Surface dose rate as a function of Teflon thickness.

6.1.3.3 Effect of source thickness on central axis depth dose rate

Figure 6.7 shows the central axis depth dose rate curves of electron energy obtained in water depths, when varying the source thickness at a constant Teflon material thickness of 0.1 cm. The source thicknesses are indicated by different symbols and colours, as listed in the key.

Figure 6.8 reflects only the curves of the Teflon-encased eye applicator sources closest to the standard applicator curve. This Figure was constructed from Figure 6.7. Figures E.2 (a) to E.2 (l), show the central axis depth dose distribution curves at the various source thicknesses with Teflon of 0.1 cm, and are given by tally per particle versus cell binned, in semi-logarithmic scale. The lines in these curves are error bars.

Table 6.1 reflects the correlation test results and the "S" in the columns signifies the source. Table 6.2 gives the summary of ANOVA F-test results where SS, df, MS, F, P-value and F-critical are sum of squares, degrees of freedom, mean of squares, F-test value, probability of obtaining a result and critical or theoretical value of the test, respectively. Table B.3 indicates the percentage differences between the standard eye applicator and the Teflon-encased eye applicator, with a Teflon thickness of 0.1 cm and source varying from 0.03 cm to 0.05 cm in thickness.

In subsection 6.1.3.4, Figure 6.9 illustrates the surface dose rate in the water phantom as a source thickness is increased from 0,001 cm to 0.1 cm at the constant Teflon thickness of 0.1 cm. A solid fitted linear line is described by the equation in the data label.

Figure 6.10 reflects the central axis depth dose rate curves in water when the source thickness is increased from 0.04 cm to 0.05 cm with a Teflon thickness of 0.125 cm. The source thicknesses are indicated by different colours and symbols, as indicated in the key. The curve for the standard eye applicator is also included for comparison purposes.

Table B.4 shows how the curves in Figure 6.10 are closer to the standard eye applicator spectrum by specifying their percentage differences. The numbers indicate the source thicknesses at a Teflon thickness of 0.125 cm. Figures from E.3 (a) to E.3 (c), show the central axis depth dose distribution curves at the various source thicknesses and Teflon thickness of 0.125 cm, and are expressed by tally per particle versus cell binned, in semi-logarithmic scale. The lines in the curves are error bars.

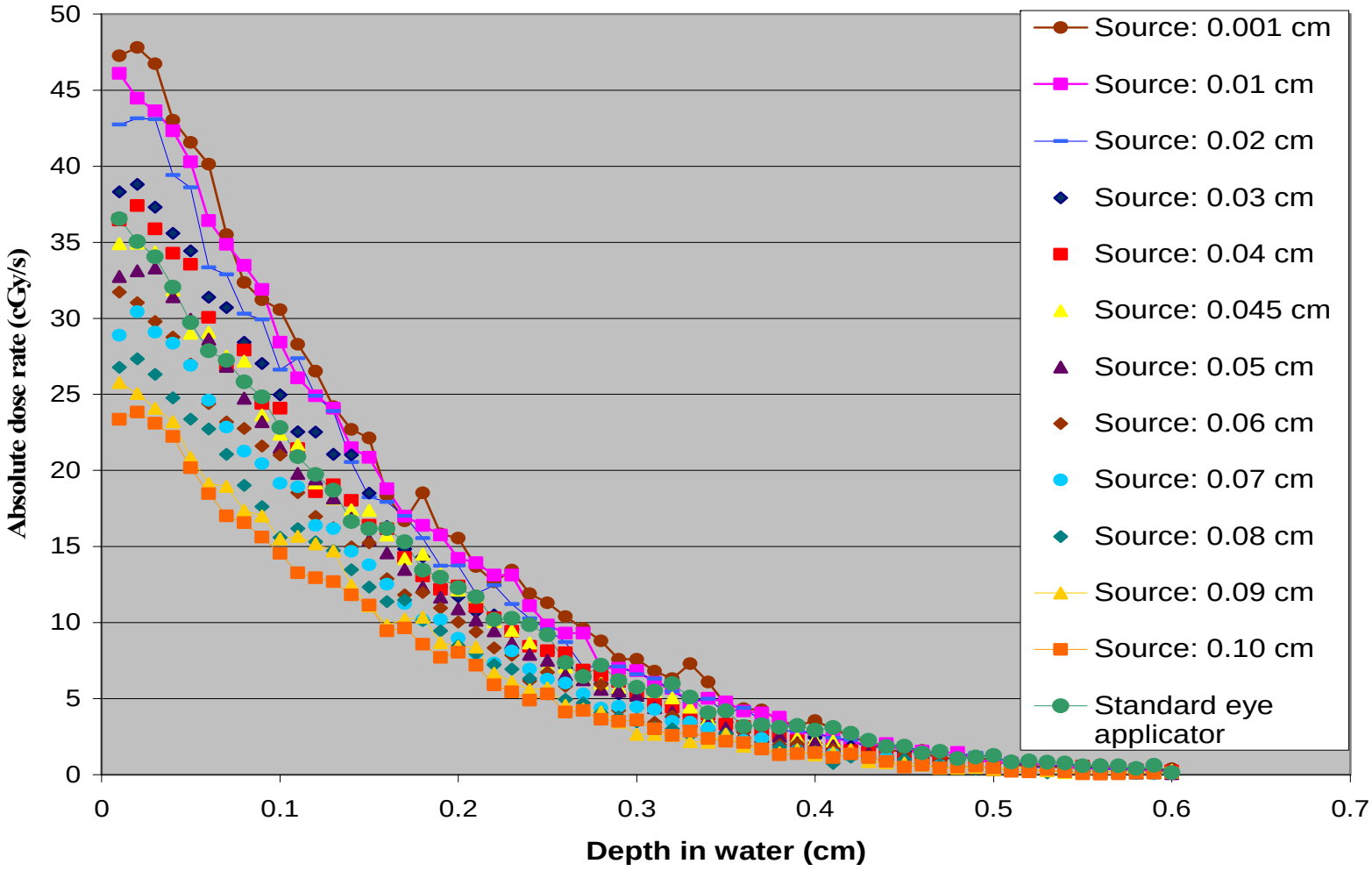

Figure 6.7: The central axis depth dose rate as a function of $SrCl_2$ thickness with 0.1 cm Teflon case, and compared to standard eye applicator.

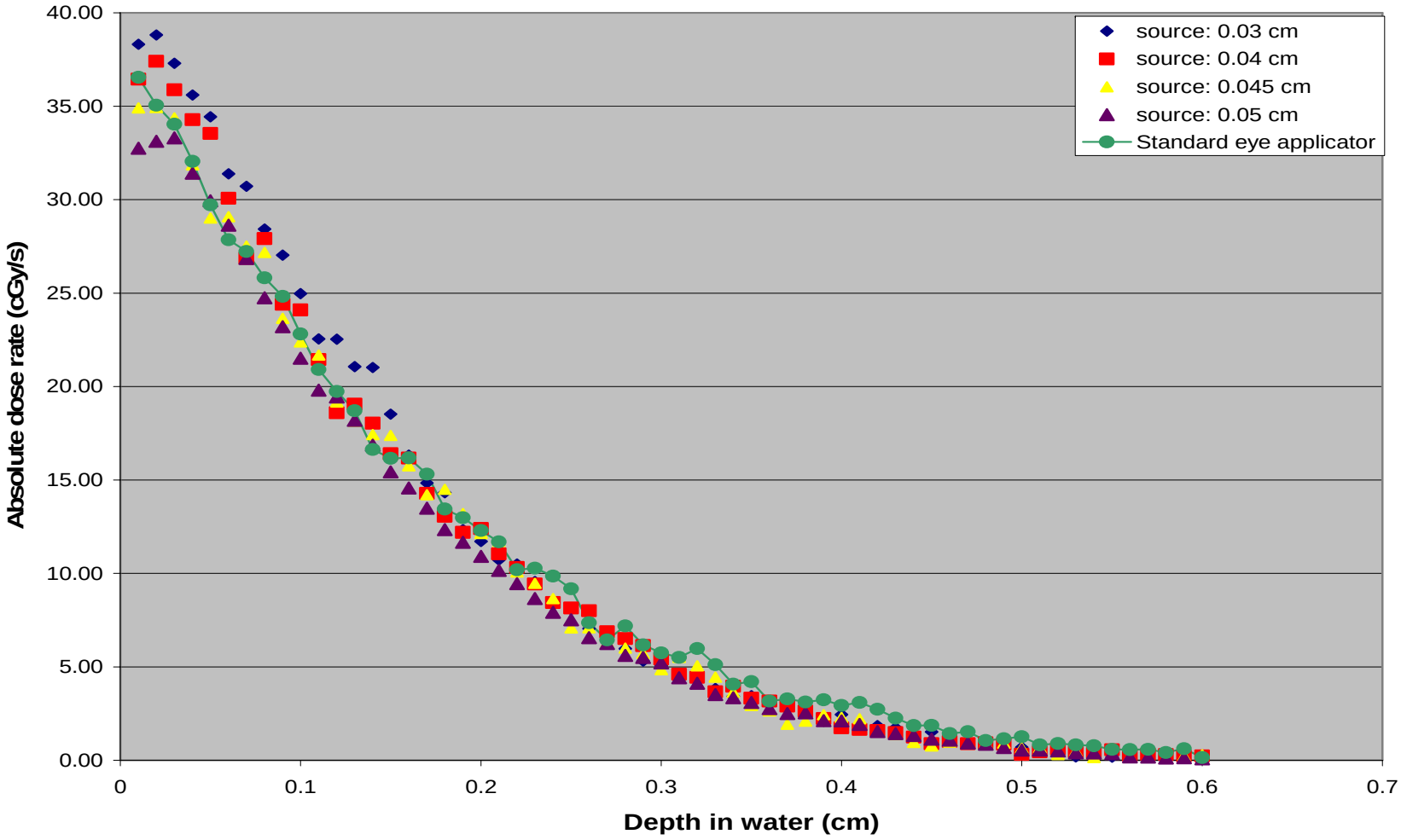

Figure 6.8: The comparable central axis depth dose rate curves of varied $SrCl_2$ thickness with 0.1 cm Teflon to the standard eye applicator.

Table 6.1: The correlation results of varied $SrCl_2$ thickness with 0.1 cm Teflon case to standard eye applicator.

	S = 0.03	S = 0.04	S = 0.045	S = 0.05	S = STD
S = 0.03	1				
S = 0.04	0.9978	1			
S = 0.045	0.9973	0.9974	1		
S = 0.05	0.9991	0.9985	0.9982	1	
S = Std	0.9971	0.9974	0.9981	0.9979	1

Table 6.2: ANOVA F-test summary results of varied $SrCl_2$ thickness with 0.1 cm Teflon case and standard eye applicator.

SUMMARY						
Groups	**count**	**Sum**	**Average**	**Variance**		
Column 1 (S = 0.03)	60	628.9507	10.48251	141.0039		
Column 2 (S = 0.04)	60	600.1222	10.00204	125.4232		
Column 3 (S = 0.045)	60	582.6096	9.71016	114.4471		
Column 4 (S = 0.05)	60	555.8081	9.263468	106.2214		
Column 5 (S = Std)	60	607.44	10.124	109.8104		
ANOVA						
Source of Variance	**SS**	**df**	**MS**	**F**	**P-value**	**F- critical**
Between Groups	50.38609	4	12.5965	0.105515	0.980535	2.402248
Within Groups	35217.45	295	119.3812			
Total	35267.84	299				

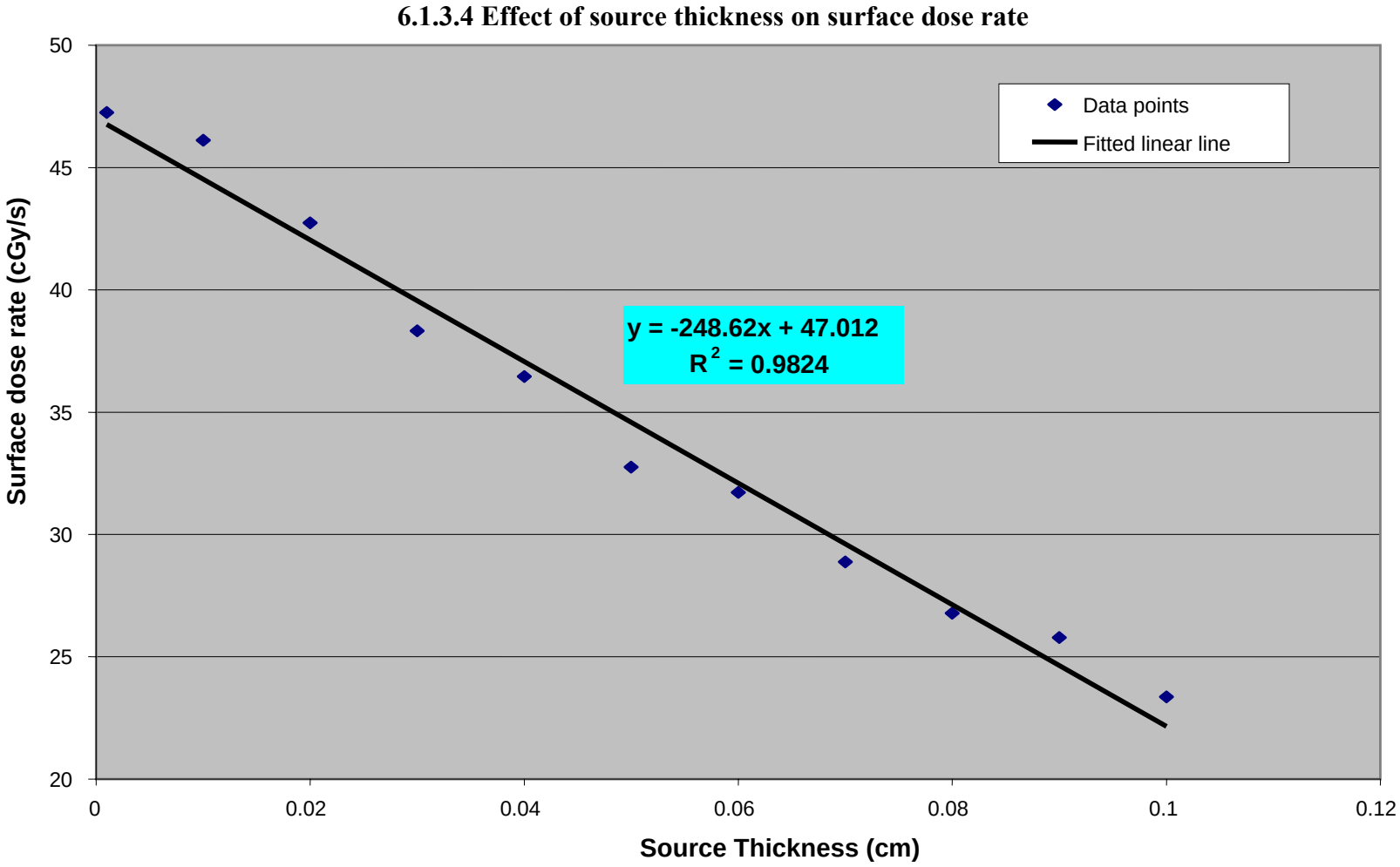

Figure 6.9: Surface dose rate as a function of the source thickness.

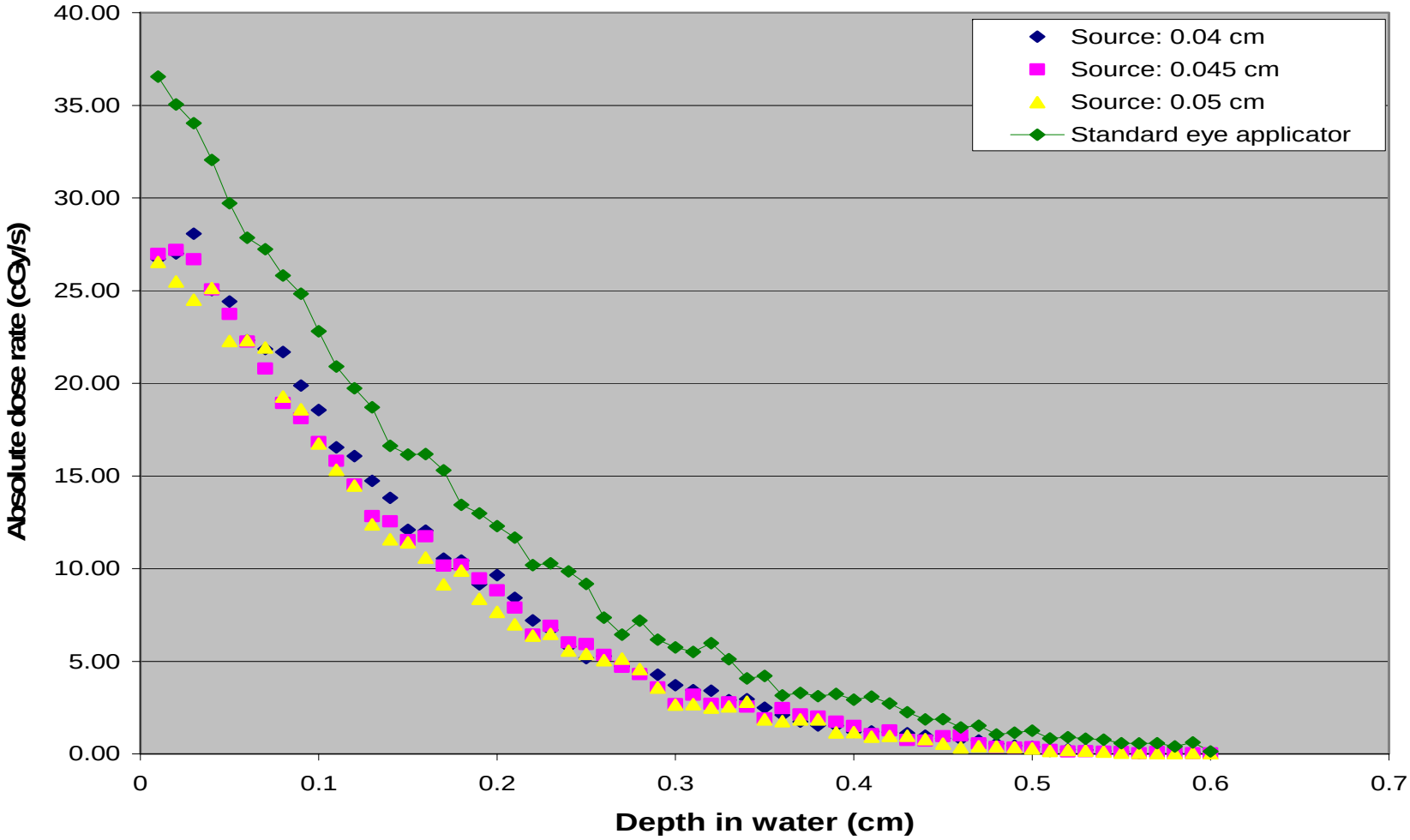

Figure 6.10: The central axis depth dose rate curves of varied $SrCl_2$ thickness with 0.125 cm Teflon and standard eye applicator.

6.1.3.5 Effect of surface source distance (SSD) on central axis depth dose rate

Figure 6.11 shows the central axis depth dose rate curves of beta particles in water as the surface source distance (SSD) increases without Teflon material, and compared to the standard eye applicator. The SSD's are indicated by different symbols and colours, as reflected in the key. Table B.5 compares the curves from Figure 6.11 by determining the percentage differences between them.

Only 0.1 cm SSD was compared to the standard eye applicator spectrum, due to the fact that this was the only one giving a curve close to that of the standard eye applicator. Figures E.4 (a) to E.4 (c) illustrate the central axis dose depth dose distribution curves, at the various SSD and are expressed by tally per particle versus cell binned in semi-logarithmic scale. The lines in the curves are error bars.

Figure 6.12 in section 6.1.3.6 shows the behaviour of the surface dose rate in the water phantom, as the SSD increases in the absence of the Teflon material of the applicator. The solid fitted linear line indicates the relationship between the surface dose rate and SSD by the equation in the Figure.

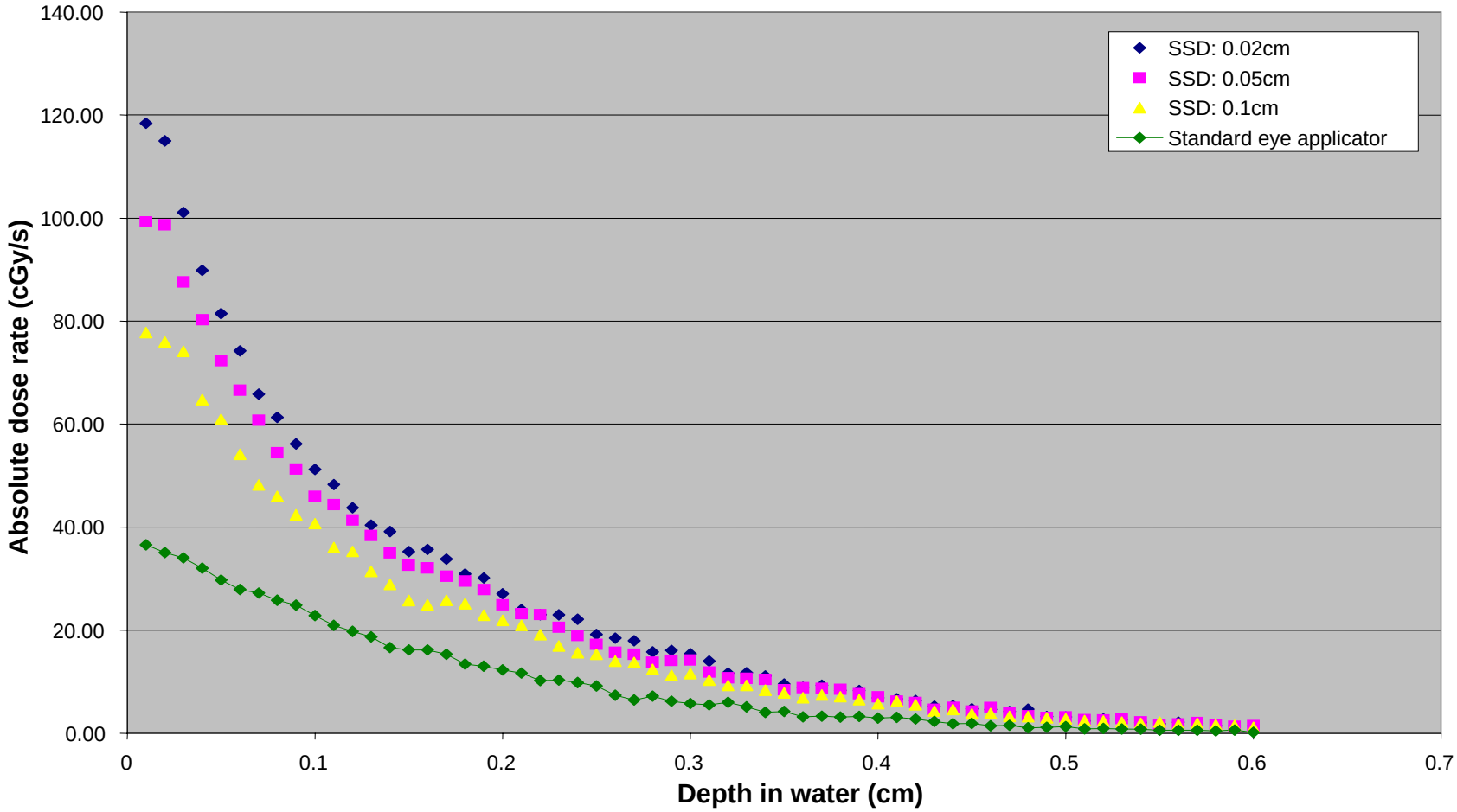

Figure 6.11: The central axis depth dose rate curves of varied SSD without Teflon material, and compared to the standard eye applicator.

6.1.3.6 Effect of surface source distance (SSD) on surface dose rate

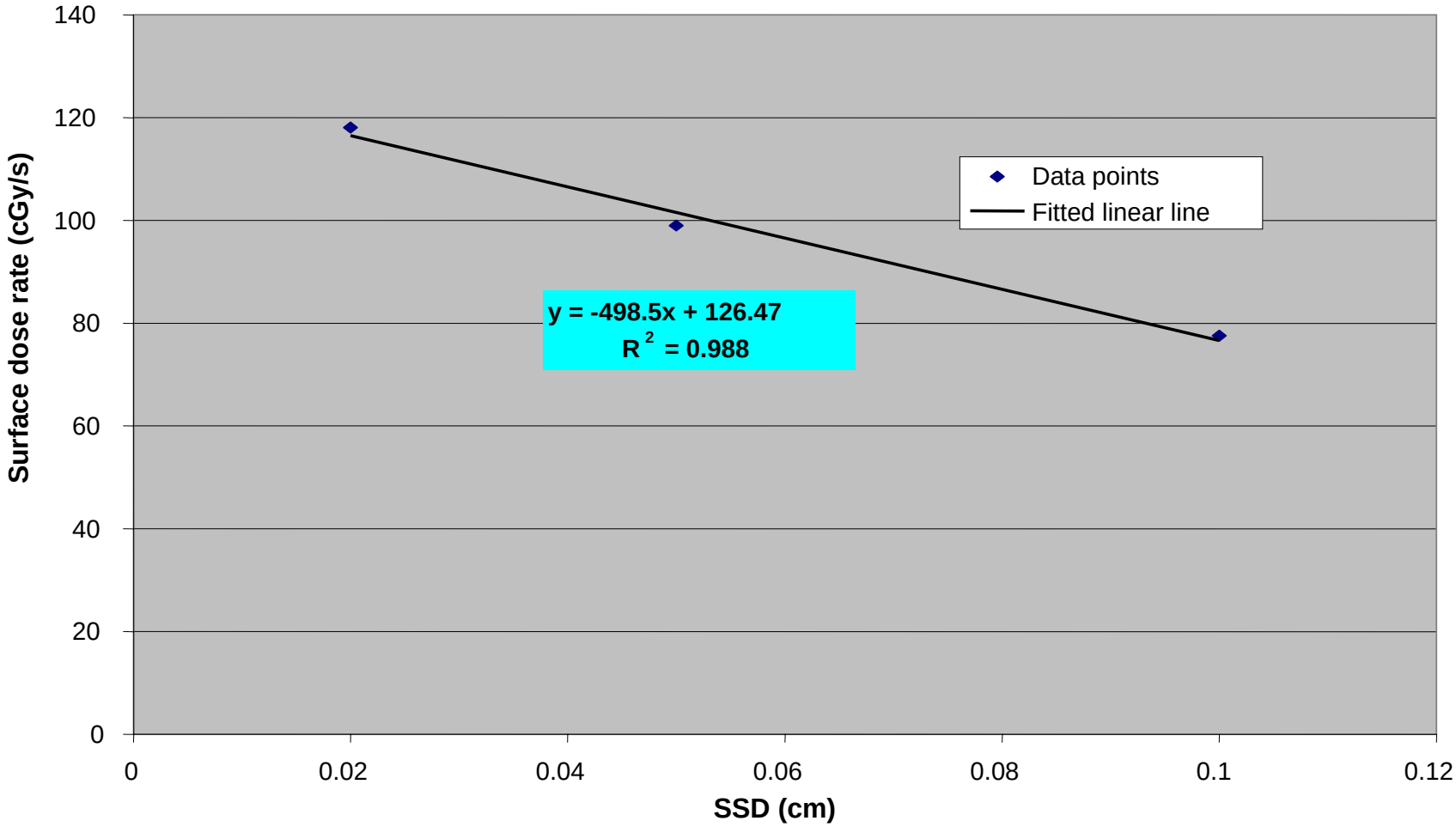

Figure 6.12: Surface dose rate as a function of surface source distance**.**

6.2 Discussion

6.2.1 Strontium spectra

6.2.1.1 Verifying the source model

The combined Sr-90 + Y-90 spectrum in Figure 6.2 was compared to Figure 6.1 (a) and Figure 6.1 (b), to validate its accuracy and correctness. This spectrum started at 1.6 tally/MeV per source particle for 0 MeV, whereas in theory [Cross *et al.*, 1983; ICRU 72, 2004], Sr-90 + Y-90 starts at 3.2 tally/MeV per source particle for 0 MeV. These differences between the theory and simulation spectrum was caused by the way in which the source was defined for simulation. The source seems to produce one beta particle for combination spectrum instead of two beta particles.

The spectrum in Figure 6.2 decreased quickly up to an energy of 0.5 MeV. This part of the spectrum is the contribution of Sr-90 beta particles, and can be confirmed by Figure 6.1 (a), where Sr-90 is effective up to 0.5460 MeV. There is one intersection point between about 0.5 MeV and 0.36 tally/MeV per source particle values of combination spectrum, where Sr-90 and Y-90 combine. From this energy value, the spectrum begins to drop off very slowly to the value of 2.281 MeV. By visual judgment of the spectrum shape and values involved, the second part of the combined beta energy spectrum of Sr-90 and Y-90, is the contribution of Y-90 beta particles.

The relative error for all spectra was ranging from 0.0023 to 0.079 (0.23% to 7.9%), and the relative error of less than 0.10 (10%) is regarded as reliable according to Briesmeister (1997) and X-5 Monte Carlo Team (2003). Therefore, the obtained spectra assume that all the portions of the problem were modeled and sampled adequately by the Monte Carlo process. Thus, the obtained spectra corresponded well with the published spectra [Cross *et al.*, 1983; ICRU 56, 1997; ICRU 72, 2004] of the Strontium isotope in shape and values, with the exception of the combined beta energy spectrum starting at the half of theoretical spectrum. Hence, it was concluded that the spectrum Sr-90 + Y-90 is valid and can be used for all simulations of this study.

6.2.1.2 Strontium spectra through the central axis of the Teflon-encased eye applicator

Figure 6.3 illustrates the relative number of emitted electrons as a function of beta particles, leaving the applicator and surfaces in front of the applicator per beta emitted from the source. This Figure also indicates the theoretical Sr-90 + Y-90 spectrum, which is an input spectrum. The integral of the area under the theoretical or input spectrum Sr-90 + Y-90 is unity, whereas the integral of the spectrum leaving the surrounding source surfaces is more than half. Thus, indicating that more than half of the emitted particles leave the source through these surfaces.

In comparing the relative number of betas emitted from the source with the number of electrons passing through surfaces on the same graph, a decrease of 8% from the input spectrum Sr-90 +Y-90 is noticed on the curves for surface 3, 5 and 6. This decrease is caused by interactions occurring in the sphere surrounding the point source, and in the air medium before reaching the surfaces of the applicator. Although, they are similar in shape and contain both Sr-90 and Y-90 components, surfaces 5, 6 and 3 are slightly different.

The percentage difference between surfaces 6 and 5 is less than 2%, as reflected in Table B.1. A percentage difference of this magnitude indicates that surfaces around the radioactive point source experience similar or equal emitted electron spectra, and the spectra are composed of both Sr-90 and Y-90 betas. Only surface 3 experiences a slightly higher percentage difference of 6.7% compared to surface 5. This is because of the fact that it is a further away from the source, and electron energies have been reduced by interaction with air and surface 5.

Surface 9 was getting 1% and less electrons, than surface 6 was getting; this proves that the Teflon material has absorbed more or almost all of the low energy Sr-90 betas, and only Y-90 betas are left. Thus, Y-90 beta particles were more penetrative than Sr-90 betas. This penetrative characteristic of Y-90 was noticed in the emitted electron energy spectra of surface 9, which is concave in shape and at the front of the applicator. It is also

noticeable on the surfaces below and on the front of the applicator. Thus, a Sr-90 beta has been suppressed, and a 0.1 cm thickness of Teflon material is sufficient to filter out the Sr-90 beta particles. Also, the spectrum emitted by the applicator is reduced further and is relatively flat, since most of the Sr-90 betas are absorbed. The nearly flat spectrum leaving the Teflon-encased eye applicator contributes to the dose curve graphs shown in appendix E [Gleckler *et al.*, 1998].

The main reason for constructing Figure 6.4 was to show clearly what is happening on the surfaces, on the front and at the back of the applicator. The electron energy spectrum calculated for surface 2, at the back of the applicator, proved to be flat. None of emitted beta particles reached this surface, since all were absorbed by the applicator materials. As the beta particles could not penetrate the 3.41 cm long stainless steel shaft of the applicator, this proves that no backing material is necessary. Hence, handling the applicator is safe.

In Figure 6.4, a decrease in electron energy spectra for all the surfaces on the front of the eye applicator is observed, and compared to the surface 9 electron energy spectrum. This is the result of a decrease in dose as the distance increases. Although all showed a maximum energy peak at 0.63 MeV, the surface 14 spectrum showed an overall percentage difference of 2.9% than surface 9. Thus, the energy of electrons that escaped from the surface of the applicator had been reduced by 2.9 energy fraction. The Figure also shows that electron energy spectra decrease with the increase in distance. Although, beyond 0.68 MeV surface 16 spectra drop below all other surface spectra (14, 15, 17 and 18) by more than 5%.

All spectra in Figure 6.4 correspond at the energies below 0.34 MeV and also at the energies greater than 2 MeV, showing small percentage differences of less than 3.7% between 0 MeV and 0.34 MeV, and less than 5% between 0.34 MeV and 0.57 MeV. Surfaces 17 and 18 spectra remain at less than 3.6%, and surfaces 14 and 15 at less than 4% for the whole spectra. The difference between surfaces 9 to 2 and 2 to 18 is more than 100% and shows a correlation only at 0 MeV and from 1.94 MeV up to 2.281 MeV.

The absence of a definite bend in the central axis depth dose curves suggests that very few Sr-90 beta particles left the Teflon-encased eye applicator, and that only those from Y-90 are present [Sinclair & Trott, 1956].

As far as the Sr-90 is concerned, it is usually in equilibrium with its daughter radionuclide, Y-90, in the common types of β-applicators. In this condition its contribution has to be added to the Y-90 absorbed dose. However, the Sr-90 contribution becomes rapidly negligible at the distances of practical interest, such as a 2 mm to 3 mm depth of water [Vynckier & Wambersie, 1982]. Because at such distances Sr-90 beta particles are completely absorbed, and there is only small contribution to the dose from scattered and bremsstrahlung radiations.

6.2.2 Central axis depth dose rate and surface dose rate in water

6.2.2.1 Effects of Teflon thickness on central axis depth dose rate and surface dose rate

From results reflected in Figure 6.5, a Teflon thickness of 0.1 cm appears to deliver a dose distribution closest to that delivered by the standard eye applicator central axis depth dose rate from 0.01 cm to 0.6 cm in depth, with a percentage difference of less than 12% on the initial depths as shown in Table B.2. The results for the other Teflon thicknesses only came close to each other, and to the standard eye applicator spectrum at around 0.4 cm depth because the electrons energy had been reduced to a greater extent at this depth and a small fraction of dose was from the scattered radiation.

From a Teflon thickness of 0.02 cm and 0 cm with a surface source distance of 0.02 cm central axis depth dose curves (Figure E.1 (b) and Figure E.1 (a)) it is clear that the curves drop off very quickly in the presence of Teflon. As Teflon thickness increases, the absolute dose rate decreases due to more attenuation, and greater bremsstrahlung production and scatter. In order to determine the effect of the thickness of the Teflon

material on dose rate, only the results up to 0.4 cm thickness are shown in Figure 6.5. The 0.45 cm and 0.5 cm Teflon thicknesses gave only scattered and bremsstrahlung radiation results leading to a small dose rate, as shown by the central axis depth dose curves of Figures E.1 (k) and E.1 (l). Thus, beyond the thickness of 0.4 cm no particles can be detected.

Figures E.1 (a) up to E.1 (l) have larger errors at the greatest depth, as the result of very few electrons reaching such depth. These effects increased as the Teflon thickness was increased, since electrons were absorbed with a thicker absorber. The thickness of Teflon material reduces the penetration depth of electrons. In the case of a Teflon thickness of 0.1 cm, a maximum penetration depth of a 0.8 cm can be estimated up to cell 60 in water (Figure E.1 (d)) as follows, adding 0.49 cm depth in water, 0.21 cm air gap between applicator and water phantom and 0.1 cm Teflon thickness penetration. This value is in the range expected for beta penetration in human tissue, as discussed in chapter 2, section 2.8.2.

Figure 6.6 illustrates that the surface dose rate decreases with an increase in the Teflon thickness, on the surface of water due to exponential attenuation. This data is fitted well by an exponential equation, which gives the attenuation coefficient as 16.14 cm^{-1} and the regression coefficient as 0.97, which implies the 97% variation of surface dose rate as a function of Teflon thickness.

The variable attenuation of the beta-particle depends on the initial energy required both to filter out lower energy betas continuously, and also to decrease the energy of the higher betas continuously. These facts, lead to the electron energy spectrum changing constantly as a function of penetration depth into medium. Thus, the electron energy or dose delivered at any point is a strong function of the initial beta spectrum [Gleckler *et al.*, 1998].

Although James (2006) explains that the attenuation coefficient for beta particles is not truly exponential as the expression for absorption or attenuation suggests, other

researchers note that exponential form curve is an artifact produced by a combination of continually varying spectra of electron energies and the scattering of particles by the absorber. As indicated in Figure 6.5 and Figure 6.6, the maximum surface dose rates of 118 cGy/s ± 1.5%, 32.75 cGy/s ± 1.5% and 0.201 cGy/s ± 36% are determined, respectively for Teflon thicknesses of 0 cm, 0.1 cm and 0.4 cm.

6.2.2.2 Effects of source thickness on central axis depth dose rate and surface dose rate

From the results indicated in Figure 6.7, it is clear that the thinner source at the constant Teflon thickness of 0.1 cm showed greater absolute dose rate, especially at the surface of water. The thicker sources in a similar condition resulted in a smaller surface dose rate, below the standard eye applicator dose rate. This effect was caused by self absorption in the source, also known as self-shielding, since thinner sources shield less beta particles and thicker sources interact with more betas.

Only four Teflon-encased eye applicator source thicknesses of 0.03 cm, 0.04 cm, 0.045 cm and 0.05 cm were closest to the standard eye applicator result. These source thicknesses are compared by percentage differences and in graphical form in Table B.3 and Figure 6.8, respectively. Further more, Table D.1 illustrates the comparison of these sources with the standard eye applicator in terms of energies and dose rates. The source thickness of 0.045 cm was the only one that was close to the standard eye applicator at a depth up to 0.14 cm, with the percentage difference of less than 5%. The remaining three source thicknesses showed slightly greater percentage difference values of ± 10 %.

Although sources of thickness 0.02 cm and 0.05 cm showed a faster drop-off in central axis depth dose curves (Figures E.2 (c) and (g)), they have less bremsstrahlung and scattered radiation. For every 0.01 cm change in source thickness there was a slight change in central axis depth dose curves, as well as in the surface dose rate (Figures E.2 (a) up to E.2 (l) and Figure 6.11).

Table 6.1 reveals that there is a strong correlation and a statistically significant relationship of 99% in results of source thicknesses 0.03 cm, 0.04 cm, 0.045 cm, 0.05 cm encased in 0.1 cm Teflon and the standard eye applicator source. The results in Table 6.1 are supported by the analysis of variances (ANOVA) F-test. The (ANOVA) F-test found the results to be statistically significant at p-value of 0.98, and accepts that sources are from the same population.

The source thickness and surface dose rate follow an inverse linear relationship with a regression fit correlation coefficient of 0.99. Thus, as source thickness increases at the constant Teflon thickness of 0.1 cm, so the surface dose rate decreases, as shown in Figure 6.9.

The main reason of simulating only source thicknesses of 0.04 cm, 0.045 cm and 0.05 cm in Teflon of thickness 0.125 cm was to make a comparison to the results of Teflon with thickness of 0.1 cm. This gives an advantage in determining the effect of increasing the Teflon thickness on the central axis depth dose rate. The increase in Teflon from 0.1 cm to 0.125 cm shows greater absorption of betas, and scatter beyond the depth of 0.54 cm of water (cell bin number 60), as reflected in Figures 6.10 and E.3 for the sources 0.04 cm, 0.045 cm and 0.05 cm. Also, the increase in Teflon thickness to 0.125 cm caused a decrease in dose rate reaching the phantom by a factor of 27%.

All the central axis depth dose rate curves of Teflon thickness of 0.125 cm gave a surface dose rate of values around 26 cGy/s, and a small enhancement peak value of about 0.87 cGy/s on average at a water depth below 0.05 cm. With the exception of source with 0.05 cm thickness which produced a small enhancement peak values of 0.63 cGy/s and 0.74 cGy/s, at a depth of 0.04 cm and 0.18 cm, respectively. The latter source thickness also experienced greatest scatter at the greater depth as compared to other sources. All the resultant spectra from Figure 6.12 were lower than the standard eye applicator spectrum by more than 20% (percentage difference) as shown in Table B.4.

6.2.2.3 Effects of surface source distance on central axis depth dose rate and surface dose rate

The effect of SSD on the central axis depth dose rate and surface dose rate was determined without Teflon material in the applicator, but with a constant source thickness. As indicated in Figure 6.11 and Figures in E.4, the central axis depth dose rate decreases with increasing SSD due to the interaction of electrons with air. Only the curve with 0.1 cm SSD was comparable to the standard eye applicator results, because others were different, especially at the surface. This curve was comparable from the surface region of the curve up to the greatest depth of the water phantom.

When the source is raised a few centimetres (Figure 6.11) above the surface of the applicator, the maximum dose rate is no longer at the surface but a fraction of a millimetre beneath it. These results are identical to the behaviour of collimated beams of electrons. The dose rate at the surface decreases with increased surface source distances [ICRP 38, 1983]. This suggests that in order to achieve results (surface dose rate) closer to that of a standard eye applicator source without Teflon, an SSD of more than 0.31 cm is required.

The required SSD can be obtained through the equation provided in Figure 6.12. The equation relates the SSD with surface dose rate. This relationship produced a correlation coefficient of 0.99, which is the 99% variation of surface dose rate due to the change in SSD. The error between fitted linear line and data points was below 5%. The fitted line is defined as the line that can give smallest differences between plotted variables. Hence, the relationship of surface dose rate and SSD was accepted as linear.

By increasing the SSD with a factor of 0.03 the surface dose rate decreased by value 19 cGy/s, whilst increasing SSD by a factor of 0.04 led to a decrease in the surface dose rate by value 21.5 cGy/s. Thus, the variation in the central axis depth dose rate curves was higher, especially at the surface region of the curves (0 cm to 0.1 cm SSDs), as shown in Table B.5. The SSD in absence Teflon material be regarded as the distance from source to water surface.

In this study, it was noticed that the eye applicator was not in close contact with the water phantom surface due to the set up geometry and the central axis depth dose rate decreased rapidly, but with a small build-up or enhancement in the water surface at a depth between 0.00 cm and 0.03 cm. This build-up was caused by the air gap between the water phantom and the applicator. The air gap was caused by the concave geometry of the applicator. Similar results were obtained by Ali and Khan (1990), where build-up curves at depth 0 gm/cm^2 to 0.1 gm/cm^2 in normalized percentage dose curves, were determined with a film and ionization chamber at a distance of 0.45 cm. They found a smooth drop off when the applicator was in contact with the film and ionization chamber.

The exponential function relationship of the Teflon-encased eye applicator source is very significant, particularly within the first few millimetres. The finite size of the Strontium source and air gap introduces additional complications at such distances, and detailed calculation of surface dose rate and the absorbed dose distribution in the central axis of the Teflon-encased eye applicator was a formidable task [Gleckler *et al.,* 1998; Ruden & Bengtsson, 1974]. The small variations in applicator dimensions change the surface dose rate significantly.

The air gap effect can be resolved clinically, by maintaining small air gap which will be filled by eye drops. Experimentally, the effect can be resolved by using the cylindrical water phantom. Then, the eye applicator can be positioned and fit in at the cylindrical side of the water phantom, such that a small air gap is maintained. These methods will lead to more accurate data as betas will experience less air attenuation.

The combination of Teflon "polymer" and a water phantom presents a mixture of material of different density and atomic number. Hence, the attenuation was different in both materials, and the flattening of the depth dose rate beyond the depth of 0.4 cm of water is due to bremsstrahlung radiation; the proportion of dose in this region is almost insignificant. Gleckler *et al*. (1998) believed that the photons from the bremsstrahlung contribution to the dose are less than 2% of the total dose.

The calculated dose rates are within ± 5% relative error up to 0.14 cm from the surface of applicator, and differ at the greatest distances. These differences increase with an increase in depth. Near the surface of the applicator the beta ray energy is high, and the highest absorbed dose rate on the surfaces of the applicator was calculated to be 118.40 cGy/s ± 1.5% for both Teflon 0 cm and SSD 0.02 cm, 47.25 cGy/s ± 2.5% for source 0.001 cm. The surface dose rate was calculated at the depth of 0.01 cm water.

The overall relative error from MCNP results ranges from 1.5% to 50% depending on simulation case, and increases with water depth and is greatest at the greater depths. On average the relative error of MCNP results was 3%. All ten statistical checks from the MCNP output files in this study have passed. The results were shown to be reliable up to a 0.2 cm depth of the water phantom with a relative error of ± 10.3%, at one standard deviation. In the future simulation variance can be found at the water depths by using the variance reduction technique, to improve on the results.

The concave applicator with planar source shows a significantly sharper decline in depth dose rate from the surface. This is due to the effective contribution of Y-90 betas and minor contribution from Sr-90 betas. Also, the central axis depth dose curves for the concave applicator show the extent of geometrical focusing, as compared with a plane standard eye applicator [Sinclair & Trott, 1956]. During the Monte Carlo calculations, the active source region was assumed to be 100% Strontium Chloride.

At the certain deep depths of water phantom no electrons were absorbed and dose distribution was from the scattered radiation, but at some depths beyond these depths the electrons were captured. This effect leads to the peaks in the Figures, as shown in Figures E.1 (e) up to (l) and E.3 (a), (b). The cause of this is that, all the remaining energies of electrons were deposited at such depths. Thus, the electron range became smaller than expected. Hence, they could not reach greatest depths.

Chapter 7

CONCLUSIONS

7.1 General conclusions

The dose distribution for a given beta-ray applicator has commonly been specified by stating the dose rate at the surface, and by providing a central-axis depth dose rate curve. This, in reality is only a partial specification of the dose from the applicator. The full specification must include the distribution throughout the region in which the dose has significant values [ICRP 38, 1983].

The absorbed dose rate at the surface of the source is considered to be the average of the dose rate across the central area of the source [Soares, 1992]. At smaller distances, very high values of absorbed dose rate can be expected. It is believed theoretically as well as experimentally that the delivered values of absorbed dose around the applicator will be accurate to a few percent, at a distance of between 0.2 cm and 0.5 cm from the source surface [Ruden & Bengtsson, 1974]. At greater distances, the residual dose is due to bremsstrahlung [Vynckier & Wambersie, 1982].

The absorbed dose rate is a sensitive function of the source size, thus for small size differences the percentage error in the dose is twice the error in the source size, as the dose is dependent upon the source area which is dependent upon the square of the radius. In addition, the central axis depth dose rate of a concave Teflon-encased eye applicator to be employed in a clinical situation can only be measured at a distance of more than 0.31 cm from the source surface owing to its geometry [Davelaar *et al.*, 1992].

7.2 Specific conclusions

In this study, the spectra corresponded well with published spectra in recent international protocols [Cross *et al.,* 1983; ICRU 56, 1997; ICRU 72, 2004], and were found to have relative errors of less than 10%. The spectra from the Teflon-encased eye applicator changed slowly with distance from the source, and their mean energy was approximately

constant [Ruden & Bengtsson, 1974]. The electron energy spectra obtained from the Teflon-encased eye applicator was similar in shape but varied slightly in value from that of the standard eye applicator studied by Maage (2002).

The input spectrum used in this study was slightly different from the one used in the study of the standard eye applicator. All the differences in the input spectra and in the dose rate results were expected, since the geometry, materials, applicator shape, size of sources, distance between the source and phantom, input spectra used and even the MCNP codes used were different. However, it was possible to minimise them. Generally, the depth dose curves determined for one beta ray source will not be accurate for another with the same radioisotope, unless the two applicators are strictly alike in all respects [ICRP 38, 1983].

The spectral characteristics of Sr-90 + Y-90 electrons varied widely with source geometry, and a certain degree of standardisation of source construction is required [Pruitt *et al*., 1988], especially when comparisons are to be made between sources. The results of the spectra at the central axis of the Teflon-encased eye applicator correlate positively with the electron energy spectra obtained by Gleckler *et al*. (1998) for the type SIA.20 applicator, and by Maage (2002) for the type SIA.8975 applicator. These results of Teflon-encased eye applicator also showed that, about 90% of the initial source dose produced is available at the surface of the Teflon-encased eye applicator for treatment.

Most of the beta particles from the Sr-90 + Y-90 source were transmitted in a forward direction. This was proven by the high number of electrons emitted from surface 6. Almost all Sr-90 beta particles are absorbed by the source encapsulation (Teflon), and no matter how thin this material is, attenuation occurs everywhere. Sr-90 betas contributed to the total dose rate through bremsstrahlung and scattered radiation, especially beyond 0.4 cm of the water phantom. Thus, the Y-90 betas were mainly responsible for the exponential attenuation of the dose rate. Only the Y-90 source was effective beyond the applicator surface.

The surface dose rate decreased with an increase in Teflon thickness through an exponential relationship, because of an increase in the attenuation of the Teflon material. With Teflon thickness of 0.1 cm and source thicknesses of 0.03 cm, 0.04 cm, 0.045 cm and 0.05 cm at SSD of 0.1 cm dose rates were found to be more accurate to the standard eye applicator. When the Teflon thickness was increased from 0.1 cm to 0.125 cm, greater absorption was experienced and the dose rate was decreased by 27%. Surface dose rate decreased in a linear relationship with an increase in source thickness, and also with SSD. The central axis depth dose rates of Sr-90 + Y-90 source decreased with increasing depth. This decrease may result in better sparing of the lens, which is located approximately 2 mm below the surface of human eye [Park *et al.*, 2008].

The build-up in depth dose curves was caused by an air gap between applicator and the water phantom, which occurs as a result of the geometry of the Teflon-encased eye applicator. But in clinical applications this air gap is minimised, since the applicator is applied directly onto the surface of the eye. These air gaps disturb the dose rate slightly. Also, a change occurs in the surface dose rate when the distance between the phantom and the applicator is altered. Thus, the existence of an air gap between the eye and the applicator surface may alter the surface dose rate. This effect of air interaction on dose distribution depends on beta energy and SSD [ICRU 56, 1997]. The absorption of photons and electrons by the Teflon material and the air gap means that more particles had to be simulated, in order to achieve statistically meaningful results at the extended depths.

The Teflon thickness, source thickness and surface source distance gave some control over the surface dose rate. A very good agreement was found between the Teflon-encased eye applicator and the standard eye applicator surface dose rates, when Teflon of 0.1 cm thickness and source thickness as shown in table 7.1 were simulated.

Table 7.1: Surface dose rates agreement results

Thickness (cm)	**Teflon-Encased**				**Standard**
Encapsulations material	0.1				0.085
Source	0.03	0.04	0.045	0.05	0.01
Dose rate (cGy/s)	38.32 ± 2.7%	36.45 ± 2.8%	34.90 ± 2.8%	32.75 ± 1.5%	36.55 ± 2.5%

Table 7.1 results reveal a 99% correlation and a statistically significant relation with the standard eye applicator, and these results were also proven by the ANOVA F-test. The latter test found these sources to be from the same population, and chances of being wrong were as low as 2%.

The resultant SSD of 0.18 cm extrapolated or calculated from Figure 6.12 without Teflon material seems to correlate with the standard eye applicator throughout the region of the electrons and bremsstrahlung. Thus, these geometries are accurate to the standard eye applicator.

Although the accuracy of the results was reduced at greater distances above 0.4 cm water phantom, the distributions cover most clinical requirements. The calculated central axis depth dose rates were within 5% up to a depth of 0.14 cm, which is advantageous in superficial irradiation treatment. In conclusion, the surface dose rate can only be defined at a depth of 0.01 cm of water, in order to estimate accurately the dose to the sclera.

The central axis depth dose rate is dependent on the following geometries: Teflon thickness, source thickness and surface source distance. Electrons could not reach the end of the water phantom due to the limited range, and the scatter could only approached more closely to about 0.68 cm depth in the water phantom. The total water phantom depth was 0.74 cm. It was possible to obtain measurements at a depth beyond the range of Y-90 beta particles (electrons), where the ionization is produced by bremsstrahlung, but the errors in these measurements were relatively high [Chhabra, 1962].

Table 6.1 and Figures 6.6, 6.9 and 6.12 showed a statistically significant perfect relationship of 99%, 97%, 99% and 99%, respectively. The deviations from the inverse square dependence are probably caused by a combination of the angular spread of the scattered-electron build-up [Cross *et al.*, 1983].

7.3 Recommendations and findings

The Teflon-encased eye applicator with geometries of 0.1 cm Teflon thickness and source thickness ranging from 0.03 cm to 0.05 cm, can therefore be manufactured and be used in clinical testing. Teflon thickness of 0.1 cm with a source thickness of 0.05 cm illustrated an estimation of maximum depth penetration of 0.8 cm for beta particles; this is within the range limits given in theory, chapter 2 section 2.8.2. The obtained results can be improved by minimising or by avoiding the air gap between Teflon-encased eye applicator and the eye in clinical situation.

The model was successfully simulated and its dosimetry was found to be comparable to that of a standard eye applicator. The designed model of a concave, Teflon-encased eye applicator fulfils its main purpose of irradiating one part of the tissue more heavily than another. The results obtained confirm the dosimetric accuracy of the Teflon-encased eye applicator, and clinical similarity in dosimetric characteristics to those of the standard eye applicator. The dose distributions will be beneficial in recurrence in pterygium, conjunctiva treatment, reducing the incidence rate of radiation-induced cataract after pterygium and glaucoma surgeries [Park *et al.*, 2008]. These results confirm that a modeled Teflon-encased eye applicator is effective, and can be used in clinical cases.

7.4 Future studies

The following recommendations are made for future studies:

1. The stability and lifespan of the Teflon material should be considered.
2. The placement of the applicator during the treatment requires investigation. Should it be held in contact with or only close to the area of treatment?

3. The effect of TLDs on the dose distribution, the accuracy and scatter effect of TLDs and Extrapolation chamber in dosimetry of the Teflon-encased eye applicator.
4. The determination of the Teflon-encased eye applicator source dose rate profile.
5. The calibration of the Teflon-encased eye applicator.

References

Ali, M.M. & Khan, F.M.; (1990). "Determination of dose rate from a ^{90}Sr ophthalmic applicator", Med. Phys, 17(3): 416 — 421.

Briesmeister, J.F.; (1997). MCNP^{TM}- A General Monte Carlo N-Particle Transport Code, Version 4B, Report LA-12625-M. Los Alamos: Los Alamos National Laboratory.

Cherry, S.R., Sorenson, J.A. & Phelps, M.E.; (2003). Physics in Nuclear Medicine. 3rd edition. Philadelphia U.S.A; Saunders. ISBN: 0-7216-8341-X.

Chhabra, A.S.; (1962). "Sr^{90}-Y^{90} (and Bremsstrahlung) Depth-Dose Measurements in Lucite", Radiology.79: 1001—1007.

Cross, W.G., Hokkanen, J., Järvinen, H., Mourtada, F., Sipilä, P., Soares C.G. & Vynckier, S.; (2001). "Calculation of beta-ray dose distribution form ophthalmic applicators and comparison with measurements in a model eye", Med. Phys. 28(7): 1385 — 1396.

Cross, W.G., Ing, H., & Freedman, N.; (1983). "A short atlas of beta-ray spectra", Phys. Med. Biol. 28(11): 1251—1260.

Davelaar, J., Schaling, D.F., Hennen, L.A. & Broerse, J.J.; (1992). "Dosimetry of ruthernium 106 eye applicators", Med. Phys. 19(3): 691— 694.

Dendy, P.P. & Heaton, B.; (1999). Physics for Diagnostic Radiology. 2nd edition. Bristol Philadelphia: U.S.A; Institute of Physics (IOP) Publishing. ISBN: 0-7503-0591-6.

Donald, T.G.; (1996). Principles of Radiological Physics. 3rd edition. New York; Churchill Living Stone. ISBN: 0-4430-4816-9.

Fraser, H. & Naunton, W.J.; (1961). "Treatment of non-malignant corneal conditions with radioactive isotopes: 5-year survey", Brit. J. Ophthal. 45: 358 — 364.

Friedell, H.L., Thomas, C.I. & Krohmer, J.S.; (1950). "Beta-Ray Application to the Eye with the Description of an Applicator Utilizing Sr^{90} and its Clinical use", Am. J. Ophthalmol. 33: 525 — 535.

Gleckler M., Valentine, J.D & Silberstein, E.B.; (1998). "Calculating lens dose and surface dose rates from ^{90}Sr ophthalmic applicators using Monte Carlo modeling", Med. Phys. 25(1): 29 — 36.

Haybittle, J.L. & Barber, R.W.; (1973). "Technical Note: Dosimetric Measurements with a Strontium-Yttrium-90 Beta Ray Source Bonded in Aluminium", Phys. Med. Biol. 18(2): 272 — 275.

Hokkanen, J., Heikkonen, J. & Holmberg, P.; (1997). "Theoretical calculations of dose distributions for beta-ray eye applicators", Med. Phys. 24(2): 211 —213.

IAEA; (2002). Calibration of photon and beta ray sources used in brachytherapy. TECDOC 1274. VIENNA; IAEA in Australia.

IAEA; (2003). Review of Radiation Oncology Physics: A handbook for Teachers and Students. Vienna Australia.

ICRP; (1983). Radionuclide Transformations Energy and Intensity of Emissions. Publication number 38: V11—13. Annals of the ICRP 38. New York; Pergamon Press.

ICRU; (1997). Dosimetry of External Beta Rays for Radiation Protection. ICRU Report 56. 7910 Woodmont Avenue, Bethesda, Maryland, 20814 USA.

ICRU; (2004). Dosimetry of Beta rays and Low-energy Photons for Brachytherapy with Sealed sources. ICRU Report 72, Volume 4 (2). Oxford University Press.

James, E.M.; (2006). Physics for Radiation Protection. 2nd edition. Germany; Weinheim Wiley-VCH. ISBN: 3-527-40611-5.

Johns, H.E. & Cunningham, J.R.; (1983). The Physics of Radiology. 4th edition. Springfield U.S.A; Charles C Thomas, Chapters 3, 5, 13. ISBN: 0-398-04669-7.

Kearsley, J.H., Fitchew, R.S. & Taylor, R.G.S.; (1988). "Adjunctive Radiotherapy with Strontium-90 in the Treatment of Conjunctival Squamous Cell Carcinoma", Int. J. Radiation Oncology Biol. Phys. 14(3): 435—443.

Khan, F.M.; (2003). The Physics of Radiation Therapy. 3rd edition. Philadelphia U.S.A; Lippincott Williams & Wilkinson. ISBN: 0-7817-3065-1.

Kirwan, J.F., Counsins, S., Venter, L., Cook, C., Stulting, A., Roux, P. & Murdoch, I.; (2006). "Effects of β radiation on success of glaucoma drainage surgery in South Africa: randomized controlled trial", BMJ. 333(7575): 942 — 947.

Kirwan, J.F., Constable, P.H., Murdoch, I.E. & Khaw, P.T.; (2003). "Beta irradiation: new uses for an old treatment: a review", Eye. 17: 207 — 215.

Klevenhagen, S.C.; (1993). Physics and Dosimetry of Therapy Electron Beams. Madison Wisconsin; Medical Physics (IOP) Publisher. ISBN: 0-944838-36-7.

Ljungberg, M., Strand, S.-E & King, M.A.; (1998). Monte Carlo Calculations in Nuclear Medicine: Applications in Diagnostic Image. Bristol Philadelphia: U.S.A; Institute of Physics (IOP). ISBN: 0-7503—0479-0.

Maage, T.S.; (2002). The Simulation of the Strontium-90 Eye Applicator using the MCNPX Monte Carlo Code, Msc Thesis, University of Limpopo (MEDUNSA).

Maboe, D.P.A.; (2001). Radiation Detector Modelling with Monte Carlo N-Particle Code, Msc Thesis, University of Limpopo (MEDUNSA). 3 — 23.

Mosia, G.J.; (2005). Evaluation and Comparison of Absorbed Dose for Electron Beams by Diamond and LiF Dosimeters, Msc Thesis, University of Limpopo (MEDUNSA). 4 — 83.

Muench, P.J., Meigooni, A.S., Nath, R. & McLaughlin, W.L.; (1991). "Photon energy dependence of the sensitivity of radiochromic film and comparison with silver halide film and LiF TLDs used for brachytherapy dosimetry", Med. Phys. 18(4): 769 —775.

NCS; (2004*)*. Quality control of sealed beta sources in Brachytherapy: Recommendations on detectors, measurement procedures and quality control of beta sources. Report 14. CH 27, 30 & 33. 11 July.2009. http://www.ncs-doc.org/download_r14.html.

Oliveira, M.L. & Caldas, L.V.E.; (2005). "A special mini-extrapolation chamber for calibration of ^{90}Sr + ^{90}Y sources", Phys. Med. Biol. 50: 2929 — 2936.

Park, Y.K., Ye, S.-J., Kim, I.I.H., Wee, W.R., Kim, M.K., Han, H.S., Son, K.-J. & Park, U.I.J.; (2008). "Potential use of P-32 ophthalmic applicator: Monte Carlo simulations for design and dosimetry", Med. Phys. 35(5): 1854 — 1858.

Pearce, J., Thomas, R. & DuSautoy, A.; (2006). "The characterization of the Advanced Markus ionization chamber for the use in reference electron dosimetry in UK", Phys. Med. Biol.51: 473 — 483.

Podgoršak, E.B.; (2006). Radiation Physics for Medical Physicists. Berlin Heilderberg New York; Springer. ISBN: 3-540-25041-7.

Pruitt, J.S., Soares, C.G. & Ehrlich, M.; (1988). NBS measurement services: Calibration of Beta-particle radiation instrumentation and sources, NBS Spec. Publ. 250-21, Washington U.S.A.

Reft, C.S., Kuhnir, F.T., Rosenberg, I. & Myrianthopoulos, L.C.; (1990). "Dosimetry of Sr-90 ophthalmic applicators", Med. Phys. 17(4): 641 — 646.

Ruden, B.-I. & Bengtsson, G.; (1974). "TLD Measurements of dose distribution around a beta-ray Applicator", Phys. Med. Biol. 19(2): 186 — 195.

Selman, J.; (1976). The Basic Physics of Radiation Therapy. 2nd edition. Springfield U.S.A; Charles C Thomas. ISBN: 0-398-03247-5.

Sinclair, W.K. & Trott, N.G.; (1956). "The Construction and Measurement of Beta-Ray Applicators for use in Ophthalmology", Br. J. Radiol. 29(337): 15 — 23.

Soares, C.G.; (1995). "Comparisons of NIST and manufacturer calibrations of ^{90}Sr + ^{90}Y ophthalmic applicators", Med. Phys. 22(9): 1487 — 1493.

Soares, C.G.; (1992). "Technical note: A method for the calibration of concave 90Sr + 90Y ophthalmic applicators", Phys. Med. Biol. 37(4): 1005 — 1007.

Soares, C.G., Vynckier, S., Järvinen, Cross, W.G., Sipilä, P., Flühs, D., Schaeken, B., Mourtada, F.A., Bass, G.A. & Williams, T.T.; (2001). "Dosimetry of beta-ray ophthalmic applicators: comparison of different measurement methods", Med. Phys. 28(7): 1373 — 1384.

Šolc, J.; (2008). "Monte Carlo calculation of dose to water of a ^{106}Ru COB-type ophthalmic plaque", IOP. Journal of Physics: Conference Series V102, 3rd McGill International Workshop, 1 — 6.

Supe, S.J., Mallikarjuna Rao, S. & Sawant, S.G.; (1975). "Dosimetry of spherical Sr^{90}-Y^{90} β ray eye applicators", Am. J. Roentgenol Radium Ther Nucl Med. 123(1): 36 — 41.

Thomas, C.I., Storaasli, J.P. & Friedell, H.L.; (1962). "Lenticular Changes Associated with Beta Radiation of the Eye and Their Significance", Radiology. 79: 588 — 597.

Viani, G.A., Stefano, E.J., De Fendi, L.I. & Fonseca, E.C.; (2008). "Long-term results and prognostic factors of fractionated strontium-90 eye applicator for pterygium", Int. J. Radiation Oncology Biol. Phys. 72(4): 1174 — 1179.

Vynckier, S. & Wambersie, A.; (1982). "Dosimetry of beta sources in radiotherapy I. The beta point source dose function", Phys. Med. Biol. 27(11): 1339 — 1347.

X-5 Monte Carlo Team; (2003), 24 April, MCNP- A General Monte Carlo N-Particle Transport Code, Version 5, Report LA-UR-03-1987, Volume I & II. California; Los Alamos National Laboratory.

Young, M.E.J.; (1983). Radiological Physics. 3rd edition. London; H.K Lewis & Co Ltd. ISBN: 0-7186-0452-0.

Glossary

TERMS AND ABBREVIATIONS

1. Terms:

Attenuation: the reduction in intensity of the primary radiation beam as penetrate matter by either absorption or scattering.

Beam quality: Beam energy specified by its spectral distribution, representing different relative intensities of photons. Thus, is penetrating ability of the radiation.

Binding energy: energy required to completely remove an electron from a given shell in an atom, increase with increase in positive charge (i.e. atomic number Z) of nucleus.

Delta rays: are electrons that acquire sufficiently high kinetic energies through hard collisions enabling them to carry this energy a significant distance away from the track of primary particle and produce their own ionizations of absorber atoms.

Dosimetry: measurement or study of radiation amount received from the radiation source

Excitation: occurs when an electron is moved from a given shell to a higher shell that is empty or does not contain full complement of electrons.

Fortran: Computer programming language.

Grenz rays: term used to describe treatment beams of very low energy.

Half-life: is the time during which the number of radioactive nuclei decays to half of the initial value of nuclei present at the time $t = 0$.

Homogenous: having similarity in structure because of common descent or of the same or similar nature.

Indirectly ionizing radiation: Uncharged particles such as neutron and photon, since they produce the charged ionizing particles as they interact with matter.

Ionization: occurs when an electron is moved from the atom, when is supplied with enough energy to overcome its binding energy in a shell.

Path length: the total distance traveled until the particle comes to rest, regardless of the direction of movement.

Phantom: Material used for determination of absorbed doses at the various depths.

Photon fluence: number of photons entered an imaginary sphere of cross-sectional small area.

Prognosis: prediction of disease course.

Projected path length: the sum of individual path lengths along the incident direction.

Radioactivity: characterized by a transformation of an unstable nucleus into a more stable entry that itself may be unstable, and will decay further through a chain of decays until a stable nuclear configuration is reached.

Recurrence: regrowth of the pterygium across the bulbar conjunctivae.

Thermoluminescence (TL): is the thermally activated phosphorescence.

2. Abbreviations:

*F8: Tally type 8 (Energy deposition tally)

$\dot{D}$: Absorbed dose rate

316 L: model or type of a stainless steel

amu: atomic mass unit

ANOVA: Analysis Of Variance

ANSI: American National Standards Institute

BGC: Bragg Gray Cavity

Bq: becquerel

cGy: centi gray

CSIR: Council for Science and Industrial Research

D: Absorbed dose

DBCN Card: Debug information card

dps: decay per second (disintegration per second)

EGS: Electron Gamma Shower

ETRAN: Electron TRANsport

F1: Tally type 1 (Number of particles crossing a surface tally or surface current tally)

FOM: figure of merit

GB: giga bites

GBq: giga Becquerel

GeV: giga electron volt

GHZ: giga hertz

Gy: gray

IAEA: International Atomic Energy Agency

ICRP: International Commission on Radiological Protection

ICRU: International Commission on Radiation Units

ISO: International Standardization Organization

ITS: Integrated TIGER Series

IV: roman number, four

J: joules

keV: kilo electron volt

kg: kilogram

LANL: Los Alamos National Laboratory

MB: mega bites

MCG: Monte Carlo Gamma

MCN: Monte Carlo Neutron

MCNG: Monte Carlo coupled Neutron-Gamma

MCNP: Monte Carlo N-Particle

MCP: Monte Carlo Photon

MCPLOT: Monte Carlo Plot, plots tally results

MEDUNSA: Medical University of South Africa

MeV: mega electron volt

NBS: National Bureau of Standards

NCS: Netherlands Commission on Radiation Dosimetry (Nederlandse Commisie voor Stralings dosimetrie)

NIST: National Institute of Standards and Technology

P-32: Phosphorus-32 radioisotope

PDF's: Probability Density Functions

R: relative error

RMI- 457: Type or model of solid water phantom used mostly for small fields and for electron beams

RSICC: Radiation Safety Information Computational Center

SDEF: source definition

SI: System International

t: time

TFC: tally fluctuation chart

TLDS: Thermoluminescence dosimeters

TTB: Thick Target Bremsstrahlung

U.S.: United State

WT1: Type of solid water phantom used for mega photon beam measurements

XSDIR: cross-section directory file

ZAID: specific isotope identifier

λ: decay constant

APPENDICES:

APPENDIX A

Sr-90 + Y-90 THEORETICAL PROPERTIES, CHARACTERISTICS AND DOSE CALCULATIONS

Table A.1: Properties and characteristics of Sr-90 + Y-90 [Cherry *et al*, 2003; James, 2006; Johns & Cunningham, 1983; Maage, 2002].

	38-Sr-90	**39-Y-90**
Possible parent nuclides	*mRb	Sr
	Rb-90	
Half-life	28.79 ± 0.33 years	64.10 hours
Transformation or decay mode	One Beta negative to Y-90	Two Beta negatives to Zr-90
Atomic mass (amu)	89.9077376 ± 0.0000029	89.9071514 ± 0.0000025
Excess mass (keV)	-85941.863 ± 2.727	-86487.861 ± 2.346
Binding Energy (E_B) (keV)	782631.486 ± 2.730	782395.131 ± 2.349
Beta decay energy (keV)	545.998 ± 1.409	2280.077 ± 1.616
spin	0^+	2-
Decay energy (MeV)	0.5460	2.2801
Yield (%)	100	99.988
Average energy (MeV)	0.1958	0.9348

* It is possible for Rb to produce Sr-90 even when is at the meta state (m is used to specify metastate).

Equations used in calculation of dose and dose rate:

Assuming that *N* is the number of histories, the following is obtained

$$1\,\text{second} = 2A_o \text{ particles} \qquad \text{(A1)}$$

Where A_o is the activity at the time t = 0 and 2 is the number of decays (beta particles). Then

$$t\,\text{second} = N \text{ particles}$$

Therefore

$$N = 2A_o t \tag{A2}$$

$$t = \frac{N}{2A_o} \tag{A3}$$

The MCNP5 code gives out the energy an MeV per source particle (E/n), where *n* is the number of particles, and by assuming that the number of histories and particles are the same, then the following relation thus holds true:

$$\left(E/N\right) = \left(E/n\right) \tag{A4}$$

$$E = \left(E/n\right) \bullet N \tag{A5}$$

Dose is defined as the energy retained or deposited in a medium by the ionizing radiation to a mass, dm of the matter. So

$$D = \frac{E}{m} \tag{A6}$$

By substituting equation A5 into A6,

$$D = \frac{\left(E/n\right) \bullet N}{m} \tag{A7}$$

Where *E* is the energy in a medium and m is the mass of the medium and both are given in Joules and Kg respectively, hence dose is given in J/Kg. Where 1 J/Kg = 1Gy = 100 rad = 100 cGy.

Since the activity of the source is needed in order to calculate the dose rate, activity is given by:

$$A(t) = A(0)e^{-\lambda t} \tag{A8}$$

Where the factor $e^{-\lambda t}$ is the fraction of the remaining activity after time t and is known as decay factor DF.

Therefore the dose rate is given by:

$$\dot{D} = \frac{D}{t} = \frac{\left[\frac{(E/n) \bullet N}{m}\right]}{\left[\frac{N}{2A_o}\right]} \tag{A9}$$

$$\dot{D} = \frac{D}{t} = \frac{(E/n) \bullet 2A_0}{m} \tag{A10}$$

In order to obtain the final dose rate the decay factor (DF) is required to account for the decayed activity of the source, hence:

$$\text{Dose rate} = \text{Dose in J/Kg} \times [\text{Activity in Bq} \times \text{DF}] \tag{A11}$$

Where 1 $Bq = 1s^{-1}$ (1 disintegration per second) and $1\,curie(Ci) = 3.7 \times 10^{10}\,Bq$

Since for Sr-90 + Y-90 the are two betas per particles per decay, then

$$\text{Dose rate} = \text{Dose in J/Kg} \times [2 \times \text{Activity in s}^{-1} \times \text{DF}] \tag{A12}$$

The activity of the source can also be given in terms of number of particles available at time t as follows:

$$A = -\frac{dN}{dt} = \lambda N \tag{A13}$$

By integrating equation A13 from initial to available particle numbers and from time zero to time t

$$\int_{N_0}^{N(t)} \frac{dN}{N} = \int_0^t -\lambda dt \tag{A14}$$

$$\ln N(t) = -\lambda t + \ln N_0 \tag{A15}$$

By plotting equation A15, on a semi-logarithmic plot it is a straight line curve, whiles on linear plot it gives an exponential curve approaching zero.

APPENDIX B

CALCULATED STUDY RESULTS

Table B.1: Percentage differences of spectra through surfaces, at the back and in front of Teflon-encased eye applicator.

Surfaces	**(%) difference**								
3 and 5	5 and 6	6 and 9	9 and 14	14 and 15	15 and 16	16 and 17	17 and 18	2 and 9	2 and 18
0.000	0.000	0.000	0.000	0.000	0.000	0.000	0.000	0.000	0.000
1.033	0.6259	196.7	8.332	3.859	2.921	3.351	3.557	200.000	200.000
2.417	0.6117	194.2	7.987	3.975	2.785	2.946	3.283	200.000	200.000
3.251	0.1879	190.1	7.162	3.880	2.789	3.051	3.446	200.000	200.000
3.364	0.0530	185.4	6.390	3.723	2.665	3.114	3.411	200.000	200.000
3.088	0.1752	179.8	6.385	3.667	2.791	2.967	3.260	200.000	200.000
2.760	0.1516	173.3	5.775	3.634	2.635	3.033	3.314	200.000	200.000
2.790	0.0955	163.9	5.725	3.568	2.561	2.996	3.373	200.000	200.000
3.119	0.2722	151.5	5.143	3.442	2.528	2.804	3.310	200.000	200.000
4.273	0.6485	132.1	5.042	3.355	2.491	2.952	3.311	200.000	200.000
6.217	1.3142	108.2	4.778	3.350	2.476	2.816	3.291	200.000	200.000
6.761	2.0804	99.7	4.535	3.290	5.242	0.043	3.304	200.000	200.000
6.117	1.8452	98.5	4.374	3.116	7.091	1.943	3.146	200.000	200.000
5.698	1.8794	97.8	4.073	3.129	8.694	3.622	3.156	200.000	200.000
5.230	1.3321	97.1	4.111	2.994	10.255	5.198	3.048	200.000	200.000
4.741	1.3461	97.9	3.770	2.931	12.203	7.218	3.146	200.000	200.000
4.360	1.0873	98.4	3.709	2.796	13.870	8.989	3.053	200.000	200.000
4.106	0.6193	99.8	3.571	2.822	14.629	9.888	3.013	200.000	200.000
3.790	0.6595	102.0	3.263	2.610	16.540	11.943	3.006	200.000	200.000
3.264	0.8091	104.3	3.038	2.423	18.815	14.318	2.794	200.000	200.000
3.069	0.2683	107.1	2.974	2.333	20.738	16.390	2.823	200.000	200.000
2.776	0.2916	110.7	2.738	2.216	23.454	19.522	2.738	200.000	200.000

2.480	0.4133	114.1	2.642	2.224	24.970	21.190	2.595	200.000	200.000
2.093	0.9785	119.2	2.327	1.875	28.518	24.893	2.575	200.000	200.000
1.903	0.2201	123.9	2.027	1.731	33.044	29.720	2.383	200.000	200.000
1.827	1.0018	129.7	1.750	1.572	37.864	34.863	2.080	200.000	200.000
1.212	1.4462	135.2	1.632	1.554	44.850	42.160	2.044	200.000	200.000
1.027	0.9799	142.8	1.466	1.126	49.979	47.716	1.754	200.000	200.000
0.854	1.4099	150.3	1.122	0.962	59.367	57.322	1.633	200.000	200.000
0.485	1.0254	157.7	0.916	0.763	72.370	70.881	1.519	200.000	200.000
0.139	1.2693	166.1	0.660	0.577	89.723	88.477	1.209	200.000	200.000
0.020	1.2343	174.3	0.486	0.449	109.623	108.783	0.914	200.000	200.000
0.389	1.1409	182.6	0.114	0.344	132.418	131.951	0.626	200.000	200.000
0.696	1.5053	189.5	0.361	0.136	164.657	164.555	0.364	200.000	200.000
1.241	1.5714	194.8	0.000	0.225	192.913	192.897	0.113	200.000	200.000
1.284	1.4712	198.4	0.000	0.000	200.000	200.000	0.939	200.000	200.000
1.883	1.1611	199.8	0.000	0.000	200.000	200.000	0.000	200.000	200.000
2.134	0.0141	200.0	0.000	0.000	0.000	0.000	0.000	0.000	0.000
2.926	0.0698	200.0	0.000	0.000	0.000	0.000	0.000	0.000	0.000
3.357	3.9071	200.0	0.000	0.000	0.000	0.000	0.000	0.000	0.000
4.183	0.7438	200.0	0.000	0.000	0.000	0.000	0.000	0.000	0.000

Table B.2: The percentage difference data of varied Teflon thickness with 0.05 cm $SrCl_2$ and standard eye applicator.

Source: 0.05 cm	**Teflon thicknesses:**								
0.00 cm	**0.02 cm**	**0.05 cm**	**0.1 cm**	**0.15 cm**	**0.2 cm**	**0.25 cm**	**0.3 cm**	**0.35 cm**	**0.4 cm**
(%) difference	**(%) difference**	**(%) difference**	**(%) difference**	**(%) difference**	**(%) difference**	**(%) difference**	**(%) difference**	**(%) difference**	**(%) difference**
105.65	81.71	41.84	10.95	59.23	106.00	148.33	172.46	191.03	197.81
106.55	81.20	46.05	5.64	50.39	107.34	148.99	175.68	191.47	197.55
99.24	82.28	48.23	2.15	58.53	106.97	150.35	173.78	193.24	198.23
94.86	76.86	48.23	1.98	49.85	106.99	199.43	176.27	192.73	197.20

93.08	78.06	50.54	0.73	53.52	105.99	147.64	175.69	189.91	198.35
90.86	75.38	47.12	2.73	59.56	107.29	151.98	180.99	191.89	197.81
82.96	71.95	47.03	1.40	62.43	115.34	153.75	181.76	192.60	196.78
81.49	73.42	45.93	4.22	54.84	120.43	156.43	186.80	190.45	198.52
77.41	67.86	45.40	6.80	59.99	114.40	158.62	176.73	190.61	199.39
76.71	70.15	48.19	5.82	66.16	113.23	162.88	185.58	193.22	198.76
79.11	67.67	49.37	5.40	66.52	117.92	156.94	187.41	194.76	198.35
75.68	68.72	50.34	1.46	64.78	119.84	146.65	185.87	196.45	197.58
73.43	70.23	45.79	2.74	71.98	118.81	150.35	187.43	197.79	199.06
80.74	72.59	48.72	1.35	63.17	121.78	161.99	186.51	199.83	198.65
74.27	73.34	45.54	4.63	61.89	110.70	162.56	191.61	199.70	197.50
75.19	60.67	41.93	10.44	74.85	116.00	160.97	187.16	197.06	199.23
75.31	60.89	39.25	12.60	73.74	136.46	164.42	191.26	196.38	198.89
78.75	70.73	45.07	8.53	82.10	128.45	164.81	187.70	198.18	199.55
79.66	65.52	42.83	10.69	77.67	130.71	176.82	190.58	196.42	200.00
75.18	61.07	42.22	11.94	75.02	123.65	167.60	190.51	198.81	200.00
69.12	62.16	41.15	13.93	87.17	125.27	178.92	187.41	198.70	199.98
77.31	69.26	53.93	7.46	61.24	127.22	170.01	189.11	197.97	198.97
76.34	68.48	44.84	17.17	83.02	125.08	176.24	193.25	200.00	200.00
76.77	62.10	35.07	21.80	79.41	137.54	174.72	188.69	200.00	200.00
70.55	58.37	33.16	19.98	87.44	145.49	183.25	189.53	199.82	199.82
85.97	74.98	58.21	11.49	67.65	148.68	176.87	195.66	200.00	200.00
94.42	86.30	60.76	3.19	71.71	131.81	177.70	192.35	200.00	200.00
74.78	66.89	38.63	24.59	89.87	139.76	183.79	194.91	200.00	200.00
89.09	75.22	47.35	11.50	101.13	136.81	185.24	195.76	200.00	200.00
91.31	68.36	41.64	9.72	89.66	156.03	185.20	188.32	199.92	199.49
87.00	78.22	46.20	22.02	96.83	135.45	188.45	196.26	200.00	200.00
64.37	60.19	31.00	36.88	103.42	151.37	179.50	196.82	200.00	200.00
78.64	61.36	40.67	37.09	113.93	148.32	188.17	198.00	200.00	200.00
92.69	72.34	45.86	19.69	87.81	156.61	186.82	199.10	200.00	200.00
77.65	73.09	29.97	30.77	106.25	168.13	196.96	199.20	200.00	200.00

95.11	88.24	60.82	13.40	92.27	143.77	197.13	200.00	200.00	200.00
95.44	79.63	47.67	27.23	83.97	156.55	196.72	200.00	200.00	200.00
90.67	73.22	43.03	20.84	100.36	158.68	189.95	200.00	200.00	200.00
87.29	59.37	44.47	42.00	96.30	160.06	197.06	200.00	200.00	200.00
80.37	60.86	27.15	32.55	115.44	170.49	197.38	200.00	200.00	200.00
73.54	56.13	10.79	47.16	130.39	182.64	193.27	200.00	200.00	200.00
79.74	64.81	20.73	56.03	121.23	156.75	199.26	200.00	200.00	200.00
79.60	77.47	31.06	44.67	120.29	184.30	199.17	200.00	200.00	200.00
96.88	80.61	42.68	33.98	109.95	162.16	190.06	200.00	200.00	200.00
86.18	81.34	19.08	49.64	102.82	185.78	200.00	200.00	200.00	200.00
104.50	84.23	41.07	28.39	102.80	175.56	200.00	200.00	200.00	200.00
93.66	59.38	28.72	49.16	133.96	165.80	200.00	200.00	199.69	199.61
126.75	93.79	12.42	20&19	96.25	190.06	200.00	200.00	200.00	200.00
94.58	87.75	8.7'	50.91	142.15	162.20	200.00	200*00	200.00	200.00
86.09	82.99	24.45	78.48	129.11	194.52	200.00	200.00	200.00	200.00
95.91	114.63	60.03	40.57	158.79	186.61	198.59	198.59	198.59	198.59
102.65	83.00	44.75	58.50	140.19	178.88	200.00	200.00	200.00	200.00
105.25	73.29	37.73	67.88	94.06	200.00	200.00	200.00	195.03	195.03
91.81	84.23	48.38	66.16	125.70	200.00	200.00	200.00	200.00	200.00
103.70	84.41	53.67	50.22	126.83	200.00	200.00	200.00	200.00	200.00
114.79	70.12	35.54	104.56	154.15	200.00	200.00	200.00	200.00	200.00
107.80	75.17	37.17	109.61	177.04	200.00	200.00	200.00	200.00	200.00
111.08	80.11	35.94	106.96	166.38	183.64	200.00	200.00	200.00	200.00
75.64	22.70	27.35	128.75	162.66	183.17	200.00	200.00	200.00	200.00
162.77	132.26	98.47	68.07	153.57	55.55	200.00	200.00	200.00	200.00

Table B.3: The percentage difference of varied $SrCl_2$ thickness with 0.1 cm Teflon and standard eye applicator.

Teflon: 0.1 cm			
Source: 0.03 cm	**0.04 cm**	**0.045 cm**	**0.05 cm**
(%) difference	**(%) difference**	**(%) difference**	**(%) difference**
4.73	0.27	4.51	10.95
10.18	6.50	0.31	5.64
9.15	5.27	0.95	2.15
10.48	6.73	0.56	1.98
14.71	12.09	2.23	0.73
11.91	7.63	4.26	2.73
12.01	1.36	1.03	1.40
9.60	7.80	5.06	4.22
8.47	1.73	4.82	6.80
9.03	5.47	1.78	5.82
7.54	2.50	3.68	5.40
13.25	5.90	2.92	1.46
11.91	1.86	2.92	2.74
23.32	8.11	4.60	1.35
13.59	1.49	7.48	4.63
0.88	0.08	2.59	10.44
3.13	6.96	7.44	12.60
6.30	2.87	7.97	8.53
5.07	6.28	1.70	10.69
4.83	0.88	1.24	11.94
8.60	5.60	0.29	13.93
2.94	1.19	1.17	7.46
7.27	8.62	8.21	17.17
14.16	15.40	13.01	21.80
12.92	11.92	24.28	19.98
4.40	8.41	3.53	11.49

2.59	6.44	1.90	3.19
18.37	9.96	17.32	24.59
15.07	0.62	7.43	11.50
13.19	5.98	16.19	9.72
16.84	17.74	0.05	22.02
23.69	29.71	17.77	36.88
28.20	33.04	15.10	37.09
17.38	2.74	10.88	19.69
19.72	23.55	34.05	30.77
0.81	0.13	16.35	13.40
7.33	12.53	44.08	27.23
0.36	16.89	35.37	20.84
43.50	36.91	29.34	42.00
17.77	51.03	27.13	32.55
48.14	60.79	36.76	47.16
38.31	53.06	55.80	56.03
25.83	41.42	47.50	44.67
44.06	40.11	58.07	33.98
20.93	71.04	80.05	49.64
25.70	34.96	37.47	28.39
37.99	53.38	53.34	49.16
1.21	11.40	12.07	20.19
31.63	28.78	24.00	50.91
58.67	120.22	76.42	78.48
34.24	58.91	26.24	40.57
87.91	40.56	80.00	58.50
127.43	57.52	53.28	67.88
92.68	68.58	109.88	66.16
111.88	4.43	39.62	50.22
69.05	71.27	86.90	104.56
81.72	59.74	92.22	109.61

77.78	28.27	81.21	106.96
96.95	91.42	89.15	128.75
46.00	48.91	83.34	68.07

Table B.4: The percentage differences of varied $SrCl_2$ thickness with 0.125 cm Teflon and standard eye applicator.

Teflon: 0.125 cm		
Source: 0.04 cm	**0.045 cm**	**0.05 cm**
(%) difference	**(%) difference**	**(%) difference**
31.12	30.16	31.70
25.95	25.25	31.60
19.22	24.18	32.54
24.59	24.47	24.16
19.62	22.40	28.63
22.08	22.37	22.09
21.95	26.76	21.55
17.42	30.75	28.99
22.16	31.27	28.69
20.57	30.14	30.61
23.33	27.75	30.79
20.39	30.37	30.69
23.66	37.20	40.57
18.51	27.96	35.77
28.78	33.41	34.45
29.27	31.84	41.72
36.86	40.38	50.42
25.22	27.29	30.46
34.63	31.28	43.26
24.01	32.79	46.38
32.42	38.65	50.26
34.34	45.13	45.91

42.23	39.21	45.28
51.96	48.20	55.53
55.91	43.21	51.94
33.02	31.66	37.02
30.86	31.21	22.51
48.69	50.07	44.41
36.19	52.70	53.37
43.19	72.59	73.37
45.89	52.81	68.72
54.46	75.41	82.15
55.33	58.96	66.21
31.73	46.12	36.09
51.07	74.67	77.52
40.23	24.67	56.34
61.59	42.62	55.43
68.03	43.07	50.56
71.75	59.92	94.79
84.23	63.78	85.53
86.75	97.57	107.42
80.16	73.19	95.36
67.96	99.74	78.71
62.06	88.18	79.74
75.90	64.66	109.06
56.23	35.03	120.58
71.62	91.29	113.36
60.94	94.31	87.38
89.29	109.84	104.54
108.20	110.39	124.56
134.78	119.27	133.69
114.43	147.62	122.01
118.40	140.86	129.85

129.28	146.93	143.57
131.11	134.08	154.91
176.01	174.15	165.42
163.95	137.87	181.72
144.53	173.18	166.50
155.02	172.04	169.44
138.95	133.84	200.00

Table B.5: The percentage differences of varied SSD without Teflon material and standard eye applicator spectra.

Teflon: 0.00 cm		**Source: 0.05 cm**
%diff	**%diff**	**%diff**
SSD (cm)	**SSD (cm)**	**SSD (cm)**
0.02 and 0.05	**0.05 and 0.1**	**0.1 and Std**
17.58	24.28	72.12
15.23	26.03	73.73
14.31	16.65	74.12
11.28	21.38	67.60
11.93	17.06	68.86
10.92	20.56	64.10
8.01	23.03	55.62
11.91	16.90	56.10
9.15	18.96	52.24
10.74	12.26	56.26
8.42	20.70	53.17
5.51	15.91	56.59
5.21	19.85	50.77
11.23	19.19	53.77
7.80	23.55	45.71
10.57	25.19	42.50

10.42	16.57	51.01
4.53	16.14	60.59
7.93	19.55	55.31
8.42	12.81	56.24
3.38	10.29	56.80
0.03	18.40	61.06
11.08	19.59	48.67
15.41	19.29	45.32
10.68	11.92	50.01
16.24	11.33	62.19
16.00	10.65	72.41
13.50	10.69	53.07
13.11	22.75	58.11
8.38	20.12	67.28
16.38	13.95	60.83
8.31	14.47	43.24
9.72	14.11	57.58
6.18	21.90	69.19
12.89	6.58	60.49
0.83	24.18	74.54
6.76	15.53	77.31
2.76	18.24	77.91
7.62	16.18	67.03
2.42	20.43	64.69
7.64	0.09	66.93
6.77	7.31	67.57
12.91	7.39	61.84
6.86	8.98	84.30
9.17	14.50	65.94
8.15	25.89	90.91
6.17	19.33	72.56

32.61	4.88	101.40
4.49	3.10	88.58
0.69	13.06	75.73
9.37	5.65	98.75
8.75	7.58	90.11
6.60	28.55	88.32
3.60	11.52	85.44
8.34	23.85	114.65
15.95	6.21	98.96
4.12	5.32	106.94
14.17	2.81	118.70
5.14	14.63	83.64
6.08	25.60	155.58

APPENDIX C

MCNP5 INPUT AND OUTPUT FILES

C.1 Example of Input files for Monte Carlo code, MCNP5:

```
Title: Strontium-90 model + water phantom
c Sr-90 dose calculations in water phantom-source thickness effect.
c
c Cell Card for water phantom
7   4 -1 -20 27 -26
8   4 -1 -20 28 -27
9   4 -1 -20 29 -28
10  4 -1 -20 30 -29
11  4 -1 -20 31 -30
12  4 -1 -20 32 -31
13  4 -1 -20 33 -32
14  4 -1 -20 34 -33
15  4 -1 -20 35 -34
16  4 -1 -20 36 -35
17  4 -1 -20 37 -36
18  4 -1 -20 38 -37
19  4 -1 -20 39 -38
20  4 -1 -20 40 -39
21  4 -1 -20 41 -40
22  4 -1 -20 42 -41
23  4 -1 -20 43 -42
24  4 -1 -20 44 -43
25  4 -1 -20 45 -44
26  4 -1 -20 46 -45
27  4 -1 -20 47 -46
28  4 -1 -20 48 -47
29  4 -1 -20 49 -48
30  4 -1 -20 50 -49
31  4 -1 -20 51 -50
32  4 -1 -20 52 -51
33  4 -1 -20 53 -52
```

```
34  4 -1 -20 54 -53
35  4 -1 -20 55 -54
36  4 -1 -20 56 -55
37  4 -1 -20 57 -56
38  4 -1 -20 58 -57
39  4 -1 -20 59 -58
40  4 -1 -20 60 -59
41  4 -1 -20 61 -60
42  4 -1 -20 62 -61
43  4 -1 -20 63 -62
44  4 -1 -20 64 -63
45  4 -1 -20 65 -64
46  4 -1 -20 66 -65
47  4 -1 -20 67 -66
48  4 -1 -20 68 -67
49  4 -1 -20 69 -68
50  4 -1 -20 70 -69
51  4 -1 -20 71 -70
52  4 -1 -20 72 -71
53  4 -1 -20 73 -72
54  4 -1 -20 74 -73
55  4 -1 -20 75 -74
56  4 -1 -20 76 -75
57  4 -1 -20 77 -76
58  4 -1 -20 78 -77
59  4 -1 -20 79 -78
60  4 -1 -20 80 -79
61  4 -1 -20 81 -80
62  4 -1 -20 82 -81
63  4 -1 -20 83 -82
64  4 -1 -20 84 -83
65  4 -1 -20 85 -84
66  4 -1 -20 86 -85
67  4 -1 -20 87 -86
68  4 -1 -20 88 -87
69  4 -1 -20 89 -88
70  4 -1 -20 90 -89
71  4 -1 -20 91 -90
```

```
72  4 -1 -20 92 -91
73  4 -1 -20 93 -92
74  4 -1 -20 94 -93
75  4 -1 -20 95 -94
76  4 -1 -20 96 -95
77  4 -1 -20 97 -96
78  4 -1 -20 98 -97
79  4 -1 -20 99 -98
80  4 -1 -20 100 -99
81 4 -1 20 -25 27 -26
82 4 -1 20 -25 28 -27
83 4 -1 20 -25 29 -28
84 4 -1 20 -25 30 -29
85 4 -1 20 -25 31 -30
86 4 -1 20 -25 32 -31
87 4 -1 20 -25 33 -32
88 4 -1 20 -25 34 -33
89 4 -1 20 -25 35 -34
90 4 -1 20 -25 36 -35
91 4 -1 20 -25 37 -36
92 4 -1 20 -25 38 -37
93 4 -1 20 -25 39 -38
94 4 -1 20 -25 40 -39
95 4 -1 20 -25 41 -40
96 4 -1 20 -25 42 -41
97 4 -1 20 -25 43 -42
98 4 -1 20 -25 44 -43
99 4 -1 20 -25 45 -44
100 4 -1 20 -25 46 -45
101 4 -1 20 -25 47 -46
102 4 -1 20 -25 48 -47
103 4 -1 20 -25 49 -48
104 4 -1 20 -25 50 -49
105 4 -1 20 -25 51 -50
106 4 -1 20 -25 52 -51
107 4 -1 20 -25 53 -52
108 4 -1 20 -25 54 -53
109 4 -1 20 -25 55 -54
```

```
110 4 -1 20 -25 56 -55
111 4 -1 20 -25 57 -56
112 4 -1 20 -25 58 -57
113 4 -1 20 -25 59 -58
114 4 -1 20 -25 60 -59
115 4 -1 20 -25 61 -60
116 4 -1 20 -25 62 -61
117 4 -1 20 -25 63 -62
118 4 -1 20 -25 64 -63
119 4 -1 20 -25 65 -64
120 4 -1 20 -25 66 -65
121 4 -1 20 -25 67 -66
122 4 -1 20 -25 68 -67
123 4 -1 20 -25 69 -68
124 4 -1 20 -25 70 -69
125 4 -1 20 -25 71 -70
126 4 -1 20 -25 72 -71
127 4 -1 20 -25 73 -72
128 4 -1 20 -25 74 -73
129 4 -1 20 -25 75 -74
130 4 -1 20 -25 76 -75
131 4 -1 20 -25 77 -76
132 4 -1 20 -25 78 -77
133 4 -1 20 -25 79 -78
134 4 -1 20 -25 80 -79
135 4 -1 20 -25 81 -80
136 4 -1 20 -25 82 -81
137 4 -1 20 -25 83 -82
138 4 -1 20 -25 84 -83
139 4 -1 20 -25 85 -84
140 4 -1 20 -25 86 -85
141 4 -1 20 -25 87 -86
142 4 -1 20 -25 88 -87
143 4 -1 20 -25 89 -88
144 4 -1 20 -25 90 -89
145 4 -1 20 -25 91 -90
146 4 -1 20 -25 92 -91
147 4 -1 20 -25 93 -92
```

```
148 4 -1 20 -25 94 -93
149 4 -1 20 -25 95 -94
150 4 -1 20 -25 96 -95
151 4 -1 20 -25 97 -96
152 4 -1 20 -25 98 -97
153 4 -1 20 -25 99 -98
154 4 -1 20 -25 100 -99
c cell card of Applicator
1 1 -8.02   -1 -2 3                          $ Stainless steel
2 0         -4 5 -3                          $ Void between source and steel
3 2 -3.052  -4 6 -5                          $ Anhydrous SrCl2 source
4 3 -2.200  -8 9 -7 (1:-3) (4:-6)            $ Teflon
5 0         -9 10                            $ Front side of Applicator
6 0         -11 (25:-100:26) #1 #2 #3 #4 #5  $ Outer appl +water & inner sphere
155 0        11                               $ Outer world

c Surface Card of water phantom
20 cz  0.02
25 cz  1.25
26 pz  -1.73 $ cells divided into 0.01cm
27 pz  -1.74
28 pz  -1.75
29 pz  -1.76
30 pz  -1.77
31 pz  -1.78
32 pz  -1.79
33 pz  -1.80
34 pz  -1.81
35 pz  -1.82
36 pz  -1.83
37 pz  -1.84
38 pz  -1.85
39 pz  -1.86
40 pz  -1.87
41 pz  -1.88
42 pz  -1.89
43 pz  -1.90
44 pz  -1.91
```

```
45 pz  -1.92
46 pz  -1.93
47 pz  -1.94
48 pz  -1.95
49 pz  -1.96
50 pz  -1.97
51 pz  -1.98
52 pz  -1.99
53 pz  -2.00
54 pz  -2.01
55 pz  -2.02
56 pz  -2.03
57 pz  -2.04
58 pz  -2.05
59 pz  -2.06
60 pz  -2.07
61 pz  -2.08
62 pz  -2.09
63 pz  -2.10
64 pz  -2.11
65 pz  -2.12
66 pz  -2.13
67 pz  -2.14
68 pz  -2.15
69 pz  -2.16
70 pz  -2.17
71 pz  -2.18
72 pz  -2.19
73 pz  -2.20
74 pz  -2.21
75 pz  -2.22
76 pz  -2.23
77 pz  -2.24
78 pz  -2.25
79 pz  -2.26
80 pz  -2.27
81 pz  -2.28
82 pz  -2.29
```

```
83 pz  -2.30
84 pz  -2.31
85 pz  -2.32
86 pz  -2.33
87 pz  -2.34
88 pz  -2.35
89 pz  -2.36
90 pz  -2.37
91 pz  -2.38
92 pz  -2.39
93 pz  -2.40
94 pz  -2.41
95 pz  -2.42
96 pz  -2.43
97 pz  -2.44
98 pz  -2.45
99 pz  -2.46
100 pz -2.47
c surface card of applicator
1 cz  0.3
2 pz  2
3 pz -1.41
4 cz  0.25
5 pz -1.419
6 pz -1.42
7 pz  0
8 cz  1
9 sz -4.0 2.482
10 pz -1.5180
11 so 4.5

c Data Cards
c Mode: Transport photons and electrons
mode: p  e
imp:p,e 1 152i 1 0
c Source definition
sdef pos 0 0 -1.419 axs 0 0 -1 rad d1
     ext d3 par 3 erg d2  dir d4 vec 0 0 -1
```

```
si1 0 0.25
sp1 -21 1 $ uniformity
sc2 Sr-90 + Y-90 spectrum according to ICRU 72 & 56
Si2 H 0 0.1 0.2 0.3 0.4 0.5 0.6 0.7 0.8 0.9 1.0 1.1  &
      1.2 1.3 1.4 1.5 1.6 1.7 1.8 1.9 2.0 2.1 2.2    $ Beta energy
sp2   0 1.32 1.285 1.165 1  0.6 0.255 0.255 0.255    &
      0.255 0.255 0.255 0.245 0.235 0.22 0.205 0.185 &
      0.165 0.135 0.105 0.075 0.04 0.015             $ Beta probabilities
sc3 length of sample volume
si3 h 0 0.001 $ Source thickness
sp3 -21 0     $ uniformity sampling
si4 h 0 1
sp4 d 0 1 $ particles direction-angulation
m1 25000 -2  14000 -1 24000 -19 &
   28000 -10 26000 -68          $ Stainless steel
m2 38000 1 17000 2              $ SrCl2 source
m3 6000 2 9000 4                $ Teflon (C2F4)
m4 1000 2 8000 1            ESTEP=60 $ Water (H2O)
*f8:pe 7 8 9 10 11 12 13 14 64i 79 80 $ Cell dose
DBCN 17j 1
fq8 f e
f11:e 2 3 5 6 9 26 27 28 29 30 T $ energy spectrum
e11: 0.022 0.044 0.066 0.088 0.11 94i 2.2
c Other cards
nps 6000000
print
cut:e j 0.02
c end
```

C.2 Example of output files for Monte Carlo code, MCNP5:

```
         Thread Name & Version = MCNP5_RSICC, 1.20

                                 _
         ._ _    _  ._   ._    |_
         | | |  (_  | |  |_)    _)
                           |
 +---------------------------------------------------------------------+
 |   This program was prepared by the Regents of the University of     |
 |California at Los Alamos National Laboratory (the University) under  |
 |  contract number W-7405-ENG-36 with the U.S. Department of Energy   |
 |(DoE).  The University has certain rights in the program pursuant to|
 |  the contract and the program should not be copied or distributed   |
 | outside your organization.  All rights in the program are reserved  |
 |by the DoE and the University.  Neither the U.S. Government nor the  |
 | University makes any warranty, express or implied, or assumes any   |
 |     liability or responsibility for the use of this software.       |
 +---------------------------------------------------------------------+

1mcnp     version 5     ld=11052003                    06/29/09 14:32:30
 ***********************************************************************      probid =  06/29/09 14:32:30
 i=soef2

    1-       Title: Strontium-90 model + water phantom
    2-       c Sr-90 dose calculations in water phantom-source thickness effect.
    3-       c
    4-       c Cell Card for water phantom
    5-       7   4 -1 -20 27 -26
    6-       8   4 -1 -20 28 -27
    7-       9   4 -1 -20 29 -28
    8-       10  4 -1 -20 30 -29
    9-       11  4 -1 -20 31 -30
   10-       12  4 -1 -20 32 -31
   11-       13  4 -1 -20 33 -32
   12-       14  4 -1 -20 34 -33
   13-       15  4 -1 -20 35 -34
   14-       16  4 -1 -20 36 -35
```

```
15-       17  4 -1 -20 37 -36
16-       18  4 -1 -20 38 -37
17-       19  4 -1 -20 39 -38
18-       20  4 -1 -20 40 -39
19-       21  4 -1 -20 41 -40
20-       22  4 -1 -20 42 -41
21-       23  4 -1 -20 43 -42
22-       24  4 -1 -20 44 -43
23-       25  4 -1 -20 45 -44
24-       26  4 -1 -20 46 -45
25-       27  4 -1 -20 47 -46
26-       28  4 -1 -20 48 -47
27-       29  4 -1 -20 49 -48
28-       30  4 -1 -20 50 -49
29-       31  4 -1 -20 51 -50
30-       32  4 -1 -20 52 -51
31-       33  4 -1 -20 53 -52
32-       34  4 -1 -20 54 -53
33-       35  4 -1 -20 55 -54
34-       36  4 -1 -20 56 -55
35-       37  4 -1 -20 57 -56
36-       38  4 -1 -20 58 -57
37-       39  4 -1 -20 59 -58
38-       40  4 -1 -20 60 -59
39-       41  4 -1 -20 61 -60
40-       42  4 -1 -20 62 -61
41-       43  4 -1 -20 63 -62
42-       44  4 -1 -20 64 -63
43-       45  4 -1 -20 65 -64
44-       46  4 -1 -20 66 -65
45-       47  4 -1 -20 67 -66
46-       48  4 -1 -20 68 -67
47-       49  4 -1 -20 69 -68
48-       50  4 -1 -20 70 -69
49-       51  4 -1 -20 71 -70
50-       52  4 -1 -20 72 -71
51-       53  4 -1 -20 73 -72
52-       54  4 -1 -20 74 -73
```

```
53-       55  4 -1 -20 75 -74
54-       56  4 -1 -20 76 -75
55-       57  4 -1 -20 77 -76
56-       58  4 -1 -20 78 -77
57-       59  4 -1 -20 79 -78
58-       60  4 -1 -20 80 -79
59-       61  4 -1 -20 81 -80
60-       62  4 -1 -20 82 -81
61-       63  4 -1 -20 83 -82
62-       64  4 -1 -20 84 -83
63-       65  4 -1 -20 85 -84
64-       66  4 -1 -20 86 -85
65-       67  4 -1 -20 87 -86
66-       68  4 -1 -20 88 -87
67-       69  4 -1 -20 89 -88
68-       70  4 -1 -20 90 -89
69-       71  4 -1 -20 91 -90
70-       72  4 -1 -20 92 -91
71-       73  4 -1 -20 93 -92
72-       74  4 -1 -20 94 -93
73-       75  4 -1 -20 95 -94
74-       76  4 -1 -20 96 -95
75-       77  4 -1 -20 97 -96
76-       78  4 -1 -20 98 -97
77-       79  4 -1 -20 99 -98
78-       80  4 -1 -20 100 -99
79-       81 4 -1 20 -25 27 -26
80-       82 4 -1 20 -25 28 -27
81-       83 4 -1 20 -25 29 -28
82-       84 4 -1 20 -25 30 -29
83-       85 4 -1 20 -25 31 -30
84-       86 4 -1 20 -25 32 -31
85-       87 4 -1 20 -25 33 -32
86-       88 4 -1 20 -25 34 -33
87-       89 4 -1 20 -25 35 -34
88-       90 4 -1 20 -25 36 -35
89-       91 4 -1 20 -25 37 -36
90-       92 4 -1 20 -25 38 -37
```

```
 91-       93 4 -1 20 -25 39 -38
 92-       94 4 -1 20 -25 40 -39
 93-       95 4 -1 20 -25 41 -40
 94-       96 4 -1 20 -25 42 -41
 95-       97 4 -1 20 -25 43 -42
 96-       98 4 -1 20 -25 44 -43
 97-       99 4 -1 20 -25 45 -44
 98-      100 4 -1 20 -25 46 -45
 99-      101 4 -1 20 -25 47 -46
100-      102 4 -1 20 -25 48 -47
101-      103 4 -1 20 -25 49 -48
102-      104 4 -1 20 -25 50 -49
103-      105 4 -1 20 -25 51 -50
104-      106 4 -1 20 -25 52 -51
105-      107 4 -1 20 -25 53 -52
106-      108 4 -1 20 -25 54 -53
107-      109 4 -1 20 -25 55 -54
108-      110 4 -1 20 -25 56 -55
109-      111 4 -1 20 -25 57 -56
110-      112 4 -1 20 -25 58 -57
111-      113 4 -1 20 -25 59 -58
112-      114 4 -1 20 -25 60 -59
113-      115 4 -1 20 -25 61 -60
114-      116 4 -1 20 -25 62 -61
115-      117 4 -1 20 -25 63 -62
116-      118 4 -1 20 -25 64 -63
117-      119 4 -1 20 -25 65 -64
118-      120 4 -1 20 -25 66 -65
119-      121 4 -1 20 -25 67 -66
120-      122 4 -1 20 -25 68 -67
121-      123 4 -1 20 -25 69 -68
122-      124 4 -1 20 -25 70 -69
123-      125 4 -1 20 -25 71 -70
124-      126 4 -1 20 -25 72 -71
125-      127 4 -1 20 -25 73 -72
126-      128 4 -1 20 -25 74 -73
127-      129 4 -1 20 -25 75 -74
128-      130 4 -1 20 -25 76 -75
```

```
129-       131 4 -1 20 -25 77 -76
130-       132 4 -1 20 -25 78 -77
131-       133 4 -1 20 -25 79 -78
132-       134 4 -1 20 -25 80 -79
133-       135 4 -1 20 -25 81 -80
134-       136 4 -1 20 -25 82 -81
135-       137 4 -1 20 -25 83 -82
136-       138 4 -1 20 -25 84 -83
137-       139 4 -1 20 -25 85 -84
138-       140 4 -1 20 -25 86 -85
139-       141 4 -1 20 -25 87 -86
140-       142 4 -1 20 -25 88 -87
141-       143 4 -1 20 -25 89 -88
142-       144 4 -1 20 -25 90 -89
143-       145 4 -1 20 -25 91 -90
144-       146 4 -1 20 -25 92 -91
145-       147 4 -1 20 -25 93 -92
146-       148 4 -1 20 -25 94 -93
147-       149 4 -1 20 -25 95 -94
148-       150 4 -1 20 -25 96 -95
149-       151 4 -1 20 -25 97 -96
150-       152 4 -1 20 -25 98 -97
151-       153 4 -1 20 -25 99 -98
152-       154 4 -1 20 -25 100 -99
153-       c cell card of Applicator
154-       1 1 -8.02   -1 -2 3                          $ Stainless steel
155-       2 0         -4 5 -3                          $ Void between source and steel
156-       3 2 -3.052  -4 6 -5                          $ Anhydrous SrCl2 source
157-       4 3 -2.200  -8 9 -7 (1:-3) (4:-6)            $ Teflon
158-       5 0         -9 10                            $ Front side of Applicator
159-       6 0         -11 (25:-100:26) #1 #2 #3 #4 #5  $ Outer appl +water & inner sphere
160-       155 0        11                               $ Outer world
161-
162-       c Surface Card of water phantom
163-       20 cz  0.02
164-       25 cz  1.25
165-       26 pz  -1.73 $ cells divided into 0.01cm
166-       27 pz  -1.74
```

```
167-       28 pz  -1.75
168-       29 pz  -1.76
169-       30 pz  -1.77
170-       31 pz  -1.78
171-       32 pz  -1.79
172-       33 pz  -1.80
173-       34 pz  -1.81
174-       35 pz  -1.82
175-       36 pz  -1.83
176-       37 pz  -1.84
177-       38 pz  -1.85
178-       39 pz  -1.86
179-       40 pz  -1.87
180-       41 pz  -1.88
181-       42 pz  -1.89
182-       43 pz  -1.90
183-       44 pz  -1.91
184-       45 pz  -1.92
185-       46 pz  -1.93
186-       47 pz  -1.94
187-       48 pz  -1.95
188-       49 pz  -1.96
189-       50 pz  -1.97
190-       51 pz  -1.98
191-       52 pz  -1.99
192-       53 pz  -2.00
193-       54 pz  -2.01
194-       55 pz  -2.02
195-       56 pz  -2.03
196-       57 pz  -2.04
197-       58 pz  -2.05
198-       59 pz  -2.06
199-       60 pz  -2.07
200-       61 pz  -2.08
201-       62 pz  -2.09
202-       63 pz  -2.10
203-       64 pz  -2.11
204-       65 pz  -2.12
```

```
205-       66 pz  -2.13
206-       67 pz  -2.14
207-       68 pz  -2.15
208-       69 pz  -2.16
209-       70 pz  -2.17
210-       71 pz  -2.18
211-       72 pz  -2.19
212-       73 pz  -2.20
213-       74 pz  -2.21
214-       75 pz  -2.22
215-       76 pz  -2.23
216-       77 pz  -2.24
217-       78 pz  -2.25
218-       79 pz  -2.26
219-       80 pz  -2.27
220-       81 pz  -2.28
221-       82 pz  -2.29
222-       83 pz  -2.30
223-       84 pz  -2.31
224-       85 pz  -2.32
225-       86 pz  -2.33
226-       87 pz  -2.34
227-       88 pz  -2.35
228-       89 pz  -2.36
229-       90 pz  -2.37
230-       91 pz  -2.38
231-       92 pz  -2.39
232-       93 pz  -2.40
233-       94 pz  -2.41
234-       95 pz  -2.42
235-       96 pz  -2.43
236-       97 pz  -2.44
237-       98 pz  -2.45
238-       99 pz  -2.46
239-       100 pz -2.47
240-       c surface card of applicator
241-       1 cz  0.3
242-       2 pz  2
```

```
3 pz -1.41
4 cz  0.25
5 pz -1.419
6 pz -1.42
7 pz  0
8 cz  1
9 sz -4.0 2.482
10 pz -1.5180
11 so 4.5

c Data Cards
c Mode: Transport photons and electrons
mode: p  e
imp:p,e 1 152i 1 0
c Source definition
sdef pos 0 0 -1.419 axs 0 0 -1 rad d1
     ext d3 par 3 erg d2  dir d4 vec 0 0 -1
si1 0 0.25
sp1 -21 1 $ uniformity
sc2 Sr-90 + Y-90 spectrum according to ICRU 72 & 56
Si2 H 0 0.1 0.2 0.3 0.4 0.5 0.6 0.7 0.8 0.9 1.0 1.1  &
      1.2 1.3 1.4 1.5 1.6 1.7 1.8 1.9 2.0 2.1 2.2    $ Beta energy
sp2   0 1.32 1.285 1.165 1  0.6 0.255 0.255 0.255    &
      0.255 0.255 0.255 0.245 0.235 0.22 0.205 0.185 &
      0.165 0.135 0.105 0.075 0.04 0.015             $ Beta probabilities
sc3 length of sample volume
si3 h 0 0.001 $ Source thickness
sp3 -21 0 $ uniformity sampling
si4 h 0 1
sp4 d 0 1 $ particles direction-angulation
m1 25000 -2  14000 -1 24000 -19 &
   28000 -10 26000 -68          $ Stainless steel
m2 38000 1 17000 2              $ SrCl2 source
m3 6000 2 9000 4                $ Teflon (C2F4)
m4 1000 2 8000 1            ESTEP=60 $ Water (H2O)
*f8:pe 7 8 9 10 11 12 13 14 64i 79 80 $ Cell dose
DBCN 17j 1
fq8 f e
```

```
  281-       f11:e 2 3 5 6 9 26 27 28 29 30 T $ energy spectrum
  282-       e11: 0.022 0.044 0.066 0.088 0.11 94i 2.2
  283-       c Other cards
  284-       nps 6000000
  285-       print
  286-       cut:e j 0.02
  287-       c end
************************************************************************************************************
1problem summary

      run terminated when   6000000 particle histories were done.
+                                                                                  06/29/09 16:42:24
      Title: Strontium-90 model + water phantom                          probid =  06/29/09 14:32:30
0
 photon creation     tracks      weight        energy         photon loss   tracks  weight    energy
                                 (per source particle)                              (per source particle)

 source                   0    0.            0.             escape          132150 2.1343E-02  2.7978E-03
                                                              energy cutoff            0    0.   2.0600E-05
                                                              time cutoff              0    0.    0.
 weight window            0    0.            0.             weight window            0    0.    0.
 cell importance          0    0.            0.             cell importance          0    0.    0.
 weight cutoff            0    0.            0.             weight cutoff            0    0.    0.
 e or t importance        0    0.            0.             e or t importance        0    0.    0.
 dxtran                   0    0.            0.             dxtran                   0    0.    0.
 forced collisions        0    0.            0.             forced collisions        0    0.    0.
 exp. transform           0    0.            0.             exp. transform           0    0.    0.
 from neutrons            0    0.            0.             compton scatter          0    0.    1.4645E-04
 bremsstrahlung      534931    8.6394E-02    3.7073E-03     capture             447242 7.2232E-02 8.0964E-04
 p-annihilation           0    0.            0.             pair production          0    0.    0.
 photonuclear             0    0.            0.             photonuclear abs         0    0.    0.
 electron x-rays      30862    4.9844E-03    5.1591E-05
 1st fluorescence     13578    2.1929E-03    1.5556E-05
 2nd fluorescence        21    3.3916E-06    6.2098E-09
     total           579392    9.3575E-02    3.7745E-03     total           579392  9.3575E-02  3.7745E-03

   number of photons banked                   565814       average time of (shakes)      cutoffs
   photon tracks per source particle      9.6565E-02       escape            1.3726E-02 tco   1.0000E+33
```

```
   photon collisions per source particle  8.3770E-02      capture           8.2599E-04 co    1.0000E-03
   total photon collisions                   502620      capture or escape 3.7682E-03 wc1  -5.0000E-01
                                                         any termination   3.7682E-03 wc2  -2.5000E-01
0
 electron creation   tracks      weight        energy     electron loss     tracks  weight     energy
                               (per source particle)                              (per source particle)
 source             6000000    9.6903E-01    5.8251E-01  escape            10266    1.6580E-03 8.3276E-04
                                                         energy cutoff     13858702 2.2383E+00 4.5429E-02
                                                         time cutoff       0        0.         0.
 weight window            0    0.            0.          weight window     0        0.         0.
 cell importance          0    0.            0.          cell importance   0        0.         0.
 weight cutoff            0    0.            0.          weight cutoff     0        0.         0.
 e or t importance        0    0.            0.          e or t importance 0        0.         0.
 pair production          0    0.            0.          scattering        0        0.        6.0049E-01
 compton recoil        9411    1.5199E-03    1.2089E-04  bremsstrahlung    0        0.        3.7061E-03
 photo-electric       53870    8.7003E-03    3.7460E-04
 photon auger             0    0.            0.
 electron auger           0    0.            0.
 knock-on           7805687    1.2607E+00    6.7460E-02
     total         13868968    2.2399E+00    6.5046E-01  total         13868968    2.2399E+00   6.5046E-01

   number of electrons banked               7868968                                  cutoffs
   electron tracks per source particle   2.3115E+00                                     tco   1.0000E+33
   electron sub-steps per source particle 5.5734E+02                                    eco   2.0000E-02
   total electron sub-steps              3344060585                                     wc1   0.0000E+00
                                                                                        wc2   0.0000E+00

 computer time so far in this run   129.51 minutes          maximum number ever in bank        20
 computer time in mcrun             129.49 minutes          bank overflows to backup file       0
 source particles per minute            4.6337E+04
 random numbers generated              15828597556          most random numbers used was    58374 in
history  1548161

 range of sampled source weights = 9.6903E-01 to 9.6903E-01
********************************************************************************
1tally  11        nps =  6000000
           tally type 1    number of particles crossing a surface.
           tally for  electrons
```

```
surface  2
     energy
   2.2000E-02   0.00000E+00 0.0000
   4.4000E-02   0.00000E+00 0.0000
   6.6000E-02   0.00000E+00 0.0000
   8.8000E-02   0.00000E+00 0.0000
   1.1000E-01   0.00000E+00 0.0000
   1.3200E-01   0.00000E+00 0.0000
   1.5400E-01   0.00000E+00 0.0000
   1.7600E-01   0.00000E+00 0.0000
   1.9800E-01   0.00000E+00 0.0000
   2.2000E-01   0.00000E+00 0.0000
   2.4200E-01   0.00000E+00 0.0000
   2.6400E-01   0.00000E+00 0.0000
   2.8600E-01   0.00000E+00 0.0000
   3.0800E-01   0.00000E+00 0.0000
   3.3000E-01   0.00000E+00 0.0000
   3.5200E-01   0.00000E+00 0.0000
   3.7400E-01   0.00000E+00 0.0000
   3.9600E-01   0.00000E+00 0.0000
   4.1800E-01   0.00000E+00 0.0000
   4.4000E-01   0.00000E+00 0.0000
   4.6200E-01   0.00000E+00 0.0000
   4.8400E-01   0.00000E+00 0.0000
   5.0600E-01   0.00000E+00 0.0000
   5.2800E-01   0.00000E+00 0.0000
   5.5000E-01   0.00000E+00 0.0000
   5.7200E-01   0.00000E+00 0.0000
   5.9400E-01   0.00000E+00 0.0000
   6.1600E-01   0.00000E+00 0.0000
   6.3800E-01   0.00000E+00 0.0000
   6.6000E-01   0.00000E+00 0.0000
   6.8200E-01   0.00000E+00 0.0000
   7.0400E-01   0.00000E+00 0.0000
   7.2600E-01   0.00000E+00 0.0000
   7.4800E-01   0.00000E+00 0.0000
   7.7000E-01   0.00000E+00 0.0000
```

```
7.9200E-01   0.00000E+00 0.0000
8.1400E-01   0.00000E+00 0.0000
8.3600E-01   0.00000E+00 0.0000
8.5800E-01   0.00000E+00 0.0000
8.8000E-01   0.00000E+00 0.0000
9.0200E-01   0.00000E+00 0.0000
9.2400E-01   0.00000E+00 0.0000
9.4600E-01   0.00000E+00 0.0000
9.6800E-01   0.00000E+00 0.0000
9.9000E-01   0.00000E+00 0.0000
1.0120E+00   0.00000E+00 0.0000
1.0340E+00   0.00000E+00 0.0000
1.0560E+00   0.00000E+00 0.0000
1.0780E+00   0.00000E+00 0.0000
1.1000E+00   0.00000E+00 0.0000
1.1220E+00   0.00000E+00 0.0000
1.1440E+00   0.00000E+00 0.0000
1.1660E+00   0.00000E+00 0.0000
1.1880E+00   0.00000E+00 0.0000
1.2100E+00   0.00000E+00 0.0000
1.2320E+00   0.00000E+00 0.0000
1.2540E+00   0.00000E+00 0.0000
1.2760E+00   0.00000E+00 0.0000
1.2980E+00   0.00000E+00 0.0000
1.3200E+00   0.00000E+00 0.0000
1.3420E+00   0.00000E+00 0.0000
1.3640E+00   0.00000E+00 0.0000
1.3860E+00   0.00000E+00 0.0000
1.4080E+00   0.00000E+00 0.0000
1.4300E+00   0.00000E+00 0.0000
1.4520E+00   0.00000E+00 0.0000
1.4740E+00   0.00000E+00 0.0000
1.4960E+00   0.00000E+00 0.0000
1.5180E+00   0.00000E+00 0.0000
1.5400E+00   0.00000E+00 0.0000
1.5620E+00   0.00000E+00 0.0000
1.5840E+00   0.00000E+00 0.0000
1.6060E+00   0.00000E+00 0.0000
```

```
   1.6280E+00   0.00000E+00 0.0000
   1.6500E+00   0.00000E+00 0.0000
   1.6720E+00   0.00000E+00 0.0000
   1.6940E+00   0.00000E+00 0.0000
   1.7160E+00   0.00000E+00 0.0000
   1.7380E+00   0.00000E+00 0.0000
   1.7600E+00   0.00000E+00 0.0000
   1.7820E+00   0.00000E+00 0.0000
   1.8040E+00   0.00000E+00 0.0000
   1.8260E+00   0.00000E+00 0.0000
   1.8480E+00   0.00000E+00 0.0000
   1.8700E+00   0.00000E+00 0.0000
   1.8920E+00   0.00000E+00 0.0000
   1.9140E+00   0.00000E+00 0.0000
   1.9360E+00   0.00000E+00 0.0000
   1.9580E+00   0.00000E+00 0.0000
   1.9800E+00   0.00000E+00 0.0000
   2.0020E+00   0.00000E+00 0.0000
   2.0240E+00   0.00000E+00 0.0000
   2.0460E+00   0.00000E+00 0.0000
   2.0680E+00   0.00000E+00 0.0000
   2.0900E+00   0.00000E+00 0.0000
   2.1120E+00   0.00000E+00 0.0000
   2.1340E+00   0.00000E+00 0.0000
   2.1560E+00   0.00000E+00 0.0000
   2.1780E+00   0.00000E+00 0.0000
   2.2000E+00   0.00000E+00 0.0000
     total      0.00000E+00 0.0000

surface  3
     energy
   2.2000E-02   2.45262E-03 0.0086
   4.4000E-02   2.86423E-02 0.0030
   6.6000E-02   2.92365E-02 0.0028
   8.8000E-02   2.81165E-02 0.0027
   1.1000E-01   2.62222E-02 0.0028
   1.3200E-01   2.39102E-02 0.0028
   1.5400E-01   2.18690E-02 0.0029
```

1.7600E-01	1.98430E-02	0.0030
1.9800E-01	1.78872E-02	0.0032
2.2000E-01	1.62539E-02	0.0033
2.4200E-01	1.48536E-02	0.0035
2.6400E-01	1.35514E-02	0.0036
2.8600E-01	1.20733E-02	0.0038
3.0800E-01	1.07514E-02	0.0040
3.3000E-01	9.77253E-03	0.0042
3.5200E-01	8.64086E-03	0.0045
3.7400E-01	7.71172E-03	0.0047
3.9600E-01	6.47346E-03	0.0051
4.1800E-01	5.73667E-03	0.0054
4.4000E-01	5.30545E-03	0.0056
4.6200E-01	4.82627E-03	0.0059
4.8400E-01	4.32188E-03	0.0062
5.0600E-01	3.70300E-03	0.0067
5.2800E-01	3.50822E-03	0.0069
5.5000E-01	3.39177E-03	0.0070
5.7200E-01	3.27194E-03	0.0071
5.9400E-01	3.16276E-03	0.0072
6.1600E-01	3.01789E-03	0.0074
6.3800E-01	2.95232E-03	0.0075
6.6000E-01	2.91194E-03	0.0075
6.8200E-01	2.77789E-03	0.0077
7.0400E-01	2.64061E-03	0.0079
7.2600E-01	2.61235E-03	0.0079
7.4800E-01	2.50075E-03	0.0081
7.7000E-01	2.39480E-03	0.0083
7.9200E-01	2.35604E-03	0.0083
8.1400E-01	2.24767E-03	0.0085
8.3600E-01	2.19147E-03	0.0086
8.5800E-01	2.14092E-03	0.0087
8.8000E-01	2.06049E-03	0.0089
9.0200E-01	1.92805E-03	0.0092
9.2400E-01	1.91174E-03	0.0092
9.4600E-01	1.85990E-03	0.0094
9.6800E-01	1.80014E-03	0.0095
9.9000E-01	1.71034E-03	0.0097

```
1.0120E+00   1.68466E-03 0.0098
1.0340E+00   1.58970E-03 0.0101
1.0560E+00   1.54464E-03 0.0103
1.0780E+00   1.48456E-03 0.0105
1.1000E+00   1.43546E-03 0.0106
1.1220E+00   1.37231E-03 0.0109
1.1440E+00   1.31078E-03 0.0111
1.1660E+00   1.26023E-03 0.0113
1.1880E+00   1.20628E-03 0.0116
1.2100E+00   1.13135E-03 0.0120
1.2320E+00   1.11003E-03 0.0121
1.2540E+00   1.05463E-03 0.0124
1.2760E+00   9.87444E-04 0.0128
1.2980E+00   9.66125E-04 0.0129
1.3200E+00   9.59180E-04 0.0130
1.3420E+00   8.87634E-04 0.0135
1.3640E+00   8.39666E-04 0.0139
1.3860E+00   7.94929E-04 0.0143
1.4080E+00   7.76356E-04 0.0144
1.4300E+00   7.13531E-04 0.0151
1.4520E+00   6.72993E-04 0.0155
1.4740E+00   6.41176E-04 0.0159
1.4960E+00   6.07422E-04 0.0163
1.5180E+00   5.84811E-04 0.0166
1.5400E+00   5.52187E-04 0.0171
1.5620E+00   5.29415E-04 0.0175
1.5840E+00   4.53507E-04 0.0189
1.6060E+00   4.43494E-04 0.0191
1.6280E+00   3.97626E-04 0.0202
1.6500E+00   3.88743E-04 0.0204
1.6720E+00   3.48206E-04 0.0216
1.6940E+00   3.11867E-04 0.0228
1.7160E+00   2.95393E-04 0.0234
1.7380E+00   2.76336E-04 0.0242
1.7600E+00   2.51625E-04 0.0253
1.7820E+00   2.20939E-04 0.0271
1.8040E+00   1.98490E-04 0.0285
1.8260E+00   1.82501E-04 0.0297
```

```
   1.8480E+00   1.67804E-04 0.0311
   1.8700E+00   1.47293E-04 0.0331
   1.8920E+00   1.21775E-04 0.0365
   1.9140E+00   9.94873E-05 0.0404
   1.9360E+00   8.86665E-05 0.0427
   1.9580E+00   7.83301E-05 0.0454
   1.9800E+00   6.94473E-05 0.0482
   2.0020E+00   4.61905E-05 0.0591
   2.0240E+00   4.00533E-05 0.0635
   2.0460E+00   3.58542E-05 0.0671
   2.0680E+00   3.02015E-05 0.0731
   2.0900E+00   1.63120E-05 0.0995
   2.1120E+00   1.53430E-05 0.1026
   2.1340E+00   1.01748E-05 0.1260
   2.1560E+00   6.94473E-06 0.1525
   2.1780E+00   2.90710E-06 0.2357
   2.2000E+00   4.84516E-07 0.5774
     total      4.08949E-01 0.0009

surface  5
     energy
   2.2000E-02   2.38043E-03 0.0087
   4.4000E-02   2.79585E-02 0.0031
   6.6000E-02   2.85030E-02 0.0028
   8.8000E-02   2.72705E-02 0.0028
   1.1000E-01   2.53870E-02 0.0028
   1.3200E-01   2.30404E-02 0.0029
   1.5400E-01   2.10060E-02 0.0030
   1.7600E-01   1.90601E-02 0.0031
   1.9800E-01   1.71244E-02 0.0032
   2.2000E-01   1.54981E-02 0.0034
   2.4200E-01   1.41395E-02 0.0035
   2.6400E-01   1.28872E-02 0.0037
   2.8600E-01   1.14971E-02 0.0039
   3.0800E-01   1.01779E-02 0.0041
   3.3000E-01   9.26023E-03 0.0043
   3.5200E-01   8.18832E-03 0.0046
   3.7400E-01   7.27566E-03 0.0049
```

3.9600E-01	6.04563E-03	0.0053
4.1800E-01	5.31256E-03	0.0056
4.4000E-01	4.91073E-03	0.0059
4.6200E-01	4.45464E-03	0.0061
4.8400E-01	3.94445E-03	0.0065
5.0600E-01	3.31506E-03	0.0071
5.2800E-01	3.11915E-03	0.0073
5.5000E-01	3.01514E-03	0.0074
5.7200E-01	2.91291E-03	0.0075
5.9400E-01	2.82247E-03	0.0076
6.1600E-01	2.69133E-03	0.0078
6.3800E-01	2.62575E-03	0.0079
6.6000E-01	2.61219E-03	0.0079
6.8200E-01	2.48266E-03	0.0081
7.0400E-01	2.36202E-03	0.0083
7.2600E-01	2.33198E-03	0.0084
7.4800E-01	2.23588E-03	0.0086
7.7000E-01	2.13655E-03	0.0087
7.9200E-01	2.10651E-03	0.0088
8.1400E-01	2.02948E-03	0.0090
8.3600E-01	1.96520E-03	0.0091
8.5800E-01	1.92805E-03	0.0092
8.8000E-01	1.85747E-03	0.0094
9.0200E-01	1.73424E-03	0.0097
9.2400E-01	1.73441E-03	0.0097
9.4600E-01	1.69177E-03	0.0098
9.6800E-01	1.62652E-03	0.0100
9.9000E-01	1.56321E-03	0.0102
1.0120E+00	1.54189E-03	0.0103
1.0340E+00	1.45484E-03	0.0106
1.0560E+00	1.40558E-03	0.0108
1.0780E+00	1.35810E-03	0.0109
1.1000E+00	1.31530E-03	0.0111
1.1220E+00	1.26507E-03	0.0113
1.1440E+00	1.21081E-03	0.0116
1.1660E+00	1.17285E-03	0.0117
1.1880E+00	1.11003E-03	0.0121
1.2100E+00	1.05608E-03	0.0124

```
1.2320E+00   1.04478E-03 0.0125
1.2540E+00   9.81307E-04 0.0129
1.2760E+00   9.21065E-04 0.0133
1.2980E+00   9.10406E-04 0.0133
1.3200E+00   8.92156E-04 0.0135
1.3420E+00   8.36436E-04 0.0139
1.3640E+00   8.03005E-04 0.0142
1.3860E+00   7.58106E-04 0.0146
1.4080E+00   7.42117E-04 0.0148
1.4300E+00   6.77354E-04 0.0155
1.4520E+00   6.51997E-04 0.0158
1.4740E+00   6.17597E-04 0.0162
1.4960E+00   5.76897E-04 0.0168
1.5180E+00   5.64461E-04 0.0169
1.5400E+00   5.35390E-04 0.0174
1.5620E+00   5.17140E-04 0.0177
1.5840E+00   4.45109E-04 0.0191
1.6060E+00   4.35418E-04 0.0193
1.6280E+00   3.96496E-04 0.0202
1.6500E+00   3.79215E-04 0.0206
1.6720E+00   3.49821E-04 0.0215
1.6940E+00   3.08960E-04 0.0229
1.7160E+00   2.94263E-04 0.0234
1.7380E+00   2.84895E-04 0.0238
1.7600E+00   2.58732E-04 0.0250
1.7820E+00   2.26915E-04 0.0267
1.8040E+00   1.92514E-04 0.0290
1.8260E+00   1.86700E-04 0.0294
1.8480E+00   1.71357E-04 0.0307
1.8700E+00   1.52461E-04 0.0325
1.8920E+00   1.26620E-04 0.0358
1.9140E+00   1.08855E-04 0.0386
1.9360E+00   9.67417E-05 0.0409
1.9580E+00   8.43058E-05 0.0438
1.9800E+00   7.25159E-05 0.0472
2.0020E+00   5.03897E-05 0.0566
2.0240E+00   4.32834E-05 0.0611
2.0460E+00   4.15069E-05 0.0624
```

```
   2.0680E+00   3.32701E-05 0.0697
   2.0900E+00   1.79271E-05 0.0949
   2.1120E+00   1.55045E-05 0.1021
   2.1340E+00   1.14669E-05 0.1187
   2.1560E+00   8.72129E-06 0.1361
   2.1780E+00   3.87613E-06 0.2041
   2.2000E+00   4.84516E-07 0.5774
     total      3.87941E-01 0.0009

surface  6
     energy
   2.2000E-02   3.58736E-03 0.0069
   4.4000E-02   4.23851E-02 0.0023
   6.6000E-02   4.56216E-02 0.0021
   8.8000E-02   4.66923E-02 0.0020
   1.1000E-01   4.59740E-02 0.0020
   1.3200E-01   4.52176E-02 0.0020
   1.5400E-01   4.40703E-02 0.0020
   1.7600E-01   4.30546E-02 0.0020
   1.9800E-01   4.13869E-02 0.0020
   2.2000E-01   3.83566E-02 0.0021
   2.4200E-01   3.73614E-02 0.0021
   2.6400E-01   3.63629E-02 0.0021
   2.8600E-01   3.52474E-02 0.0021
   3.0800E-01   3.23691E-02 0.0022
   3.3000E-01   3.01216E-02 0.0023
   3.5200E-01   2.91322E-02 0.0024
   3.7400E-01   2.82121E-02 0.0024
   3.9600E-01   2.66537E-02 0.0025
   4.1800E-01   1.86550E-02 0.0029
   4.4000E-01   1.77598E-02 0.0030
   4.6200E-01   1.74301E-02 0.0030
   4.8400E-01   1.68600E-02 0.0031
   5.0600E-01   1.29424E-02 0.0035
   5.2800E-01   8.81238E-03 0.0043
   5.5000E-01   8.75133E-03 0.0043
   5.7200E-01   8.69028E-03 0.0043
   5.9400E-01   8.56592E-03 0.0043
```

```
6.1600E-01   8.47063E-03 0.0044
6.3800E-01   8.41475E-03 0.0044
6.6000E-01   8.42832E-03 0.0044
6.8200E-01   8.33319E-03 0.0044
7.0400E-01   8.22563E-03 0.0044
7.2600E-01   8.20496E-03 0.0044
7.4800E-01   8.06396E-03 0.0045
7.7000E-01   8.06752E-03 0.0045
7.9200E-01   7.96351E-03 0.0045
8.1400E-01   7.80491E-03 0.0045
8.3600E-01   7.85966E-03 0.0045
8.5800E-01   7.80362E-03 0.0045
8.8000E-01   7.76163E-03 0.0046
9.0200E-01   7.64163E-03 0.0046
9.2400E-01   7.66908E-03 0.0046
9.4600E-01   7.60674E-03 0.0046
9.6800E-01   7.54553E-03 0.0046
9.9000E-01   7.52244E-03 0.0046
1.0120E+00   7.42973E-03 0.0047
1.0340E+00   7.37773E-03 0.0047
1.0560E+00   7.35786E-03 0.0047
1.0780E+00   7.24949E-03 0.0047
1.1000E+00   7.23156E-03 0.0047
1.1220E+00   7.01741E-03 0.0048
1.1440E+00   6.90952E-03 0.0048
1.1660E+00   6.91033E-03 0.0048
1.1880E+00   6.85913E-03 0.0048
1.2100E+00   6.64982E-03 0.0049
1.2320E+00   6.55680E-03 0.0050
1.2540E+00   6.54210E-03 0.0050
1.2760E+00   6.45973E-03 0.0050
1.2980E+00   6.34280E-03 0.0050
1.3200E+00   6.05807E-03 0.0052
1.3420E+00   5.99589E-03 0.0052
1.3640E+00   5.98555E-03 0.0052
1.3860E+00   5.94663E-03 0.0052
1.4080E+00   5.68289E-03 0.0053
1.4300E+00   5.50540E-03 0.0054
```

```
   1.4520E+00   5.53463E-03 0.0054
   1.4740E+00   5.42384E-03 0.0054
   1.4960E+00   5.36149E-03 0.0055
   1.5180E+00   4.92349E-03 0.0057
   1.5400E+00   4.90363E-03 0.0057
   1.5620E+00   4.83838E-03 0.0058
   1.5840E+00   4.84871E-03 0.0058
   1.6060E+00   4.59192E-03 0.0059
   1.6280E+00   4.30816E-03 0.0061
   1.6500E+00   4.32059E-03 0.0061
   1.6720E+00   4.24501E-03 0.0062
   1.6940E+00   4.18008E-03 0.0062
   1.7160E+00   3.57476E-03 0.0067
   1.7380E+00   3.46445E-03 0.0068
   1.7600E+00   3.43312E-03 0.0068
   1.7820E+00   3.42731E-03 0.0069
   1.8040E+00   3.07845E-03 0.0072
   1.8260E+00   2.68793E-03 0.0077
   1.8480E+00   2.67388E-03 0.0078
   1.8700E+00   2.60767E-03 0.0079
   1.8920E+00   2.56907E-03 0.0079
   1.9140E+00   2.00993E-03 0.0090
   1.9360E+00   1.89236E-03 0.0092
   1.9580E+00   1.85521E-03 0.0093
   1.9800E+00   1.83486E-03 0.0094
   2.0020E+00   1.58227E-03 0.0101
   2.0240E+00   9.75008E-04 0.0129
   2.0460E+00   9.91966E-04 0.0128
   2.0680E+00   9.89705E-04 0.0128
   2.0900E+00   9.46422E-04 0.0131
   2.1120E+00   5.30061E-04 0.0175
   2.1340E+00   3.77761E-04 0.0207
   2.1560E+00   3.64356E-04 0.0210
   2.1780E+00   3.49982E-04 0.0215
   2.2000E+00   2.71329E-04 0.0244
     total      1.14570E+00 0.0003

surface  9
```

energy		
2.2000E-02	1.54884E-04	0.0341
4.4000E-02	1.63589E-03	0.0111
6.6000E-02	1.70033E-03	0.0105
8.8000E-02	1.82340E-03	0.0100
1.1000E-01	1.97004E-03	0.0095
1.3200E-01	2.14528E-03	0.0091
1.5400E-01	2.26996E-03	0.0088
1.7600E-01	2.41063E-03	0.0085
1.9800E-01	2.54484E-03	0.0083
2.2000E-01	2.64610E-03	0.0081
2.4200E-01	2.74155E-03	0.0079
2.6400E-01	2.84395E-03	0.0078
2.8600E-01	2.86898E-03	0.0078
3.0800E-01	2.96072E-03	0.0076
3.3000E-01	3.02596E-03	0.0075
3.5200E-01	3.07022E-03	0.0074
3.7400E-01	3.07571E-03	0.0075
3.9600E-01	3.15711E-03	0.0073
4.1800E-01	3.20152E-03	0.0073
4.4000E-01	3.18602E-03	0.0073
4.6200E-01	3.19118E-03	0.0073
4.8400E-01	3.17293E-03	0.0073
5.0600E-01	3.21606E-03	0.0073
5.2800E-01	3.22849E-03	0.0072
5.5000E-01	3.21008E-03	0.0073
5.7200E-01	3.19328E-03	0.0073
5.9400E-01	3.20604E-03	0.0073
6.1600E-01	3.23770E-03	0.0072
6.3800E-01	3.17939E-03	0.0073
6.6000E-01	3.14160E-03	0.0073
6.8200E-01	3.09654E-03	0.0074
7.0400E-01	3.09073E-03	0.0074
7.2600E-01	3.07619E-03	0.0074
7.4800E-01	3.03485E-03	0.0075
7.7000E-01	2.97041E-03	0.0075
7.9200E-01	2.93649E-03	0.0076
8.1400E-01	2.91598E-03	0.0076

8.3600E-01	2.84153E-03	0.0077
8.5800E-01	2.84960E-03	0.0077
8.8000E-01	2.71200E-03	0.0079
9.0200E-01	2.70198E-03	0.0079
9.2400E-01	2.66613E-03	0.0079
9.4600E-01	2.62995E-03	0.0080
9.6800E-01	2.55711E-03	0.0081
9.9000E-01	2.47410E-03	0.0082
1.0120E+00	2.43372E-03	0.0083
1.0340E+00	2.38721E-03	0.0084
1.0560E+00	2.29887E-03	0.0085
1.0780E+00	2.25074E-03	0.0086
1.1000E+00	2.13526E-03	0.0088
1.1220E+00	2.09489E-03	0.0089
1.1440E+00	2.04385E-03	0.0090
1.1660E+00	1.99072E-03	0.0091
1.1880E+00	1.89414E-03	0.0093
1.2100E+00	1.83002E-03	0.0095
1.2320E+00	1.76800E-03	0.0097
1.2540E+00	1.68353E-03	0.0099
1.2760E+00	1.57952E-03	0.0102
1.2980E+00	1.51476E-03	0.0105
1.3200E+00	1.44240E-03	0.0107
1.3420E+00	1.35390E-03	0.0110
1.3640E+00	1.27767E-03	0.0114
1.3860E+00	1.17511E-03	0.0118
1.4080E+00	1.12036E-03	0.0121
1.4300E+00	1.04769E-03	0.0125
1.4520E+00	9.77431E-04	0.0130
1.4740E+00	9.06368E-04	0.0134
1.4960E+00	8.05104E-04	0.0143
1.5180E+00	7.30812E-04	0.0150
1.5400E+00	6.73800E-04	0.0156
1.5620E+00	6.16305E-04	0.0163
1.5840E+00	5.18432E-04	0.0178
1.6060E+00	4.98567E-04	0.0181
1.6280E+00	4.03279E-04	0.0202
1.6500E+00	3.63226E-04	0.0212

```
   1.6720E+00   3.12674E-04 0.0228
   1.6940E+00   2.61639E-04 0.0249
   1.7160E+00   2.14641E-04 0.0276
   1.7380E+00   1.81048E-04 0.0299
   1.7600E+00   1.43901E-04 0.0335
   1.7820E+00   1.09501E-04 0.0384
   1.8040E+00   8.25292E-05 0.0443
   1.8260E+00   5.70114E-05 0.0532
   1.8480E+00   3.95688E-05 0.0639
   1.8700E+00   2.34183E-05 0.0830
   1.8920E+00   1.79271E-05 0.0949
   1.9140E+00   8.07527E-06 0.1414
   1.9360E+00   2.26108E-06 0.2673
   1.9580E+00   1.61505E-07 1.0000
   1.9800E+00   0.00000E+00 0.0000
   2.0020E+00   0.00000E+00 0.0000
   2.0240E+00   0.00000E+00 0.0000
   2.0460E+00   0.00000E+00 0.0000
   2.0680E+00   0.00000E+00 0.0000
   2.0900E+00   0.00000E+00 0.0000
   2.1120E+00   0.00000E+00 0.0000
   2.1340E+00   0.00000E+00 0.0000
   2.1560E+00   0.00000E+00 0.0000
   2.1780E+00   0.00000E+00 0.0000
   2.2000E+00   0.00000E+00 0.0000
     total      1.67233E-01 0.0011

surface  26
     energy
   2.2000E-02   1.47293E-04 0.0336
   4.4000E-02   1.57500E-03 0.0109
   6.6000E-02   1.64251E-03 0.0103
   8.8000E-02   1.76558E-03 0.0098
   1.1000E-01   1.91142E-03 0.0093
   1.3200E-01   2.07260E-03 0.0089
   1.5400E-01   2.19276E-03 0.0086
   1.7600E-01   2.33456E-03 0.0084
   1.9800E-01   2.45634E-03 0.0082
```

```
2.2000E-01   2.55792E-03 0.0080
2.4200E-01   2.65079E-03 0.0078
2.6400E-01   2.75657E-03 0.0077
2.8600E-01   2.76271E-03 0.0077
3.0800E-01   2.85396E-03 0.0075
3.3000E-01   2.90677E-03 0.0075
3.5200E-01   2.96750E-03 0.0074
3.7400E-01   2.96282E-03 0.0074
3.9600E-01   3.04260E-03 0.0073
4.1800E-01   3.07926E-03 0.0072
4.4000E-01   3.06876E-03 0.0073
4.6200E-01   3.07603E-03 0.0072
4.8400E-01   3.06230E-03 0.0073
5.0600E-01   3.09460E-03 0.0072
5.2800E-01   3.12852E-03 0.0072
5.5000E-01   3.09541E-03 0.0072
5.7200E-01   3.07700E-03 0.0072
5.9400E-01   3.08104E-03 0.0072
6.1600E-01   3.10526E-03 0.0072
6.3800E-01   3.07329E-03 0.0072
6.6000E-01   3.03452E-03 0.0073
6.8200E-01   3.00174E-03 0.0073
7.0400E-01   2.97186E-03 0.0074
7.2600E-01   2.95926E-03 0.0074
7.4800E-01   2.92066E-03 0.0074
7.7000E-01   2.86850E-03 0.0075
7.9200E-01   2.83022E-03 0.0075
8.1400E-01   2.81520E-03 0.0076
8.3600E-01   2.73316E-03 0.0077
8.5800E-01   2.74511E-03 0.0077
8.8000E-01   2.62333E-03 0.0078
9.0200E-01   2.60508E-03 0.0079
9.2400E-01   2.57472E-03 0.0079
9.4600E-01   2.53515E-03 0.0080
9.6800E-01   2.46296E-03 0.0081
9.9000E-01   2.39545E-03 0.0082
1.0120E+00   2.35265E-03 0.0083
1.0340E+00   2.30775E-03 0.0084
```

1.0560E+00	2.22296E-03	0.0085
1.0780E+00	2.17564E-03	0.0086
1.1000E+00	2.07793E-03	0.0088
1.1220E+00	2.03545E-03	0.0089
1.1440E+00	1.97909E-03	0.0090
1.1660E+00	1.93419E-03	0.0091
1.1880E+00	1.84875E-03	0.0093
1.2100E+00	1.78076E-03	0.0095
1.2320E+00	1.71906E-03	0.0097
1.2540E+00	1.64089E-03	0.0099
1.2760E+00	1.54383E-03	0.0102
1.2980E+00	1.46986E-03	0.0105
1.3200E+00	1.41075E-03	0.0107
1.3420E+00	1.33097E-03	0.0110
1.3640E+00	1.24973E-03	0.0114
1.3860E+00	1.15202E-03	0.0118
1.4080E+00	1.09840E-03	0.0121
1.4300E+00	1.03089E-03	0.0125
1.4520E+00	9.62088E-04	0.0130
1.4740E+00	8.95709E-04	0.0134
1.4960E+00	7.90569E-04	0.0143
1.5180E+00	7.21283E-04	0.0150
1.5400E+00	6.62657E-04	0.0156
1.5620E+00	6.07099E-04	0.0163
1.5840E+00	5.11649E-04	0.0178
1.6060E+00	4.94045E-04	0.0181
1.6280E+00	3.96819E-04	0.0202
1.6500E+00	3.60318E-04	0.0212
1.6720E+00	3.10736E-04	0.0228
1.6940E+00	2.60993E-04	0.0249
1.7160E+00	2.12057E-04	0.0276
1.7380E+00	1.80078E-04	0.0299
1.7600E+00	1.43578E-04	0.0335
1.7820E+00	1.09501E-04	0.0384
1.8040E+00	8.22062E-05	0.0443
1.8260E+00	5.70114E-05	0.0532
1.8480E+00	3.95688E-05	0.0639
1.8700E+00	2.34183E-05	0.0830

```
   1.8920E+00   1.79271E-05 0.0949
   1.9140E+00   8.07527E-06 0.1414
   1.9360E+00   2.26108E-06 0.2673
   1.9580E+00   1.61505E-07 1.0000
   1.9800E+00   0.00000E+00 0.0000
   2.0020E+00   0.00000E+00 0.0000
   2.0240E+00   0.00000E+00 0.0000
   2.0460E+00   0.00000E+00 0.0000
   2.0680E+00   0.00000E+00 0.0000
   2.0900E+00   0.00000E+00 0.0000
   2.1120E+00   0.00000E+00 0.0000
   2.1340E+00   0.00000E+00 0.0000
   2.1560E+00   0.00000E+00 0.0000
   2.1780E+00   0.00000E+00 0.0000
   2.2000E+00   0.00000E+00 0.0000
     total      1.61789E-01 0.0011

surface  27
     energy
   2.2000E-02   1.49069E-04 0.0337
   4.4000E-02   1.63637E-03 0.0111
   6.6000E-02   1.68709E-03 0.0104
   8.8000E-02   1.81322E-03 0.0099
   1.1000E-01   1.97150E-03 0.0094
   1.3200E-01   2.08762E-03 0.0090
   1.5400E-01   2.20406E-03 0.0087
   1.7600E-01   2.31114E-03 0.0085
   1.9800E-01   2.44341E-03 0.0083
   2.2000E-01   2.53919E-03 0.0081
   2.4200E-01   2.64837E-03 0.0079
   2.6400E-01   2.65919E-03 0.0079
   2.8600E-01   2.73429E-03 0.0078
   3.0800E-01   2.78758E-03 0.0077
   3.3000E-01   2.85816E-03 0.0076
   3.5200E-01   2.91065E-03 0.0075
   3.7400E-01   2.98058E-03 0.0074
   3.9600E-01   2.97138E-03 0.0074
   4.1800E-01   2.99060E-03 0.0074
```

```
4.4000E-01   3.00432E-03 0.0074
4.6200E-01   2.98930E-03 0.0074
4.8400E-01   3.03194E-03 0.0073
5.0600E-01   3.05407E-03 0.0073
5.2800E-01   3.03759E-03 0.0073
5.5000E-01   3.03598E-03 0.0073
5.7200E-01   3.02419E-03 0.0073
5.9400E-01   3.03856E-03 0.0073
6.1600E-01   3.01466E-03 0.0073
6.3800E-01   2.95216E-03 0.0074
6.6000E-01   2.94925E-03 0.0074
6.8200E-01   2.92793E-03 0.0074
7.0400E-01   2.92438E-03 0.0074
7.2600E-01   2.84605E-03 0.0075
7.4800E-01   2.81181E-03 0.0076
7.7000E-01   2.79582E-03 0.0076
7.9200E-01   2.75867E-03 0.0077
8.1400E-01   2.68777E-03 0.0078
8.3600E-01   2.68987E-03 0.0078
8.5800E-01   2.58392E-03 0.0079
8.8000E-01   2.56971E-03 0.0079
9.0200E-01   2.51965E-03 0.0080
9.2400E-01   2.49687E-03 0.0080
9.4600E-01   2.40691E-03 0.0082
9.6800E-01   2.34102E-03 0.0083
9.9000E-01   2.34474E-03 0.0083
1.0120E+00   2.27400E-03 0.0084
1.0340E+00   2.18630E-03 0.0086
1.0560E+00   2.14334E-03 0.0087
1.0780E+00   2.05726E-03 0.0089
1.1000E+00   1.99411E-03 0.0090
1.1220E+00   1.94630E-03 0.0091
1.1440E+00   1.89527E-03 0.0092
1.1660E+00   1.81419E-03 0.0094
1.1880E+00   1.74135E-03 0.0096
1.2100E+00   1.69403E-03 0.0098
1.2320E+00   1.60423E-03 0.0100
1.2540E+00   1.49473E-03 0.0104
```

1.2760E+00	1.45646E-03	0.0105
1.2980E+00	1.38669E-03	0.0108
1.3200E+00	1.30173E-03	0.0111
1.3420E+00	1.22873E-03	0.0115
1.3640E+00	1.13054E-03	0.0119
1.3860E+00	1.06367E-03	0.0123
1.4080E+00	1.01926E-03	0.0126
1.4300E+00	9.45775E-04	0.0131
1.4520E+00	8.66153E-04	0.0137
1.4740E+00	7.67474E-04	0.0145
1.4960E+00	7.06748E-04	0.0151
1.5180E+00	6.46668E-04	0.0158
1.5400E+00	5.96601E-04	0.0164
1.5620E+00	4.97598E-04	0.0180
1.5840E+00	4.82417E-04	0.0183
1.6060E+00	3.98595E-04	0.0202
1.6280E+00	3.53051E-04	0.0214
1.6500E+00	3.10090E-04	0.0228
1.6720E+00	2.52594E-04	0.0253
1.6940E+00	2.11249E-04	0.0276
1.7160E+00	1.79594E-04	0.0300
1.7380E+00	1.39056E-04	0.0341
1.7600E+00	1.05140E-04	0.0392
1.7820E+00	8.43058E-05	0.0438
1.8040E+00	5.66884E-05	0.0534
1.8260E+00	4.02148E-05	0.0634
1.8480E+00	2.34183E-05	0.0830
1.8700E+00	1.58275E-05	0.1010
1.8920E+00	1.00133E-05	0.1270
1.9140E+00	2.90710E-06	0.2357
1.9360E+00	4.84516E-07	0.5774
1.9580E+00	0.00000E+00	0.0000
1.9800E+00	0.00000E+00	0.0000
2.0020E+00	0.00000E+00	0.0000
2.0240E+00	0.00000E+00	0.0000
2.0460E+00	0.00000E+00	0.0000
2.0680E+00	0.00000E+00	0.0000
2.0900E+00	0.00000E+00	0.0000

```
   2.1120E+00   0.00000E+00 0.0000
   2.1340E+00   0.00000E+00 0.0000
   2.1560E+00   0.00000E+00 0.0000
   2.1780E+00   0.00000E+00 0.0000
   2.2000E+00   0.00000E+00 0.0000
     total      1.56345E-01 0.0012

surface  28
     energy
   2.2000E-02   1.39379E-04 0.0346
   4.4000E-02   1.55077E-03 0.0113
   6.6000E-02   1.63363E-03 0.0106
   8.8000E-02   1.74603E-03 0.0101
   1.1000E-01   1.90609E-03 0.0095
   1.3200E-01   2.05742E-03 0.0091
   1.5400E-01   2.16046E-03 0.0089
   1.7600E-01   2.25316E-03 0.0086
   1.9800E-01   2.32568E-03 0.0085
   2.2000E-01   2.44891E-03 0.0083
   2.4200E-01   2.49946E-03 0.0082
   2.6400E-01   2.60912E-03 0.0080
   2.8600E-01   2.65628E-03 0.0079
   3.0800E-01   2.70473E-03 0.0078
   3.3000E-01   2.75221E-03 0.0077
   3.5200E-01   2.77563E-03 0.0077
   3.7400E-01   2.83135E-03 0.0076
   3.9600E-01   2.81552E-03 0.0076
   4.1800E-01   2.87480E-03 0.0075
   4.4000E-01   2.91097E-03 0.0075
   4.6200E-01   2.90629E-03 0.0075
   4.8400E-01   2.92212E-03 0.0075
   5.0600E-01   2.94408E-03 0.0074
   5.2800E-01   2.91113E-03 0.0075
   5.5000E-01   2.92858E-03 0.0074
   5.7200E-01   2.91566E-03 0.0075
   5.9400E-01   2.91210E-03 0.0075
   6.1600E-01   2.87286E-03 0.0075
   6.3800E-01   2.88675E-03 0.0075
```

```
6.6000E-01   2.83216E-03 0.0076
6.8200E-01   2.82198E-03 0.0076
7.0400E-01   2.77402E-03 0.0076
7.2600E-01   2.72379E-03 0.0077
7.4800E-01   2.72605E-03 0.0077
7.7000E-01   2.69472E-03 0.0077
7.9200E-01   2.61929E-03 0.0079
8.1400E-01   2.58279E-03 0.0079
8.3600E-01   2.56067E-03 0.0079
8.5800E-01   2.52368E-03 0.0080
8.8000E-01   2.43760E-03 0.0081
9.0200E-01   2.41628E-03 0.0082
9.2400E-01   2.36702E-03 0.0083
9.4600E-01   2.27448E-03 0.0084
9.6800E-01   2.25914E-03 0.0085
9.9000E-01   2.20196E-03 0.0086
1.0120E+00   2.13849E-03 0.0087
1.0340E+00   2.08229E-03 0.0088
1.0560E+00   2.01236E-03 0.0090
1.0780E+00   1.96019E-03 0.0091
1.1000E+00   1.90108E-03 0.0092
1.1220E+00   1.84730E-03 0.0093
1.1440E+00   1.76251E-03 0.0096
1.1660E+00   1.70146E-03 0.0097
1.1880E+00   1.64671E-03 0.0099
1.2100E+00   1.55869E-03 0.0102
1.2320E+00   1.47810E-03 0.0104
1.2540E+00   1.41769E-03 0.0107
1.2760E+00   1.33791E-03 0.0110
1.2980E+00   1.26895E-03 0.0113
1.3200E+00   1.19401E-03 0.0116
1.3420E+00   1.11762E-03 0.0120
1.3640E+00   1.03993E-03 0.0125
1.3860E+00   9.77754E-04 0.0128
1.4080E+00   9.32209E-04 0.0132
1.4300E+00   8.44512E-04 0.0138
1.4520E+00   7.56168E-04 0.0146
1.4740E+00   6.79292E-04 0.0154
```

```
   1.4960E+00   6.43437E-04 0.0158
   1.5180E+00   5.84326E-04 0.0166
   1.5400E+00   4.77733E-04 0.0184
   1.5620E+00   4.70627E-04 0.0185
   1.5840E+00   3.94235E-04 0.0202
   1.6060E+00   3.44652E-04 0.0216
   1.6280E+00   3.04438E-04 0.0230
   1.6500E+00   2.45973E-04 0.0256
   1.6720E+00   2.14156E-04 0.0275
   1.6940E+00   1.72488E-04 0.0306
   1.7160E+00   1.38087E-04 0.0342
   1.7380E+00   1.03686E-04 0.0395
   1.7600E+00   8.49518E-05 0.0436
   1.7820E+00   5.76574E-05 0.0529
   1.8040E+00   3.87613E-05 0.0645
   1.8260E+00   2.60024E-05 0.0788
   1.8480E+00   1.51815E-05 0.1031
   1.8700E+00   1.17899E-05 0.1170
   1.8920E+00   2.90710E-06 0.2357
   1.9140E+00   6.46022E-07 0.5000
   1.9360E+00   0.00000E+00 0.0000
   1.9580E+00   0.00000E+00 0.0000
   1.9800E+00   0.00000E+00 0.0000
   2.0020E+00   0.00000E+00 0.0000
   2.0240E+00   0.00000E+00 0.0000
   2.0460E+00   0.00000E+00 0.0000
   2.0680E+00   0.00000E+00 0.0000
   2.0900E+00   0.00000E+00 0.0000
   2.1120E+00   0.00000E+00 0.0000
   2.1340E+00   0.00000E+00 0.0000
   2.1560E+00   0.00000E+00 0.0000
   2.1780E+00   0.00000E+00 0.0000
   2.2000E+00   0.00000E+00 0.0000
     total      1.48654E-01 0.0012

surface  29
     energy
   2.2000E-02   1.47777E-04 0.0338
```

```
4.4000E-02   1.47810E-03 0.0116
6.6000E-02   1.57807E-03 0.0108
8.8000E-02   1.72149E-03 0.0101
1.1000E-01   1.84019E-03 0.0097
1.3200E-01   1.92159E-03 0.0094
1.5400E-01   2.04595E-03 0.0091
1.7600E-01   2.17580E-03 0.0088
1.9800E-01   2.24573E-03 0.0086
2.2000E-01   2.33811E-03 0.0085
2.4200E-01   2.43146E-03 0.0083
2.6400E-01   2.48460E-03 0.0082
2.8600E-01   2.53612E-03 0.0081
3.0800E-01   2.62236E-03 0.0079
3.3000E-01   2.61138E-03 0.0079
3.5200E-01   2.67873E-03 0.0078
3.7400E-01   2.73493E-03 0.0077
3.9600E-01   2.72411E-03 0.0078
4.1800E-01   2.79614E-03 0.0076
4.4000E-01   2.77272E-03 0.0077
4.6200E-01   2.82731E-03 0.0076
4.8400E-01   2.82538E-03 0.0076
5.0600E-01   2.78048E-03 0.0076
5.2800E-01   2.80034E-03 0.0076
5.5000E-01   2.83167E-03 0.0076
5.7200E-01   2.78355E-03 0.0076
5.9400E-01   2.79178E-03 0.0076
6.1600E-01   2.75124E-03 0.0077
6.3800E-01   2.75819E-03 0.0077
6.6000E-01   2.72427E-03 0.0077
6.8200E-01   2.68487E-03 0.0078
7.0400E-01   2.62091E-03 0.0079
7.2600E-01   2.63318E-03 0.0078
7.4800E-01   2.61962E-03 0.0079
7.7000E-01   2.56874E-03 0.0079
7.9200E-01   2.49494E-03 0.0080
8.1400E-01   2.47895E-03 0.0081
8.3600E-01   2.44600E-03 0.0081
8.5800E-01   2.36702E-03 0.0083
```

```
8.8000E-01   2.33181E-03 0.0083
9.0200E-01   2.31292E-03 0.0084
9.2400E-01   2.22280E-03 0.0085
9.4600E-01   2.20536E-03 0.0086
9.6800E-01   2.12864E-03 0.0087
9.9000E-01   2.07066E-03 0.0088
1.0120E+00   2.03141E-03 0.0089
1.0340E+00   1.96068E-03 0.0091
1.0560E+00   1.88864E-03 0.0093
1.0780E+00   1.84972E-03 0.0093
1.1000E+00   1.81532E-03 0.0094
1.1220E+00   1.69952E-03 0.0097
1.1440E+00   1.66560E-03 0.0098
1.1660E+00   1.60359E-03 0.0100
1.1880E+00   1.51928E-03 0.0103
1.2100E+00   1.45113E-03 0.0105
1.2320E+00   1.37376E-03 0.0108
1.2540E+00   1.29818E-03 0.0112
1.2760E+00   1.23503E-03 0.0114
1.2980E+00   1.17301E-03 0.0117
1.3200E+00   1.10292E-03 0.0121
1.3420E+00   1.00876E-03 0.0127
1.3640E+00   9.59665E-04 0.0130
1.3860E+00   9.00877E-04 0.0134
1.4080E+00   8.24646E-04 0.0140
1.4300E+00   7.38887E-04 0.0148
1.4520E+00   6.73154E-04 0.0155
1.4740E+00   6.06291E-04 0.0163
1.4960E+00   5.67530E-04 0.0169
1.5180E+00   4.91461E-04 0.0181
1.5400E+00   4.58514E-04 0.0188
1.5620E+00   3.84706E-04 0.0205
1.5840E+00   3.39484E-04 0.0218
1.6060E+00   2.95555E-04 0.0234
1.6280E+00   2.46942E-04 0.0256
1.6500E+00   2.05112E-04 0.0281
1.6720E+00   1.69904E-04 0.0308
1.6940E+00   1.40510E-04 0.0339
```

```
   1.7160E+00   1.03040E-04 0.0396
   1.7380E+00   8.43058E-05 0.0438
   1.7600E+00   5.58809E-05 0.0538
   1.7820E+00   4.23144E-05 0.0618
   1.8040E+00   2.27723E-05 0.0842
   1.8260E+00   1.61505E-05 0.1000
   1.8480E+00   1.29204E-05 0.1118
   1.8700E+00   3.06860E-06 0.2294
   1.8920E+00   1.13054E-06 0.3780
   1.9140E+00   1.61505E-07 1.0000
   1.9360E+00   0.00000E+00 0.0000
   1.9580E+00   0.00000E+00 0.0000
   1.9800E+00   0.00000E+00 0.0000
   2.0020E+00   0.00000E+00 0.0000
   2.0240E+00   0.00000E+00 0.0000
   2.0460E+00   0.00000E+00 0.0000
   2.0680E+00   0.00000E+00 0.0000
   2.0900E+00   0.00000E+00 0.0000
   2.1120E+00   0.00000E+00 0.0000
   2.1340E+00   0.00000E+00 0.0000
   2.1560E+00   0.00000E+00 0.0000
   2.1780E+00   0.00000E+00 0.0000
   2.2000E+00   0.00000E+00 0.0000
     total      1.40968E-01 0.0012

surface  30
     energy
   2.2000E-02   1.26782E-04 0.0365
   4.4000E-02   1.42109E-03 0.0119
   6.6000E-02   1.49651E-03 0.0111
   8.8000E-02   1.61941E-03 0.0105
   1.1000E-01   1.73198E-03 0.0100
   1.3200E-01   1.87072E-03 0.0095
   1.5400E-01   1.96810E-03 0.0093
   1.7600E-01   2.08067E-03 0.0090
   1.9800E-01   2.18598E-03 0.0088
   2.2000E-01   2.22554E-03 0.0087
   2.4200E-01   2.32067E-03 0.0085
```

```
2.6400E-01   2.36395E-03 0.0084
2.8600E-01   2.46312E-03 0.0082
3.0800E-01   2.50253E-03 0.0081
3.3000E-01   2.49930E-03 0.0081
3.5200E-01   2.61106E-03 0.0080
3.7400E-01   2.63205E-03 0.0079
3.9600E-01   2.63771E-03 0.0079
4.1800E-01   2.67695E-03 0.0078
4.4000E-01   2.72766E-03 0.0077
4.6200E-01   2.68131E-03 0.0078
4.8400E-01   2.68373E-03 0.0078
5.0600E-01   2.66726E-03 0.0078
5.2800E-01   2.72556E-03 0.0077
5.5000E-01   2.67001E-03 0.0078
5.7200E-01   2.65951E-03 0.0078
5.9400E-01   2.65515E-03 0.0078
6.1600E-01   2.64481E-03 0.0078
6.3800E-01   2.61719E-03 0.0079
6.6000E-01   2.59313E-03 0.0079
6.8200E-01   2.55857E-03 0.0080
7.0400E-01   2.53014E-03 0.0080
7.2600E-01   2.52837E-03 0.0080
7.4800E-01   2.47103E-03 0.0081
7.7000E-01   2.42533E-03 0.0082
7.9200E-01   2.41580E-03 0.0082
8.1400E-01   2.37138E-03 0.0083
8.3600E-01   2.31906E-03 0.0083
8.5800E-01   2.24977E-03 0.0085
8.8000E-01   2.23039E-03 0.0085
9.0200E-01   2.16191E-03 0.0086
9.2400E-01   2.13236E-03 0.0087
9.4600E-01   2.06468E-03 0.0089
9.6800E-01   2.01817E-03 0.0089
9.9000E-01   1.98571E-03 0.0090
1.0120E+00   1.90932E-03 0.0092
1.0340E+00   1.83373E-03 0.0094
1.0560E+00   1.79675E-03 0.0095
1.0780E+00   1.76832E-03 0.0096
```

```
1.1000E+00   1.65624E-03 0.0099
1.1220E+00   1.60827E-03 0.0100
1.1440E+00   1.55885E-03 0.0102
1.1660E+00   1.49683E-03 0.0104
1.1880E+00   1.39573E-03 0.0108
1.2100E+00   1.35002E-03 0.0109
1.2320E+00   1.26475E-03 0.0113
1.2540E+00   1.20822E-03 0.0116
1.2760E+00   1.13280E-03 0.0119
1.2980E+00   1.07256E-03 0.0123
1.3200E+00   1.00230E-03 0.0127
1.3420E+00   9.11375E-04 0.0133
1.3640E+00   8.89410E-04 0.0135
1.3860E+00   7.97029E-04 0.0142
1.4080E+00   7.24836E-04 0.0149
1.4300E+00   6.53774E-04 0.0157
1.4520E+00   6.03869E-04 0.0164
1.4740E+00   5.42497E-04 0.0172
1.4960E+00   4.85001E-04 0.0182
1.5180E+00   4.33642E-04 0.0193
1.5400E+00   3.91974E-04 0.0203
1.5620E+00   3.34316E-04 0.0220
1.5840E+00   2.87641E-04 0.0237
1.6060E+00   2.47588E-04 0.0255
1.6280E+00   2.03012E-04 0.0282
1.6500E+00   1.61990E-04 0.0316
1.6720E+00   1.37764E-04 0.0342
1.6940E+00   1.04332E-04 0.0393
1.7160E+00   8.17217E-05 0.0445
1.7380E+00   6.12105E-05 0.0514
1.7600E+00   4.03763E-05 0.0632
1.7820E+00   2.66484E-05 0.0778
1.8040E+00   1.51815E-05 0.1031
1.8260E+00   1.22744E-05 0.1147
1.8480E+00   4.84516E-06 0.1826
1.8700E+00   1.77656E-06 0.3015
1.8920E+00   1.61505E-07 1.0000
1.9140E+00   0.00000E+00 0.0000
```

```
   1.9360E+00   0.00000E+00 0.0000
   1.9580E+00   0.00000E+00 0.0000
   1.9800E+00   0.00000E+00 0.0000
   2.0020E+00   0.00000E+00 0.0000
   2.0240E+00   0.00000E+00 0.0000
   2.0460E+00   0.00000E+00 0.0000
   2.0680E+00   0.00000E+00 0.0000
   2.0900E+00   0.00000E+00 0.0000
   2.1120E+00   0.00000E+00 0.0000
   2.1340E+00   0.00000E+00 0.0000
   2.1560E+00   0.00000E+00 0.0000
   2.1780E+00   0.00000E+00 0.0000
   2.2000E+00   0.00000E+00 0.0000
     total      1.33431E-01 0.0013

surface union total
     energy
   2.2000E-02   9.28559E-03 0.0054
   4.4000E-02   1.08283E-01 0.0019
   6.6000E-02   1.13099E-01 0.0017
   8.8000E-02   1.12568E-01 0.0017
   1.1000E-01   1.08914E-01 0.0017
   1.3200E-01   1.04323E-01 0.0017
   1.5400E-01   9.97866E-02 0.0017
   1.7600E-01   9.55236E-02 0.0017
   1.9800E-01   9.06005E-02 0.0018
   2.2000E-01   8.48643E-02 0.0018
   2.4200E-01   8.16468E-02 0.0018
   2.6400E-01   7.85189E-02 0.0018
   2.8600E-01   7.48393E-02 0.0019
   3.0800E-01   6.97303E-02 0.0019
   3.3000E-01   6.58081E-02 0.0020
   3.5200E-01   6.29751E-02 0.0020
   3.7400E-01   6.04169E-02 0.0020
   3.9600E-01   5.65212E-02 0.0020
   4.1800E-01   4.73235E-02 0.0023
   4.4000E-01   4.56464E-02 0.0023
   4.6200E-01   4.43825E-02 0.0023
```

```
4.8400E-01   4.28248E-02 0.0024
5.0600E-01   3.77170E-02 0.0026
5.2800E-01   3.32714E-02 0.0028
5.5000E-01   3.29300E-02 0.0028
5.7200E-01   3.25283E-02 0.0028
5.9400E-01   3.22358E-02 0.0028
6.1600E-01   3.18064E-02 0.0028
6.3800E-01   3.14598E-02 0.0028
6.6000E-01   3.12274E-02 0.0028
6.8200E-01   3.06854E-02 0.0029
7.0400E-01   3.01403E-02 0.0029
7.2600E-01   2.99161E-02 0.0029
7.4800E-01   2.93846E-02 0.0029
7.7000E-01   2.89224E-02 0.0029
7.9200E-01   2.84815E-02 0.0029
8.1400E-01   2.79341E-02 0.0030
8.3600E-01   2.76066E-02 0.0030
8.5800E-01   2.71917E-02 0.0030
8.8000E-01   2.65844E-02 0.0030
9.0200E-01   2.60217E-02 0.0031
9.2400E-01   2.57751E-02 0.0031
9.4600E-01   2.52749E-02 0.0031
9.6800E-01   2.47392E-02 0.0031
9.9000E-01   2.42686E-02 0.0032
1.0120E+00   2.37959E-02 0.0032
1.0340E+00   2.31802E-02 0.0032
1.0560E+00   2.26710E-02 0.0032
1.0780E+00   2.21540E-02 0.0033
1.1000E+00   2.15623E-02 0.0033
1.1220E+00   2.08865E-02 0.0034
1.1440E+00   2.03363E-02 0.0034
1.1660E+00   1.98844E-02 0.0035
1.1880E+00   1.92214E-02 0.0035
1.2100E+00   1.85019E-02 0.0036
1.2320E+00   1.79195E-02 0.0036
1.2540E+00   1.73213E-02 0.0037
1.2760E+00   1.66538E-02 0.0037
1.2980E+00   1.61052E-02 0.0038
```

```
1.3200E+00   1.53635E-02 0.0039
1.3420E+00   1.46713E-02 0.0040
1.3640E+00   1.41752E-02 0.0040
1.3860E+00   1.35661E-02 0.0041
1.4080E+00   1.29211E-02 0.0042
1.4300E+00   1.21578E-02 0.0043
1.4520E+00   1.16985E-02 0.0044
1.4740E+00   1.10802E-02 0.0045
1.4960E+00   1.05442E-02 0.0046
1.5180E+00   9.68096E-03 0.0048
1.5400E+00   9.25248E-03 0.0049
1.5620E+00   8.79558E-03 0.0050
1.5840E+00   8.28119E-03 0.0051
1.6060E+00   7.74984E-03 0.0053
1.6280E+00   7.00982E-03 0.0055
1.6500E+00   6.73526E-03 0.0056
1.6720E+00   6.34086E-03 0.0057
1.6940E+00   5.95212E-03 0.0058
1.7160E+00   5.09356E-03 0.0063
1.7380E+00   4.77507E-03 0.0065
1.7600E+00   4.51731E-03 0.0066
1.7820E+00   4.30509E-03 0.0067
1.8040E+00   3.76760E-03 0.0071
1.8260E+00   3.26580E-03 0.0076
1.8480E+00   3.14855E-03 0.0077
1.8700E+00   2.98672E-03 0.0078
1.8920E+00   2.86753E-03 0.0079
1.9140E+00   2.23814E-03 0.0089
1.9360E+00   2.08277E-03 0.0092
1.9580E+00   2.01817E-03 0.0093
1.9800E+00   1.97683E-03 0.0094
2.0020E+00   1.67885E-03 0.0101
2.0240E+00   1.05834E-03 0.0128
2.0460E+00   1.06933E-03 0.0127
2.0680E+00   1.05318E-03 0.0128
2.0900E+00   9.80661E-04 0.0130
2.1120E+00   5.60908E-04 0.0174
2.1340E+00   3.99403E-04 0.0206
```

```
    2.1560E+00   3.80022E-04 0.0210
    2.1780E+00   3.56765E-04 0.0214
    2&2000E+00   r.72298E-04 0.0244
      total      2.85101E+00 0.0004

 thare are no nonzero tallies in the tally fluctuation chart bin for tally  11

1tally   8        nps =  6000000
           tally type 8*   energy deposition                              units   met
           tally for  photons   electrons

        cell
        7        1.38495E-05 0.0251
        8        1.40106E-05 0.0243
        9        1.36972E-05 0.0247
       10        1.26092E-05 0.0257
       11        1.21807E-05 0.0265
       12        1.17626E-05 0.0269
       13        1.04070E-05 0.0303
       14        9.48203E-06 0.0354
       15        9.14914E-06 0.0315
       16        8.95804E-06 0.0318
       17        8.29410E-06 0.0365
       18        7.77549E-06 0.0363
       19        7.09064E-06 0.0347
       20        6.65151E-06 0.0388
       21        6.48807E-06 0.0382
       22        5.38197E-06 0.0410
       23        4.89160E-06 0.0421
       24        5.43018E-06 0.0399
       25        4.63749E-06 0.0430
       26        4.55598E-06 0.0445
       27        4.00975E-06 0.0510
       28        3.71451E-06 0.0497
       29        3.93323E-06 0.0475
       30        3.48597E-06 0.0481
       31        3.30937E-06 0.0538
       32        3.04715E-06 0.0542
```

33	2.81394E-06	0.0561
34	2.57323E-06	0.0606
35	2.22142E-06	0.0629
36	2.22259E-06	0.0671
37	1.99594E-06	0.0716
38	1.84960E-06	0.0812
39	2.13989E-06	0.0682
40	1.78698E-06	0.0739
41	1.34743E-06	0.0765
42	1.27069E-06	0.0878
43	1.24660E-06	0.0825
44	1.04170E-06	0.0891
45	9.49351E-07	0.0944
46	1.04238E-06	0.1026
47	8.82010E-07	0.1150
48	7.37102E-07	0.1107
49	6.12447E-07	0.1140
50	6.12173E-07	0.1253
51	4.72845E-07	0.1374
52	4.51074E-07	0.1374
53	4.69283E-07	0.1531
54	2.75489E-07	0.1923
55	3.62089E-07	0.1845
56	3.35957E-07	0.1758
57	2.70763E-07	0.1887
58	1.96311E-07	0.1980
59	1.71622E-07	0.2587
60	1.55542E-07	0.2591
61	1.50848E-07	0.2419
62	1.25199E-07	0.2298
63	1.87260E-07	0.2304
64	9.23981E-08	0.3025
65	1.07024E-07	0.3197
66	9.50304E-08	0.3012
67	1.16613E-07	0.2793
68	1.40314E-07	0.3143
69	1.09729E-07	0.3437
70	2.84561E-08	0.5407

```
       71        5.78657E-08 0.5272
       72        5.35571E-08 0.5112
       73        2.10606E-08 0.4933
       74        4.25856E-08 0.4662
       75        3.96623E-08 0.5132
       76        1.62356E-08 0.8433
       77        4.76211E-19 0.2370
       78        4.41984E-19 0.2403
       79        1.14322E-10 1.0000
       80        5.22470E-19 0.2466


================================================================================================================
========================

          results of 10 statistical checks for the estimated answer for the tally fluctuation chart (tfc)
bin of tally   8

tfc bin     --mean-- ------relative error--------- -variance of the variance----  -figure of merit-- -pdf-
behavior    behavior  value decrease decrease rate  value decrease decrease rate  value behavior  slope

desired      random   <0.10  yes   1/sqrt(nps)    <0.10  yes    1/nps           constant random   >3.00
observed     random    0.03  yes   yes             0.00  yes     yes            constant random   10.00
passed?      yes       yes   yes   yes             yes   yes     yes               yes     yes    yes


================================================================================================================
========================
1tally fluctuation charts

                     tally   11                                  tally    8
      nps      mean     error   vov  slope    fom      mean     error   vov  slope    fom
    512000   0.0000E+00 0.0000 0.0000  0.0 0.0E+00   1.2791E-05 0.1057 0.0865  0.0 8.1E+00
   1024000   0.0000E+00 0.0000 0.0000  0.0 0.0E+00   1.3542E-05 0.0667 0.0324 10.0      10
   1536000   0.0000E+00 0.0000 0.0000  0.0 0.0E+00   1.3863E-05 0.0511 0.0187 10.0      12
   2048000   0.0000E+00 0.0000 0.0000  0.0 0.0E+00   1.4277E-05 0.0420 0.0122 10.0      13
   2560000   0.0000E+00 0.0000 0.0000  0.0 0.0E+00   1.4092E-05 0.0370 0.0092 10.0      13
```

```
   3072000   0.0000E+00 0.0000 0.0000  0.0 0.0E+00   1.3913E-05 0.0335 0.0074 10.0      13
   3584000   0.0000E+00 0.0000 0.0000  0.0 0.0E+00   1.4076E-05 0.0305 0.0058 10.0      14
   4096000   0.0000E+00 0.0000 0.0000  0.0 0.0E+00   1.3971E-05 0.0286 0.0049 10.0      14
   4608000   0.0000E+00 0.0000 0.0000  0.0 0.0E+00   1.3884E-05 0.0273 0.0042 10.0      13
   5120000   0.0000E+00 0.0000 0.0000  0.0 0.0E+00   1.3728E-05 0.0267 0.0047 10.0      13
   5632000   0.0000E+00 0.0000 0.0000  0.0 0.0E+00   1.3724E-05 0.0259 0.0048 10.0      12
   6000000   0.0000E+00 0.0000 0.0000  0.0 0.0E+00   1.3849E-05 0.0251 0.0043 10.0      12

************************************************************************************************************
************
 dump no.    4 on file runtpg   nps =   6000000     coll = 3344563205    ctm =  129.49   nrn = 15828597556


         4 warning messages so far.


 run terminated when   6000000 particle histories were done.

 computer time =  129.51 minutes

 mcnp     version 5     11052003                     06/29/09 16:42:24         probid =  06/29/09 14:32:30
```

APPENDIX D

ENERGY AND DOSE RATE CALCULATED RESULTS

Table D.1: The calculated energies and dose rates deposited by Teflon-encased and standard eye applicators.

Teflon: 0.1 cm	Source: 0.03 cm		0.04 cm		0.045 cm		0.05 cm		Standard applicator	
Depth	Energy	Dose rate	Energy	Dose rate	Energy	Dose rate	Energy	Dose rate	Energy	Dose rate
(cm)	(J/part)	(cGy/s)	(J/part)	(cGy/s)	(J/part)	(cGy/s)	(J/part)	(cGy/s)	(J/part)	(cGy/s)
0.00-0.01	1.80E-18	38.32	1.71E-18	36.45	1.64E-18	34.90	1.54E-18	32.75	4.29E-19	36.55
0.01-0.02	1.82E-18	38.81	1.76E-18	37.40	1.64E-18	34.94	1.56E-18	33.13	4.12E-19	35.05
0.02-0.03	1.75E-18	37.30	1.68E-18	35.88	1.61E-18	34.37	1.56E-18	33.31	4.00E-19	34.04
0.03-0.04	1.67E-18	35.60	1.61E-18	34.28	1.50E-18	31.86	1.48E-18	31.42	3.76E-19	32.05
0.04-0.05	1.62E-18	34.44	1.58E-18	33.54	1.36E-18	29.02	1.41E-18	29.94	3.49E-19	29.72
0.05-0.06	1.47E-18	31.39	1.41E-18	30.07	1.37E-18	29.09	1.34E-18	28.63	3.27E-19	27.86
0.06-0.07	1.44E-18	30.71	1.26E-18	26.86	1.29E-18	27.51	1.26E-18	26.85	3.2E-19	27.23
0.07-0.08	1.33E-18	28.42	1.31E-18	27.92	1.28E-18	27.18	1.16E-18	24.75	3.03E-19	25.82
0.08-0.09	1.27E-18	27.03	1.15E-18	24.40	1.11E-18	23.64	1.09E-18	23.20	2.92E-19	24.83
0.09-0.10	1.17E-18	24.97	1.13E-18	24.09	1.05E-18	22.39	1.01E-18	21.52	2.68E-19	22.81
0.10-0.11	1.06E-18	22.55	1.01E-18	21.44	1.02E-18	21.69	9.30E-19	19.81	2.46E-19	20.91
0.11-0.12	1.06E-18	22.53	8.73E-19	18.60	9.00E-19	19.17	9.13E-19	19.44	2.32E-19	19.73
0.12-0.13	9.89E-19	21.07	8.95E-19	19.05	8.52E-19	18.15	8.54E-19	18.19	2.2E-19	18.7
0.13-0.14	9.87E-19	21.02	8.47E-19	18.04	8.18E-19	17.43	7.92E-19	16.86	1.95E-19	16.63
0.14-0.15	8.69E-19	18.52	7.70E-19	16.40	8.16E-19	17.38	7.25E-19	15.43	1.9E-19	16.16
0.15-0.16	7.67E-19	16.32	7.59E-19	16.17	7.40E-19	15.76	6.84E-19	14.58	1.9E-19	16.18
0.16-0.17	6.97E-19	14.84	6.71E-19	14.28	6.67E-19	14.21	6.34E-19	13.50	1.8E-19	15.31
0.17-0.18	6.72E-19	14.31	6.13E-19	13.06	6.81E-19	14.50	5.79E-19	12.34	1.58E-19	13.44
0.18-0.19	5.79E-19	12.34	5.72E-19	12.19	6.20E-19	13.19	5.48E-19	11.66	1.52E-19	12.98
0.19-0.20	5.50E-19	11.71	5.82E-19	12.40	5.70E-19	12.14	5.12E-19	10.91	1.44E-19	12.29
0.20-0.21	5.03E-19	10.72	5.19E-19	11.04	5.50E-19	11.71	4.77E-19	10.16	1.37E-19	11.68
0.21-0.22	4.93E-19	10.49	4.84E-19	10.31	4.73E-19	10.07	4.44E-19	9.46	1.2E-19	10.19
0.22-0.23	4.49E-19	9.56	4.43E-19	9.43	4.45E-19	9.47	4.06E-19	8.65	1.21E-19	10.28
0.23-0.24	4.01E-19	8.55	3.96E-19	8.44	4.07E-19	8.66	3.72E-19	7.91	1.16E-19	9.85
0.24-0.25	3.79E-19	8.07	3.83E-19	8.15	3.32E-19	7.08	3.53E-19	7.51	1.08E-19	9.18
0.25-0.26	3.31E-19	7.04	3.76E-19	8.01	3.33E-19	7.09	3.08E-19	6.56	8.65E-20	7.36

0.26-0.27	3.10E-19	6.61	3.23E-19	6.87	2.96E-19	6.31	2.93E-19	6.24	7.56E-20	6.44
0.27-0.28	2.81E-19	5.98	3.06E-19	6.51	2.82E-19	6.00	2.64E-19	5.62	8.44E-20	7.19
0.28-0.29	2.49E-19	5.31	2.88E-19	6.13	2.68E-19	5.71	2.58E-19	5.50	7.25E-20	6.17
0.29-0.30	2.37E-19	5.04	2.54E-19	5.42	2.28E-19	4.85	2.45E-19	5.22	6.75E-20	5.75
0.30-0.31	2.18E-19	4.65	2.16E-19	4.60	2.58E-19	5.50	2.07E-19	4.41	6.46E-20	5.5
0.31-0.32	2.21E-19	4.71	2.08E-19	4.43	2.37E-19	5.05	1.93E-19	4.12	7.02E-20	5.98
0.32-0.33	1.81E-19	3.85	1.72E-19	3.66	2.09E-19	4.45	1.65E-19	3.51	6E-20	5.11
0.33-0.34	1.61E-19	3.42	1.86E-19	3.96	1.71E-19	3.63	1.57E-19	3.34	4.79E-20	4.07
0.34-0.35	1.62E-19	3.45	1.56E-19	3.32	1.37E-19	2.93	1.45E-19	3.09	4.95E-20	4.21
0.35-0.36	1.47E-19	3.13	1.49E-19	3.16	1.24E-19	2.64	1.30E-19	2.76	3.71E-20	3.16
0.36-0.37	1.44E-19	3.06	1.36E-19	2.90	9.04E-20	1.93	1.17E-19	2.50	3.87E-20	3.29
0.37-0.38	1.47E-19	3.13	1.24E-19	2.63	9.87E-20	2.10	1.19E-19	2.53	3.67E-20	3.12
0.38-0.39	9.78E-20	2.08	1.05E-19	2.23	1.14E-19	2.44	9.93E-20	2.12	3.8E-20	3.24
0.39-0.40	1.15E-19	2.45	8.16E-20	1.74	1.08E-19	2.30	9.91E-20	2.11	3.45E-20	2.93
0.40-0.41	8.88E-20	1.89	7.75E-20	1.65	1.04E-19	2.22	8.97E-20	1.91	3.63E-20	3.09
0.41-0.42	8.70E-20	1.85	7.44E-20	1.59	7.17E-20	1.53	7.21E-20	1.54	3.21E-20	2.73
0.42-0.43	8.19E-20	1.74	6.97E-20	1.48	6.44E-20	1.37	6.74E-20	1.43	2.66E-20	2.26
0.43-0.44	5.58E-20	1.19	5.82E-20	1.24	4.51E-20	0.96	6.20E-20	1.32	2.18E-20	1.86
0.44-0.45	7.12E-20	1.52	4.18E-20	0.89	3.59E-20	0.77	5.29E-20	1.13	2.2E-20	1.87
0.45-0.46	5.19E-20	1.10	4.72E-20	1.00	4.57E-20	0.97	5.05E-20	1.07	1.68E-20	1.43
0.46-0.47	4.89E-20	1.04	4.16E-20	0.89	4.16E-20	0.89	4.35E-20	0.93	1.8E-20	1.53
0.47-0.48	4.87E-20	1.04	4.40E-20	0.94	4.37E-20	0.93	4.03E-20	0.86	1.23E-20	1.05
0.48-0.49	3.93E-20	0.84	4.04E-20	0.86	4.27E-20	0.91	3.21E-20	0.68	1.35E-20	1.15
0.49-0.50	3.23E-20	0.69	1.47E-20	0.31	3.09E-20	0.66	2.58E-20	0.55	1.48E-20	1.26
0.50-0.51	2.76E-20	0.59	2.12E-20	0.45	3.11E-20	0.66	2.58E-20	0.55	9.77E-21	0.83
0.51-0.52	1.65E-20	0.35	2.80E-20	0.60	1.42E-20	0.30	2.31E-20	0.49	1.05E-20	0.9
0.52-0.53	8.53E-21	0.18	2.13E-20	0.45	2.26E-20	0.48	1.90E-20	0.40	9.58E-21	0.82
0.53-0.54	1.33E-20	0.28	1.77E-20	0.38	6.57E-21	0.14	1.82E-20	0.39	9.01E-21	0.77
0.54-0.55	7.70E-21	0.16	2.61E-20	0.55	1.67E-20	0.36	1.63E-20	0.35	6.86E-21	0.58
0.55-0.56	1.30E-20	0.28	1.27E-20	0.27	9.62E-21	0.20	8.39E-21	0.18	6.65E-21	0.57
0.56-0.57	1.14E-20	0.24	1.47E-20	0.31	7.90E-21	0.17	7.95E-21	0.17	6.83E-21	0.58
0.57-0.58	8.47E-21	0.18	1.45E-20	0.31	5.55E-21	0.12	5.84E-21	0.12	4.86E-21	0.41
0.58-0.59	1.01E-20	0.22	1.08E-20	0.23	1.13E-20	0.24	6.31E-21	0.13	7.27E-21	0.62
0.59-0.60	4.12E-21	0.09	1.08E-20	0.23	1.38E-20	0.29	3.24E-21	0.07	1.65E-21	0.14

APPENDIX E

CENTRAL AXIS DEPTH DOSE CURVES

E.1: Effects of Teflon thickness on central axis depth dose curves

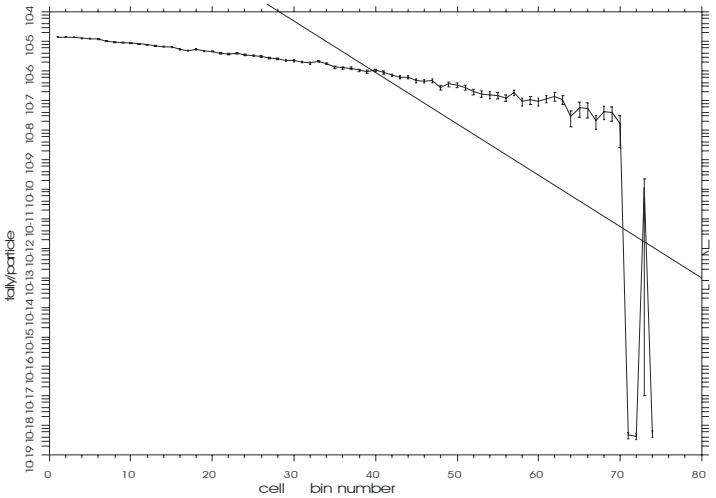

Figure E.1 (a): Teflon thickness of 0 cm and SSD of 0.02 cm

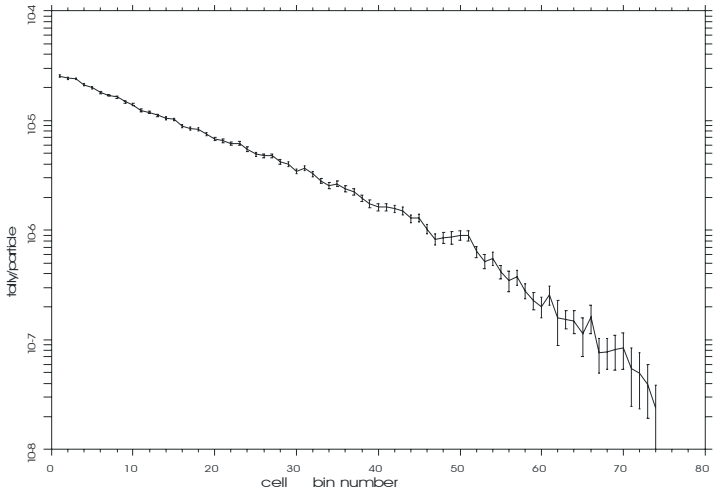

Figure E.1 (b): Teflon thickness of 0.02 cm

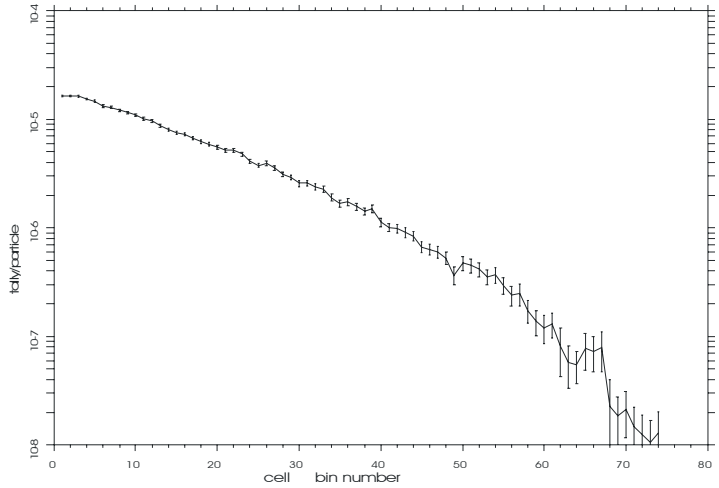

Figure E.1 (c): Teflon thickness of 0.05 cm

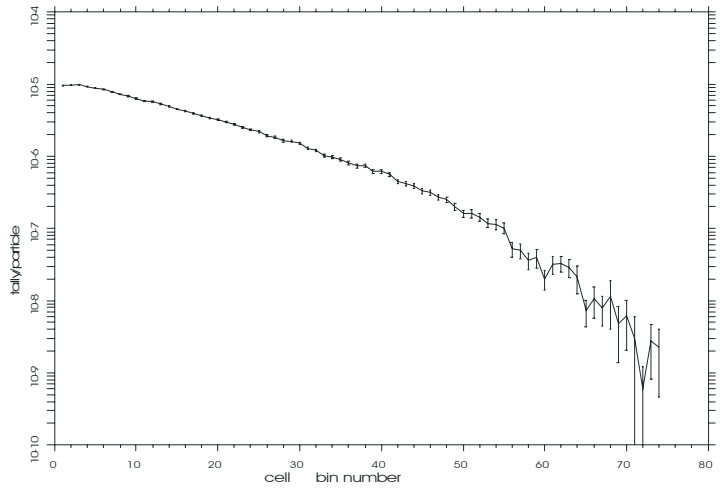

Figure E.1 (d): Teflon thickness of 0.1 cm

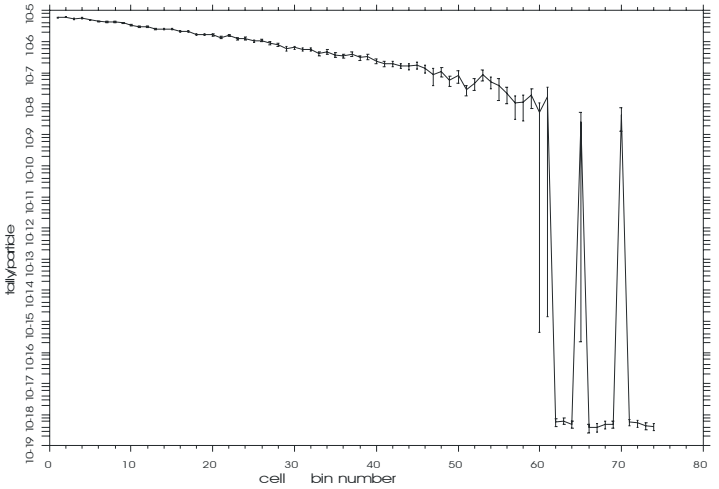

Figure E.1 (e): Teflon thickness of 0.15 cm

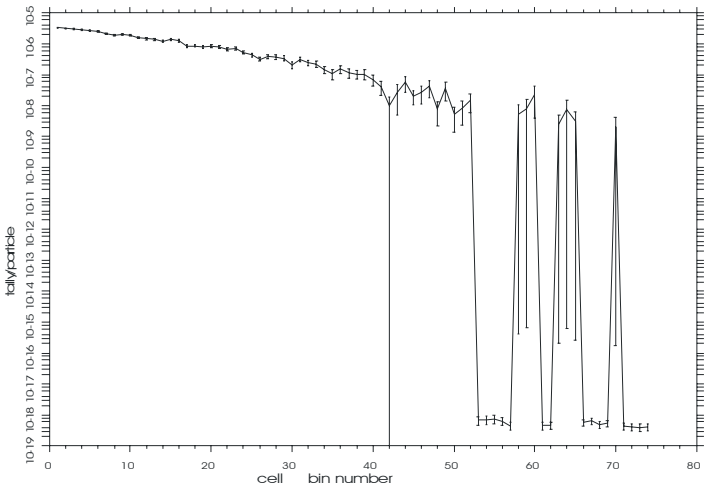

Figure E.1 (f): Teflon thickness of 0.2 cm

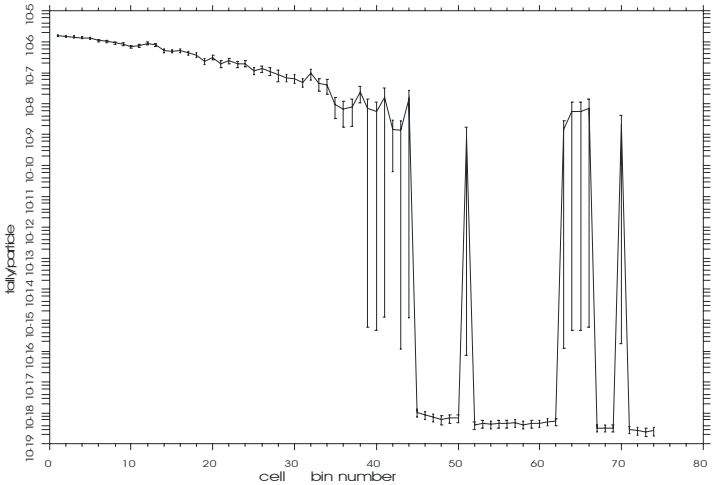

Figure E.1 (g): Teflon thickness of 0.25 cm

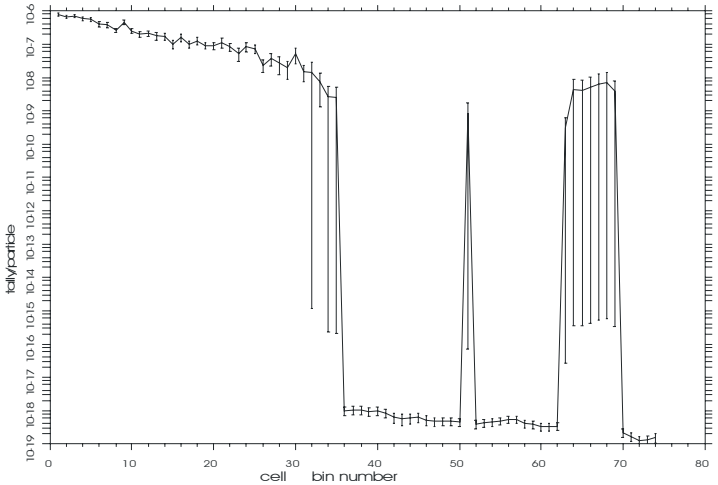

Figure E.1 (h): Teflon thickness of 0.3 cm

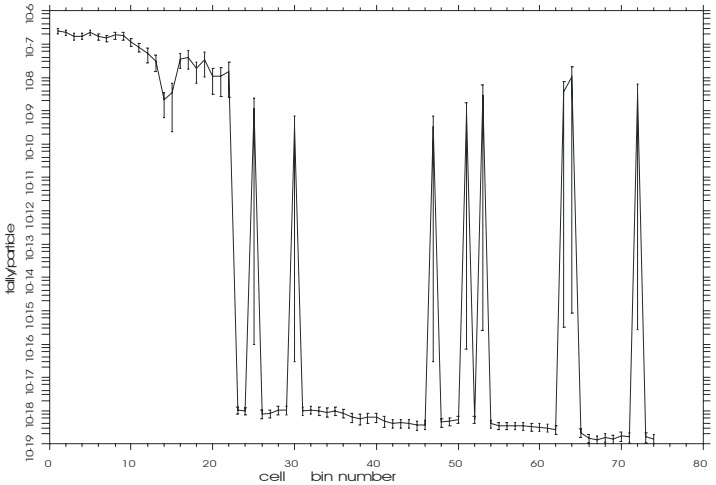

Figure E.1 (i): Teflon thickness of 0.35 cm

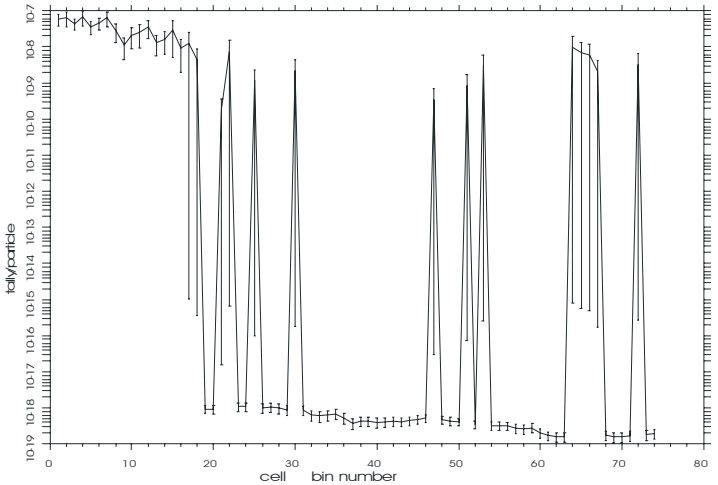

Figure E.1 (j): Teflon thickness of 0.4 cm

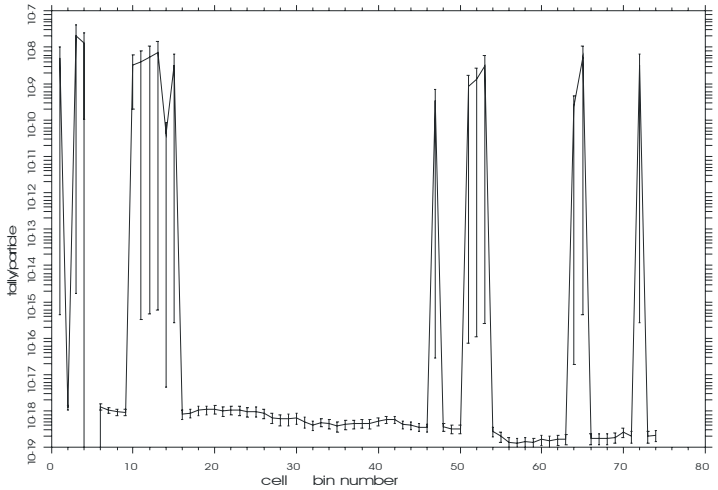

Figure E.1 (k): Teflon thickness of 0.45 cm

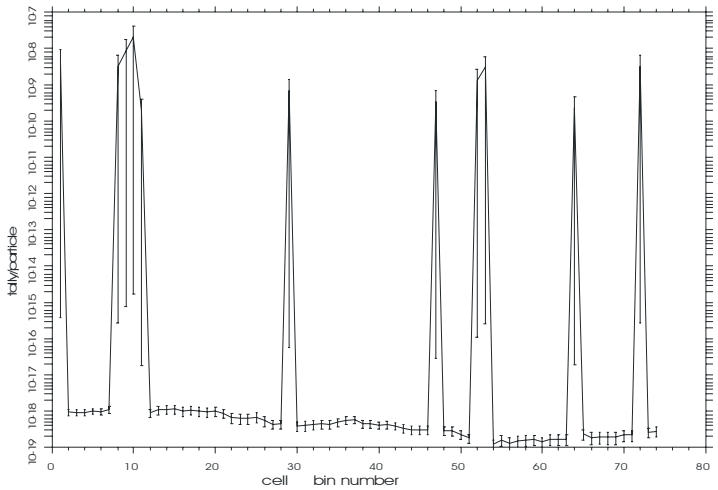

Figure E.1 (l): Teflon thickness of 0.5 cm

E.2: Effects of Source thickness on central axis depth dose curves with 0.1 cm Teflon thickness

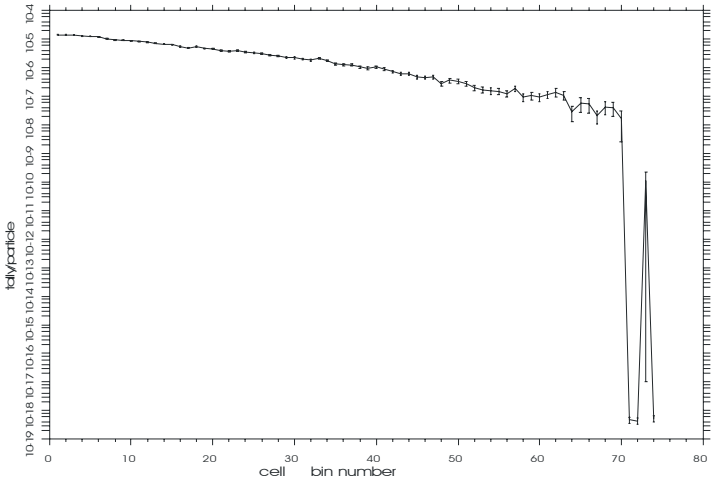

Figure E.2 (a): Source thickness of 0.001 cm

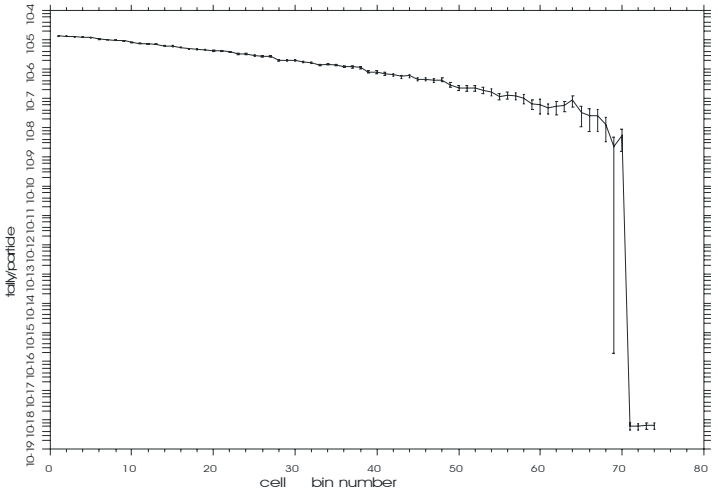

Figure E.2 (b): Source thickness of 0.01 cm

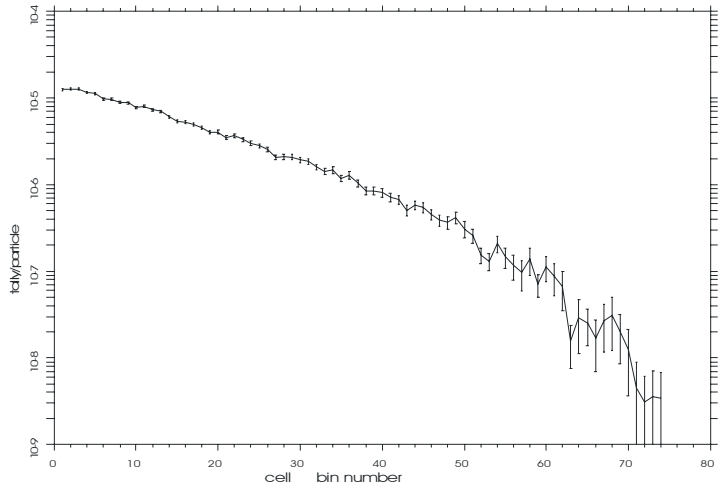

Figure E.2 (c): Source thickness of 0.02 cm

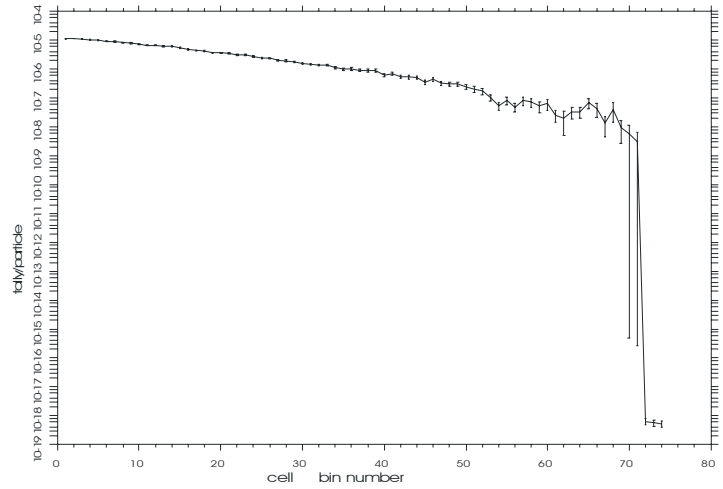

Figure E.2 (d): Source thickness of 0.03 cm

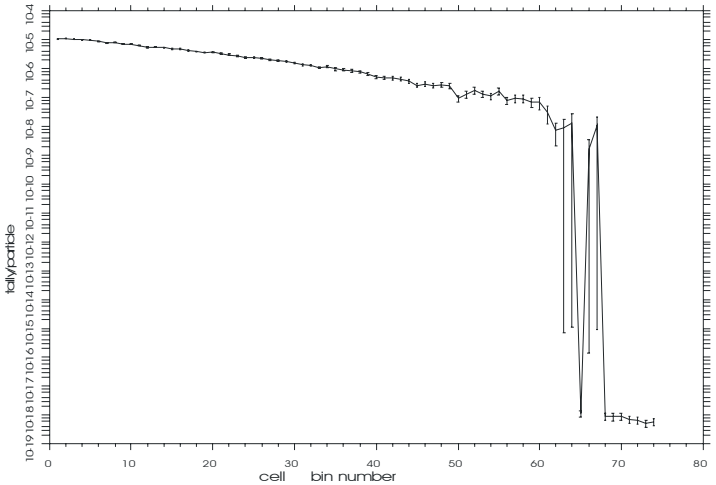

Figure E.2 (e): Source thickness of 0.04 cm

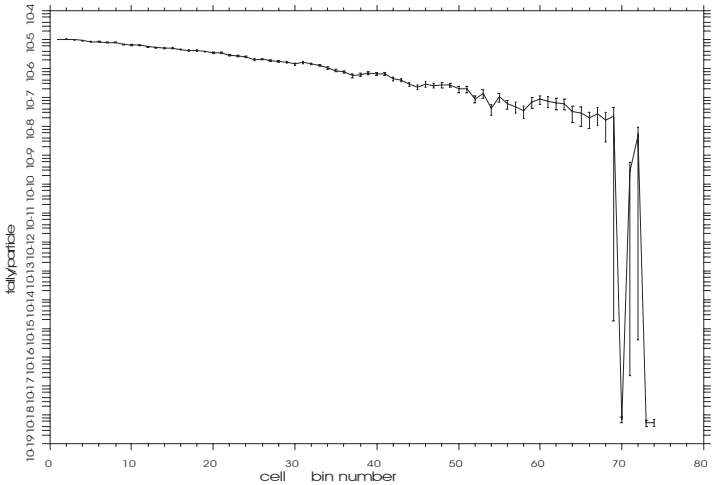

Figure E.2 (f): Source thickness of 0.045 cm

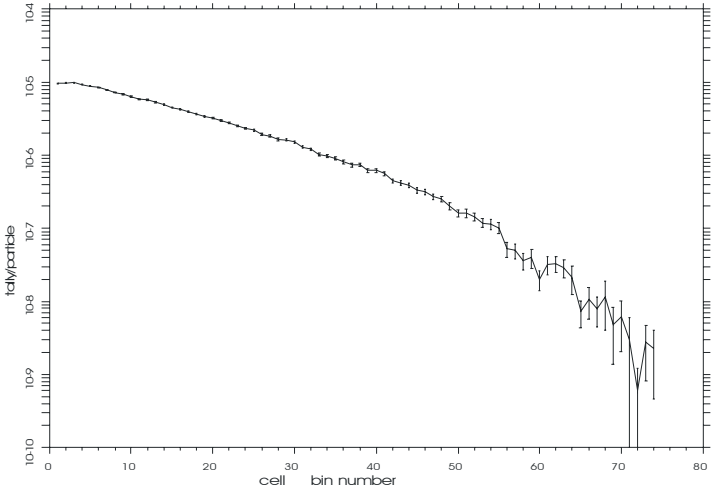

Figure E.2 (g): Source thickness of 0.05 cm

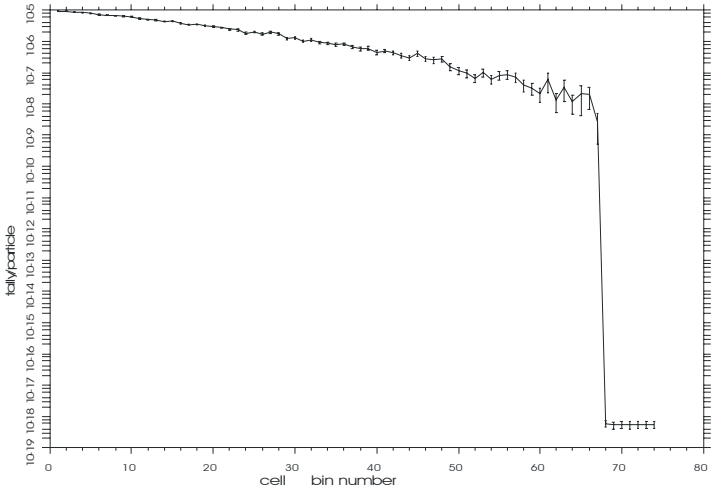

Figure E.2 (h): Source thickness of 0.06 cm

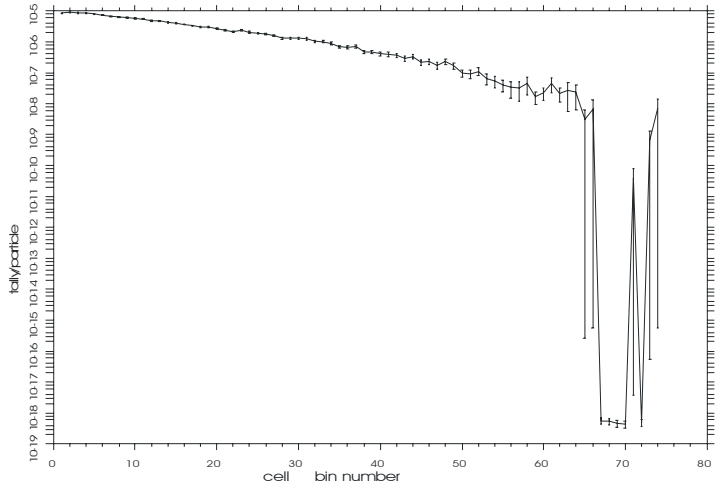

Figure E.2 (i): Source thickness of 0.07 cm

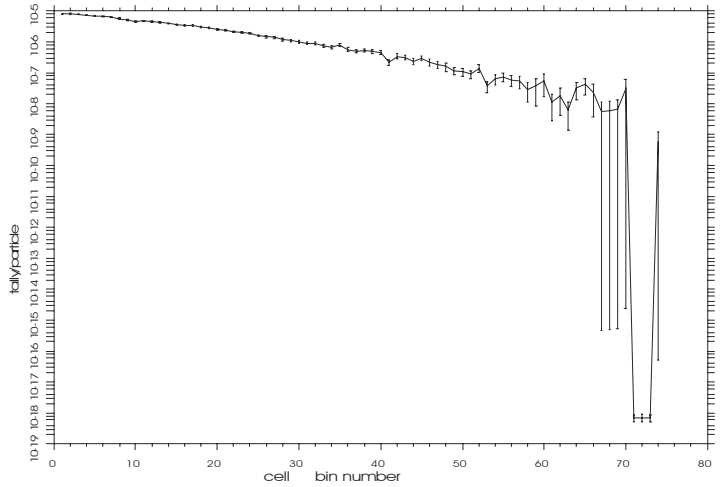

Figure E.2 (j): Source thickness of 0.08 cm

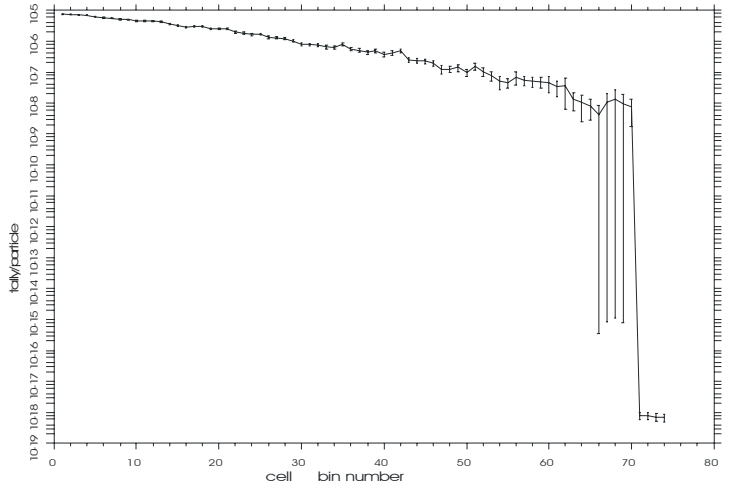

Figure E.2 (k): Source thickness of 0.09 cm

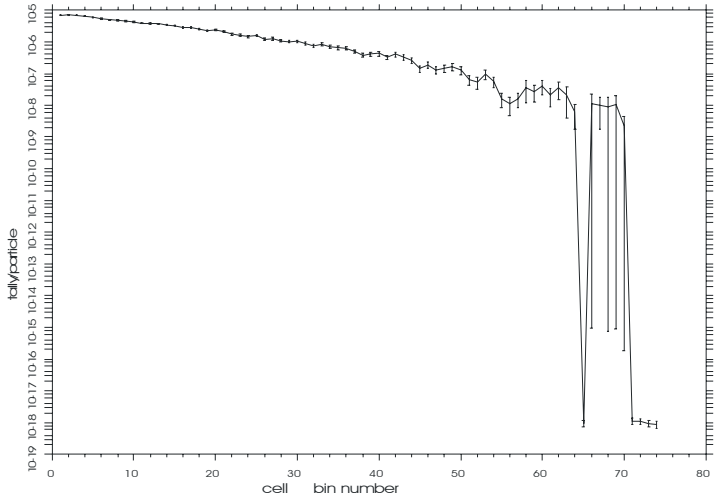

Figure E.2 (l): Source thickness of 0.10 cm

E.3: Effects of source thickness on central axis depth dose curves with 0.125 cm Teflon thickness

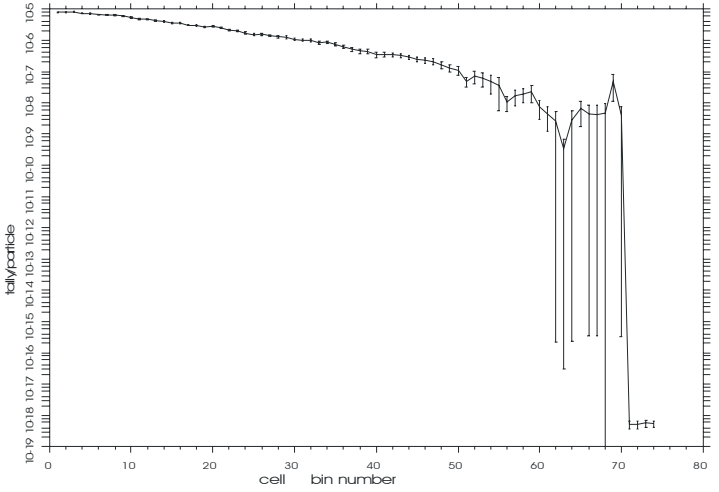

Figure E.3 (a): Source thickness of 0.04 cm

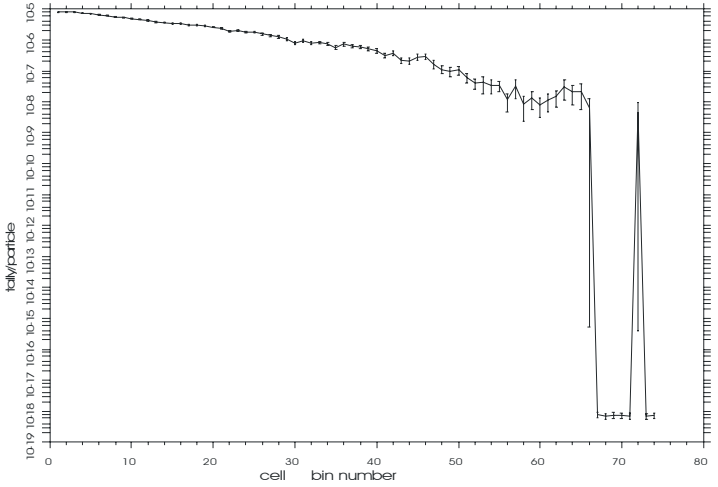

Figure E.3 (b): Source thickness of 0.045 cm

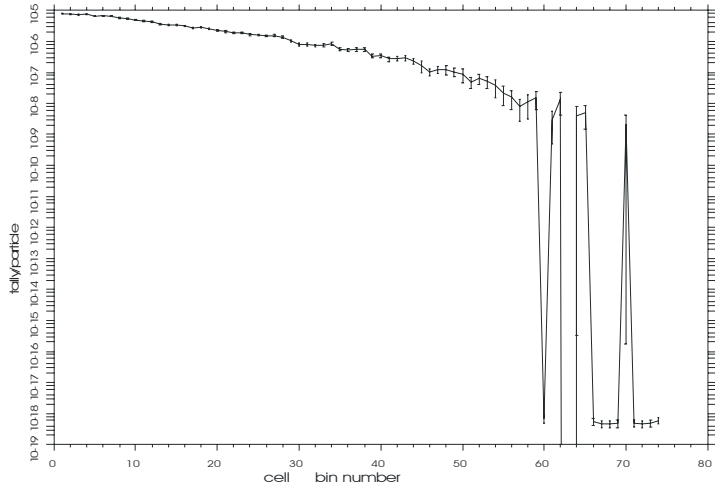

Figure E.3 (c): Source thickness of 0.05 cm

E.4: Effects of surface source distance on central axis depth dose curves

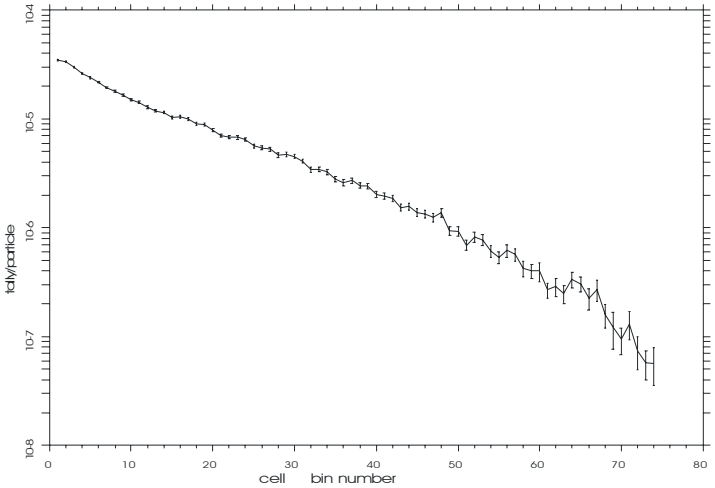

Figure E.4 (a): SSD of 0.02 cm

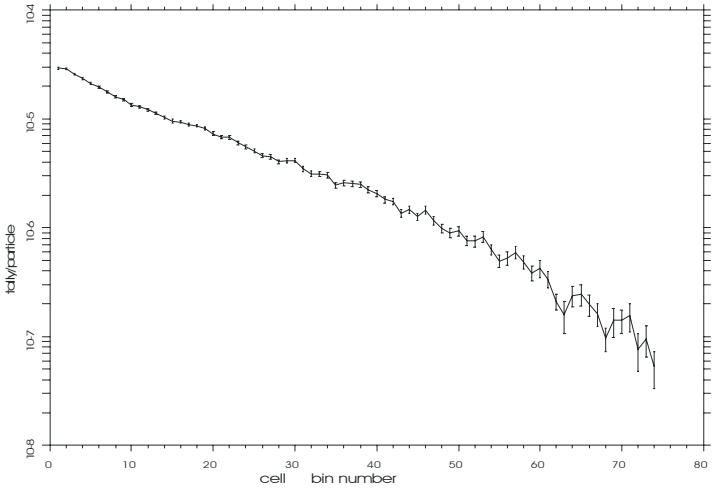

Figure E.4 (b): SSD of 0.05 cm

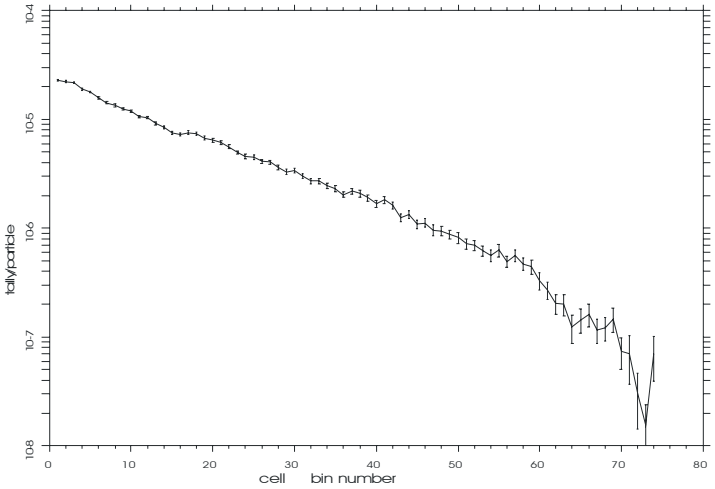

Figure E.4 (c): SSD of 0.1 cm